NASA TECHNICAL NOTE

NASA TN D-2186

DESIGN, TESTS, AND ANALYSIS OF A HOT STRUCTURE FOR LIFTING REENTRY VEHICLES

by Richard A. Pride, Dick M. Royster, and Bobbie F. Helms

Langley Research Center
Langley Station, Hampton, Va.

NATIONAL AERONAUTICS AND SPACE ADMINISTRATION • WASHINGTON, D. C. • APRIL 1964

DESIGN, TESTS, AND ANALYSIS OF A HOT STRUCTURE FOR LIFTING REENTRY VEHICLES

By Richard A. Pride, Dick M. Royster,
and Bobbie F. Helms

Langley Research Center
Langley Station, Hampton, Va.

NATIONAL AERONAUTICS AND SPACE ADMINISTRATION

For sale by the Office of Technical Services, Department of Commerce,
Washington, D.C. 20230 -- Price $2.75

DESIGN, TESTS, AND ANALYSIS OF A HOT STRUCTURE FOR LIFTING REENTRY VEHICLES

By Richard A. Pride, Dick M. Royster,
and Bobbie F. Helms

SUMMARY

A large structural model of a lifting reentry vehicle has been designed and fabricated to incorporate design concepts applicable to a radiation-cooled vehicle. Thermal-stress-alleviating features of the model are discussed. The structure successfully survived all environmental tests, which included approximately 100 cycles of room-temperature loading and 33 cycles of combined loading and heating up to temperatures of 1,600° F. Measured temperatures are presented for all parts of the model for tests at 1,600° F. Comparisons made between measured and calculated strains and deflections for the model show satisfactory agreement.

Environmental tests on model components include corrugation-stiffened skin panels subjected to various combinations of heat, load, random intense noise, and wind-tunnel flutter and corrugated shear webs subjected to combined heat and load. Tests were generally carried to failure. Results by analytical methods are presented wherever possible, and the correlation with the experimental behavior of the components is satisfactory. Component behavior also shows that the concepts employed in the large model were designed with an adequate margin of strength.

INTRODUCTION

Design of lifting reentry vehicles of low wing loading can be based on radiative thermal-protection systems. One such radiative system, the hot structure, subjects the load-carrying material to high temperatures with large variations in temperature throughout the structure. These conditions present difficult thermal-stress problems and have prompted investigation of structural concepts which are designed to cope with the thermal environment while maintaining a load-carrying capability. Preliminary results of such an investigation were reported in reference 1.

The present paper further describes the design and fabrication of the full-scale structural model of a lifting reentry glider presented in reference 1 and also presents the detailed structural response of the model to applied loads and heating which simulate the reentry environment. Studies were also made in depth

of buckling, shear, and bending deformations and response to acoustic and wind-tunnel flutter tests of two of the more unusual components of the structural model - namely, corrugated-skin panels and shear webs.

SYMBOLS

A	cross-sectional area, sq in.
a	distance between applied loads, in.
B, C	empirical correction terms
b	width of element, in.
c	spar-cap depth, in.
D	diameter of hole or cutout, in.
d	depth of shear web, in.
E	modulus of elasticity, psi
G	shear modulus of elasticity, psi
$\overline{GJ}$	effective torsional stiffness, lb-in.^{2}
H	distance from neutral axis of beam to centroid of spar cap (fig. 2(c)), in.
h	distance between centroid and outside cover of spar cap (fig. 2(c)), in.
I	moment of inertia, in.^{4}
l	length of element, in.
M	bending moment, in-lb
n	exponent in stress-strain equation (D3)
P	concentrated load, lb
q	shear flow, lb/in.
S	planform area of reentry vehicle, sq ft
s	distance around perimeter of cross section, in.
T	temperature, ^{o}F

$\bar{T}$	average temperature, $^{\circ}F$
t	thickness, in.
W	gross weight of reentry vehicle, lb
x, y	coordinates
α	coefficient of thermal expansion, in./in./$^{\circ}F$
β	angle of support rotation, radians
γ	shear strain
δ	deflection, in.
ϵ	strain
ζ	empirical postbuckling factor
θ	angle of twist, radians
μ	Poisson's ratio
ρ	radius of curvature, in.
σ	stress, psi
τ	shear stress, psi
ϕ	angle of slope at end of beam, radians

Subscripts:

B	bottom, with respect to testing configuration of model
cr	buckling
f	failure
i, j	any particular element or part
T	top, with respect to testing configuration of model
ult	ultimate
y	yield
σ	stress

LIFTING REENTRY GLIDER

STRUCTURAL DESIGN

A full-scale structural model of the forward portion of a lifting reentry vehicle was designed, fabricated, and tested. Figure 1 is a photograph of this model during assembly and instrumentation. The model is triangular in planform and cross section with a length of 12 feet, a width at the base of 7 feet, and a height at the base of $2\frac{3}{4}$ feet. These dimensions provide a planform area of 47 square feet with a sweep angle of 75°. In order to provide the greatest variety of test information, this structural model was designed with a nonsymmetrical cross section in order to be more representative of a general class of reentry vehicles. Skin panels and internal structure were designed so that the model could be heated and loaded from either side to simulate either a flat-bottomed or a V-bottomed reentry vehicle.

Initial design guidelines specified a glider configuration with W/S = 30 lb/sq ft and a limit load factor of 7 at room temperature. Simulated reentry heat input was specified for only one surface so that a peak heat-shield temperature of 2,500° F would be reached. Based on observations made in reference 2, a temperature of 2,500° F on the metallic outer surface of a heat shield containing passive fibrous insulation would correspond to a temperature of about 1,600° F in the primary skin structure. For these particular tests, heat was applied only to the flat planform surface so as to reach a peak temperature of 1,600° F. No heat shields, leading edges, or nose cap were used on the model.

Interior

The internal structure of the model consists of an approximately orthogonal arrangement of transverse frames and two main beams (fig. 2). The skin panels are designed so that air loads are transmitted only to the transverse frames. These frames in turn transmit the loads to the two main beams. All load-carrying members operate at elevated temperatures because the heat transfer from the skin panels is principally by radiation throughout the internal structure with conduction a secondary means of heat transfer. The principal thermal forces are alleviated by designing an essentially determinate structure so as not appreciably to restrict thermal displacements.

Corrugated shear webs are used in both the transverse frames and the main beams to carry the shear loads, and at the same time, to permit differential thermal expansion between the top and bottom spar caps without a large buildup of thermal stress. Reference 3 shows that shear webs of corrugated material may be designed to be efficient with regard to shear strength and stiffness.

Details of the two types of corrugated webs are shown in figure 2(b). The main-beam web is a standard 60° corrugation and is spotwelded between the channels of the main-beam spar cap as shown in figure 2(b). The transverse-frame

web has a specially designed corrugation to provide extreme flexibility normal to the web between the two channels which make up the transverse cap. This flexibility is needed to allow the skin-panel expansion joints to expand or contract freely without a large buildup of thermal stress in the skins. The transverse shear webs are spliced to the main-beam webs at their intersection.

Spar-cap details are shown in figure 2(c). Primary bending stiffness for the model is provided by the spar caps of the two main beams. Because of the taper in depth of the main beams as well as taper in depth of individual spar caps, the lettered dimensions change with station and are tabulated along with the section properties in table I. Transverse-frame spar caps consist of two channels of constant cross section. In order to help isolate thermally the main beams from the skin panels, the transverse-frame channels cross on the outside of the main-beam spar cap (fig. 1). One channel in each frame is firmly attached to the main beam with a clip angle, but the other channel is freely floating so that the expansion-joint action is not restricted.

Exterior

The exterior of the model is covered with corrugated skin panels with the axis of the corrugations alined as shown in figure 3. These skin panels serve a dual purpose; air loads are carried fore and aft to the supporting internal frames, and torsional stiffness is provided for the model. Expansion joints (see fig. 3(c)) in the transverse frames which extend around the model cross section at 2-foot longitudinal intervals help to alleviate thermal stresses but prevent the skins from contributing any bending stiffness to the model. The station numbers shown in figures 2(a) and 3(b) designate longitudinal locations measured in inches from the apex shown in figure 3(b).

The skin panels are attached to the outside flanges of the transverse-frame caps by blind riveting (fig. 3(c)). Skin panels are fabricated by seam welding two pieces of 0.0107-inch-thick sheet. The outer sheet is beaded slightly to stiffen the sheet against local buckling and to preset a pattern which deforms uniformly when thermal expansion across the beads is restrained by the attachment to the transverse frames. The inner sheet is formed to a 60°, 1/2-inch flat corrugation and stops short of the edge of the outer sheet. A Z-stiffener provides the transition from the inner sheet to the outer sheet along the attached edges as shown in figure 3(c). The skin panels are attached only to the transverse frames and do not come in contact with the main-beam cap. The expansion-joint tie acts as a joint seal and allows the transverse-frame channels to move relative to each other as the skin panels move, so that their shear stiffness can be utilized for torsional stiffness of the model. For aerodynamic smoothness, the expansion joint is covered with a strip which is fastened on the upstream side.

Material

All parts of the structural model were fabricated from Inconel X. This material was selected because, as an established commercial alloy, it was readily available, could be readily formed and spotwelded in the annealed condition,

could be heattreated after fabrication, and had the strength capabilities to meet the design requirements. Four thicknesses of sheet were used. The average thicknesses for various parts of the model were 0.0107-inch sheet for skin panels and transverse-frame shear webs, 0.0193-inch sheet for main-beam shear webs, 0.0317-inch sheet for transverse-frame caps, and 0.0502-inch sheet for main-beam caps. The average weight of the internal structure in this model is 1.5 lb/sq ft and the average weight of the skin panels is 1.0 lb/sq ft based on the wetted area of the model.

Prior to heat treatment, the skin panels were assembled on the transverse frames. All of the rivet holes needed for final assembly were drilled. Blind rivets were driven in 50 percent of the rivet holes (fig. 3(c)). The assembly was mounted inside a heavy structural-steel frame as shown in figure 3(d) to prevent handling damage during transportation to and from heat treatment. During heat treatment, both the assembled model and frame were placed in the furnace with the model freely suspended from the top of the frame so that no external restraint of thermal expansion occurred.

The model was heattreated 2 hours at 1,400° F in a large gas-fired furnace. Heating and cooling in the furnace were controlled at rates which kept temperature differences throughout the model less than 100° F at any time. Results from references 4 to 6 showed that optimum short-time tensile strength could be obtained by heattreating annealed Inconel X sheet at 1,400° F for times from 1 to 4 hours. In order to insure that all parts of the large model were at 1,400° F for at least 1 hour, a 2-hour heattreating exposure was used. Material properties resulting from this heat treatment are given in table II.

After heattreating the large model, all rivets were drilled out, skin panels were removed, and the entire structure was examined for cracks. No warping was observed for the assembly or for individual parts. Several small cracks were discovered in a longitudinal riveted joint between skin panels and leading-edge closing web. These were stopped by drilling a small hole at the end of each crack, and a reinforcing strip was riveted over the affected region of the closing web. The frequency of these reinforcements can be seen in figure 4(a) by the presence of extra rivets in the single horizontal rivet connection shown. This joint was designed to be nonload carrying and the presence of cracks and repairs thereto was not considered to have an appreciable effect on the subsequent behavior of the model.

After attaching thermocouple and strain-gage instrumentation, the skin panels were reassembled on the transverse frames with rivets driven in all of the rivet holes.

Instrumentation

Response of various parts of the model to loading and heating was measured by 84 strain gages and 300 thermocouples installed inside the model after heat treatment, and by two load cells, four thermocouples, 24 deflectometers, and one transit attached to or reading on various exterior portions of the model. The location of the various transducers is shown in figure 5. Details of transducer

installation and data recording as well as a discussion of data accuracy are given in appendix A.

Test Apparatus

Loads were applied to the model cantilevered from a support as shown in figure 4(a). Two hydraulic jacks loaded the model through a whippletree system so as to approximate the bending moments and shears in the transverse frames and main beams that would be produced by a uniformly distributed airload on the flat side of the model. Whippletree loads were applied to loading straps which extended through the model expansion joints and were spotwelded to the shear webs at the intersections of transverse frames with either main beams or leading edges (see fig. 3(a)).

The loads applied to the model were transferred to the model support through four pins (pin holes are shown at right end of model in fig. 1). The support structure and the loading jacks were bolted into the reinforced concrete laboratory floor.

Elevated-temperature tests were run by radiantly heating the flat side of the model with a large quartz-lamp radiator (fig. 4(b)). For the lamp configuration shown, heating was designed to produce isotherms parallel to the leading edges of the model. The radiator was divided into seven zones, each operated by a separate ignitron tube power supply and controlled by a computer which continuously compared model temperature response with the programed temperature desired as plotted on a time-based curve.

Three-phase electrical power was distributed to the lamp units through a system of bare copper tubing mounted behind the lamp units and supported on high-temperature ceramic electrical insulation. This arrangement eliminated the possibility of fire in overheated electrical insulation. Maximum power capacity for the radiator was 2,800 kilowatts.

Cooling the quartz lamps for long-time high-temperature use was accomplished by blowing air across the lamp ends and the quartz envelopes. Cooling air at a pressure of 30 psi and a volume flow of 1,300 standard cubic feet/minute was distributed in the high-temperature areas through gold-plated stainless-steel tubing.

The radiator is shown raised for checkout in figure 4(b). Before a test, the radiator was lowered so that it was parallel to, and about 4 inches above, the flat surface of the model.

MODEL TEST RESULTS AND DISCUSSION

Structural behavior of the model was studied first at room temperature for three types of load application and second at various combinations of loading and elevated temperatures simulating reentry environments. All tests on the model simulated heating and loading conditions for a flat-bottom reentry

configuration. For testing convenience the model was mounted with the flat side up (fig. 4). All references to top or bottom in this report refer to the test orientation of the model; thus the top skin refers to the flat side. An overall observation of the model behavior is that the model responded elastically throughout the cyclic loading and heating history. This elastic response was indicated by absence of permanent set in the measured strains upon removal of load and by the cumulative total measured permanent deflection at the tip of only 0.06 inch (less than 3 percent of maximum cyclic deflection).

Room-Temperature Loading

The strain and deflection response to room-temperature loading is given in tables III to VII.

For each location of the application of load on the model (tables III to VI) one preload and two load cycles were applied up to the loads indicated in the tables in order to record all readings from the instrumentation. Loads were increased or decreased continuously at a rate of about 1,000 pounds per minute.

For the concentrated-load bending tests, a single jack loaded particular stations on the model. The jack load was divided so as to be applied symmetrically to the two main beams or the two leading-edge load points at the selected station. Thus the 1,000-pound load applied at any station in table III or V is divided to place 500 pounds on each of the two main beams or on each of the two leading edges.

Room-temperature deflections.- Deflections measured at the various stations for concentrated loads symmetrically applied to the model at room temperature are listed in table III. The tabulated values are averages of slopes for straight lines fitted to the experimental deflection-load data for the two symmetrical locations (main beam or leading edge). Interference between the loading apparatus and the deflectometer connections resulted in a loss of deflection measurements for a few combinations as noted by the blank spots in table III.

Experimental deflections of the model at various stations for distributed loads are given in table IV and are plotted in figure 6(a). The three loads represent approximately one-third, two-thirds, and the maximum applied load. The whippletrees (fig. 4(a)) were designed to distribute the hydraulic jack load so as to simulate a uniform airload, and several checks indicated that individual load points were receiving applied loads within 4 percent of their calculated value.

A comparison is shown in figure 6(a) between the measured deflections and calculated deflections on the main beams for the same values of applied distributed load. Agreement is reasonable at the tip of the model (7 percent), but is less satisfactory at stations towards the root. Calculated deflections consist of three parts, bending deflections, shear deflections, and deflections due to support motion. A comparison is shown in figure 6(b) of the influence of these three factors considered in the calculated deflections. Although bending is predominant, support deformation and shear both contribute significantly to the

total beam deflection. The two main beams are assumed to carry all of the applied loads inasmuch as the expansion joints between skin panels were designed to be flexible under direct loads. Details of the theoretical analysis are presented in appendix B.

Room-temperature shear strains.- Experimental strains in various parts of the model responded to applied loads at room temperature in a generally predictable manner. Strains increased linearly with increase of applied load. Some of the special characteristics designed into the model resulted in a few unusual responses.

The shear strain in the corrugated webs of the main beams is plotted in figure 7(a) for 1,000-pound concentrated-load applications at various stations and shows the influence of the depthwise taper in the main beam as well as the effect of access hole cutouts in the web.

Shear strain was measured with back-to-back rosette gages attached to the corrugated web at station 188 (fig. 5(b)). Rosettes at two other stations developed electrical grounds and were not read. The measured shear strain at station 188 decreased as the point of load application moved toward the tip of the model. As the applied load moved toward the tip, the bending moment at station 188 increased and accordingly the vertical component of the compressive thrust in the inclined spar cap also increased. Increase in the spar cap vertical component produced a decrease in the shear force remaining to be carried by the web. The curve labeled "Uniform strain distribution" in figure 7(a) is calculated by dividing the shear force by the web cross-sectional area and the shear modulus. The shear strain is assumed to be uniformly distributed across the depth of the web. This is shown experimentally to be a valid assumption for solid corrugated shear web beams in a subsequent section entitled "Component Tests." However, reference to figures 2(a) and 5(b) shows that the rosette gage at station 188 is close to a circular cutout in the web. The cutout proximity causes an increased strain at the gage location. Strain distributions around cutouts in corrugated shear webs described in the section "Component Tests" indicate that a strain concentration factor of 1.8 should be applied to the uniform shear strains calculated for station 188. The curve labeled "Strain concentration factor, 1.8" in figure 7(a) is calculated by increasing the uniform calculated shear strain 1.8 times. This operation gives reasonable agreement with the experimental strain.

Room-temperature axial strains.- Axial strains due to bending in the spar caps of the main beams are shown in figure 7(b) for concentrated load applications at various stations. Axial strains shown were measured with gages at various locations in the cross section at station 155.

The strains in figure 7(b) are plotted as the parameter strain-moment ratio ϵ/M in order to compare directly values for the concentrated load at various stations. Particular values of strain can be read directly from table V. The two curves shown are the calculated y/EI values for the top and bottom spar caps at station 155 obtained on the basis of the measured dimensions (fig. 2 and table I). Measured strains from corresponding gages on both left and right main beams are presented. The agreement shown between measured and calculated strains

is satisfactory for cases where the concentrated load was applied at considerable distance from the gage cross section, for example, load at station 47 or 72. However, as the point of load application moves closer to the strain gages, individual gage readings deviate quite markedly from the calculated values. Averages of left and right beam readings reduce the deviation considerably but do not eliminate it. The manner in which the concentrated load is distributed from the loading strap into the corrugated shear web and from the web into the spar caps apparently produces local disturbances in the cross-sectional strain-distribution pattern which extend for some length along the beam from the point of load application.

Average values of axial strain in the top and bottom spar caps is shown in figure 7(c) as a function of location along the length of the beams for the maximum value of distributed load applied (9,986 lb). Averages are for both left and right main beams and the numbers indicate the number of strain-gage readings which were averaged for a particular point. The curves are the calculated MH/EI values of average strain for the same value of distributed load (9,986 lb). The agreement between measured and calculated average axial strain is satisfactory with the exception of one point on the top spar cap at station 192. However, this is a single gage reading at one particular point in the cross section and as shown in the previous figure 7(b), individual gage readings may deviate considerably.

The strains shown in figure 7 are for typical responses of the main beams to applied bending loads. Since the model was designed so that the skin panels would transfer only local air loads and would provide torsional stiffness, the response of the skin panels to the overall bending is of interest. As shown in table V, the only strains measured by any of the gages on the skin panels at station 158 occurred when the concentrated load was applied at the leading edges of station 144. These strains are probably the result of local distortions of the skin panels due to bending of the transverse frame at station 144 to which they are attached.

Room-temperature angular twist.- In addition to the room-temperature bending tests, a torsion test was made to determine the ability of the model with its special design features to withstand torque loadings. A torque was applied at station 96 up to a maximum value of 16,650 in-lb by deadweight loading the two leading-edge load points antisymmetrically. The reaction to the torque was taken out through the main beams into the model support at station 205 in the same manner as reactions to bending loads were carried. Vertical deflections of the model at various stations were measured and are listed in table VII along with the experimental angles of twist determined from these deflections.

A comparison of measured angle of twist with calculated values obtained from two elementary methods is shown in figure 8. In the first method, the torsion is assumed to be carried in the shell of a torque box. Details of this method are discussed in appendix B.

The second method for calculating angle of twist in the model assumes that all of the applied torque is carried by the two main beams by differential bending, one beam deflecting up and the other beam deflecting down. Bending deflections have been discussed in an earlier section. The total angle of twist

at any station then becomes the bending deflection of one main beam divided by the distance from the model center line to the beam.

Experimentally, the model twisted about 5 times more than would be calculated when the skins were assumed to form a torque box, and about 10 times less than calculated when the two main beams were assumed to carry the torque by differential bending.

Elevated Temperatures and Loads Programing

The elevated temperature tests were run by programing both load and temperature on the model simultaneously. Figure 9 shows a typical programed test environment for a time of 20 minutes. Since the model was a research specimen, no attempt was made to duplicate the effects of any specific reentry trajectory. Ramp function inputs were used to simplify the analysis of results. The temperature along the structural leading edge of the flat top heated surface was increased at a rate of 10° F per second up to a maximum of $1,600^{\circ}$ F, then held constant for about 15 minutes, and finally decreased at a programed rate of 10° F per second. The temperature at the center line of station 182 (near the back) on the heated surface was programed to increase at a rate of 8.6° F per second so as to arrive at a maximum of $1,385^{\circ}$ F at the same time as the leading edge reached $1,600^{\circ}$ F. Temperatures at other locations on the heated surface were programed similarly to arrive at maximum temperatures between $1,385^{\circ}$ F and $1,600^{\circ}$ F. About midway in the program, a load pulse of 6,700 pounds was applied hydraulically. (See fig. 9.)

The experimental response of the model to the programed heating and loading of figure 9 is given in table VIII. Temperatures measured at many locations in the model are listed in table VIII for various times from the start of heating for the $1,600^{\circ}$ F combined heating and loading test. In general all the thermocouples measuring temperatures in a particular part of the model are grouped together in the table and can be located by reference to the table headings and the instrumentation drawings (fig. 5). The four parts of table VIII correspond to the four heating cycles required to record all the instrumentation. The first heating cycle (table VIII(a)) was used primarily to record strains and associated temperatures in order to minimize temperature cycling effects on the strain gages. The load pulse applied during this cycle was 889 pounds. Examination of the spar-cap temperatures indicated that considerably more load could be safely carried, and accordingly, a load pulse of 6,472 pounds was applied on the second, third, and fourth cycles. Cyclic repeatability of data is discussed in appendix A.

The temperatures in table VIII are considered to be representative for either load pulse, since neither deformations produced by heating nor any particular change in temperature that could be attributed to loading were observed when the load was applied or removed. However, the strains must be associated only with the smaller load pulse (table VIII(a)), and the deflections must be associated with the larger load pulse (table VIII(b)).

Temperature Distribution

Temperatures not only vary widely at various stations on the model at any particular time but also vary with time. Figure 10 presents temperature distributions in various parts of the model at a fixed time of 7 minutes from the start of heating. Seven minutes was selected as it was near the time of maximum model deflection due to heating.

Top skin.- Temperatures in the top skin 4 inches beneath the radiator are shown in figure 10(a). The temperature controllers brought this surface up to approximately these temperatures in 2.5 minutes and then held it constant. The programed pattern of isotherms parallel to the leading edges is evident with highest temperatures along the leading edges and lower temperatures in the interior. However, many deviations from the programed pattern are also evident and indicate the influence of factors which could not be controlled. Dead spots exist in the mechanical arrangement of the quartz heat lamps (fig. 4(b)) which though minimized in the radiator design, produced local cold spots in the heated surface. As the model interior heated up, the model deflected away from the radiator so that the distance between lamps and heated surface was increased. The radiator was designed to minimize the effect of model deflection by controlling the portion over the model from station 48 to station 96 separately from the remainder of the radiator. Control thermocouples in the cross sections at sections 84 and 182 maintained the programed temperature within $\pm 10^{\circ}$ F throughout the cycle. Temperatures in other cross sections were generally lower than the control temperature because of the increased distance from the radiator. Conduction into the heat sinks formed by the transverse frames produced temperature variations in the skin panel length between frames as shown by the three longitudinal groups of thermocouples in figure 10(a). With the exception of the rear panel (stations 168 to 192) the left side of the top skin was hotter throughout the entire test than the right side. An overall difference in temperature of about 100° F can be seen between symmetrically located thermocouples on the left and right sides for which no explanation has been found. The maximum difference in measured temperatures in the entire top skin after 7 minutes of heating was 515° F while the programed difference was 215° F.

Bottom skin.- Temperatures in the bottom skin after 7 minutes of heating are shown in figure 10(b). The bottom skin is heated primarily by radiation through the model interior from the top skin, and loses heat to the outside by radiation to the test enclosure and by natural convection of air past the inclined lower surfaces. A pattern of isotherms parallel to the leading edges is also evident in the bottom skin. However, the isotherms are more a function of distance from the top skin than of the isotherm pattern in the top skin. The maximum difference in measured temperatures in the bottom skin after 7 minutes is 644° F. A comparison of temperature variation in the top and bottom skins at station 157 after 7 minutes of heating is shown in figure 10(c). The magnitude of temperature at any point is proportional to the perpendicular distance from the temperature curve to the model cross section. The general trend of the programed temperature variation in the top skin is evident, as is the effect of the left side being hotter than the right. Local temperature variations due to radiator dead spots and model heat sinks show up as minor effects in this particular cross section.

Transverse frame.- A similar comparison of temperature variation in an adjacent transverse frame at station 144 is shown in figure 10(d). The temperatures shown around the outside of the frame were measured at the midpoint of the transverse frame caps (fig. 5(d)). Temperatures in the top cap are several hundred degrees lower than the corresponding skin temperatures (fig. 10(c)), and the variations across the width of the model are reduced. Heating of the top spar cap was primarily by conduction. The bottom-spar-cap temperatures are very similar to the corresponding bottom-skin temperatures since both are heated primarily by radiation through the model interior, and the 7 minutes of heating time is sufficient to establish approximate equilibrium. The transverse-spar-cap temperature on top dips in the vicinity of the junction with the main beams as a result of conduction into the colder main beam. Transverse-cap temperature also dips on the bottom in the vicinity of the main beams because the main-beam spar cap shields the transverse cap from radiation. Transverse-frame shear-web temperatures along two corrugation elements at station 144 (fig. 10(d)) indicate heating by radiation from the top skin. Shear webs have smaller heat losses than the bottom skin because as an interior member the web reradiates only to other parts of the model, all of which are heated considerably above room temperature.

Main beams.- Temperature distribution along the main-beam spar caps is shown in figure 10(e) for the right beam after 7 minutes of heating. Heating of both top and bottom spar caps is by radiation since the main beams lie beneath the top skin, and the only points of contact are through the transverse caps at the junctions with the transverse frames. The shielding effect of the transverse frames is quite evident from the temperature dips in figure 10(e). Obtaining average temperatures for each 24-inch length between transverse frames requires a certain amount of engineering judgment or a considerable increase in the number of thermocouples used. The temperature distribution shown represents the largest difference in temperature between the top and bottom spar caps; however, because of the mass involved the actual temperatures of both continued to increase throughout the duration of the heating cycle.

Temperature variation with time.- Variation of temperature with time is shown in figure 11 for four selected points in the top and bottom skins and top and bottom spar caps of the right main beam at station 157. The top skin shows a response very similar to the programed input (fig. 9) with the exception of the region near the end of the test when natural cooling took place at a slower rate than the maximum programed cooling rate. As noted previously, heating of the main-beam spar caps and bottom skin occurred primarily by radiation from the top skin and the temperature responses are functions of the distances from the top skin and relative masses. From 5 to 10 minutes elapsed after the top skin reached equilibrium before the other elements essentially reached equilibrium.

Model Response to Temperature and Load

Vertical deflection.- Since the spar caps of the main beams provide the longitudinal bending stiffness for the model, spar-cap-temperature response to heating results in beam curvature and deflection. Vertical tip deflection of the model is shown in figure 12(a) for the 1,600° F combined heating and loading test. The experimental model deflection is compared with the calculated deflection

(see appendix B) for most of the heating and loading cycle. The model deflection reaches a value of nearly 3 inches due to spar-cap-temperature difference at an exposure time of about 7 minutes corresponding to the maximum temperature difference between top and bottom spar caps. Beyond an exposure time of 7 minutes, deflection due to temperature difference decreases even though the absolute spar temperatures were still increasing.

The hump in the deflection curve is produced by the load pulse applied during the heating cycle. Note that deflection due to heating is about 3 times the deflection due to loading. The rapid decrease in deflection at 1,050 seconds corresponds to the time when peak heat input ceased and the model began to cool rapidly.

Horizontal deflections.- The effect of the left side of the model being heated more than the right side (as mentioned previously) also shows up in the left and right main-beam temperatures. (See tables VIII(c) and (d).) The left beam, being hotter, expands more in every element of length than the right beam, and this expansion produces a horizontal bending of the model. The measured horizontal tip deflection resulting from this "left-side-hotter" condition is shown in figure 12(b). The deflection can be seen to be simply a function of heating and is independent of the applied vertical load pulse. These measurements were taken optically with a transit and were not read beyond the start of cooling in the heat cycle. A reading taken much later after the model had returned to room temperature indicated, however, that the deflection was completely elastic and no residual horizontal deflection remained.

Spar-cap strains.- Variation of temperature in the cross section of the main-beam spar caps is shown in figure 13 for the top right spar cap at several times during the heating cycle. The solid curves are drawn through measured temperatures for the 1,600° F test (table VIII); the dashed curves are drawn through temperatures obtained during the 1,000° F test (table IX). The large differences in temperature around the cross section during the early part of the heating cycle indicate that the shape and distance of various parts of the spar cap from the radiating top skin are significant in determining temperature. Even after considerable time has elapsed, differences of more than 100° F exist. A somewhat similar pattern of temperature variation occurred in the bottom spar cap.

Temperature variations in the spar caps such as shown in figure 13 produce local thermal stresses and strains and have a secondary effect on beam bending deflections, since the average temperature of the spar cap will be influenced by the temperature distribution.

Strains due to combined thermal and load stress are presented in figure 14 for both top and bottom main-beam spar caps at two times during the 1,000° F test tabulated in table IX. The two times presented represent: (1) a case of thermal strain with essentially no load and (2) a case of combined thermal and applied load strain. Calculated strains are based on an analysis which divides the spar caps into 12 parts, assumes a linear variation of total strain with distance from the neutral axis (plane cross sections remain plane), and sums the forces and moments for the 12 parts of the cross section so as to equate them to

the applied forces and moments. Variation of temperatures in the 12 parts requires 12 sets of material properties. The resulting equations were solved with high-speed digital computing machines and the curves in figure 14 were drawn through the results. The differences shown in figure 14 between load and no-load calculated curves represent primarily strains due to load, but also have some additional strain due to a change in the temperature distribution between times 317 seconds and 665 seconds.

The measured strains show good agreement with the calculated thermal strains for the no-load case but show some of the same lack of agreement at individual points for combined load and thermal strain that was previously indicated for room-temperature loading (fig. 7(b)). However, the average level of measured strain is in good agreement with the calculated strain.

Prior to the four cycles at 1,600° F listed in table VIII, the model had been subjected to about 100 cycles of distributed loading at room temperature in the manner given by tables IV and VI, and 28 cycles of combined heating and loading in the manner given by figure 9 at various levels of peak temperature between 400° F and 1,600° F.

COMPONENT DESIGN AND TEST

As a means of developing a better understanding of the structural deformations and strength of the specific corrugated shear-web and skin-panel designs used in the structural concept model and of developing design modifications, 15 shear-web beams and 15 skin-panel specimens were designed, fabricated, and tested under a variety of conditions.

CORRUGATED SHEAR WEBS

Specimens

Two series of corrugated shear-web beams were designed, built, and tested. Tests were conducted on the beams under combinations of heat and load. The basic specimen concept is the same as described in reference 3. Details of the specimens are shown in figure 15. The shear-web specimens incorporating the same web design as the reentry glider model main beams (60° by 1-inch flat corrugation) are detailed in figure 15(a). Similar shear-web beams utilizing the special corrugation of the reentry-glider-model transverse frames are detailed in figure 15(b).

All beams tested are listed in table X. All specimens were made of Inconel X heat treated 2 hours at 1,400° F in the same way as the reentry glider model. Most of the beams were fabricated by spotwelding the corrugated shear web to spar-cap angles in a manner duplicating the connections in the reentry-glider model. For the purpose of studying means of improving shear-web strength without

destroying the thermal expansion capabilities, several other beams were fabricated with a doubler strip along the edges of the corrugation. Also, several of the beams had circular cutouts in the center of the web to study their influence on beam behavior.

Test Setups

The test setup is illustrated in figure 16. Room-temperature testing is shown in figure 16(a) and the construction of a quartz lamp radiator for controlling the elevated temperature tests is shown in figure 16(b). One bank of lamps has not been installed, so the location of the specimen relative to the radiator elements can be seen. In both of these setups a vertical load is applied to the tip of the shear-web beam with a hydraulic jack. The beam is cantilevered from a rigid backstop. Tip deflections of the beam are measured with a flexible cantilever-type deflectometer mounted above the beam (fig. 16(a)).

The heavy flanges and end plates shown bolted to the spar-cap angles form a frame which distributes the concentrated load uniformly to the shear web and carries all of the bending moment. Thus, the corrugated web is essentially loaded in pure shear.

Tests, Results and Discussion

Room-temperature load tests were made to evaluate the performance of the spot-welded connections between corrugations and spar caps and to provide a reference from which to judge the effects of other parameters. Elevated-temperature tests were made to study the behavior of corrugations at temperature and under load. The two temperature profiles programed (fig. 17) were selected to cover the range of shear-web temperatures experienced in the reentry glider model. Experimentally good correlation is shown with the programed temperatures, and the 1,200° to 900° F temperature gradient is reasonably close to the temperature pattern at station 160 for the reentry model at a time midway through the loading cycle in the 1,600° F test (table VIII(a) and fig. 5(c)).

Shear deflection.- Variation of tip shear deflection for beams utilizing the two types of corrugated web is shown in figure 18. The largest effects are due to the change in corrugation design from the 60° by 1-inch flat corrugation (fig. 18(a)) to the model transverse-frame corrugation (fig. 18(b)). This change in design results in 24 times more deflection for the same load on the transverse-frame corrugation than on the 60° corrugation.

The addition of the doubler strip along the connected edges of the web has little effect on the beam stiffness for the 60° corrugation but doubles the initial stiffness of the transverse-frame corrugation. The presence of cutouts reduces the stiffness of the 60° corrugation considerably but has little effect on the already flexible transverse-frame corrugation. These effects can be seen experimentally in figure 18 but might be difficult to calculate quantitatively. Deflections for the basic corrugations can be calculated with reasonable accuracy by use of the developed length of either corrugation along with considerations of

the additional flexibility of the special transverse-frame corrugation. (See appendix C.)

Failure strength.- The influence of temperature and doubler strips on the strength of corrugated shear webs is shown in figure 19. Shear-web strength is degraded by temperature. Addition of doublers along the connected edges of the shear webs generally increased the strength. Buckling and failure strength calculations are made in appendix C.

Several different modes of failure were experienced by the shear-web beams as listed in table X. Spot-welded connections between web corrugations and spar-cap angles failed in shear along both the top and bottom edges of specimens 1, 2, and 10. Specimens 3, 8, and 11 had similar spot-weld failures along the hottest edge only. Local shear buckling of the flat elements of the 60° corrugation followed by maximum load occurred for the two specimens with doublers along the connections (specimens 4 and 5). Figure 20(a) is a photograph of this type of failure. The 60° corrugation beams with cutouts had extensive distortion around the cutout leading to a general buckling type failure for specimens 6 and 7. A special type of general instability was experienced by most of the transverse-frame corrugation beams. An example of this type is shown in figure 20(b) and the failure can best be described as a twisting and falling over of the corrugations with the sharp crease horizontally along the center line occurring at failure or just after failure. Two tests of the transverse-frame corrugation at 1,200° F failed by web-cap connection failure but also displayed evidence of overall instability. The low stress level at failure and the general instability mode are both indicative that the large proportion of the edge of the web which is unsupported is a major factor in the failure. Adding a doubler strip along this edge increases the initial beam stiffness but does not change the mode of failure or produce a significant increase in strength.

The presence of cutouts in a shear web is a practical necessity for access in most structures. In corrugated shear webs, these tests show a decided reduction in strength even when the cutout is reinforced with a stiffener around the edge of the hole (table X).

Shear strain.- The extensive distortion and the low failure loads for the 60° corrugation beams with cutouts indicated excessive strains around the cutout. Measurements were made at a number of locations on the web for an elastic load using Tuckerman optical strain gages alined at 45° and 135° with respect to the corrugation vertical center line. These shear strains are shown in figure 21 as measured on specimen 6. A similar distribution was found for specimen 7 which had a stiffener around the cutout. The strain distribution becomes very erratic, even at some distance from the cutout as shown in figure 21. The general level of strain appears to be higher than in the beam without a cutout as shown by the three numbers in parentheses across the center, which are test values from specimen 1. Calculated average shear strain for specimen 1 is in good agreement with these experimental values.

Strength-unit weight.- A comparison of strength weight ratios for the various design modifications in the shear webs is given in figure 22. As would be expected, the extreme flexibility designed into the transverse-frame corrugation

makes it less efficient for carrying shear than the 60° corrugation. Unstiffened cutouts are very detrimental to strength for both types of corrugation. Adding a stiffener to the corrugation does not fully restore the loss of strength weight. Use of a doubler strip to improve spot-weld connections is quite beneficial to the 60° corrugations. However, the doubler size should be optimized for greatest efficiency. On the transverse-frame corrugation, the increase in strength is offset by the added weight when the doubler is used.

SKIN PANELS

Normal Air-Load and Heat Tests

Specimens.- Nine corrugation-stiffened skin panel specimens typical of the skin panels used in the structural concept model of a lifting reentry glider (fig. 3) have been subjected to a variety of load and heat tests that generally were carried to destruction. Two views of the basic test specimens are shown in figure 23. The dimensions and method of construction are the same as given in figure 3(c) for the reentry model with the exception that most of these specimens are 24.5 inches square. All were fabricated from Inconel X and heat treated 2 hours at 1,400° F in the same manner as the model. Expansion-joint and transverse-frame details are the same for the skin panels as for the reentry model, except that the frame is rectangular and designed to support the skin panel in the test fixture for loading.

Test setups.- Normal-pressure loads are uniformly applied over the surface of the skin panels by use of the test setup shown in figure 24(a). The test panel is shown fitted into a square hole cut in the top of the cylindrical box. The ends of the panel (left front and right rear in fig. 24(a)) overlapped the top of the box. The sides of the panel (right front and left rear in fig. 24(a)) fit closely against spring-loaded side members so that they were free to deflect up or down with the center of the panel and yet would maintain a tight seal for the reduced air pressure. The box was connected to an air ejector which could maintain reduced pressures in the box while handling large volumes of air due to leaks. Uniformly distributed load on the panel resulted from the pressure difference between atmospheric pressure on the outside and reduced pressure on the inside of the box. Panel deflections were measured with deflectometers installed on the outside and well above the panel so as not to interfere with heating. Deflection transfer rods connected the deflectometers to the panel surface. The transfer-rod ends were made from alumina rod so as to receive a minimum of influence from heating in the vicinity of the radiator.

The radiator is shown in figure 24(b) installed over the panel surface. It consists of quartz-lamp heater units similar to those used on the large model (fig. 4(b)) and on the shear-web component tests (fig. 16(b)). Side reflectors are utilized to cut down edge losses from the radiator. The deflectometer support frame shown in figure 24(a) fits around and above the radiator. The transfer rods extend through small holes in the back side of the radiator reflector units. All thermocouple and strain-gage-instrumentation leads on the bottom of the skin panels are brought out through a vacuum seal in the side wall of the box.

Location of the various types of instrumentation is shown in figure 25. Not all of the instrumentation shown was used in every test, but reference to the appropriate instrumentation is made for each test in table XI. Discussion of test-data acquisition in appendix A for the large reentry model is generally applicable to the skin-panel tests as well.

Normal Air Load and Heat Results and Discussion

Temperature distribution.- Two types of heating are considered (fig. 26(a)). In the first, the entire surface of the panel is heated uniformly either to a constant temperature level or at a constant temperature rise rate. In the second, the surface of the panel is heated uniformly along lines parallel to the corrugations, but along lines perpendicular to the corrugations the heating is controlled so as to produce a constant temperature gradient of 300° F between the edges of the panel and the center line. As shown in figure 26(a), the panel edges are at 1,300° F and the center line is at 1,600° F. This gradient is larger than any programed on the large model skin panels (fig. 10(a)) but was selected in order to magnify any effects which might have resulted from the model program. The same gradient was applied to another test specimen but at a lower temperature level (600° F to 300° F) in order to separate effects of material degradation from effects of thermal gradient.

Both the uniform and gradient types of heating shown in figure 26(a) result in a temperature difference of about 200° F between the heated surface and the bottoms of the corrugations, which produces a more severe gradient in the corrugation element than exists in the panel planform. In order better to study this gradient, additional thermocouples were installed in the cross section of one corrugation element as shown in figure 26(b), and the temperature distribution was obtained corresponding to the uniform heating at 1,600° F after equilibrium had been reached. Temperatures in the single-thickness beaded portion of the skin are considerably higher than the temperatures in the double-thickness seam-welded flat portion where all control thermocouples were located both in the skin-panel test specimens and in the large model.

The temperature distribution around each corrugation element shown in figure 26(b) was for steady-state equilibrium temperatures. Corresponding temperatures were obtained during the transient phase of heating the panel up to the peak temperatures. Figure 26(c) shows how the temperatures respond through the panel element as a function of time from the start of heating for a programed temperature-rise rate of 10° per second up to a peak of 1,540° F. The difference in temperature between the hottest and coldest parts reaches a maximum at a heating time of about 60 seconds and remains essentially constant from that time on, even though the temperature level increases considerably. Thermal stresses in the panel element can be related to this temperature difference.

The influence of heating rate on this temperature difference between the hottest and coldest parts of the panel element is shown in figure 26(d) for temperature-rise rates from 10° per second to 70° per second. A curve has been faired through the maximum temperature difference points for each rise-rate

curve. This gives the point at which maximum thermal stress will exist in various parts of the panel element.

Buckling.- If the compressive thermal stress in the panel elements becomes large enough, local buckling of the compressed parts will occur. This occurrence of buckling was observed experimentally in the beaded part of the skin and is detailed in table XI(f) for two skin panels which were heated at various increasing temperature-rise rates up to a maximum temperature of 1,200° F. After each cycle of heating the number of buckles occurring in the skin panel due to the temperature-rise rates was counted. The mode of local buckling was a series of sharp creases with convex curvature forming across the concave curvature of the beaded part in a manner typical of curved plate buckling. The buckles snapped in suddenly and audibly during heating and remained as permanent buckles after the panel cooled. A few buckles were present in the panel from fabrication. Initial imperfections and deviations in temperature distribution in the panel caused additional buckles to occur at nearly all temperature-rise rates. A plot of the number of buckles as a function of temperature-rise rate gives a curve which breaks sharply at a rise rate associated with thermal buckling of the panel. This break occurred at a temperature-rise rate of 36.5° per second for specimen 6 and 20.5° per second for specimen 7. Based on the data from specimen 5 (fig. 26(d)) these critical temperature-rise rates correspond to maximum temperature differences in the panel elements of 805° F and 630° F for specimens 6 and 7, respectively. The normal load of 288 lb/sq ft carried by specimen 7 corresponds to bending stress My/I of 20,400 psi in the beaded part.

No evidence of buckling was observed in the room-temperature loading test on specimen 1. Examination of the strain-gage data in table XI(a) indicates that under room-temperature loading, the tension side of the corrugations becomes highly plastic in bending, whereas the compressive strain in the beaded part increases very slowly with increasing load. The maximum compressive stress reached in the beaded part at room temperature is slightly less than 50,000 psi.

In order to establish an end-point value for compressive buckling stress of the beaded part of the skin panels, two test specimens were fabricated for compression testing (table XI(h)). Each specimen consisted of a single element of the corrugated skin panel; however, the 60° by 1/2-inch flat corrugated sheet was made from 0.0193-inch-thick sheet in place of 0.0107-inch sheet used in the other panels. This increase in thickness was to preclude compressive buckling of the flat parts prior to that of the beaded part. Experimental buckling stresses for the beaded part of these two specimens averaged 63,800 psi.

An interaction curve drawn through the experimental buckling results is shown in figure 27. Combinations of compression load stress and maximum temperature differences which produce buckling can be determined from the curve.

Theoretical calculations for the compressive buckling stress of the beaded element were also made utilizing information in reference 7, and several assumptions. The beaded part was assumed to be a long, simply supported curved plate of constant radius. Based on averages of measurements made on several panels, the radius-thickness ratio for the bead was 220. Applying the empirical coefficients to the curved-plate buckling equation, as worked out in reference 7, gave

a calculated compressive buckling stress of 71,100 psi, which is in reasonable agreement with the experimental value.

Bending deflections.- Normal air loads applied over the surface of the skin panels produced bending strains and deflections which became quite large prior to failure. Figure 28(a) presents the experimental load-deflection curves for the various skin panels tested under combinations of load and temperature as detailed in tables XI(a) to (d) and (g). Initial straight-line portions indicate loading ranges which are elastic, and the curved portions indicate the effects of plasticity prior to failure.

The panels used in two room-temperature tests did not fail by any detectable method. The center deflection became so large that it was impossible for the vacuum box to maintain a tight seal along the edges and the leakage exceeded the capability of the ejector system. The curve marked "Room temperature - previously buckled" is for specimen 7 which was loaded to failure at room temperature after having been cycled to 1,200° F eight times at various temperature-rise rates. The panel surface was uniformly covered with permanent buckles in the beaded portions, and a slight residual set in deflection was present at the start of loading. However, with all the apparent visible damage, the panel responded to load in a manner similar to the undamaged specimen.

The three curves in figure 28(a) at various elevated temperatures were obtained by applying the steady-state temperature conditions first and then loading to failure. Two of the panels failed by sudden collapse as the load was being increased, and the panel tested at a uniform temperature of 1,600° F experienced a peak load, then continued to deflect as attempts were made unsuccessfully to increase the load, and finally collapsed as the other panels. The initial negative deflection shown in figure 28(a) for these three specimens results from the panel response to the thermal gradient through the cross section of each element. Very little effect of the planform gradient is evident in the initial thermal deflection; however, as the load is increased, the better material properties in the lower temperature parts of the panel show a tendency to stiffen the entire panel with a resultant increase in failure load over the uniform temperature case.

Comparison of calculated load-deflection curves with the experimental room temperature and the uniform temperature of 1,600° F is shown in figure 28(b). Details of the calculations are given in appendix D. The agreement shown at room temperature is reasonable, especially in the plastic portion where small uncertainties in stress-strain curves at large plastic strains can produce large effects. For the test at 1,600° F the calculations give good agreement with the initial thermal deflection which is elastic and thus requires only a knowledge of elastic modulus. Under load, however, the uncertainty in material yield and plastic stresses shows up in deviation between calculated and experimental deflections.

Acoustic Tests

Specimens.- Four skin-panel specimens were subjected to an intense random noise environment. Each test specimen was approximately 12 inches wide by

48 inches long and consisted of two 12-inch-wide skin panels with an expansion joint between them. This assembly was supported on a heavy framework around all four sides with the regular transverse frame and shear web supporting the two panels at the expansion joint. The first two specimens were fabricated in the same manner as the large reentry model, which included indirect resistance welding of one flange of the Z-stiffener to the crests of the corrugated inner skin (fig. 3(c)). Based on observation of the start of acoustic failure in these two specimens as detailed in table XII, and discussed later, a modification was made in the fabrication of the last two acoustic test specimens. The indirect resistance welding was replaced with a blind rivet between the flange of the Z-stiffener and each corrugation crest of the panel.

Test setup.- The acoustic tests (table XII) were performed in the random noise environment of a 12-inch-diameter air jet at the Langley Research Center. This facility consists of a circular pipe having four sharp 90° bends upstream of the jet exit and the noise spectra adjacent to the exhaust jet are similar to spectra produced by jet or rocket engines. A more complete description is given in reference 8.

Figure 29 shows a photograph of a skin-panel specimen mounted at the jet exit. For all tests the back side of the specimen support box was closed off from the noise environment by a backup plate. As shown in figure 29, the specimen is alined with the long axis parallel to the air flow. The skin-panel corrugations are also parallel to the air flow. Tests were made with the panel in this position and with the specimen and corrugation axis perpendicular to the air flow. Changes in specimen orientation were made to insure adequate coverage by the noise field. In both positions the specimens were mounted a few inches below the boundary of the jet exhaust in a region of essentially constant sound pressure.

For testing at elevated temperature, the specimen was mounted well below the boundary of the jet exhaust, and a radiator of quartz-lamp heaters was placed between the specimen and the jet. The sound-pressure level was reduced on the specimen, primarily because of the greater distance between specimen and jet-exhaust boundary.

All acoustic tests were made by exposing the specimen to the desired sound-pressure level for an interval of time, then stopping the noise and examining the specimen in detail for evidence of failure or cracking. After each examination, the exposure to noise would be continued for another interval of time, and the process would be repeated until significant failures had been observed.

Tests and discussion.- The acoustic test results as given in table XII show several interesting qualitative effects. Specimens 10 and 11 developed skin cracks initially at about the same time after 40 minutes of exposure to a sound-pressure level of 160 db. No effect was evident from testing orientation. The extent of skin cracking is shown at the end of the test (121 min) for specimen 10 in figure 30. Close examination of specimen 10 after the 121 minutes revealed that many of the indirect resistance welds between the flange of the Z-stiffener and the bottoms of the skin corrugations had been broken as shown in figure 31. Since these welds were an area of potential weakness, they were

observed more closely during the test of specimen 11. The indirect resistance welds were noted to be failing considerably earlier than the appearance of cracks in the skin.

An attempt to strengthen this weld area resulted in a modification of specimens 12 and 13 to replace the indirect resistance welds with blind rivets. Specimen 12 carried the 160-db noise for almost twice as long as specimen 10 or 11 before skin cracking started. Once started, the cracks grew with continued exposure and fragments of skin actually broke loose as shown in figure 32. It should be noted, however, that the first failures noted in specimen 12 occurred in spot welds between the transverse frame and transverse shear web, well beneath the surface of the panel. Thus, it appears that for this type of structure, intense noise can start failures beneath the outside surface as easily or even more easily than on the surface.

The test at 1,600° F on specimen 13, which also had the riveted modification, showed that after 5 minutes the Monel rivets attaching the skin panels to the expansion joint and transverse frame had failed badly. These rivets were replaced with a new set and testing was resumed at a maximum temperature of 1,200° F and a sound pressure level of 151 db. The exposure times listed in table XII for specimen 13 are times at combined noise and maximum temperature. The noise was started first and then the specimen was heated to temperature so that for the 180 minutes tabulated, the specimen actually was exposed to the noise level for 216 minutes. No evidence of skin-panel cracking was detected. The welds in the shear web again were a source of early failure in the structure.

Wind-Tunnel Flutter Tests

Two skin-panel specimens were flutter tested in the Langley Unitary Plan wind tunnel. Each specimen was 24.5 inches square with an expansion joint along one edge. They were mounted in a panel support fixture which held them parallel to the flow in the tunnel test section and about 12 inches out from one side wall. One panel was mounted with its corrugations parallel to the air flow and the other was mounted with the corrugations perpendicular to the flow. A quartz-lamp heater was constructed in the tunnel side wall in order to produce high temperatures in the specimen and to simulate the aerodynamic heating effects of higher velocities. The tunnel was operated at a constant Mach number of 1.87 for all the tests, and the dynamic pressure was slowly increased throughout each test until the panel fluttered or until the maximum operating condition for the tunnel was reached.

The three panel flutter tests on two specimens listed in table XIII initially pointed up a serious problem. As shown in table XIII a corrugation-stiffened skin panel with the corrugations oriented perpendicular to the direction of air flow fluttered and was totally destroyed in about 10 seconds at the supersonic test conditions. A similar panel was turned 90° so that the corrugations were parallel to the flow. It did not show any indication of flutter up to the maximum dynamic pressure at which the tunnel could be operated. A recent analysis of this problem is presented in reference 9. The analysis shows that

large reductions in flutter stiffness may be induced by small deviations in flow angularity with respect to the axis of the corrugations.

The test temperatures of 125° F for these first two tests were the equilibrium operating temperature of the tunnel at high dynamic pressure. The third test was a repeat of the second one with corrugation parallel to the air flow; however, when maximum dynamic pressure was reached, the quartz-lamp radiator was energized and brought the panel temperature up to 600° F with no flutter evident. Under static conditions, the radiator could easily produce temperatures of 1,600° F on the panel, but under the supersonic, high-dynamic-pressure conditions the panel was aerodynamically cooled so that a temperature of 600° F was the maximum that could be achieved.

CONCLUSIONS

A full-scale structural model of a lifting reentry glider was built and design concepts of corrugated sheetmetal and special expansion joints were incorporated so as to alleviate thermal stresses but maintain load-carrying ability in the presence of the large temperature variations throughout the model such as would be encountered in a lifting reentry. The environmental test results with this model as well as with numerous components indicates that the design concepts functioned satisfactorily and enabled the model successfully to withstand the imposed loads and heating at levels simulating a reentry. The following specific conclusions were made as a result of the tests and analysis conducted on the model and components.

MODEL

1. Bending deflections resulting from loads and elevated temperatures can be approximated with reasonable accuracy by elementary theory even though tip deflections due to temperature differences may be two to three times as large as those due to loading.

2. Average axial strains due to bending loads show good correlation with calculated averages both at room and elevated temperatures. Strains due to thermal stress are small compared with strains due to load.

3. Torsional stiffness is provided by the corrugation-stiffened skin panels although not to the extent indicated by calculations made by assuming elementary torque-box behavior.

CORRUGATED SHEAR WEBS

4. Elastic shear stiffness as measured by beam tip deflection can be calculated adequately by using developed lengths of corrugation and by considering an additional flexibility designed into the transverse-frame type of corrugation.

5. Shear strains in solid corrugated webs are uniform and predictable. Cutouts in the webs increase the general level of strain and make it highly nonuniform.

6. Failure of the 60° flat corrugations with a doubler strip along the connected edges was by local buckling of the corrugation elements at the design stress. Without the doubler strips, failures occurred in the web-spar cap connections at somewhat lower stress levels. Cutouts with or without stiffeners reduced the strength considerably.

7. Strength of the transverse-frame corrugation was consistently low with or without doublers and/or cutouts. The extra flexibility designed into this corrugation produced a low-stress general instability failure.

CORRUGATION-STIFFENED SKIN PANELS

8. Buckling of the beaded-surface elements occurred at high compressive stress levels which could be produced by thermal stresses due to high transient heating rates or combinations of thermal stress and stress due to normal air loads.

9. Bending stiffnesses and deflections are predictable at room and elevated temperatures from zero to maximum load.

10. Failures under normal air load at all temperature levels occurred at large center deflections with highly plastic stresses.

11. Resistance to 160-db random frequency noise lasted about 40 minutes at room temperature before cracks appeared in the surface along the edges of the panels. Crack growth was slow but progressive. No cracks were evident in the skin after 180 minutes of exposure to 151 db at 1,200° F.

12. Panel flutter of corrugation-stiffened skin panels did not occur at either room or elevated temperature in supersonic air flow parallel to the corrugation axis. With the air flow across the panel surface perpendicular to the corrugation axis, panel flutter destroyed the specimen.

Langley Research Center,
National Aeronautics and Space Administration,
Langley Station, Hampton, Va., January 2, 1964.

APPENDIX A

TEST DATA ACQUISITION

Data have been acquired in a series of tests on the lifting reentry model, skin panel components, and shear-web components at room temperature and elevated temperatures. All three types of specimens were instrumented with strain gages, thermocouples, load cells, and deflectometers. The sections which follow discuss installation and data accuracy specifically for the glider model with its 414 transducers. However, the comments are generally applicable to the other two types of test specimen.

DATA RECORDING

Electrical signals from 414 transducers were recorded on magnetic tape in a central data recording facility at the Langley Research Center which had a capability for handling 99 analog transducers. Recording and readout accuracy is approximately 0.1 percent of full-scale signal. All room-temperature load tests had to be made twice to handle 84 strain gages on one test and 24 deflectometers on the next test. Heat and load tests had to be made four times at each temperature level in order to record all working transducers. A transit was used to measure optically the lateral deflection of the nose of the model.

CYCLIC REPEATABILITY

Repeatability of heat input for the four cycles at 1,600° F was monitored from cycle to cycle by seven temperature-control thermocouples located at various points on the heated surface and by one thermocouple located near the center of the heated surface. Readings of the seven control thermocouples are tabulated for one of the cycles in table VIII(b). The other cycles repeated within ±10° F. The one data thermocouple, No. 132, is tabulated in each of the four cycles and repeats within ±10° F.

In addition 9 of the thermocouples associated with strain gages that are listed in table VIII(a) are also reported in table VIII(c) or VIII(d) in order better to define temperature distributions in the cross sections of the spar-cap members. These thermocouples (thermocouples 95, 99, 101, 103, 105, 107, 113, 114, and 116) indicate that the first heating cycle was 10° to 20° hotter than the third or fourth cycle with respect to the bottom cap members but was within ±5° for the top cap members.

Vertical tip deflection of the model was also monitored from cycle to cycle. Deflections showed the same trend as in figure 12(a) with the maximum cycle-to-cycle difference in deflection of 0.075 inch (2.6%) occurring at 400 seconds test time.

Accuracy of the various transducers on this 1,600° F test is difficult to assess precisely. However, the following remarks should give an indication of the accuracy obtainable.

LOAD CELLS

Two load cells were located in the whippletree linkage as shown in figure 4(a). Load-cell output was calibrated at room temperature against a universal hydraulic testing machine having an accuracy of ±0.5 percent of indicated load. Output at a 3,000-pound load was about 1/4 full scale on the recorder for each load cell. Thus, loads at room temperature are accurate to about ±1 percent. During the 1,600° F test, however, the load-cell temperatures were observed to rise from 75° F to 117° F in a linear fashion according to thermocouples welded to the outside case. After the fourth heating cycle listed in table VIII, another similar heating cycle was imposed on the model but with the loading jacks disconnected so that the load cells were unloaded throughout the heating cycle. Their output indicated an apparent tensile load increasing linearly from zero to about 280 pounds during the cycle. This drift in zero load output probably is caused by thermal gradients through the interior of the load cell. All loads in the 1,600° F test have been corrected for this apparent drift with temperature.

Negative (compression) loads at the start and end of the heating cycle, table VIII(a) or (b) are the result of the friction in the hydraulic loading jacks. During a cycle the loading was maintained at a prescribed level by monitoring hydraulic pressure delivered by a pumping unit to the two jacks. At the start of a heating cycle, the model would deflect downward and tended to compress the load cells and the jacks. Until positive loading began, the friction in the system prevented the operator from maintaining close control of a small preload.

DEFLECTOMETERS

Model vertical deflections were measured by 24 deflectometers mounted on steel base plates beneath the model (fig. 4(a)). Deflectometers consisted of aluminum cantilever beams with four strain gages mounted near the root of each beam, wired to form a Wheatstone bridge with maximum sensitivity to a given tip deflection. A furnace check had established that drift of an unrestrained deflectometer when heated slowly from room temperature to 150° F was negligible. Actual temperature changes monitored on the mounting plates beneath an asbestos shield indicated temperature changes of less than 10° F during the heating cycle.

Piano wire (0.016-inch diameter) connected the deflectometers to the load points on the lower surface of the model. Locations are shown in figure 5(g). Thermocouples were welded to the piano wires at stations 47, 120, and 192. The most severe temperatures were recorded at station 47 and are tabulated in table VIII(b) as TC 294 to TC 296 (fig. 5(c)). These thermocouples reached equilibrium temperatures at the same time as the heated skin and the corresponding

thermal expansion of the piano wire is calculated to be 0.014 inch. The expansion is 0.5 percent of the peak experimental deflections and has been neglected.

THERMOCOUPLES

Thermocouple locations on the model are shown in figures 5(c) to 5(f). Thermocouples used were No. 30 chromel-alumel wire with high-temperature varnish-impregnated glass-braid insulation. Thermocouple accuracy was ±5° from 32° F to 530° F and ±0.5 percent from 530 to 2,300° F. Installation was made by spot welding the individual chromel and alumel wires to the model approximately 1/16 inch apart, alined so as to minimize the thermal gradient between them. All skin thermocouples were installed on inside surfaces in order to be shielded from direct radiation from the heat lamps. Cold junctions were inside 24-pin AN cable connectors where a transition was made from the chromel-alumel leads to copper leads. These plugs were mounted in a rack about 25 feet from the model. Temperature of the plugs was monitored throughout the test and remained within 1° of the room temperature. All 304 thermocouples were working satisfactorily at the start of the 1,600° F tests. As noted in table VIII four thermocouples either failed or began reading erratically during the 1,600° cycles.

STRAIN GAGES

Strain gages were applied in various locations as shown in figures 5(a) and 5(b). For measurements at room temperature, 44 foil strain gages of various types were used. Gage errors including bridge-voltage fluctuations were less than ±1 percent of indicated strain. Recorder error corresponded to less than ±5 microinches per inch. Skin panel riveting and model mounting in the test setup produced failures in 8 of the 44 room-temperature gages. One additional gage failed during the various load cycles prior to heating.

For measurements at elevated temperatures, 40 foil gages of two types were used. Eighteen of these were inoperative prior to the 1,600° F test as follows: 9 gage failures (3 during model assembly, 2 during room-temperature load tests, 4 during heating cycles), and 9 gage installations which had been cycled to temperatures exceeding 800° F. An upper temperature limit of 800° F was selected for prior cycling based on cycle-to-cycle repeatability as discussed in a subsequent paragraph.

Spar caps were instrumented with gages nominally rated for temperatures to 600° F and skin panels with gages rated for much higher temperatures. Installations were made with a ceramic-type cement cured at 600° F for 1 hour. Gage leads of stainless-steel-clad copper wire were attached to short strips of nichrome foil by spot welding; these strips in turn were spot welded to the gage tabs. A three-wire lead system was used to compensate for temperature effects in the lead wires.

Temperature compensation of the gages was not attempted because of the large thermal gradients expected. Gage installation temperatures were obtained by thermocouples spotwelded to the model on the gage center line within 1/2 inch of the gage. Strain-gage bridges were balanced at the start of the heating and loading cycle and total output was recorded as a function of time during the cycle. This output was then corrected twice to obtain strain readings caused by stress. The apparent strain due to temperature was subtracted from the total output and the residual strain was corrected for change in gage factor at temperature.

Apparent strain due to temperature was obtained by installing a gage and thermocouple on a 1 by 6 by 0.03 inch strip of heat treated Inconel X, mounting the strip as a free cantilever beam under a radiant heater, and cycling the assembly through a temperature history corresponding to that which the large model had been exposed to. Results are plotted in figure 33 for one gage of each type. Temperature rise rates varied considerably with respect to different gage locations in the large model as well as with respect to time or temperature level. For calibration purposes, each gage was cycled four times to each of a series of successively greater temperatures corresponding to the large model programed peak temperature. For peak temperature less than the lowest shown in figure 33, no effect of cycling or cycling rate was ascertained. At higher cyclic temperatures an effect of cycling is produced and the apparent strain correction to be made depends on the prior temperature history of the gage.

For the <600° type gage apparent strains are less than 280 microinches per inch with a cycle-to-cycle repeatability of ±15 microinches per inch up to 800° F. For the >600° type gage apparent strains become very large exceeding 8,000 microinches per inch at 800° F although the cycle-to-cycle repeatability is less than ±50 microinches per inch at temperatures up to 800° F. At temperatures greater than 800° F, cycle-to-cycle repeatability becomes very poor exceeding ±1,000 microinches per inch.

No attempt was made to verify the manufacturer's gage factor variation with temperature, figure 33(c). However, evaluation of similar type gages on stainless steel at the National Bureau of Standards indicated good repeatability of gage factor. These evaluations also indicated low drift in gage output at constant temperatures up to 700° F.

APPENDIX B

STRUCTURAL CONCEPT MODEL ANALYSIS

The design of a large structural concept model of a lifting reentry glider has been discussed in the body of this paper. The feasibility of the design concepts for thermal stress relief was demonstrated by a test program. This appendix develops appropriate methods of analysis.

RESPONSE TO ROOM-TEMPERATURE BENDING LOADS

Beam Bending

The main beams are divided into seven elements as shown in figure 34 to facilitate calculation for all the variables involved. The different element lengths are chosen so that elements begin or end at points of load application on the model. The root of the beam, station 205, is assumed to be fixed; that is,

$$\left(\frac{dy}{dx}\right)_{205} = 0 \tag{B1}$$

$$(y)_{205} = 0 \tag{B2}$$

Each element is assumed to have a constant curvature over its length equal to the curvature at the element midpoint. Thus at station 192, the slope can be written

$$\left(\frac{dy}{dx}\right)_{192} = \left(\frac{dy}{dx}\right)_{205} + l_1\left(\frac{1}{\rho_1}\right) \tag{B3}$$

and the element deflection can be written as the product of the average element slope and length:

$$(y)_{192} = (y)_{205} + \frac{1}{2}\left[\left(\frac{dy}{dx}\right)_{205} + \left(\frac{dy}{dx}\right)_{192}\right] l_1 \tag{B4}$$

and at station 168

$$\left(\frac{dy}{dx}\right)_{168} = \left(\frac{dy}{dx}\right)_{192} + l_2\left(\frac{1}{\rho_2}\right) \tag{B5}$$

$$(y)_{168} = (y)_{192} + \frac{1}{2}\left[\left(\frac{dy}{dx}\right)_{192} + \left(\frac{dy}{dx}\right)_{168}\right] l_2 \tag{B6}$$

and so on to station 47 at the tip

$$\left(\frac{dy}{dx}\right)_{47} = \left(\frac{dy}{dx}\right)_{72} + l_7\left(\frac{1}{\rho_7}\right) \tag{B7}$$

$$(y)_{47} = (y)_{72} + \frac{1}{2}\left[\left(\frac{dy}{dx}\right)_{72} + \left(\frac{dy}{dx}\right)_{47}\right] l_7 \tag{B8}$$

which when expanded, substituted into, and reduced gives the tip deflection

$$\begin{aligned}\delta_{bending} &= (y)_{47} \\ &= 1970\left(\frac{1}{\rho_1}\right) + 3192\left(\frac{1}{\rho_2}\right) + 2616\left(\frac{1}{\rho_3}\right) \\ &\quad + 2040\left(\frac{1}{\rho_4}\right) + 1464\left(\frac{1}{\rho_5}\right) + 888\left(\frac{1}{\rho_6}\right) + 312\left(\frac{1}{\rho_7}\right)\end{aligned} \tag{B9}$$

The element curvature terms in equation (B9) can be expressed for a general case as

$$\left(\frac{1}{\rho_i}\right) = \left(\frac{M}{EI}\right)_i \qquad (i = 1,2,3 \ldots 7) \tag{B10}$$

For room-temperature loading the bending moment in equation (B10) is evaluated at the midpoint of each element of length. The moment of inertia of the cross section at the midpoint of each element can be obtained from the information given in table I.

Beam Shear

Deflection calculations for the shear deformations of the main beams are made by using the same seven elements of length as in the bending calculations (fig. 34). The assumption is made that the shear stress in the corrugated webs of the main beams is uniformly distributed across the depth of the web inasmuch as the corrugations reduce the bending stiffness of the webs to a negligible quantity. Thus the shear deflection of any element is

$$\left(\delta_{shear}\right)_i = \gamma_i \times (\text{Developed length})_i \tag{B11}$$

The developed length of the 60° corrugated webs used in the main beams (fig. 2(b)) is $4/3$ of the linear length. The shear deflection at any station along the beam is the sum of the shear deflections in the individual elements from the root out to the station in question. Thus, for the shear deflection at the tip,

$$\left(\delta_{shear}\right)_{47} = \sum_{i=1}^{7} (\gamma_i)\left(\frac{4}{3}\right)(l_i) = \frac{4}{3}\sum_{i=1}^{7}\left(\frac{\tau l}{G}\right)_i \tag{B12}$$

The shear stress in each element is an average stress since the shear stress varies along the length of the beam because of the tapered depth. The bending moment is assumed to be carried completely by axial forces in the spar caps. Due to the inclination of the bottom spar cap, shear is carried by the webs and the vertical component of the axial force in the bottom spar cap. Thus when the appropriate values of load, length, depth, and thickness are substituted into equation (B12), the tip deflection of the model due to shear for a distributed load becomes

$$\left(\delta_{shear}\right)_{47} = \frac{4.8P_{192}}{G_1} + \frac{46.8P_{168}}{G_2} + \frac{90.0P_{144}}{G_3} + \frac{130.3P_{120}}{G_4} + \frac{172.2P_{96}}{G_5} + \frac{213.0P_{72}}{G_6} + \frac{196.0P_{47}}{G_7} \tag{B13}$$

The numerical subscripts on the applied loads P designate the station at which load is applied, and those on the shear moduli G designate the element of beam length (fig. 34) to which they apply. At room temperature, $G = 12.0 \times 10^6$ psi in all elements.

Support Deformation

Deflections of the model under applied loads are influenced by deformation of the model support. The calculations derived in the section "Beam Bending" were based on the assumption of a fixed root. However, an experimental determination showed that the model support deformed elastically at the root whenever the model was loaded. This elastic-support deformation produces two types of deflection in the model which are the result of:

(1) Support deflection

$$\delta_{support} = 6.50(10)^{-7}P \tag{B14}$$

(2) Support rotation

$$\beta_{support} = 1.55(10)^{-9}M_{205} \tag{B15}$$

Support deflection occurs when a load P is applied anywhere on the model and results in an equal amount of model deflection at every station. Support rotation occurs also when a load P is applied anywhere on the model, but the amount of rotation is proportional to the bending moment produced at station 205 (the root) by the load and therefore is dependent upon the location of the load. Support rotation will produce, at any point on the model, a deflection which is proportional to the distance from that point to the support.

Thus, support deflection and rotation produce a model deflection at any station which is expressed as

$$\delta_{support\ motion} = 6.50(10)^{-7}P + 1.55(10)^{-9}\left(M_{205}\right)(205 - \bar{x}) \tag{B16}$$

where $\bar{x}$ is the number of the station at which the deflection is being calculated; thus, at the tip of the model,

$$\left(\delta_{support\ motion}\right)_{47} = 6.50(10)^{-7}P + 1.55(10)^{-9}\left(M_{205}\right)(158) \tag{B17}$$

RESPONSE TO ROOM-TEMPERATURE TORSION LOADS

Calculations for the angle of twist produced by an applied torque on the model are made with the torsion assumed to be carried in the shell of a torque box composed of skin panels and closure pieces along the structural leading edges. The angle of twist is

$$\theta = \frac{Pa}{\overline{GJ}} \tag{B18}$$

$$\overline{GJ} = \frac{4A^2}{\oint \frac{ds}{Gt}} \tag{B19}$$

The line integral ds/Gt is evaluated by summing the lengths of various parts of the perimeter around the cross section of the model. Each part is divided by its shear modulus and thickness prior to summing. The thickness used for corrugated skin panels in the torsional analysis is obtained from the effective thickness of the panel in plane shear. For the type of corrugation used (fig. 3(c)) the effective thickness of the panel becomes 1.75 times the thickness of a single sheet.

Adjusting the effective thickness for the 22.5 inches of panel and 1.5 inches of expansion joint in each 24-inch length of structure gives an average effective thickness for the corrugated skin panels, $\bar{t}_{skin} = 0.0166$ inch. The corrugated closure pieces along the structural leading edges of the model have an effective thickness, $\bar{t} = 0.0080$ inch.

The model length was divided into elements 24 inches long (fig. 34) as in the bending calculations, and the torque box in each element was assumed to have the properties of the midlength cross section. At station 192 the skin-panel torque box ended, and the torque was assumed to be carried into the model support at station 205 by differential bending of the two main beams. The total angle of twist at any station was calculated by summing the increments of twist in each element from the root out to the station in question. Angles of twist calculated on the basis that the torsion is carried by the skin panels are about 5 times smaller than the experimental angles of twist, as shown in figure 8.

RESPONSE TO COMBINED HEATING AND BENDING LOADS

Calculated deflections shown in figure 12(a) are based on equation (B9) with the following expression used for curvature in place of equation (B10)

$$\left(\frac{1}{\rho_i}\right) = \left(\frac{\alpha_T \bar{T}_T - \alpha_B \bar{T}_B}{H_T + H_B}\right)_i + \left(\frac{M}{EI}\right)_i \qquad (i = 1,2,3 \ldots 7) \qquad \text{(B20)}$$

For combined heating and loading cases, the curvature becomes a function of the temperatures in the top and bottom spar caps of each element of beam length as well as a function of bending moment. Measured temperatures in the spar caps are tabulated in table VIII. However, these temperatures must be corrected in order to give an appropriate average temperature. Figure 10(e) indicates the kind of variation in temperature that occurs along the length of the spar caps at any given time. Figure 13 illustrates the variation in temperature that occurs in the cross section of the spar caps. Correction terms given in figure 35 have been obtained from a series of plots similar to figures 10(e) and 13. These correction terms are used to calculate the average temperature of a spar cap in any element from the measured midpoint temperature as in the following equations

$$\left(\bar{T}_T\right)_i = B_i\left(T_T\right)_i \qquad \text{(B21)}$$

and

$$\left(\bar{T}_B\right)_i = C_i\left(T_B\right)_i \qquad (i = 1,2,3 \ldots 7) \qquad \text{(B22)}$$

Particular values of the coefficient of thermal expansion α in equation (B20) are calculated from the following expression at appropriate temperatures:

$$\alpha = 7.575(10)^{-6} - 1.210(10)^{-10}T + 7.112(10)^{-13}T^2 \qquad \text{(B23)}$$

This expression for α was obtained by fitting a curve to the experimental data given in reference 5 by the method of least squares.

When bending moments are applied to the main beams in the presence of temperature, the value of the modulus of elasticity for the material in the last term of equation (B20) must be evaluated at the average of the temperatures in the top and bottom spar caps of any element. An expression for the modulus of elasticity at any temperature for Inconel X heat treated 2 hours at 1,400° F that was obtained by the method of least squares by fitting the appropriate experimental data in table II and references 4 to 6 is as follows:

$$E = 31.657(10)^6 - 1649.3T - 3.9936T^2 \qquad \text{(B24)}$$

Equations (B13) and (B17) for beam-shear and support-motion effects were also used in the deflection calculation made during the applied load pulse. A different value of G was used in each term of equation (B13) corresponding to the average temperature of each element. The value of G is reduced at elevated temperature in the same ratio as the modulus of elasticity E is reduced (eq. (B24)).

One additional contribution to the calculated deflection shown in figure 12(a) is determined as follows: Static deflection of the model tip at room temperature due to the deadweight of the model and its whippletree loading fixtures is calculated to be 0.175 inch for the 1,400-pound load. This deflection was on the model when the instrumentation was zeroed at room temperature prior to the test and is not included in any measured or calculated deflections presented in this paper. However, as the main beams heated up, their material moduli of elasticity decreased with temperature and resulted in an increase in the static, deadweight deflection, which was measured by the deflectometers and is included as an additional contribution to calculated tip deflection. Maximum value of this additional deflection increment was calculated to be 0.036 inch. Considering the variation in temperatures in the main beams the agreement between measured and calculated deflections in figure 12(a) is satisfactory.

APPENDIX C

CORRUGATED SHEAR-WEB COMPONENT ANALYSIS

Tests of 15 corrugated shear-web beams under combinations of heat and load were reported in the body of this paper and in table X. Details of the methods of analysis are given in this appendix.

SHEAR DEFLECTIONS

Corrugated shear-web deflections can be calculated with reasonable accuracy by use of elementary principles of elasticity and strength of materials. In addition, for the tip-loaded cantilevered beam, it is assumed that all the bending moment is resisted by the beam flanges and all the shear is uniformly carried by the developed length of the corrugated web. Further, the "picture-frame" construction of flanges and plates is assumed not to restrain shear deflections of the web.

Tip deflection for the 60° corrugation beam (fig. 15(a)) is calculated for elastic loading as follows:

$$\delta = \gamma \times (\text{Developed length})$$

$$= \frac{\tau}{G} \times (\text{Developed length})$$

$$= \frac{P}{tdG} \times (\text{Developed length})$$

$$= \frac{P}{(0.0181)(17.98)(12)(10)^6}(1.333)(33.5) \qquad \text{(C1)}$$

$$\delta = 1.143(10)^{-5}P \qquad \text{(C2)}$$

This relationship between load and calculated elastic deflection for the 60° corrugation is plotted as a solid line in figure 18(a). If applied, corrections for plasticity and elevated temperature would be of the right sense to correlate with the experiments.

When the corresponding dimensions for the transverse frame corrugation beam are substituted into equation (C2), the calculated deflection is only about 10 percent of the experimental value and indicates that a different mode of elastic deformation occurs when the transverse frame corrugation is loaded.

Figure 36(a) is a schematic of the deformation which can occur as a result of the shear flow q bending the elements (2) and (3) as cantilever beams. The center, beaded element (1) which is not attached to either spar cap is essentially floating on the two cantilever elements and thus displaces sideways when they bend so that an effective shear displacement of the element that can be calculated in the following manner occurs. Element (1) not only displaces sideways, but also bends as shown in figure 36(b) and in accordance with the following equations:

For all elements

$$\frac{d^2y}{dx^2} = \frac{M}{EI} \tag{C3}$$

For element (1)

$$\phi = \left(\frac{dy}{dx}\right)_{x=0} = \frac{1}{EI}\left(-\frac{M_1 b_1}{2}\right) \tag{C4}$$

Element (2) or (3) bends as shown in figure 36(c) and in accordance with the following equations:

For element (2) or (3)

$$\phi = \left(\frac{dy}{dx}\right)_{x=0} = \frac{1}{EI}\left[M_1 b_2 - \left(\frac{qb_1}{2}\right)\frac{b_2^2}{2}\right] \tag{C5}$$

$$(y)_{x=0} = \frac{1}{EI}\left[\left(\frac{qb_1}{2}\right)\frac{b_2^3}{3} - \frac{M_1 b_2^2}{2}\right] \tag{C6}$$

When the end slopes of elements (1) and (2) are equated, equations (C4) and (C5) give

$$M_1 = \frac{\left(\frac{qb_1}{2}\right)b_2^2}{\left(2b_2 + b_1\right)} \tag{C7}$$

from which the tip deflection of element (2) becomes

$$(y)_{x=0} = \left[\frac{\left(\frac{qb_1}{2}\right)b_2^3}{3EI}\right]\left[1 - \frac{3}{4\left(1 + \frac{b_1}{2b_2}\right)}\right] \tag{C8}$$

If the numerical values $b_1 = 1.66$ in., $b_2 = 0.50$ in., and $EI = 25.44$ lb-in.^{2} are substituted in equation (C8),

$$(y)_{x=0} = 9.76(10)^{-4}q$$

$$= 5.66(10)^{-5}P \qquad \text{(C9)}$$

Since the shear flow acts in one direction along the top of the corrugated web and in the opposite direction along the bottom, the cantilever elements (2) and (3) deflect correspondingly with no motion occurring at the center. If the variation in deflection with distance above or below the web center is assumed to be linear, the effective shear strain in element (1) becomes

$$\gamma_{eff} = \left[\frac{(y)_{\text{element (2)}}}{2}\right]\left(\frac{1}{d/2}\right) = 1.312(10)^{-5}P \qquad \text{(C10)}$$

Tip deflection for the transverse-frame corrugation beam becomes

$$\delta = \gamma \times (\text{Developed length of web}) + \gamma_{eff} \times (\text{Developed length of element (1)})$$

$$= 2.26(10)^{-5}P + 31.68(10)^{-5}P$$

or

$$\delta = 33.94(10)^{-5}P \qquad \text{(C11)}$$

This analysis and the test results indicated that the transverse-frame corrugation was extremely flexible and large tip deflections occurred with load. Because of the large deflection, a special calibration test was made of the flange and end-plate assembly without a shear web. The calibration test established experimental stiffnesses of the flange assemblies of 670 lb/in. at room temperature. Thus tip deflection for the transverse-frame corrugation beam corrected for flange stiffness is

$$\delta = 27.60(10)^{-5}P \qquad \text{(C12)}$$

Comparison of equation (C2) with equation (C12) shows that the transverse-frame corrugation has 24 times the deflection of the 60° by 1-inch flat corrugation for the same applied load. Equation (C12) is plotted as the solid line in figure 18(b) where it is compared with the experimental deflections for the various

transverse-frame corrugation beams. Corrections to the deflection equation (C12) for plasticity and elevated temperature could be made and qualitatively would be in the right direction to correlate with the experimental deflections shown in figure 18.

BUCKLING AND FAILURE LOADS

Because the extreme flexibility of the model transverse-frame corrugation resulted in large deflections prior to failure, the beam failure loads listed in table X need to be corrected for the increment of total load carried by the flanges. The column headed "Flange load" lists the increment of load calculated to be carried by the flanges at failure, based on the experimental flange stiffness (670 lb/in. at room temperature) and the test beam deflection at failure. Flange loads are subtracted from "Beam failure loads" in order to calculate the average experimental shear stress in the web at failure (table X).

The flange load correction to be made to the beam failure loads in table X is normally considered insignificant in this type of test. However, the large deflections and low failure loads for the transverse-frame corrugations made a correction necessary. The flanges carry from 10 to 30 percent of the beam load for the transverse-frame corrugation at failure. For the more standard 60° corrugation, the flange load is only 2 to 5 percent.

Four types of failure are indicated in table X. Two of these can be calculated quite readily. The web-cap spotweld connection fails by shearing the spot welds. The average strength at failure is the ultimate shear stress times the ratio of spotweld connection area to maximum potential connection area.

$$\tau_f = \tau_{ult}\left(\frac{A_{connection}}{A_{beam}}\right) \tag{C13}$$

The calculated curves in figure 19 for web-cap connection strength are based on values of shear ultimate stress equal to one-half the tensile ultimate stress for the material at test temperature. The area of spotweld connection is evaluated in terms of the side of a square whose area would equal the rectangular area enclosing the spotweld pattern on each corrugation.

Thus, for the 60° corrugation,

$$\tau_f = \tau_{ult}\left[\frac{(0.86)(0.018)}{(2.00)(0.018)}\right] = 0.430\tau_{ult} \tag{C14}$$

and for the model transverse-frame corrugation,

$$\tau_f = \tau_{ult}\left[\frac{(0.38)(0.010)}{(3.36)(0.010)}\right] = 0.113\tau_{ult} \tag{C15}$$

Web-cap connection strength for the beams with doublers is not calculated but would be greater by the amount of increase in the connection-sheet thickness.

Element buckling is calculated for the flat-plate elements in either of the two corrugation designs by assuming them to be long, simply supported plates buckling elastically in shear. Thus,

$$\tau_{cr} = \frac{5.35\pi^2 E}{12(1 - \mu^2)}\left(\frac{t}{b}\right)^2 \qquad (C16)$$

The modulus of elasticity is evaluated at appropriate test temperature. The presence or absence of doublers along the edges of the web does not have any significant effect on the element buckling stress as determined by equation (C16).

Shear-web strengths shown in figure 19 indicate that for the range covered (80° to 1,200° F) temperature has about the same effect on strength regardless of the mode of failure.

The 60° corrugation web-cap connection failures are indicative of the problem of achieving sufficient connection area in corrugated webs to carry the high shear stresses required of efficient beams. Adding the doubler strips along the connected edges increased the connection area sufficiently to reach a shear stress at least as great as the element buckling stress for this particular design. The doubler had no particular effect on element buckling stress and at the high stress level, element buckling and maximum strength can be expected to be equal. The agreement between calculated element buckling and experimental maximum strength is adequate for the 60° corrugation (fig. 19).

APPENDIX D

SKIN-PANEL COMPONENT ANALYSIS

Tests of nine corrugation-stiffened skin panels subjected to heat and normal air load were reported in the body of this paper and table XI. Methods of deflection analysis are given in this appendix.

Comparison of calculated load-deflection curves with the experimental room temperature and 1,600° F uniform cases is shown in figure 28(b). The agreement shown at room temperature is reasonable especially in the plastic portion where small uncertainties in stress-strain curves at large plastic strains can produce large effects. For the test at 1,600° F the calculations give good agreement with the initial thermal deflection which is elastic and thus requires only a knowledge of elastic modulus. Under load, however, the uncertainty in material yield and plastic stresses shows up in deviation between calculated and experimental deflections. Calculations for the center deflection of any of the corrugation-stiffened skin panels are based on several assumptions. The panel is assumed to bend under load and temperature in the same manner as a simply supported beam rather than as a plate since the bending stiffness across the corrugation is essentially negligible compared to the bending stiffness parallel to the corrugations. The beam, which is assumed to represent the skin panel, is composed of one corrugation element and associated beaded cover sheet 1.5 inches wide, which is the basic repeating element in the skin-panel design (fig. 37(a)).

Distributed normal load on the beam (fig. 37(a)) produces the bending-moment diagram (fig. 37(b)) from which, after considerable effort, the beam curvature diagram (fig. 37(c)) is constructed with temperature effects included. Deflection of the beam is calculated by utilizing the first moment of the area under the curve of beam curvature. The moment is taken with respect to the end of the beam.

In the elastic stress range, beam curvature is related to bending moment by the expression, $\frac{1}{\rho} = \frac{M}{EI}$, in which EI is constant for all values of moment. For plastic bending, the relationship is not constant and must be evaluated at every value of moment as in the bending-moment-curvature plot of figure 37(d). At any station along the length of the beam, curvature can be expressed in terms of any two strains in the cross section and the distance between the strain locations, if the total strain is assumed to vary linearly with distance from the neutral axis. Thus,

$$\frac{1}{\rho} = \frac{\epsilon_i - \epsilon_j}{y} \qquad (i \neq j) \qquad (D1)$$

and the strain can be expressed as thermal expansion plus strain due to stress

$$\epsilon = \alpha T + \epsilon_\sigma \qquad (D2)$$

In order to evaluate temperatures and stresses, the cross section of the beam is divided into parts (12 parts were used in this analysis). Temperatures of each of the 12 parts are determined by reference to temperature-distribution curves similar to those in figure 26(b). The coefficient of thermal expansion is calculated from equation (B23) for the appropriate temperatures.

The calculation process begins with the assumption of two values of total strain for equation (D1) and calculating the corresponding total strains in each of the 12 parts. Strains due to stress can then be calculated (eq. (D2)), and the plastic stresses corresponding to these strains can be determined by use of a suitable stress-strain relation. Hill's equation (ref. 10) is used here:

$$\epsilon_\sigma = \frac{\sigma}{E} + 0.002\left(\frac{\sigma}{\sigma_y}\right)^n \tag{D3}$$

Values of E, σ_y, and n have been determined by fitting least-square curves to data obtained from stress-strain tests of Inconel X. The equation for E has been previously given as equation (B24).

$$\left.\begin{aligned} \sigma_y &= 121{,}000 - 14.34T \qquad (0 < T < 1{,}290^\circ\ F) \\ \sigma_y &= 361{,}600 - 201.0T \qquad (1{,}290^\circ\ F < T < 1{,}800^\circ\ F) \end{aligned}\right\} \tag{D4}$$

$$n = 40.0 + 0.0120T - 1.906(10)^{-5}T^2 \tag{D5}$$

Forces in the beam cross section corresponding to the stresses calculated by equation (D3) are summed for the 12 parts. Because no axial forces are applied to the beam, static equilibrium requires the summation of forces to be equal to zero. Generally, the first assumptions of strain in equation (D1) will not result in summation of force equal to zero, so new values of strain will have to be assumed and the calculation repeated until force equilibrium is achieved. When force summation equals zero, a summation of moments due to the forces in each part can be made, and this will be the bending moment which is in equilibrium with the particular set of strains assumed. Beam curvature can also be calculated (eq. (D1)) and a point can be plotted to begin generating a moment-curvature plot such as figure 37(d). This particular point gives the beam curvature at any station along the length of the beam where the bending moment is equal to the calculated value. Repeating the foregoing calculation procedure for other sets of assumed strains will produce additional points through which the moment-curvature curve can be drawn (fig. 37(d)). The initial offset at zero moment is the curvature due to temperature differences through the cross section at the start of loading and results in an initial center deflection at zero load as shown in figure 28.

The calculation procedure outlined applies to combined heating and loading cases. Corresponding calculations for loading at room temperature are simplified

somewhat by having a constant temperature for all parts of the beam and therefore only one set of material properties. However, the plastic stress-strain relations must be observed where needed.

Calculations for the panels tested at room temperature indicated that stresses on the compression side of the beam remained well below the local buckling stresses of the several parts which were compressed. However, for the 1,600° uniform heating tests, both the beaded part and the double-thickness seam-welded flat part were at high temperatures with resulting low stress-strain curves compared with the parts on the tension side of the beam. In order to maintain equilibrium of forces, the strains on the compression side became large along with those on the tension side as the beam bent plastically. Both the beaded part and the double-thickness flat part were strained beyond their calculated buckling strains. They were assumed to be stabilized even in the postbuckling condition by the other parts of the beam, but their effectiveness in carrying load was reduced to less than that given by the stress-strain curves.

An effective stress-strain curve for the buckled parts can be calculated with the help of the following observations. The stress-shortening curves for both flat and curved plates beyond buckling have been described in reference 11 with the following type of equations:

$$\frac{\sigma_{effective}}{\sigma_{edge}} = \zeta \sqrt{\frac{\epsilon_{cr}}{\epsilon_{edge}}} \tag{D6}$$

where the empirical factor

$$\zeta = 1 + 0.28\left(1 - \sqrt{\frac{\epsilon_{cr}}{\epsilon_{edge}}}\right)^3 \tag{D7}$$

The edge stress and edge strain are evaluated from the stress-strain curve of the material and the effective stress applies to the same edge strain. The buckling strain is evaluated for a flat plate having the same dimensions as the curved plate. Results of such calculations applied to two parts of the beam are shown in figure 38. There is a region immediately after buckling for the curved plate that is not properly calculated by the equivalent flat plate method as pointed out in reference 11. In this region the curve is faired using engineering judgment. The method as worked out in reference 11 was applied to plates which buckled at elastic stresses. It is assumed that the same method will apply to plates which buckle well out in the plastic range.

Using the effective stress-strain curves in place of the material stress-strain curves for the parts of the beam which buckled does not change the procedure for calculating the moment-curvature plot of figure 37(d). It does result, however, in a lower moment-curvature curve (labeled "postbuckling" in fig. 37(d)) than would have existed if buckling had not occurred.

REFERENCES

1. Pride, Richard A., Royster, Dick M., and Helms, Bobbie F.: Experimental Study of a Hot Structure for a Reentry Vehicle. NASA TM X-314, 1960.

2. Anderson, Melvin S., and Stroud, C. W.: Experimental Observations of Aerodynamic and Heating Tests on Insulating Heat Shields. NASA TN D-1237, 1962.

3. Peterson, James P., and Card, Michael F.: Investigation of the Buckling Strength of Corrugated Webs in Shear. NASA TN D-424, 1960.

4. Hughes, Philip J., Inge, John E., and Prosser, Stanley B.: Tensile and Compressive Stress-Strain Properties of Some High-Strength Sheet Alloys at Elevated Temperatures. NACA TN 3315, 1954.

5. Kurg, Ivo M.: Tensile Properties of Inconel X Sheet Under Rapid-Heating and Constant-Temperature Conditions. NACA TN 4065, 1957.

6. Schmidt, F. W., Farquhar, John, and Kurg, Ivo M.: Effects of Various Aging Heat Treatments and Solution-Annealing and Aging Heat Treatments on Tensile, Creep, and Stress-Rupture Strengths of Inconel X Sheet to Temperatures of 1,400° F. NASA TN D-374, 1960.

7. Batdorf, S. B., Schildcrout, Murry, and Stein, Manuel: Critical Combinations of Shear and Longitudinal Direct Stress for Long Plates With Transverse Curvature. NACA TN 1347, 1947.

8. Edge, Philip M., Jr.: Random-Noise Testing of Aircraft and Missile Components With the Aid of a Laboratory Air Jet. Shock Vibration and Associated Environments Bulletin, No. 27, Pt. II, Dept. of Defense, June 1959, pp. 169-174.

9. Bohon, Herman L.: Flutter of Flat Rectangular Orthotropic Panels With Biaxial Loading and Arbitrary Flow Direction. NASA TN D-1949, 1963.

10. Hill, H. N.: Determination of Stress-Strain Relations From "Offset" Yield Strength Values. NACA TN 927, 1944.

11. Peterson, James P., Whitley, Ralph O., and Deaton, Jerry W.: Structural Behavior and Compressive Strength of Circular Cylinders With Longitudinal Stiffening. NASA TN D-1251, 1962.

TABLE I.- DIMENSIONS, AREAS, AND MOMENTS OF INERTIA OF MAIN BEAMS FOR STRUCTURAL CONCEPT MODEL

Station	H_T, in. (fig. 2(c))	H_B, in. (fig. 2(c))	c, in. (fig. 2(c))	h_T, in. (fig. 2(c))	h_B, in. (fig. 2(c))	Cross-sectional area (single spar cap), $in.^2$		I (single beam), $in.^4$	d, in.
						Top	Bottom		
47	1.68	1.56	0.994	0.324	0.316	0.1705	0.1780	1.08	3.38
72	3.30	3.06	1.153	.343	.470	.3988	.4288	8.37	6.95
96	4.71	4.38	1.306	.398	.508	.4141	.4441	17.69	9.77
120	6.12	5.11	1.459	.453	.546	.4302	.4602	31.10	12.61
144	7.50	7.06	1.612	.507	.583	.4445	.4745	48.70	15.43
168	8.83	8.47	1.765	.562	.620	.4600	.4900	71.50	18.26
192	10.28	9.75	1.917	.617	.658	.4752	.5052	98.40	21.08
[a]205	11.03	10.47	2.000	-----	-----	------	------	118.00	22.61

[a]Properties at station 205 are those which would exist if the spar caps extended back from station 192 without interruption. Local stiffening and discontinuities in vicinity of station 205 make actual values unknown.

TABLE II.- MATERIAL PROPERTIES OF INCONEL X SHEET

Heattreated 2 hours at 1,400° F; air cooled in furnace

Specimen	Thickness, in.	Temperature, °F	E, psi	σ_y, psi	σ_{ult}, psi	Elongation in 2 inches, percent
Tensile tests						
1	0.0100	80	31.0×10^6	118.3×10^3	159.5×10^3	14
2	.0100	80	31.3	131.0	166.5	12
3	.0183	80	31.3	119.0	163.2	18
4	.0187	80	30.8	118.0	160.0	14
5	.0326	80	31.2	125.8	174.6	18
6	.0331	80	31.3	128.3	175.0	23
7	.0494	80	31.6	123.8	181.0	16
8	.0497	80	31.8	122.5	179.0	28
9	.0187	1,600	17.5	38.1	39.7	4
10	.0101	1,600	18.1	32.9	34.3	4
Compression tests						
11	0.0100	80	32.1×10^6	----------	[a]112.0×10^3	
12	.0100	80	31.8	----------	[a]112.5	

Spotweld shear tests at room temperature (heattreated after spotwelding)

Specimen	Number of spotwelds	Thickness, in.	Maximum load, lb	Cycles to failure
13	[b]1	0.0103	301	1
14	1	.0102	325	1
15	1	.0102	306	1
16	1	.0321	2,120	1
17	1	.0318	2,120	1
18	1	.0314	2,040	1
19	1	.0516	2,775	1
20	1	.0517	2,215	1
21	1	.0515	2,760	1
22	1	.0188	850	1
23	1	.0188	864	1
24	1	.0189	815	1
25	1	.0189	800	30
26	1	.0187	800	51
27	1	.0189	760	260
28	1	.0189	760	448
29	1	.0184	715	331
30	1	.0186	715	689
31	[c]9	.0190	2,930	1
32	9	.0188	2,900	1
33	9	.0182	2,770	4,803
34	9	.0182	2,700	3,548
35	9	.0187	2,700	4,154
36	9	.0185	2,700	896

[a]Ultimate stress in compression is crippling stress for cylindrical test specimen, 3/4-inch diameter by 3-inch length, double-wrapped 0.0107 sheet, with four lines of spotwelds equally spaced around the circumference.

[b]Spotweld in single lap joint at center of tensile specimen.

[c]Nine spotwelds in lap joint are in three rows of three each.

TABLE III.- EXPERIMENTAL DEFLECTION COEFFICIENTS FOR CONCENTRATED LOAD SYMMETRICALLY APPLIED TO MODEL AT ROOM TEMPERATURE

[Location designated MB is main beam; LE is leading edge]

Deflection at -		For 1,000-lb load applied at station and location -										
Station	Location	47 MB	72 LE	96 MB	120 MB	120 LE	144 MB	144 LE	168 MB	168 LE	192 MB	192 LE
47	MB	0.4600	0.3343	0.2280	0.1458	0.1454	0.0823	0.0826	0.0384	0.0393	0.0100	0.0092
72	LE	.3260	.2580	.1803	.1200	.1210	.0710	.0711	.0333	.0339	.0082	.0081
96	MB	.2200	.1867	------	.1033	.1048	.0634	.0640	.0303	.0315	.0072	.0087
96	LE	.2140	.1777	.1429	.0997	.1022	.0612	.0616	.0298	.0302	.0071	.0070
120	MB	.1400	.1200	.1000	------	.0840	.0545	.0550	.0273	.0277	.0059	.0072
120	LE	.1360	.1200	.0995	.0814	------	.0538	.0561	.0291	.0272	.0058	.0070
144	MB	.0787	.0727	.0596	.0516	.0538	------	.0440	.0237	.0244	.0047	.0068
144	LE	.0780	.0662	.0580	.0506	.0528	.0405	------	.0223	.0272	.0044	.0056
168	MB	.0378	.0347	.0305	.0276	.0283	.0239	.0242	------	.0182	.0035	.0058
168	LE	.0368	.0328	.0306	.0274	.0278	.0240	.0242	.0156	------	.0032	.0123
192	MB	.0112	.0102	.0083	.0071	.0067	.0056	.0058	.0047	.0040	------	------
192	LE	.0094	.0085	.0083	.0078	.0084	.0066	.0064	.0048	.0120	.0002	------

TABLE IV.- EXPERIMENTAL DEFLECTIONS FOR DISTRIBUTED LOAD SYMMETRICALLY APPLIED TO MODEL AT ROOM TEMPERATURE

[Location designated MB is main beam; LE is leading edge]

Station	Location	Distribution of applied load	Deflections for applied loads of -		
			3,492 lb	7,036 lb	9,986 lb
47	MB	0.1355	0.546	1.090	1.540
72	LE	.0576	.448	.896	1.260
96	MB	.0378	.334	.668	.938
96	LE	.0859	.335	.670	.941
120	MB	.0657	.240	.481	.678
120	LE	.0910	.251	.503	.708
144	MB	.0918	.158	.316	.423
144	LE	.0967	.171	.341	.480
168	MB	.1151	.086	.163	(a)
168	LE	.1041	.109	.216	.304
192	MB	.0671	.023	.047	(a)
192	LE	.0517	.037	.074	(a)

[a]Deflection exceeded capability of deflectometer.

TABLE V.- EXPERIMENTAL STRAINS FOR CONCENTRATED LOADS SYMMETRICALLY APPLIED TO MODEL AT ROOM TEMPERATURE

[Locations designated MB are on main beams; LE are on leading edges. Eleven gages were inoperative: gages 51, 52, 58, 63, 65, 73 to 75, 108, 115, and 130. Fourteen gages did not indicate a response greater than the recorder error: gages 54, 55, 56, 121, 122, 124 to 127, 129, 131 to 134]

Gage	Strain, μin./in., for 1,000-pound load applied at station and location -								
	47 MB	72 LE	96 MB	120 LE	120 MB	144 LE	144 MB	168 LE	168 MB
53	-38	-61	-84	-106	-106	-125	-128	-125	-148
57	228	137	34	3	----	----	----	----	----
59	-25	-12	----	----	----	----	----	----	----
60	-263	-162	-40	6	5	-5	3	----	----
61	250	182	106	56	60	----	-5	-2	----
62	198	135	63	24	23	8	9	----	----
64	-260	-204	-170	-62	-62	28	14	----	----
66	236	200	150	133	134	100	102	63	72
67	-236	-194	-160	-120	-120	-83	-80	-32	-39
68	-250	-194	-148	-92	-92	-44	-41	18	13
69	239	182	112	71	73	24	20	----	----
70	239	178	102	62	63	12	6	-2	----
71	242	184	128	79	81	31	30	----	----
72	242	185	117	81	82	33	30	----	----
76	-215	-172	-138	-100	-97	-47	-55	----	3
77	-284	-212	-152	-84	-81	-3	-10	15	5
78	-256	-192	-132	-74	-71	----	-6	13	4
79	-194	-152	-114	-67	-70	-39	-34	-10	-3
80	-143	-112	-86	-53	-56	-32	-28	-9	----
81	-205	-156	-113	-59	-66	-37	-26	-10	-4
82	-214	-162	-117	-61	-65	-33	-23	-14	-5
83	----	----	----	----	----	2	----	17	----
84	----	----	----	----	----	----	----	15	----
85	-4	-3	----	-3	-3	-28	----	-92	15
86	-3	-2	----	----	----	17	----	56	9
87	1	----	----	----	----	7	----	38	----
88	2	----	----	----	----	----	----	31	-2
89	----	----	----	----	----	-6	----	-70	2
90	-2	----	----	----	----	----	----	-46	4
91	----	----	----	-3	----	18	----	----	----
92	----	----	----	-3	----	27	-3	9	----
93	----	----	----	-6	----	-30	5	12	----
94	----	----	----	-10	----	-57	10	-23	----
95	254	206	148	112	114	66	68	9	2
96	262	218	158	122	122	72	76	10	----
97	244	189	132	75	77	32	29	6	2
98	242	186	106	80	82	32	30	----	----
99	199	132	51	----	3	-46	-58	-13	3
100	210	(a)	(a)	(a)	(a)	(a)	-38	-13	----
101	-206	-143	-77	-22	-20	36	42	18	2
102	-189	-128	-70	-16	-15	38	45	17	3
103	-278	-210	-169	-119	-118	-50	-60	9	----
104	-254	-204	-158	-112	-108	-48	-56	9	5
105	-170	-118	-68	-13	-16	20	32	----	-4
106	-184	-130	-88	-29	-31	8	19	-7	-4
107	-238	-192	-149	-97	-101	-65	-62	-21	-4
109	----	----	----	----	----	----	----	10	----
110	----	----	----	----	----	----	----	13	3
111	-4	----	----	----	----	-26	----	-84	16
112	-2	----	----	----	----	----	----	----	----
113	2	----	----	----	2	9	----	----	----
114	----	----	----	----	----	----	----	24	----
116	-3	----	----	----	----	----	2	----	5
117	----	----	----	-4	----	14	----	----	----
118	----	----	----	-5	----	26	----	6	----
119	----	----	----	-14	----	-76	13	-32	----
120	----	----	----	-9	----	-53	10	-22	----
123	----	----	----	----	----	8	----	----	----
128	----	----	----	----	----	5	----	----	----

[a]Gage became unstable during tests.

TABLE VI.- EXPERIMENTAL STRAINS FOR DISTRIBUTED LOADS SYMMETRICALLY APPLIED TO MODEL AT ROOM TEMPERATURE

[Thirteen gages were inoperative: gages 51, 52, 58, 63 to 65, 73 to 75, 100, 108, 115, and 130. Sixteen gages did not indicate a response greater than the recorder error: gages 54 to 56, 121 to 129, and 131 to 134]

Gage	Strain, μin./in., for applied load of -		
	3,492 lb	7,036 lb	9,986 lb
53	-325	-655	-930
57	155	311	443
59	-20	-40	-54
60	-180	-364	-516
61	242	485	687
62	180	360	508
66	470	972	1,422
67	-379	-755	-1,061
68	-291	-589	-843
69	259	520	736
70	243	487	691
71	279	560	795
72	279	560	796
76	-293	-583	-818
77	-294	-595	-846
78	-253	-505	-715
79	-245	-482	-674
80	-183	-361	-501
81	-243	-486	-689
82	-245	-494	-702
83	8	16	22
84	3	7	10
85	-51	-103	-148
86	-32	-63	-90
87	19	37	52
88	13	26	40
89	-28	-57	-81
90	-20	-39	-55
91	4	10	15
92	9	20	28

Gage	Strain, μin./in., for applied load of -		
	3,492 lb	7,036 lb	9,986 lb
93	-17	-33	-47
94	-28	-57	-80
95	341	678	961
96	364	729	1,030
97	263	549	781
98	276	558	794
99	107	218	314
101	-143	-285	-401
102	-118	-233	-326
103	-360	-729	-1,035
104	-326	-653	-926
105	-128	-251	-346
106	-158	-314	-440
107	-329	-663	-944
109	5	9	12
110	3	6	9
111	-46	-90	-128
112	9	-142	-159
113	6	12	17
114	11	22	32
116	-16	-30	-40
117	3	7	11
118	8	17	23
119	-37	-76	-108
120	-26	-51	-71

TABLE VII.- TORSION TEST AT ROOM TEMPERATURE

[16,650 in-lb torque applied at station 96]

Station	Deflection, in.				Angle of twist, radians	
	Right leading edge	Right main beam	Left main beam	Left leading edge	Leading edge	Main beam
47	0.007	-----	------	-0.009	$2,400 \times 10^{-6}$	----------
72	.022	-----	------	-.025	2,315	----------
96	.054	0.020	-0.022	-.045	(a)	$2,415 \times 10^{-6}$
120	.032	.016	-.018	-.034	1,405	1,557
144	.032	.013	-.014	-.033	1,110	1,015
168	.035	.009	-.009	-.035	985	640
192	.037	.002	-.002	-.032	815	130

[a]Not computed, deflections influenced by application of concentrated loads to produce torque.

TABLE VIII.- MEASURED VALUES OF LOAD, STRAIN, TEMPERATURE, AND DEFLECTION FOR 1,600° F TEST

[Strain-gage (SG) readings are corrected for temperature, microinches/inch.
Thermocouple (TC) readings are temperatures, °F.
Deflectometer (Defl) readings are in inches.]

(a) First heating cycle: 3 loads, 22 strain gages, 38 strain-gage thermocouples, 6 skin-corrugation-detail thermocouples, 8 longitudinal-spar-web thermocouples

Time, sec	Total load, lb	Left load, lb	Right load, lb	Strain, μin./in., at -								Temperature, °F, at -							
				SG 101	SG 102	SG 103	SG 104	SG 105	SG 106	SG 107	SG 111	TC 101	TC 102	TC 103	TC 104	TC 105	TC 106	TC 107	TC 111
0	0	0	0	-1	-14	1	-6	-5	5	2	-3	82	86	81	85	82	82	80	83
30	-61	-22	-39	-3	-16	3	-4	-5	13	10	-3	82	86	82	85	82	82	80	83
60	-91	-30	-61	-9	-22	3	-7	-5	19	19	2	83	88	83	87	84	84	81	84
90	-76	-24	-52	-17	-32	-13	-11	-22	24	26	2	87	93	88	93	89	90	85	88
121	-204	-87	-117	-20	-35	-15	23	-36	36	52	3	96	106	99	105	102	108	93	99
151	-158	-63	-95	-46	-57	-37	43	-83	24	85	13	118	136	120	132	133	149	113	118
181	-218	-95	-123	-55	-76	-19	106	-166	-38	150	36	152	180	147	167	184	214	143	144
261	-121	-48	-73	-52	-73	34	280	-394	-261	307	83	272	324	240	279	354	414	250	220
322	-89	-31	-58	3	-47	112	407	-501	-401	416	90	371	436	319	369	479	553	344	279
382	33	29	4	79	-29	212	516	-554	-490	457	84	466	537	400	455	587	665	442	334
401	56	40	16	108	-27	250	544	-552	-509	461	82	494	564	424	479	616	693	471	350
416	322	174	148	118	-30	253	538	-563	-530	441	76	516	586	442	498	637	714	494	361
431	783	404	379	118	-38	226	505	-573	-556	396	76	536	605	460	516	657	734	517	372
492	889	437	452	187	-19	307	570	-545	-561	365	84	606	674	523	582	724	801	595	408
552	861	423	438	236	9	391	625	-511	-524	327	78	660	727	576	637	774	847	658	439
612	841	415	426	283	13	454	673	-467	-458	318	75	703	767	617	678	811	883	708	465
642	853	421	432	292	12	478	693	-436	-421	305	76	721	782	637	694	826	897	727	474
672	857	424	433	319	17	500	721	-402	(a)	313	71	737	796	654	707	840	907	745	483
703	842	416	426	340	20	516	736	-378		320	61	752	806	668	719	852	916	762	491
733	861	426	435	361	28	525	752	-347		334	61	764	817	682	729	862	925	775	499
793	865	431	434	400	56	561	780	-261		354	57	782	830	701	745	878	938	796	509
823	538	262	276	439	91	618	825	-195		391	58	790	835	710	750	884	941	805	513
853	-43	-25	-18	481	133	699	903	-120		467	70	795	839	714	755	889	946	811	517
884	22	21	1	492	154	715	910	-61		480	64	799	843	722	759	893	948	817	519
914	59	34	25	509	180	724	922	8		492	65	804	846	727	762	896	952	822	520
974	84	40	44	548	245	745	949	(a)		525	63	810	850	733	767	902	956	830	524
1035	47	23	24	584	312	778	974			555	66	817	854	741	771	908	960	837	529
1065	60	31	29	599	348	790	985			589	61	820	855	744	771	909	961	839	530
1096	254	127	127	601	378	758	954			596	56	816	851	737	767	898	948	832	528
1126	44	19	25	614	413	741	932			560	57	788	818	710	741	860	903	809	507
1187	113	56	57	646	509	713	900			481	55	700	720	635	660	756	788	737	442
1247	100	54	46	646	524	657	770			409	52	609	626	553	577	657	682	656	378
1308	40	22	18	614	527	607	700			375	52	531	546	482	503	576	593	580	328
1369	93	49	44	572	521	536	624			348	46	466	479	424	441	506	520	512	286
1430	16	11	5	525	510	490	574			347	41	413	423	376	389	449	460	456	254
1491	74	41	33	494	501	434	519	↓	↓	330	35	367	377	335	347	402	410	408	224

[a]Strain gage exceeded 900° F.

TABLE VIII.- MEASURED VALUES OF LOAD, STRAIN, TEMPERATURE, AND DEFLECTION FOR 1,600° F TEST - Continued

(a) First heating cycle: 3 loads, 22 strain gages, 38 strain-gage thermocouples, 6 skin-corrugation-detail thermocouples, 8 longitudinal-spar-web thermocouples - Continued

Time, sec	Strain, μin./in., at -										Temperature, °F, at -									
	SG 112	SG 116	SG 119	SG 120	SG 129	SG 131	SG 132	SG 122	SG 123	SG 124	TC 112	TC 116	TC 119	TC 120	TC 129	TC 131	TC 132	TC 122	TC 123	TC 124
0	-7	1	-5	-7	-35	-25	34	-1	-2	-3	82	83	82	82	80	80	85	79	82	83
30	-13	11	-9	-8	-170	-248	-137	-4	-2	1	83	84	82	83	136	141	400	82	83	83
60	-10	27	-7	-4	-613	-703	-959	-20	-9	2	84	87	84	85	342	390	701	95	91	88
90	-6	35	-4	-2	-2124	-1897	-2248	-29	-24	6	88	96	89	89	640	698	987	128	110	99
121	5	53	0	7	-3554	-3818	(b)	-77	-54	3	98	118	103	102	969	1010	1294	208	154	121
151	34	68	7	42	(b)	(b)		-235	-153	2	116	167	135	129	1252	1192	1406	379	247	170
181	60	78	33	76				-499	-371	-1	139	235	180	167	1288	1216	1412	566	345	233
261	97	153	86	142				-633	-1109	-124	207	418	314	290	1315	1252	1432	789	539	387
322	114	187	114	178				-733	-1491	-285	256	531	406	382	1332	1263	1433	836	631	467
382	114	197	133	203				-789	-1742	-188	302	618	485	463	1345	1271	1436	865	694	525
401	117	198	143	213				-761	-1772	-442	315	639	507	485	1344	1274	1438	872	710	539
416	113	198	147	214				-702	-1785	-454	323	655	522	500	1342	1273	1436	875	720	550
431	108	199	143	214				-645	-1870	-465	332	668	538	516	1342	1274	1434	879	731	560
492	125	224	145	222				-548	-1938	-528	358	711	593	567	1344	1278	1434	888	760	590
552	120	462	150	232				-449	-2046	-572	381	741	637	609	1349	1281	1434	898	784	614
612	127	820	163	241				-370	-2228	-606	404	762	669	639	1354	1284	1436	905	803	634
642	135	924	167	251				-331	-2262	-628	411	769	682	652	1354	1289	1442	908	812	642
672	135	370	180	276				-271	-2304	-649	417	775	689	658	1356	1289	1443	912	821	652
703	137	381	203	306				-236	-2345	-655	423	780	694	664	1357	1289	1440	915	828	661
733	143	416	214	333				-217	-2405	-663	428	784	700	670	1357	1290	1442	917	834	667
793	148	441	221	344				-179	-2477	-671	434	792	713	680	1360	1290	1441	919	842	676
823	151	459	232	356				-174	-2481	-666	438	795	716	683	1359	1291	1441	922	845	679
853	158	470	248	373				-121	-2540	-695	441	797	719	685	1359	1290	1441	922	848	683
884	159	491	268	384				-109	-2544	-685	443	800	722	686	1362	1291	1441	924	851	685
914	171	511	260	377				-116	-2565	-695	443	801	724	689	1359	1290	1431	923	854	687
974	173	551	306	406				-149	-2618	-710	447	806	726	691	1361	1291	1441	925	857	690
1035	195	592	302	416				-81	-2622	-693	454	809	730	694	1366	1292	1442	927	862	693
1065	206	616	313	428				-54	-2606	-686	456	808	731	696	1304	1292	1442	914	857	692
1096	167	605	304	425				-56	-2742	-649	454	790	726	691	1076	1117	1094	840	824	673
1126	150	516	306	416				66	-2662	-560	440	742	692	662	868	877	852	737	753	625
1187	99	444	351	396				154	-2274	-439	390	626	588	572	597	595	476	573	612	520
1247	56	407	358	362				98	-2012	-329	338	526	492	485	455	448	335	466	500	432
1308	28	388	341	343				80	-1923	-246	296	449	415	413	366	358	262	391	417	363
1369	16	374	312	305				26	-1600	-188	258	388	354	357	303	298	217	337	353	310
1430	5	364	300	300				-7	-1490	-133	232	338	309	313	258	256	188	294	304	267
1491	-4	358	283	284				-24	-1383	-92	204	300	272	277	225	225	156	261	265	234

[b]Signal went off scale on recorder.

TABLE VIII.- MEASURED VALUES OF LOAD, STRAIN, TEMPERATURE, AND DEFLECTION FOR 1,600° F TEST - Continued

(a) First heating cycle: 3 loads, 22 strain gages, 38 strain-gage thermocouples, 6 skin-corrugation-detail thermocouples, 8 longitudinal-spar-web thermocouples - Continued

Time, sec	Strain, μin./in., at -				Temperature, °F, at -														
	SG 125	SG 126	SG 127	SG 128	TC 125	TC 126	TC 127	TC 128	TC 96	TC 95	TC 98	TC 99	TC 109	TC 110	TC 113	TC 114	TC 117	TC 118	TC 133
0	-5	3	-2	-2	83	79	81	82	83	79	83	83	82	81	83	83	82	83	87
30	-4	0	0	-2	84	81	83	83	84	79	83	83	87	86	92	102	87	88	407
60	-5	-10	3	-4	91	87	88	93	89	82	85	85	121	119	129	157	115	118	724
90	-27	-22	12	9	110	101	102	119	113	98	95	93	192	190	198	249	171	181	1027
121	-81	-53	20	2	155	133	134	186	177	140	125	116	314	314	315	395	269	288	1355
151	-173	-116	19	-133	235	195	201	312	313	241	199	170	504	504	513	618	432	458	1466
181	-240	-205	0	-391	312	261	283	428	467	371	312	251	698	697	746	843	618	644	1467
261	-322	-507	-164	-846	472	414	456	630	806	681	645	527	985	972	1061	1096	929	942	1478
322	-285	-724	-288	-978	542	493	544	717	977	856	850	723	1055	1037	1120	1144	1016	1022	1476
382	-327	-630	-374	-1098	593	536	601	777	1083	978	985	864	1087	1065	1151	1171	1055	1058	1479
401	-255	-860	-372	-1137	598	549	614	787	1106	1006	1013	897	1094	1070	1157	1176	1063	1066	1481
416	-193	-898	-388	-1241	601	557	623	798	1122	1025	1033	920	1098	1074	1161	1179	1067	1071	1479
431	-232	-896	-424	-1252	611	564	633	805	1136	1042	1049	940	1102	1077	1164	1182	1074	1076	1477
492	-336	-910	-450	-1429	641	589	667	841	1177	1093	1096	998	1115	1088	1173	1189	1091	1091	1476
552	-375	-856	-506	-1534	664	604	691	865	1202	1126	1125	1031	1123	1094	1179	1193	1105	1101	1476
612	-428	-900	-478	-1541	677	618	712	882	1216	1146	1142	1051	1127	1097	1186	1198	1114	1109	1479
642	-379	-891	-475	-1508	676	621	717	887	1222	1154	1148	1058	1129	1098	1188	1199	1118	1112	1486
672	-286	-962	-484	-1487	681	627	723	895	1225	1159	1153	1065	1131	1099	1191	1202	1122	1115	1486
703	-164	-1062	-500	-1467	679	636	731	901	1230	1164	1157	1071	1133	1101	1194	1204	1126	1119	1485
733	-233	-1110	-506	-1418	687	639	736	905	1233	1168	1161	1075	1134	1102	1196	1206	1129	1121	1488
793	-211	-1117	-500	-1371	693	645	744	914	1235	1172	1166	1081	1136	1103	1200	1209	1131	1123	1487
823	-184	-1077	-511	-1328	693	642	748	917	1237	1173	1168	1083	1137	1104	1202	1212	1133	1124	1487
853	-225	-1152	-509	-1295	693	648	751	919	1238	1175	1169	1085	1137	1104	1203	1213	1135	1125	1487
884	-189	-1185	-504	-1268	691	650	753	921	1239	1177	1170	1087	1137	1103	1204	1213	1135	1125	1489
914	-192	-1144	-520	-1264	695	648	754	923	1239	1178	1171	1088	1138	1104	1205	1215	1136	1126	1487
974	-240	-1159	-541	-1227	697	647	760	929	1243	1181	1174	1091	1141	1106	1207	1218	1139	1128	1489
1035	-346	-1008	-581	-1159	697	639	762	929	1245	1183	1176	1094	1142	1107	1208	1217	1141	1129	1491
1065	-229	-1084	-576	-1127	695	644	759	924	1246	1184	1177	1094	1142	1107	1203	1213	1142	1129	1492
1096	-229	-1055	-570	-1069	682	632	737	882	1236	1177	1172	1087	1125	1090	1164	1169	1128	1114	1129
1126	-87	-854	-452	-982	603	570	679	787	1163	1118	1126	1043	1016	983	1041	1031	1036	1019	887
1187	94	-626	-317	-616	461	451	566	620	1003	972	987	920	796	770	799	780	830	815	511
1247	210	-374	-281	-507	358	358	460	496	869	845	858	804	630	608	626	609	670	658	358
1308	196	-253	-275	-497	292	292	385	413	766	746	756	708	514	492	507	493	556	544	278
1369	196	-168	-215	-467	243	243	329	350	683	665	673	631	428	409	421	410	470	458	228
1430	161	-126	-168	-445	212	209	283	297	615	599	606	567	364	346	357	348	405	393	195
1491	172	-90	-146	-453	185	185	249	264	557	542	548	513	315	298	307	301	354	342	173

TABLE VIII.- MEASURED VALUES OF LOAD, STRAIN, TEMPERATURE, AND DEFLECTION FOR 1,600° F TEST - Continued

(a) First heating cycle: 3 loads, 22 strain gages, 38 strain-gage thermocouples, 6 skin-corrugation-detail thermocouples, 8 longitudinal-spar-web thermocouples - Concluded

Time, sec	Temperature, °F, at -																	
	TC 134	TC 121	TC 130	TC 108	TC 115	TC 135	TC 136	TC 137	TC 138	TC 139	TC 140	TC 197	TC 198	TC 199	TC 200	TC 201	TC 279	TC 280	TC 281
0	77	79	80	80	82	82	84	83	80	82	80	78	78	78	78	78	77	77	78
30	142	81	361	80	82	83	85	84	149	215	319	79	79	79	79	79	78	78	79
60	403	96	616	81	85	88	89	88	358	448	570	85	87	85	84	84	85	86	85
90	717	140	897	86	93	103	101	99	648	725	849	108	115	109	102	98	108	109	105
121	1035	253	1207	97	113	136	126	119	967	1027	1150	169	189	171	148	135	169	173	158
151	1217	490	1449	124	162	207	183	167	1244	1289	1393	308	355	310	253	216	314	319	279
181	1244	702	1470	162	234	297	259	232	1278	1319	1416	475	548	473	387	315	489	498	425
261	1281	908	1474	298	441	487	437	395	1306	1341	1426	797	635	759	655	534	789	785	691
322	1293	958	1487	413	572	580	527	480	1323	1357	1439	894	908	844	755	641	879	869	790
382	1303	989	1491	526	670	646	593	540	1337	1369	1446	952	951	894	812	714	936	923	856
401	1306	995	1491	559	694	626	609	555	1336	1369	1446	965	961	905	826	733	950	936	873
416	1307	999	1488	584	713	674	620	567	1335	1367	1443	974	968	912	835	745	961	946	886
431	1307	1003	1488	607	728	685	631	577	1335	1368	1444	983	974	920	843	756	970	955	897
492	1310	1014	1486	688	778	717	662	608	1337	1369	1443	1009	996	943	868	792	1002	984	936
552	1314	1025	1489	750	811	743	689	632	1343	1375	1447	1025	1009	959	888	818	1027	1008	967
612	1317	1034	1494	796	834	764	711	653	1349	1381	1452	1037	1019	970	902	838	1048	1029	993
642	1322	1036	1491	814	843	774	720	661	1349	1381	1452	1042	1023	975	907	847	1056	1037	1003
672	1322	1041	1494	828	848	783	731	671	1351	1383	1454	1046	1027	979	914	856	1064	1045	1012
703	1323	1044	1496	841	854	791	740	680	1353	1385	1455	1050	1032	984	921	864	1069	1050	1020
733	1326	1046	1497	851	859	798	747	686	1353	1385	1455	1053	1034	987	925	870	1074	1055	1026
793	1325	1048	1499	867	867	806	756	695	1356	1389	1459	1057	1037	991	930	877	1082	1063	1036
823	1326	1051	1498	873	870	810	760	699	1355	1388	1458	1058	1039	993	932	882	1086	1067	1041
853	1325	1052	1499	878	873	813	762	702	1356	1388	1458	1059	1040	994	933	883	1089	1069	1044
884	1326	1053	1500	882	875	816	766	705	1358	1391	1460	1060	1041	995	935	886	1092	1072	1048
914	1326	1053	1495	886	877	819	768	706	1355	1388	1457	1061	1043	996	936	887	1095	1076	1051
974	1328	1056	1497	892	881	822	771	709	1358	1390	1459	1064	1045	999	939	891	1100	1081	1058
1035	1329	1059	1504	896	887	827	776	712	1363	1396	1465	1066	1047	1000	942	894	1105	1085	1062
1065	1328	1040	1394	895	885	826	776	712	1302	1330	1372	1062	1042	996	939	893	1098	1078	1057
1096	1149	945	1072	885	861	799	753	693	1079	1083	1073	1025	997	955	902	863	1046	1028	1016
1126	917	822	788	856	809	735	697	644	868	852	807	926	885	853	813	789	959	934	932
1187	634	632	456	769	683	602	576	534	594	554	485	756	700	675	648	646	803	776	787
1247	483	511	327	676	576	493	474	443	451	414	353	634	574	549	526	536	694	665	682
1308	392	427	259	594	491	412	397	371	362	331	281	543	483	458	438	453	612	583	602
1369	324	365	213	522	423	349	337	316	300	272	230	473	414	390	372	391	546	516	533
1430	276	318	184	462	370	300	290	273	255	232	198	417	361	339	324	344	491	461	477
1491	241	281	163	412	327	262	253	239	223	203	175	372	319	299	285	305	445	416	432

TABLE VIII.- MEASURED VALUES OF LOAD, STRAIN, TEMPERATURE, AND DEFLECTION FOR 1,600° F TEST - Continued

(b) Second heating cycle: 3 loads, 19 deflections, 66 top skin thermocouples, 8 transverse frame web thermocouples, 3 deflectometer wire thermocouples, 1 air thermocouple

Time, sec	Total load, lb	Left load, lb	Right load, lb	Temperature, °F, at TC 132	Deflection, in., at -															
					Defl 1	Defl 2	Defl 5	Defl 8	Defl 9	Defl 12	Defl 13	Defl 14	Defl 15	Defl 16	Defl 17	Defl 18	Defl 19	Defl 20	Defl 21	Defl 22
0	-2	-1	-1	77	-0.001	0.001	0	0	0.001	0.001	0.001	0	0	0.001	0	0	0	0.001	0	0
30	-54	-20	-34	400	-.002	-.002	.005	.003	.010	.008	.012	-.001	-.001	.011	.015	.001	0	.013	.017	.001
60	-75	-32	-43	706	.020	.018	.011	.013	.016	.022	.021	-.003	-.002	.023	.030	-.003	-.002	.029	.037	0
90	-58	-22	-36	977	.080	.084	.041	.043	.041	.056	.044	.002	.004	.046	.056	-.002	0	.056	.064	.001
121	-121	-54	-67	1280	.231	.241	.107	.109	.090	.119	.081	.013	.018	.087	.097	0	.003	.097	.102	.002
151	-108	-47	-61	1389	.578	.595	.253	.253	.186	.244	.142	.044	.051	.151	.144	.010	.014	.148	.140	.004
181	-95	-41	-54	1393	1.011	1.039	.427	.424	.294	.383	.199	.084	.094	.209	.176	.022	.026	.183	.149	.006
241	-37	-13	-24	1410	1.866	1.915	.776	.764	.500	.648	.292	.171	.187	.308	.210	.052	.057	.226	.150	.011
302	-53	-21	-32	1419	2.482	2.548	1.037	1.017	.643	.835	.350	.243	.264	.368	.217	.078	.081	.239	.150	.014
332	-90	-38	-52	1422	2.668	2.741	1.122	1.099	.689	.893	.366	.267	.290	.384	.217	.089	.090	.239	.150	.016
362	-55	-21	-34	1426	2.789	2.865	1.184	1.156	.725	.938	.380	.288	.312	.396	.219	.098	.098	.240	.150	.018
393	-65	-26	-39	1430	2.832	2.912	1.215	1.185	.742	.959	.387	.302	.325	.402	.218	.106	.104	.238	.149	.021
423	-66	-27	-39	1430	2.831	2.908	1.226	1.196	.750	.968	.389	.311	.335	.403	.216	.112	.108	.237	.149	.023
484	-71	-66	-15	1430	2.734	2.803	1.208	1.179	.740	.957	.385	.317	.342	.400	.212	.119	.115	.233	.148	.027
544	-98	-68	-30	1430	2.580	2.645	1.159	1.133	.718	.927	.377	.318	.340	.389	.206	.123	.118	.227	.147	.030
605	-114	-76	-38	1430	2.431	2.490	1.112	1.086	.695	.896	.367	.315	.338	.379	.203	.125	.120	.224	.146	.031
620	479	242	237	1428	2.491	2.552	1.162	1.131	.735	.945	.396	.340	.365	.405	.224	.142	.133	.240	.149	.036
635	2157	1093	1064	1431	2.725	2.791	1.321	1.283	.855	1.098	.478	.380	.445	.485	.277	.182	.168	.292	.151	.048
650	3609	1830	1779	1430	2.929	3.001	1.460	1.412	.945	1.229	.544	.385	.514	.548	.324	.197	.173	.336	.151	.059
666	4469	2267	2202	1428	3.041	3.113	1.538	1.486	.973	1.287	.560	.386	.554	.578	.352	.198	.173	.362	.151	.066
696	5740	2915	2825	1425	3.199	3.275	(b)	(b)	.987	1.304	.568	.387	.614	.603	.392	.199	.173	.398	.151	.075
726	6365	3231	3134	1425	3.263	3.341	↓	↓	.989	1.304	.569	.388	.643	.608	.399	.199	.173	(b)	.151	.080
787	6453	3203	3250	1428	3.220	3.299	↓	↓	.989	1.305	.569	.388	.649	.649	.399	.199	.174	↓	.152	.080
817	6472	3193	3279	1429	3.203	3.281	↓	↓	.989	1.306	.569	.388	.651	.610	.399	.199	.174	↓	.152	.081
847	6454	3180	3274	1426	3.179	3.255	↓	↓	.989	1.306	.569	.388	.650	.609	.399	.199	.174	↓	.152	.082
863	2533	1250	1283	1427	2.570	2.632	1.291	1.254	.858	1.104	.494	.385	.469	.498	.290	.192	.172	.310	.151	.056
878	1449	709	740	1429	2.382	2.442	1.174	1.143	.774	.993	.438	.375	.415	.444	.255	.175	.164	.273	.150	.048
908	249	112	137	1434	2.159	2.215	1.038	1.016	.672	.867	.373	.330	.352	.380	.213	.144	.137	.233	.147	.039
969	-152	-87	-65	1434	2.061	2.116	.983	.964	.636	.818	.350	.311	.330	.356	.197	.132	.125	.218	.144	.037
1030	-175	-96	-79	1438	2.043	2.099	.974	.957	.630	.816	.349	.309	.328	.355	.196	.132	.126	.217	.143	.036
1076	-102	-64	-38	1143	1.985	2.040	.944	.928	.604	.780	.322	.304	.324	.333	.166	.131	.125	.191	.119	.035
1106	-36	-31	-5	901	1.789	1.842	.859	.847	.545	.704	.283	.290	.308	.291	.133	.126	.121	.156	.085	.032
1137	-39	-33	-6	670	1.550	1.598	.757	.749	.477	.617	.241	.267	.285	.248	.102	.118	.115	.121	.053	.031
1198	-83	-52	-31	430	1.184	1.220	.601	.594	.377	.482	.186	.225	.237	.186	.065	.100	.097	.078	.021	.025
1258	-119	-69	-50	318	.974	1.004	.505	.499	.316	.401	.152	.193	.202	.151	.045	.084	.082	.056	.007	.020
1319	-142	-82	-60	256	.850	.875	.444	.448	.277	.348	.132	.171	.176	.128	.035	.073	.071	.044	.001	.016
1379	-163	-86	-67	215	.766	.790	.402	.395	.249	.311	.116	.151	.155	.112	.029	.063	.061	.036	-.002	.012
1440	-163	-92	-71	187	.706	.728	.369	.361	.227	.282	.105	.135	.139	.100	.025	.054	.053	.030	-.003	.010
1501	-162	-91	-71	168	.657	.679	.340	.334	.208	.258	.095	.122	.125	.090	.021	.048	.047	.026	-.004	.007
1802	-212	-106	-106	165	.442	.457	.208	.202	.122	.151	.058	.060	.059	.055	.017	.020	.019	.018	-.001	0

[b]Signal went off scale on recorder.

TABLE VIII.- MEASURED VALUES OF LOAD, STRAIN, TEMPERATURE, AND DEFLECTION FOR 1,600° F TEST - Continued

(b) Second heating cycle: 3 loads, 19 deflections, 66 top skin thermocouples, 8 transverse frame web thermocouples, 3 deflectometer wire thermocouples, 1 air thermocouple - Continued

Time, sec	Deflection, in., at -		Temperature, °F, at - ·																	
	Defl 23	Defl 24	TC 1	TC 2	TC 3	TC 4	TC 5	TC 6	TC 7	TC 8	TC 289	TC 9	TC 10	TC 11	TC 12	TC 13	TC 14	TC 15	TC 16	TC 17
0	0	0	77	82	102	81	76	76	81	84	76	78	78	95	99	86	80	77	77	76
30	.001	.018	240	387	395	365	425	365	368	346	240	206	265	353	355	342	344	330	352	380
60	0	.042	549	684	651	663	750	650	679	631	573	442	513	591	584	578	619	564	620	681
90	.001	.074	843	969	918	941	1023	908	957	930	899	689	780	847	780	810	885	805	866	946
121	.002	.118	1167	1273	1232	1267	1322	1198	1282	1248	1227	1009	1097	1159	1052	1123	1218	1127	1148	1238
151	.005	.130	1501	1507	1419	1425	1420	1301	1426	1484	1537	1367	1385	1393	1228	1301	1399	1270	1261	1335
181	.007	.131	1514	1517	1427	1434	1420	1309	1429	1488	1554	1418	1395	1415	1276	1318	1408	1288	1271	1326
241	.012	.131	1518	1511	1424	1427	1423	1314	1422	1473	1553	1446	1393	1407	1317	1337	1411	1319	1279	1329
302	.017	.131	1509	1514	1414	1427	1428	1317	1426	1467	1551	1453	1397	1411	1323	1361	1427	1328	1287	1334
332	.019	.131	1510	1513	1414	1432	1430	1318	1430	1469	1552	1453	1397	1415	1328	1369	1438	1337	1292	1337
362	.021	.131	1512	1511	1412	1427	1431	1318	1428	1462	1549	1458	1396	1419	1332	1377	1444	1344	1300	1342
393	.022	.131	1514	1510	1413	1426	1434	1321	1425	1462	1552	1463	1400	1422	1336	1382	1448	1346	1301	1346
423	.024	.131	1518	1512	1413	1424	1431	1317	1422	1461	1549	1467	1399	1424	1338	1388	1452	1348	1305	1346
484	.027	.131	1517	1510	1419	1426	1430	1315	1428	1464	1551	1465	1397	1423	1349	1402	1465	1345	1306	1346
544	.028	.131	1518	1514	1414	1424	1428	1314	1429	1466	1553	1467	1402	1426	1346	1410	1473	1346	1307	1349
605	.029	.131	1518	1510	1414	1424	1427	1311	1427	1464	1553	1471	1402	1424	1349	1412	1473	1349	1304	1349
620	.033	.131	1520	1510	1415	1424	1424	1309	1425	1462	1555	1471	1403	1428	1349	1409	1473	1354	1306	1347
635	.044	.131	1517	1511	1416	1425	1428	1313	1426	1462	1552	1469	1402	1430	1350	1415	1475	1351	1314	1350
650	.053	.131	1517	1510	1417	1425	1429	1313	1426	1461	1554	1467	1401	1433	1352	1419	1475	1350	1322	1350
666	.059	.131	1515	1510	1417	1424	1428	1310	1426	1461	1551	1464	1398	1432	1351	1419	1475	1349	1320	1347
696	.067	.131	1514	1506	1418	1427	1426	1310	1428	1461	1554	1461	1399	1436	1354	1419	1477	1351	1322	1344
726	.072	.131	1514	1509	1419	1426	1425	1308	1429	1462	1553	1462	1400	1437	1355	1424	1478	1353	1326	1344
787	.073	.131	1514	1505	1415	1429	1426	1308	1432	1460	1552	1462	1399	1436	1353	1420	1480	1360	1328	1343
817	.074	.131	1515	1508	1417	1425	1428	1310	1428	1461	1553	1464	1403	1441	1355	1420	1477	1360	1332	1347
847	.075	.131	1514	1511	1421	1427	1424	1307	1429	1464	1555	1465	1405	1443	1358	1422	1478	1356	1325	1343
863	.053	.131	1519	1511	1423	1427	1425	1309	1431	1465	1555	1471	1406	1441	1359	1422	1479	1354	1320	1346
878	.046	.131	1521	1513	1422	1429	1425	1309	1434	1467	1555	1473	1408	1431	1358	1423	1484	1358	1313	1349
908	.038	.131	1521	1512	1422	1434	1431	1313	1437	1470	1557	1474	1411	1427	1360	1431	1490	1355	1310	1355
969	.034	.131	1518	1518	1422	1437	1429	1312	1437	1476	1558	1475	1417	1434	1363	1439	1497	1352	1308	1356
1030	.034	.131	1523	1516	1422	1439	1429	1312	1438	1476	1562	1485	1422	1437	1361	1434	1496	1364	1311	1357
1076	.034	.131	1511	1351	1188	1219	1117	1004	1203	1297	1532	1469	1331	1258	1169	1247	1304	1108	1062	1070
1106	.032	.122	972	1018	875	933	869	790	918	971	1042	948	905	956	906	995	1049	860	860	854
1137	.029	.084	656	714	638	680	635	596	671	697	750	643	614	698	701	779	823	620	662	658
1198	.024	.038	363	386	384	440	397	391	447	431	471	366	350	427	476	555	591	386	444	454
1258	.019	.017	257	268	273	328	291	288	341	323	347	268	258	314	363	431	452	280	332	341
1319	.016	.008	207	214	216	268	235	230	281	258	272	220	211	250	296	350	365	227	266	273
1379	.012	.003	176	182	182	229	201	193	237	215	223	187	181	209	250	294	305	193	223	228
1440	.009	0	156	160	159	201	177	168	207	185	191	165	161	181	217	253	262	170	193	198
1501	.007	-.001	142	145	144	181	159	152	186	164	169	150	146	162	194	224	229	153	172	176
1802	.001	.002	142	139	144	157	143	117	155	142	146	164	157	164	182	216	219	172	162	163

TABLE VIII.- MEASURED VALUES OF LOAD, STRAIN, TEMPERATURE, AND DEFLECTION FOR 1,600° F TEST - Continued

(b) Second heating cycle: 3 loads, 19 deflections, 66 top skin thermocouples, 8 transverse frame web thermocouples, 3 deflectometer wire thermocouples, 1 air thermocouple - Continued

Time, sec	Temperature, °F, at -																			
	TC 18	TC 19	TC 20	TC 21	TC 22	TC 23	TC 24	TC 25	TC 26	TC 27	TC 28	TC 29	TC 30	TC 31	TC 32	TC 33	TC 34	TC 35	TC 36	TC 37
0	79	103	83	77	77	86	112	81	77	77	78	82	110	85	78	77	77	77	77	77
30	371	370	341	230	198	292	403	300	275	226	197	331	398	302	255	230	444	326	402	279
60	683	601	620	517	433	482	635	552	511	517	398	607	631	536	568	607	673	494	676	588
90	969	850	917	815	682	714	881	817	762	814	620	892	880	778	872	924	909	708	954	906
121	1306	1155	1249	1162	989	1012	1186	1154	1098	1140	914	1200	1178	1088	1186	1216	1171	968	1248	1224
151	1454	1344	1516	1509	1310	1252	1361	1317	1261	1452	1232	1450	1358	1241	1481	1467	1355	1199	1477	1500
181	1458	1364	1543	1547	1360	1280	1373	1338	1266	1483	1259	1454	1360	1254	1486	1471	1371	1272	1505	1540
241	1481	1390	1561	1571	1367	1301	1380	1342	1256	1506	1257	1443	1351	1256	1473	1466	1370	1332	1514	1532
302	1495	1403	1577	1581	1374	1319	1383	1346	1260	1517	1264	1443	1348	1260	1471	1457	1394	1385	1543	1549
332	1505	1409	1581	1583	1375	1324	1388	1355	1268	1517	1261	1442	1349	1265	1471	1455	1394	1396	1550	1551
362	1510	1415	1579	1586	1377	1324	1395	1352	1263	1520	1266	1439	1354	1263	1473	1453	1399	1404	1555	1553
393	1513	1420	1581	1590	1381	1329	1402	1350	1262	1525	1267	1439	1361	1266	1480	1454	1396	1404	1555	1552
423	1513	1424	1583	1592	1381	1331	1405	1349	1260	1529	1271	1441	1365	1267	1481	1454	1397	1409	1558	1552
484	1520	1435	1585	1591	1384	1334	1421	1360	1268	1531	1275	1444	1377	1276	1479	1456	1400	1416	1566	1554
544	1521	1435	1589	1591	1389	1342	1425	1362	1273	1534	1277	1449	1384	1284	1486	1460	1398	1412	1565	1564
605	1521	1438	1588	1594	1392	1345	1429	1365	1277	1537	1282	1453	1391	1288	1496	1458	1391	1409	1560	1562
620	1522	1438	1588	1594	1393	1345	1430	1364	1277	1538	1286	1455	1391	1290	1497	1455	1391	1409	1560	1565
635	1523	1438	1587	1591	1391	1345	1431	1363	1274	1536	1285	1450	1391	1286	1486	1449	1387	1408	1558	1549
650	1522	1439	1585	1592	1389	1344	1433	1362	1270	1532	1287	1445	1389	1286	1493	1453	1389	1413	1563	1554
666	1522	1439	1584	1592	1389	1347	1433	1361	1267	1530	1285	1441	1389	1284	1494	1450	1385	1417	1564	1555
696	1524	1439	1581	1588	1387	1348	1437	1365	1271	1530	1288	1439	1389	1289	1490	1456	1399	1431	1574	1553
726	1524	1438	1582	1588	1384	1347	1437	1364	1269	1527	1285	1437	1389	1289	1487	1455	1400	1434	1574	1558
787	1526	1435	1579	1589	1387	1345	1436	1369	1274	1528	1288	1436	1386	1290	1488	1460	1402	1438	1578	1557
817	1524	1437	1582	1589	1386	1350	1438	1363	1268	1530	1290	1440	1390	1292	1490	1460	1406	1440	1582	1564
847	1523	1439	1584	1592	1388	1350	1440	1364	1270	1532	1294	1444	1395	1293	1493	1464	1402	1437	1579	1563
863	1525	1444	1587	1595	1393	1349	1441	1369	1276	1538	1291	1450	1399	1297	1499	1462	1409	1437	1581	1566
878	1528	1445	1590	1598	1395	1350	1443	1376	1289	1544	1295	1461	1406	1305	1500	1456	1400	1424	1571	1566
908	1531	1447	1593	1599	1397	1350	1446	1381	1297	1547	1295	1466	1409	1312	1503	1456	1404	1421	1568	1560
969	1533	1453	1601	1602	1400	1358	1450	1385	1306	1550	1299	1476	1413	1316	1508	1463	1401	1415	1569	1559
1030	1534	1453	1603	1610	1407	1361	1451	1389	1311	1558	1308	1478	1414	1321	1516	1464	1399	1413	1566	1563
1076	1311	1239	1450	1583	1391	1207	1229	1188	1116	1536	1274	1344	1195	1129	1478	1429	1227	1258	1435	1497
1106	1047	958	1129	1110	908	894	949	922	852	1095	828	998	907	868	1058	1000	940	976	1119	1080
1137	813	744	847	827	632	630	746	687	627	829	565	719	703	665	798	705	684	729	855	794
1198	578	500	543	530	380	367	530	465	417	549	343	449	496	462	541	485	448	495	601	533
1258	444	371	399	388	300	277	419	338	318	413	266	350	397	362	425	400	355	388	474	416
1319	363	294	313	303	248	228	348	278	260	330	224	295	337	301	350	341	297	318	392	335
1379	305	243	256	247	211	195	295	236	222	276	195	252	291	257	297	299	255	268	335	280
1440	262	209	218	210	185	174	255	206	195	237	174	221	257	224	256	270	225	235	294	240
1501	232	186	190	184	169	159	229	185	175	208	159	198	232	198	227	244	201	210	263	213
1802	209	176	167	169	172	176	242	188	174	183	182	192	241	189	197	204	201	212	245	214

TABLE VIII.- MEASURED VALUES OF LOAD, STRAIN, TEMPERATURE, AND DEFLECTION FOR 1,600° F TEST - Continued

(b) Second heating cycle: 3 loads, 19 deflections, 66 top skin thermocouples, 8 transverse frame web thermocouples, 3 deflectometer wire thermocouples, 1 air thermocouple - Continued

Time, sec	Temperature, °F, at -																			
	TC 38	TC 39	TC 40	TC 41	TC 42	TC 43	TC 44	TC 45	TC 46	TC 47	TC 48	TC 49	TC 50	TC 51	TC 52	TC 53	TC 54	TC 55	TC 56	TC 57
0	77	77	77	77	77	82	83	83	84	76	76	76	76	76	75	77	77	82	78	77
30	173	297	384	197	102	263	295	287	248	117	106	256	337	259	247	106	104	280	362	233
60	466	551	649	547	182	474	528	503	411	182	202	450	595	456	429	176	154	438	553	361
90	759	810	889	865	305	720	788	751	610	259	335	650	835	669	641	277	222	623	762	524
121	1063	1080	1149	1173	478	1019	1086	1037	884	370	504	897	1115	929	922	420	331	862	1015	748
151	1362	1308	1356	1469	723	1277	1331	1282	1147	535	695	1019	1219	1058	1060	610	485	1073	1210	980
181	1409	1334	1396	1499	920	1325	1363	1309	1195	707	839	1039	1227	1073	1084	765	614	1137	1245	1054
241	1403	1337	1382	1476	1134	1357	1387	1325	1225	956	1024	1066	1242	1084	1118	967	822	1189	1264	1116
302	1395	1342	1371	1456	1217	1378	1402	1328	1255	1073	1105	1081	1250	1092	1135	1061	958	1239	1294	1160
332	1398	1341	1364	1451	1233	1383	1409	1332	1258	1099	1126	1088	1254	1094	1138	1087	1002	1251	1303	1166
362	1391	1337	1363	1445	1242	1382	1417	1332	1257	1116	1140	1092	1256	1094	1138	1105	1035	1265	1310	1177
393	1388	1337	1359	1441	1249	1386	1419	1334	1260	1127	1150	1096	1260	1096	1142	1119	1058	1269	1310	1179
423	1391	1338	1362	1443	1253	1386	1419	1334	1257	1134	1157	1097	1259	1096	1142	1129	1077	1277	1314	1181
484	1399	1345	1366	1451	1258	1387	1423	1332	1263	1144	1166	1099	1258	1095	1142	1142	1100	1287	1321	1192
544	1409	1352	1368	1463	1263	1389	1425	1342	1273	1158	1170	1099	1258	1095	1147	1150	1112	1288	1319	1189
605	1407	1355	1370	1467	1264	1390	1426	1339	1269	1160	1172	1098	1255	1094	1146	1157	1123	1286	1314	1186
620	1407	1350	1369	1465	1265	1390	1425	1337	1270	1164	1173	1097	1254	1093	1144	1159	1124	1285	1314	1186
635	1407	1346	1364	1461	1266	1391	1425	1342	1272	1166	1174	1102	1258	1098	1148	1161	1127	1287	1314	1189
650	1400	1345	1366	1455	1267	1392	1427	1339	1273	1169	1176	1105	1260	1101	1152	1163	1137	1296	1324	1202
666	1403	1342	1363	1454	1269	1393	1428	1337	1275	1167	1177	1106	1258	1102	1153	1166	1146	1299	1326	1207
696	1413	1345	1368	1449	1271	1395	1431	1338	1278	1171	1179	1106	1257	1103	1152	1170	1160	1315	1343	1231
726	1401	1345	1366	1448	1273	1397	1429	1336	1280	1172	1180	1105	1257	1105	1151	1172	1170	1319	1345	1236
787	1419	1350	1372	1457	1274	1398	1442	1334	1282	1172	1182	1107	1258	1104	1153	1176	1176	1322	1349	1240
817	1423	1356	1376	1459	1276	1400	1433	1338	1283	1177	1183	1107	1260	1105	1154	1178	1182	1325	1351	1243
847	1419	1357	1377	1461	1278	1401	1435	1338	1284	1178	1183	1105	1257	1103	1152	1178	1184	1323	1349	1240
863	1411	1364	1382	1467	1278	1399	1435	1338	1278	1176	1183	1103	1256	1101	1150	1178	1183	1320	1350	1231
878	1409	1362	1379	1472	1276	1396	1434	1343	1274	1177	1181	1099	1256	1098	1150	1176	1176	1306	1330	1210
908	1409	1362	1380	1477	1274	1395	1427	1342	1278	1181	1181	1099	1258	1098	1151	1175	1158	1300	1325	1196
969	1416	1365	1384	1486	1275	1398	1429	1351	1278	1185	1183	1097	1255	1096	1148	1176	1143	1296	1321	1192
1030	1418	1367	1387	1489	1278	1399	1433	1348	1280	1187	1185	1097	1256	1096	1148	1180	1145	1293	1317	1191
1076	1407	1307	1302	1480	1237	1281	1297	1206	1143	1150	1090	882	971	874	917	1112	1103	1150	1175	1075
1106	1013	945	975	1058	1083	998	999	905	867	988	971	721	769	699	732	1000	968	911	904	813
1137	763	697	726	777	913	748	733	652	630	789	834	569	582	537	565	875	794	707	670	602
1198	518	472	494	517	647	466	448	388	388	483	608	393	380	353	365	667	550	503	451	404
1258	411	382	403	409	491	338	328	289	289	348	465	299	280	264	268	527	426	404	366	323
1319	350	328	343	348	397	267	262	236	238	289	373	241	225	213	215	426	350	339	299	274
1379	303	288	300	302	333	221	220	202	202	248	311	203	189	182	182	354	295	292	259	237
1440	267	257	268	267	286	189	190	177	177	223	265	176	166	160	158	304	256	255	228	210
1501	244	231	241	242	251	168	169	159	159	203	232	157	149	145	142	270	228	227	203	190
1802	220	231	215	239	197	165	162	167	170	214	183	138	127	120	127	223	243	206	205	209

TABLE VIII.- MEASURED VALUES OF LOAD, STRAIN, TEMPERATURE, AND DEFLECTION FOR 1,600° F TEST - Continued

(b) Second heating cycle: 3 loads, 19 deflections, 66 top skin thermocouples, 8 transverse frame web thermocouples, 3 deflectometer wire thermocouples, 1 air thermocouple - Concluded

Time, sec	Temperature, °F, at -																		Lateral defl. sta. 47
	TC 271	TC 272	TC 273	TC 274	TC 275	TC 276	TC 277	TC 278	TC 282	TC 283	TC 284	TC 285	TC 286	TC 287	TC 288	TC 294	TC 295	TC 296	TC 297	
0	77	77	77	77	78	77	77	77	77	77	81	79	112	80	79	77	75	75	75	0
30	79	79	79	79	79	78	77	78	230	432	371	390	400	366	375	116	79	75	75	0
60	92	91	91	93	93	90	88	86	557	776	665	685	678	661	666	146	82	76	75	0
90	133	129	125	139	134	124	119	113	862	1087	934	963	950	949	957	160	86	78	78	.010
121	242	233	218	261	239	214	198	181	1185	1430	1220	1265	1228	1260	1268	176	93	81	88	.050
151	482	462	423	485	432	380	346	313	1511	1520	1487	1496	1434	1404	1385	170	95	83	101	.130
181	723	693	631	647	576	511	469	426	1546	1562	1504	1503	1443	1410	1386	166	94	82	104	.200
241	917	884	825	800	732	667	621	569	1560	1561	1502	1499	1442	1409	1385	174	100	84	109	.410
302	989	956	907	878	818	761	713	659	1560	1561	1499	1500	1447	1408	1384	160	98	85	116	.600
332	1011	979	935	907	850	792	745	692	1560	1561	1499	1499	1443	1407	1383	155	99	85	119	.680
362	1028	998	956	931	874	820	774	723	1560	1561	1501	1499	1443	1408	1385	154	107	84	120	.740
393	1043	1013	975	951	896	842	797	746	1560	1564	1499	1500	1446	1408	1384	159	106	85	125	.810
423	1054	1026	990	968	915	862	818	767	1560	1564	1500	1499	1448	1408	1387	162	96	86	125	.870
484	1072	1046	1011	993	941	891	849	803	1560	1568	1500	1500	1448	1408	1387	158	92	86	130	.940
544	1086	1060	1027	1012	962	913	873	827	1561	1568	1501	1500	1442	1407	1383	159	91	86	130	.980
605	1094	1070	1036	1024	975	929	891	847	1561	1568	1501	1499	1442	1407	1385	173	92	85	135	1.020
620	1097	1072	1039	1027	979	932	894	851	1562	1569	1501	1498	1443	1407	1386	172	93	85	138	1.025
635	1099	1074	1041	1030	982	936	898	854	1562	1571	1501	1497	1444	1407	1387	173	93	85	138	1.030
650	1100	1076	1043	1032	984	939	901	858	1563	1570	1501	1497	1444	1407	1386	170	95	84	139	1.035
666	1102	1077	1044	1035	987	943	905	861	1563	1570	1501	1497	1449	1407	1387	167	96	83	139	1.040
696	1104	1079	1047	1038	991	947	911	867	1567	1571	1501	1496	1450	1407	1386	174	96	85	138	1.045
726	1106	1083	1050	1044	996	952	915	872	1567	1571	1501	1499	1449	1407	1387	173	98	86	136	1.050
787	1109	1086	1053	1050	1002	959	924	881	1569	1571	1502	1499	1451	1409	1389	156	97	86	141	1.055
817	1112	1088	1055	1051	1006	962	927	885	1569	1571	1502	1498	1451	1409	1389	165	98	87	140	1.060
847	1114	1091	1059	1051	1008	964	928	888	1569	1572	1502	1499	1452	1410	1389	173	98	87	144	1.065
863	1115	1091	1059	1053	1007	965	929	889	1569	1573	1505	1500	1457	1410	1390	168	98	86	144	1.070
878	1116	1092	1060	1054	1007	967	930	889	1569	1573	1505	1500	1458	1411	1390	166	97	85	147	1.070
908	1117	1094	1062	1055	1009	968	933	892	1569	1574	1509	1500	1459	1411	1389	162	95	86	145	1.075
969	1121	1098	1065	1059	1014	972	937	897	1569	1578	1510	1501	1461	1414	1391	165	100	88	148	1.075
1030	1126	1102	1071	1065	1020	979	944	903	1571	1579	1516	1501	1460	1420	1392	161	98	86	150	1.080
1076	1104	1080	1049	1023	981	943	911	873	1341	1382	1270	1345	1232	1220	1100	120	86	80	135	1.070
1106	993	967	944	935	895	863	836	801	1038	1052	963	1014	930	934	844	108	83	78	122	1.040
1137	871	848	834	837	802	772	748	716	760	803	710	720	718	714	620	100	82	77	113	-----
1198	687	673	667	685	651	620	598	568	480	580	521	412	501	480	410	98	80	77	100	-----
1258	571	561	557	578	543	512	491	464	366	475	441	293	384	360	305	101	80	77	96	-----
1319	488	480	476	498	465	434	413	386	(c)	(c)	(c)	(c)	(c)	(c)	(c)	93	78	76	90	-----
1379	425	419	417	436	405	371	351	327	↓	↓	↓	↓	↓	↓	↓	92	79	75	86	-----
1440	376	372	370	386	357	325	305	283								92	80	76	83	-----
1501	336	333	331	345	318	287	268	247								90	78	75	83	-----
1802	232	228	226	244	228	209	195	183								84	77	75	77	-----

[c]Thermocouple readings terminated when temperature controllers were stopped.

TABLE VIII.- MEASURED VALUES OF LOAD, STRAIN, TEMPERATURE, AND DEFLECTION FOR 1,600° F TEST - Continued

(c) Third heating cycle: 1 top skin thermocouple, 36 bottom skin thermocouples, 57 right longitudinal spar cap thermocouples

Time, sec	Temperature, °F, at -																			
	TC 132	TC 59	TC 60	TC 61	TC 62	TC 63	TC 64	TC 65	TC 66	TC 67	TC 68	TC 69	TC 70	TC 71	TC 72	TC 73	TC 74	TC 75	TC 76 (e)	TC 77
0	78	76	(d)	75	76	77	77	77	77	76	78	76	77	77	77	77	77	77	76	77
30	389	80	↓	76	78	79	78	79	79	77	79	79	78	79	78	81	79	78	69	79
60	695	95		79	84	93	87	88	86	82	89	90	85	85	85	98	91	85	71	87
90	968	139		89	101	132	108	112	105	95	118	116	102	102	102	134	120	101	74	105
121	1266	245		111	142	235	160	170	151	132	191	180	144	140	145	209	193	135	86	145
151	1386	466		153	224	453	283	300	252	201	359	315	234	223	239	367	352	204	133	226
181	1397	679		197	316	670	462	458	376	280	578	491	336	316	345	562	527	284	195	320
251	1416	849	467	275	468	854	744	682	588	421	853	737	513	494	519	805	729	433	320	485
312	1421	877	532	320	537	890	823	752	673	498	920	805	600	585	602	870	788	519	396	573
372	1424	890	568	355	575	906	853	788	719	547	949	836	650	637	651	902	822	580	446	633
399	1428	894	579	361	586	909	862	799	733	562	958	845	665	648	666	910	834	603	463	656
414	1423	895	584	366	592	912	865	803	738	566	962	850	673	656	675	916	842	614	472	668
429	1423	898	590	367	598	914	870	809	745	574	965	854	682	665	681	920	846	626	479	679
499	1426	903	610	384	616	919	883	827	769	597	978	870	712	690	710	934	870	673	506	727
559	1430	905	623	397	629	925	889	836	780	613	984	881	729	702	729	942	885	709	525	761
619	1431	911	631	405	639	927	895	846	791	623	991	890	743	712	747	953	898	740	539	790
649	1428	912	(d)	405	641	929	898	848	794	626	993	895	751	724	752	955	904	755	545	803
679	1429	913	↓	412	642	930	898	849	795	633	994	897	756	733	757	959	908	765	549	811
709	1430	913		415	645	931	899	851	798	636	995	900	762	740	762	961	910	775	555	821
739	1434	915		418	649	932	902	854	801	638	997	902	764	743	768	966	913	783	556	830
799	1435	916		419	654	933	906	858	806	641	999	906	772	747	774	969	919	797	561	841
829	1436	917		425	656	933	905	858	807	643	1000	908	774	743	775	971	922	805	569	848
859	1438	916		423	658	934	906	861	809	645	1001	909	774	747	780	973	926	810	570	852
889	1438	918		424	659	936	908	863	811	648	1002	911	778	753	783	975	926	813	568	855
919	1437	920		424	660	936	909	864	811	650	1005	913	782	753	785	977	928	817	573	860
949	1442	921		425	661	939	910	865	813	654	1006	914	782	754	787	979	931	821	573	862
979	1442	923		424	664	939	913	868	815	655	1007	915	780	756	791	982	933	825	578	867
1039	1417	923		429	667	941	916	871	819	657	1010	918	790	768	794	984	933	828	583	870
1069	1157	891		417	653	910	899	851	801	637	986	894	774	754	778	956	912	821	581	860
1100	916	780		389	601	802	824	773	735	586	893	812	718	701	716	862	826	780	548	813
1130	681	667		352	533	690	733	683	656	524	789	720	646	628	645	759	734	728	502	755
1190	435	498		286	414	520	581	539	523	410	617	578	524	499	521	596	595	633	413	652
1251	322	397		236	330	415	475	440	428	327	504	481	434	405	430	489	506	557	346	571
1311	259	329		201	271	345	404	374	363	268	425	411	364	341	363	413	442	494	296	502
1372	218	280		177	227	294	349	323	312	224	364	358	310	289	311	355	389	439	258	444
1433	189	244		158	197	255	307	283	272	193	318	316	267	250	271	307	349	394	229	398
1493	170	215	↓	144	174	225	271	251	240	170	282	283	233	221	238	271	314	354	207	357

[d] Intermittent short in thermocouple.

[e] Readings low and erratic.

TABLE VIII.- MEASURED VALUES OF LOAD, STRAIN, TEMPERATURE, AND DEFLECTION FOR 1,600° F TEST - Continued

(c) Third heating cycle: 1 top skin thermocouple, 36 bottom skin thermocouples, 57 right longitudinal spar cap thermocouples - Continued

Time, sec	Temperature, °F, at -																		
	TC 78	TC 79	TC 80	TC 81	TC 82	TC 83	TC 84	TC 85	TC 86	TC 87	TC 88	TC 89	TC 90	TC 91	TC 92	TC 93	TC 94	TC 310	TC 311	TC 312
0	77	77	77	77	76	77	77	77	77	77	77	77	76	76	77	77	77	76	77	78
30	80	79	79	79	78	80	79	77	78	78	77	77	78	78	78	79	77	76	77	78
60	94	93	89	91	89	95	91	80	83	82	78	79	81	83	84	85	80	76	77	78
90	132	124	105	115	106	131	117	89	94	90	80	85	90	95	100	101	88	77	77	79
121	225	191	131	164	135	210	175	110	120	109	84	100	108	124	137	139	107	77	78	81
151	420	319	175	261	188	359	295	157	177	148	93	126	146	180	211	213	145	79	80	87
181	618	468	229	376	252	527	440	220	255	204	108	152	192	243	291	293	188	81	83	98
251	813	686	354	584	391	750	635	367	430	333	152	211	295	369	444	442	287	91	95	154
312	867	769	445	690	481	828	702	480	531	417	201	257	367	445	524	524	368	95	101	184
372	899	817	517	753	555	874	745	572	596	478	261	304	423	495	573	575	440	104	113	237
399	912	831	546	772	588	889	757	604	615	499	292	321	441	513	588	591	468	109	119	262
414	918	839	563	782	605	895	764	621	626	507	311	332	451	522	597	598	483	110	122	275
429	923	847	581	790	620	902	773	637	635	518	321	340	461	531	603	605	496	113	127	287
499	943	872	646	824	688	926	807	692	669	562	407	375	496	563	625	628	548	123	144	344
559	956	889	691	842	734	941	826	725	687	588	459	397	519	579	641	647	578	135	161	387
619	968	903	727	856	764	951	842	749	704	612	502	416	537	599	650	658	598	143	177	416
649	972	908	741	864	777	956	848	757	709	622	522	422	541	601	658	662	608	149	186	437
679	975	910	750	865	784	958	854	765	713	628	539	425	544	604	661	667	615	153	194	447
709	978	914	758	865	792	960	858	769	718	635	555	430	547	605	666	673	621	158	203	460
739	981	916	765	871	796	962	861	776	721	643	569	432	552	612	668	677	625	163	210	470
799	986	917	772	873	806	964	865	784	728	654	593	442	562	620	671	682	632	172	227	489
829	987	921	778	874	808	964	868	788	731	657	601	442	567	623	673	683	632	177	235	498
859	990	922	780	876	812	967	870	792	733	660	608	445	569	625	674	683	636	181	242	505
889	991	924	784	877	813	967	870	795	736	664	616	449	573	628	675	685	636	186	250	512
919	994	926	786	879	814	968	875	796	738	668	622	451	575	631	676	686	640	190	259	518
949	994	928	788	880	816	969	875	799	740	671	627	454	575	628	679	690	644	195	267	524
979	997	931	790	884	819	972	879	802	743	674	631	458	577	631	679	690	643	198	273	529
1039	1000	931	792	885	820	973	879	806	747	679	641	459	580	635	686	696	656	205	287	537
1069	973	917	788	875	817	958	865	800	737	672	640	451	571	620	668	677	646	208	292	539
1100	878	852	769	813	793	881	803	760	690	641	632	430	538	579	622	626	619	210	297	537
1130	778	773	735	739	755	795	734	703	625	596	615	406	494	516	556	563	574	211	300	530
1190	625	641	649	612	667	656	623	587	504	502	567	354	406	413	441	449	477	210	301	510
1251	528	554	572	522	586	563	545	492	413	424	509	307	335	331	356	364	399	208	302	480
1311	456	489	505	452	513	491	483	418	345	358	455	272	285	282	291	302	339	205	300	455
1372	402	437	450	400	455	438	436	362	295	306	402	239	246	242	245	256	294	201	296	426
1433	357	393	404	357	407	391	395	317	257	267	358	215	216	211	210	221	257	196	291	398
1493	320	357	364	319	363	353	360	281	227	235	317	195	194	188	185	195	230	193	285	375

TABLE VIII.- MEASURED VALUES OF LOAD, STRAIN, TEMPERATURE, AND DEFLECTION FOR 1,600° F TEST - Continued

(c) Third heating cycle: 1 top skin thermocouple, 36 bottom skin thermocouples, 57 right longitudinal spar cap thermocouples - Continued

Time, sec	Temperature, °F, at -																			
	TC 141	TC 142	TC 143	TC 144	TC 145	TC 146	TC 147	TC 148	TC 149	TC 150	TC 151	TC 152	TC 153	TC 154	TC 155	TC 156 (e)	TC 307	TC 308	TC 309	TC 163
0	78	77	78	78	78	78	78	78	78	78	78	77	77	77	78	76	76	77	77	77
30	77	78	78	78	78	78	78	78	78	78	78	77	77	77	78	76	76	76	78	77
60	79	80	80	79	79	79	79	79	79	79	80	79	78	79	78	77	76	77	78	78
90	84	90	86	86	85	86	87	85	83	85	84	84	81	85	81	77	76	77	78	80
121	96	119	104	107	105	107	108	105	94	104	94	99	89	102	88	77	76	77	79	87
151	125	180	145	160	156	160	163	155	122	153	117	137	108	144	105	77	76	78	80	100
181	172	262	199	248	241	246	248	236	172	234	159	203	142	224	142	77	77	79	82	118
251	328	499	372	505	495	492	496	472	346	472	321	424	292	499	313	86	77	81	90	165
312	472	688	546	718	708	701	702	667	523	669	495	621	467	738	509	224	78	84	99	204
372	595	822	706	874	866	858	851	817	687	822	663	779	645	906	693	596	79	87	109	241
399	638	863	765	922	916	908	898	865	748	872	727	834	715	958	761	702	80	89	115	256
414	660	882	795	945	939	932	920	889	780	897	761	861	752	981	795	741	80	89	116	264
429	680	899	822	964	960	953	940	910	809	920	792	886	787	1001	827	775	81	91	119	272
499	753	952	916	1025	1025	1020	1004	981	912	996	906	973	914	1066	941	894	82	95	130	306
559	793	976	965	1053	1055	1050	1033	1015	969	1034	971	1019	986	1098	1003	962	84	100	141	329
619	820	989	995	1070	1072	1069	1051	1035	1004	1059	1014	1050	1032	1119	1043	1007	85	104	152	350
649	829	994	1005	1076	1079	1075	1058	1043	1017	1069	1029	1062	1048	1127	1058	1024	86	106	157	359
679	837	998	1013	1080	1084	1080	1063	1048	1027	1076	1042	1072	1061	1134	1071	1038	86	108	162	367
709	844	1001	1019	1084	1088	1084	1068	1053	1035	1083	1052	1080	1072	1139	1081	1050	87	110	166	375
739	849	1003	1024	1088	1091	1088	1071	1058	1041	1088	1060	1087	1080	1143	1089	1059	88	113	171	382
799	858	1007	1031	1094	1097	1094	1077	1065	1051	1097	1073	1097	1092	1148	1101	1074	90	117	180	394
829	861	1008	1034	1095	1099	1096	1080	1067	1055	1101	1078	1101	1097	1150	1106	1079	90	119	184	399
859	864	1010	1036	1098	1101	1099	1082	1070	1059	1105	1083	1106	1101	1152	1109	1085	91	121	187	404
889	867	1011	1038	1099	1103	1101	1084	1072	1062	1108	1087	1110	1104	1153	1112	1089	92	123	190	409
919	869	1012	1040	1101	1105	1102	1086	1074	1065	1110	1090	1113	1107	1154	1115	1093	92	125	194	412
949	870	1013	1042	1103	1106	1104	1088	1076	1068	1113	1093	1116	1109	1156	1117	1097	93	127	197	416
979	872	1015	1043	1104	1109	1106	1090	1078	1070	1115	1096	1118	1112	1158	1120	1101	94	129	200	419
1039	875	1017	1047	1108	1112	1110	1094	1082	1075	1121	1102	1123	1116	1162	1125	1107	95	133	205	425
1069	871	1005	1042	1100	1106	1103	1086	1075	1073	1117	1101	1120	1116	1159	1125	1109	96	135	208	425
1100	855	970	1022	1065	1076	1073	1053	1043	1056	1086	1084	1093	1104	1131	1114	1099	97	136	210	416
1130	826	919	989	1009	1023	1022	999	991	1022	1033	1050	1045	1075	1076	1085	1051	97	137	209	401
1190	746	805	893	881	897	898	875	873	921	912	950	941	982	946	990	948	97	137	203	367
1251	663	706	793	773	787	788	769	771	818	809	847	831	883	836	892	815	98	137	196	334
1311	589	627	702	684	696	698	682	687	728	724	755	748	795	750	806	690	98	137	190	304
1372	524	551	625	612	622	624	611	618	652	654	677	680	718	680	734	598	98	137	182	278
1433	469	505	559	552	561	562	552	560	586	596	611	622	653	622	672	502	97	136	177	255
1493	424	457	503	501	509	509	501	510	530	546	553	573	598	572	619	424	97	134	171	234

[e]Readings low and erratic.

TABLE VIII.- MEASURED VALUES OF LOAD, STRAIN, TEMPERATURE, AND DEFLECTION FOR 1,600° F TEST - Continued

(c) Third heating cycle: 1 top skin thermocouple, 36 bottom skin thermocouples, 57 right longitudinal spar cap thermocouples - Continued

Time, sec	Temperature, °F, at -																			
	TC 164	TC 165	TC 166	TC 167	TC 168	TC 169	TC 170	TC 171	TC 172	TC 173	TC 174	TC 175	TC 176	TC 177	TC 184	TC 185	TC 186	TC 187	TC 188	TC 189
0	77	77	78	77	77	77	77	77	78	77	77	77	77	78	78	77	78	78	78	78
30	77	77	78	77	77	78	77	77	77	77	77	77	77	77	78	78	79	78	78	78
60	78	77	79	78	79	79	78	78	79	78	79	78	79	78	83	85	85	83	80	81
90	82	80	82	81	81	84	83	81	83	81	83	80	84	80	99	108	106	100	89	93
121	92	87	92	90	91	98	95	89	93	87	95	87	97	84	140	169	161	145	119	127
151	115	103	113	110	110	127	123	109	121	103	124	104	129	98	239	306	280	251	194	202
181	147	125	144	140	140	169	163	140	164	132	171	134	184	123	373	450	414	386	307	298
251	234	193	240	231	234	289	282	238	297	235	315	241	355	222	666	719	690	665	579	542
312	311	258	336	323	327	400	395	333	422	342	446	353	513	330	856	892	868	846	778	732
372	382	323	428	412	420	504	502	428	538	451	570	467	663	445	983	1016	993	972	923	863
399	409	350	465	448	458	544	544	467	584	497	619	513	720	494	1022	1055	1033	1013	970	904
414	424	365	486	468	479	567	567	489	609	523	646	542	750	522	1041	1074	1052	1032	992	925
429	438	380	505	487	499	588	588	510	632	548	671	569	778	549	1057	1089	1068	1048	1012	942
499	494	445	584	566	582	668	674	599	725	653	774	681	884	667	1108	1143	1121	1102	1073	997
559	532	493	635	620	638	720	727	661	785	728	841	760	946	752	1133	1168	1147	1128	1102	1022
619	560	534	674	660	681	758	767	713	830	789	891	824	987	821	1149	1184	1164	1145	1120	1038
649	572	552	688	677	699	773	784	734	849	814	912	849	1003	849	1154	1189	1169	1150	1127	1044
679	583	568	701	691	714	785	796	753	864	836	929	872	1015	874	1158	1193	1173	1155	1131	1048
709	592	582	712	703	727	796	808	770	878	855	944	891	1025	896	1161	1196	1177	1158	1135	1052
739	599	594	722	714	738	806	818	785	890	872	956	907	1032	913	1165	1200	1180	1161	1139	1055
799	610	615	739	730	756	820	833	809	908	898	976	934	1042	941	1170	1205	1185	1166	1144	1061
829	614	623	743	737	763	825	839	819	916	908	983	944	1046	952	1172	1207	1187	1168	1147	1063
859	619	631	748	743	769	831	843	827	922	917	990	953	1050	961	1174	1209	1189	1170	1148	1065
889	622	638	753	748	775	835	848	835	928	925	995	960	1052	968	1176	1211	1191	1172	1150	1067
919	624	644	756	752	780	838	853	841	932	932	1000	966	1054	974	1178	1213	1193	1174	1152	1069
949	627	649	760	756	784	842	855	846	936	937	1004	971	1056	979	1180	1215	1194	1175	1154	1070
979	627	655	766	762	789	845	860	851	939	942	1008	976	1058	984	1182	1218	1197	1178	1156	1073
1039	632	663	770	767	795	851	867	860	947	951	1015	984	1063	992	1186	1222	1201	1182	1160	1076
1069	631	662	765	763	791	844	862	858	946	953	1013	983	1062	994	1177	1206	1186	1171	1154	1061
1100	618	652	741	745	773	819	838	843	923	940	992	971	1040	986	1126	1145	1130	1122	1116	1014
1130	593	632	707	714	741	778	798	815	884	911	953	945	998	964	1054	1066	1057	1054	1056	951
1190	524	577	623	633	659	682	702	742	788	835	859	875	894	899	911	919	915	913	922	827
1251	460	520	542	550	578	595	612	666	698	754	771	798	799	827	798	805	802	801	809	724
1311	404	467	473	479	505	519	535	597	620	679	693	725	719	760	708	713	712	711	718	641
1372	357	420	417	421	443	457	470	533	552	612	625	658	652	699	635	639	637	637	643	573
1433	319	378	369	371	393	405	418	479	495	552	566	599	595	645	575	577	575	575	581	516
1493	286	341	329	330	350	362	373	431	446	500	514	546	545	596	524	525	522	523	528	469

TABLE VIII.- MEASURED VALUES OF LOAD, STRAIN, TEMPERATURE, AND DEFLECTION FOR 1,600° F TEST - Continued

(c) Third heating cycle: 1 top skin thermocouple, 36 bottom skin thermocouples, 57 right longitudinal spar cap thermocouples - Concluded

Time, sec	Temperature, °F, at -													
	TC 190	TC 191	TC 192	TC 193	TC 194	TC 195	TC 196	TC 95	TC 97	TC 99	TC 101	TC 103	TC 105	TC 107
0	78	77	77	77	78	78	78	77	78	78	77	77	76	77
30	78	78	77	77	78	78	78	77	78	77	77	77	77	77
60	82	79	79	78	79	78	79	81	79	79	78	79	78	78
90	93	88	85	81	83	81	83	97	86	87	81	84	83	81
121	121	113	102	88	93	86	93	140	109	110	91	96	95	89
151	191	178	136	105	116	100	116	244	166	165	112	117	126	107
181	293	286	179	129	146	122	149	378	262	248	145	143	177	136
251	562	571	293	205	226	195	242	658	523	492	247	221	327	226
312	761	783	397	285	300	275	333	841	729	698	345	298	455	318
372	893	931	493	368	372	359	426	970	881	849	442	376	565	414
399	933	977	531	404	402	395	465	1011	931	898	480	410	607	454
414	952	999	552	423	419	415	488	1031	954	921	501	427	628	477
429	969	1018	571	442	433	434	509	1048	975	942	522	445	648	499
499	1020	1077	647	522	499	516	598	1103	1039	1006	604	518	726	591
559	1044	1105	695	578	547	574	658	1130	1070	1036	658	572	774	654
619	1059	1123	732	624	586	620	707	1147	1088	1054	700	613	809	703
649	1065	1129	746	642	600	639	727	1153	1095	1060	717	631	824	723
679	1069	1133	759	658	613	655	742	1157	1100	1065	731	645	836	740
709	1073	1137	769	672	626	668	756	1161	1104	1069	743	659	846	755
739	1076	1140	778	684	636	681	768	1164	1107	1073	754	670	855	767
799	1082	1146	794	703	651	700	787	1169	1114	1079	771	688	869	787
829	1084	1148	798	711	659	708	794	1171	1115	1082	778	695	875	795
859	1086	1150	805	718	664	715	800	1173	1118	1084	784	703	880	801
889	1088	1152	809	723	670	720	806	1175	1120	1086	789	708	883	807
919	1090	1154	812	728	675	725	811	1176	1121	1087	793	711	887	812
949	1091	1156	816	733	678	729	816	1178	1123	1089	798	716	891	817
979	1094	1158	821	738	684	735	820	1181	1125	1091	802	723	894	821
1039	1098	1162	825	744	689	741	827	1185	1129	1095	807	726	901	829
1069	1087	1157	815	741	681	737	823	1175	1124	1087	803	720	896	827
1100	1039	1120	785	727	658	725	801	1127	1093	1054	783	700	870	810
1130	972	1057	742	700	627	699	766	1059	1039	1000	749	671	824	782
1190	837	920	648	628	552	627	685	919	912	877	663	598	719	704
1251	728	806	563	552	481	552	607	806	801	768	580	524	626	625
1311	641	714	490	484	423	484	536	715	710	680	506	459	546	553
1372	571	640	430	426	371	427	476	641	635	608	445	405	482	490
1433	513	578	380	377	331	379	425	579	573	546	393	358	428	437
1493	465	526	340	337	296	339	380	526	520	495	350	320	382	391

TABLE VIII.- MEASURED VALUES OF LOAD, STRAIN, TEMPERATURE, AND DEFLECTION FOR 1,600° F TEST - Continued

(d) Fourth heating cycle: 1 top skin thermocouple, 18 left longitudinal spar cap thermocouples, 73 transverse frame cap thermocouples

Time, sec	Temperature, °F, at -																	
	TC 132	TC 301	TC 302	TC 303	TC 157	TC 158	TC 159	TC 160	TC 161	TC 162	TC 304	TC 305	TC 306	TC 179	TC 180	TC 181	TC 182	TC 183	TC 178
0	79	77	77	78	79	80	79	79	79	79	76	77	77	79	79	79	79	79	79
30	399	77	78	78	79	80	79	79	80	79	76	77	77	79	79	79	79	79	79
60	700	77	78	78	82	83	81	81	82	80	76	77	78	81	80	81	81	81	81
90	980	77	78	79	91	94	87	88	89	84	76	77	78	86	85	85	85	87	83
121	1279	78	79	81	120	126	108	107	110	95	76	77	79	99	97	97	99	102	93
151	1380	79	80	86	182	196	161	154	160	125	77	78	80	127	123	127	130	138	116
176	1390	81	82	93	251	277	232	217	232	171	77	79	82	157	152	166	169	186	149
236	1402	84	86	111	458	511	446	426	482	343	77	80	86	239	239	284	289	335	264
297	1414	93	96	160	662	744	665	646	741	540	78	83	97	323	339	414	421	502	397
357	1416	102	109	204	813	912	838	818	921	711	79	87	107	399	437	537	549	658	531
385	1417	106	113	224	860	965	896	877	975	774	80	89	111	430	479	588	603	720	588
400	1417	107	116	232	881	988	923	905	998	803	81	90	113	445	501	614	631	751	617
415	1417	109	120	244	900	1009	947	930	1018	831	81	91	115	460	522	639	657	781	646
430	1417	113	124	258	916	1025	968	952	1035	855	81	92	119	475	542	662	682	808	673
485	1420	121	137	296	958	1068	1025	1013	1082	928	83	96	128	518	608	738	765	893	763
545	1421	130	152	339	983	1094	1064	1056	1115	983	84	100	138	555	664	803	835	958	840
605	1421	138	167	375	997	1111	1088	1085	1137	1021	85	104	148	584	708	853	889	1002	899
635	1424	143	175	392	1001	1116	1097	1095	1145	1035	86	106	153	594	725	872	910	1017	921
665	1425	147	183	406	1005	1120	1104	1104	1151	1047	87	108	157	603	739	889	928	1030	941
695	1429	152	191	419	1008	1124	1110	1111	1156	1057	88	110	162	612	750	903	942	1040	957
726	1428	157	199	433	1010	1127	1116	1118	1161	1066	89	113	165	618	761	915	955	1047	970
786	1430	165	213	458	1014	1133	1125	1128	1166	1079	90	117	175	630	778	935	975	1058	991
816	1431	169	223	468	1016	1135	1129	1133	1168	1084	91	119	179	634	784	942	984	1062	998
846	1432	174	230	478	1017	1137	1132	1137	1169	1088	92	121	183	637	789	948	991	1066	1004
877	1432	177	239	488	1018	1139	1135	1140	1171	1091	93	123	186	640	795	954	996	1068	1008
907	1437	181	245	494	1019	1141	1138	1144	1173	1095	93	125	190	642	799	958	1002	1070	1013
937	1437	185	253	502	1021	1143	1141	1147	1174	1098	94	127	193	644	803	963	1007	1072	1016
967	1433	189	259	507	1022	1144	1143	1149	1175	1100	95	129	196	647	806	967	1010	1075	1020
1028	1429	196	274	520	1025	1148	1148	1154	1179	1106	97	133	201	651	812	974	1017	1079	1026
1058	1253	200	281	525	1021	1145	1149	1155	1179	1108	97	135	202	651	813	975	1019	1079	1028
1088	988	202	287	525	995	1119	1128	1136	1160	1099	98	136	204	637	799	961	1006	1066	1021
1119	751	203	292	522	949	1067	1078	1090	1107	1068	98	137	203	611	771	925	973	1028	997
1179	458	205	297	503	834	932	951	968	972	966	99	138	198	537	686	824	881	923	919
1240	333	206	298	480	731	812	838	857	855	866	99	137	193	467	600	728	789	824	836
1301	262	204	297	453	648	715	747	768	763	784	99	137	186	408	522	645	708	739	760
1361	219	202	295	429	580	638	671	694	688	714	98	136	180	360	457	574	637	667	693
1422	191	199	291	403	522	575	610	634	627	656	98	135	174	319	404	515	577	607	637
1483	171	196	286	380	473	520	556	581	575	607	98	134	169	286	359	464	523	553	588

TABLE VIII.- MEASURED VALUES OF LOAD, STRAIN, TEMPERATURE, AND DEFLECTION FOR 1,600° F TEST - Continued

(d) Fourth heating cycle: 1 top skin thermocouple, 18 left longitudinal spar cap thermocouples, 73 transverse frame cap thermocouples - Continued

Time, sec	Temperature, °F, at -																		
	TC 202	TC 203	TC 204	TC 205	TC 206	TC 207	TC 208	TC 209	TC 216	TC 217	TC 218	TC 219	TC 221	TC 222	TC 223	TC 224	TC 231	TC 232	TC 233	TC 234
0	78	80	79	78	79	79	79	79	79	80	79	79	80	79	79	79	79	79	79	79
30	80	82	80	76	79	80	81	86	92	86	85	85	85	81	79	80	79	79	79	79
60	109	103	99	78	79	82	99	119	139	112	121	123	113	104	84	84	81	79	81	80
90	180	149	155	86	82	92	138	189	226	164	195	203	174	161	94	97	88	81	88	85
121	309	232	264	107	89	123	211	312	366	258	318	338	284	268	129	132	104	83	104	96
151	535	364	468	161	103	197	249	527	587	419	509	545	462	464	208	213	139	90	136	117
176	760	482	692	221	116	287	514	739	769	565	669	710	622	674	305	304	176	100	167	137
236	1021	681	996	360	152	502	843	1041	1016	829	912	950	897	1013	541	508	273	134	242	190
297	1085	775	1085	464	186	663	996	1127	1100	970	1004	1043	1039	1137	717	661	365	178	312	241
357	1108	818	1119	527	211	760	1059	1158	1135	1051	1042	1079	1125	1187	821	761	443	228	369	286
385	1114	829	1127	548	221	788	1075	1165	1145	1077	1052	1088	1152	1201	851	792	472	252	392	303
400	1116	835	1130	555	226	800	1083	1168	1149	1090	1056	1091	1166	1206	865	806	487	264	401	312
415	1118	839	1133	562	231	810	1088	1170	1153	1102	1061	1095	1179	1211	876	819	501	277	412	320
430	1120	843	1135	568	236	819	1094	1173	1158	1114	1064	1098	1190	1215	886	830	514	289	421	328
485	1128	854	1143	585	251	843	1107	1179	1169	1148	1075	1107	1224	1226	912	861	557	330	449	352
545	1134	861	1148	597	268	858	1117	1186	1177	1175	1082	1112	1248	1233	930	882	593	368	467	376
605	1138	865	1152	604	282	867	1124	1191	1181	1192	1088	1117	1262	1237	941	895	619	404	489	391
635	1138	867	1154	607	285	871	1126	1192	1183	1198	1089	1117	1267	1237	944	899	629	419	498	399
665	1139	869	1155	609	289	873	1127	1192	1183	1202	1091	1119	1271	1238	948	903	639	433	503	406
695	1140	870	1156	611	294	875	1128	1192	1185	1205	1092	1120	1273	1239	950	904	646	444	506	410
726	1142	872	1157	611	300	877	1129	1194	1186	1208	1094	1121	1275	1240	952	907	653	455	507	414
786	1144	874	1158	616	303	881	1131	1196	1189	1212	1097	1123	1280	1241	955	912	666	474	515	421
816	1144	876	1159	616	307	882	1132	1198	1191	1214	1098	1125	1282	1242	957	914	671	480	515	423
846	1144	876	1159	616	311	883	1132	1198	1192	1215	1098	1125	1283	1242	958	915	676	488	518	427
877	1145	877	1161	619	312	885	1133	1200	1194	1217	1099	1126	1285	1243	960	918	681	494	520	428
907	1146	877	1161	620	315	886	1134	1201	1196	1219	1100	1127	1287	1244	961	919	686	499	521	430
937	1147	879	1162	621	314	887	1134	1202	1198	1220	1102	1129	1289	1246	963	921	689	505	526	432
967	1148	880	1163	622	320	888	1136	1203	1198	1222	1103	1130	1290	1247	964	922	691	510	529	434
1028	1152	882	1167	626	327	892	1140	1207	1203	1226	1106	1131	1294	1251	968	927	697	517	527	441
1058	1148	873	1164	625	327	890	1138	1202	1197	1222	1091	1112	1288	1247	966	925	697	519	524	440
1088	1096	827	1091	599	320	857	1079	1137	1126	1177	1017	1031	1239	1181	932	889	679	518	504	428
1119	942	760	971	551	305	793	970	1012	1004	1088	912	925	1153	1068	865	822	639	511	474	407
1179	706	615	742	454	271	659	743	763	778	897	706	723	970	839	719	681	547	482	399	360
1240	549	500	584	380	236	553	586	594	625	750	559	575	828	675	604	568	466	441	334	315
1301	443	414	473	327	208	472	478	478	516	640	457	469	718	556	516	483	402	397	283	274
1361	369	349	391	287	187	408	402	397	435	553	382	392	627	466	447	417	350	356	244	240
1422	314	300	329	255	169	358	345	336	373	483	327	334	555	397	393	365	308	319	214	215
1483	272	261	283	231	156	316	301	290	325	427	285	289	495	343	349	323	275	288	191	195

TABLE VIII.- MEASURED VALUES OF LOAD, STRAIN, TEMPERATURE, AND DEFLECTION FOR 1,600° F TEST - Continued

(d) Fourth heating cycle: 1 top skin thermocouple, 18 left longitudinal spar cap thermocouples, 73 transverse frame cap thermocouples - Continued

Time, sec	Temperature, °F, at -																		
	TC 236	TC 210	TC 211	TC 113	TC 243	TC 212	TC 213	TC 214	TC 114	TC 220	TC 215	TC 225	TC 226	TC 115	TC 251	TC 227	TC 228	TC 229	TC 116	TC 235
0	79	80	79	79	78	79	82	80	79	79	79	79	78	78	79	79	79	79	78	79
30	79	127	142	89	84	81	154	163	100	85	81	79	79	78	80	80	79	79	78	79
60	83	212	248	125	112	96	263	287	156	113	98	81	81	81	82	83	82	84	81	82
90	95	338	399	197	172	139	414	453	250	172	142	88	86	89	90	95	89	97	91	92
121	132	525	617	315	276	224	627	686	399	281	232	103	100	109	112	123	108	130	113	117
151	222	791	909	520	464	395	896	971	626	470	407	136	130	157	162	189	147	200	163	173
176	333	963	1066	720	668	597	1043	1103	811	669	607	177	171	216	224	261	192	272	219	238
236	599	1161	1219	1016	988	934	1204	1231	1059	976	932	307	298	375	389	438	318	430	361	390
297	781	1223	1264	1110	1091	1043	1254	1272	1139	1074	1035	441	431	520	537	586	443	555	486	517
357	884	1245	1282	1145	1128	1084	1272	1286	1166	1108	1072	554	544	632	650	693	541	645	584	613
385	913	1251	1286	1154	1137	1095	1275	1289	1173	1117	1081	595	586	671	689	729	577	677	619	646
400	926	1253	1288	1158	1142	1100	1277	1291	1176	1121	1085	615	606	690	708	747	594	691	635	662
415	937	1256	1289	1161	1145	1105	1279	1292	1178	1124	1089	633	624	707	724	763	610	706	650	677
430	947	1257	1291	1164	1149	1109	1279	1293	1180	1127	1092	649	641	722	740	777	624	718	663	690
485	970	1263	1296	1174	1159	1121	1284	1296	1188	1136	1102	697	688	768	785	818	663	754	702	728
545	986	1269	1301	1182	1168	1131	1289	1301	1195	1144	1110	733	725	803	819	850	693	782	732	758
605	995	1275	1305	1188	1175	1138	1291	1302	1198	1150	1117	756	748	825	841	871	714	802	753	778
635	999	1275	1305	1190	1177	1140	1291	1303	1199	1151	1118	764	756	833	849	879	722	808	761	785
665	1001	1276	1305	1191	1178	1142	1291	1302	1200	1152	1119	771	762	839	856	884	728	814	767	791
695	1002	1276	1305	1192	1179	1143	1292	1303	1201	1153	1120	776	768	845	861	889	732	817	771	795
726	1004	1276	1305	1193	1181	1145	1293	1304	1202	1154	1122	781	773	850	866	895	735	822	775	800
786	1008	1278	1307	1195	1183	1148	1295	1306	1205	1157	1124	789	781	858	874	902	744	829	783	807
816	1010	1281	1311	1198	1185	1150	1298	1310	1207	1159	1126	793	784	861	878	906	747	832	786	810
846	1011	1282	1311	1199	1187	1150	1300	1312	1209	1161	1128	796	788	865	881	909	749	835	789	813
877	1013	1284	1314	1201	1189	1154	1303	1315	1211	1163	1130	798	790	867	884	912	752	838	792	816
907	1015	1286	1314	1203	1191	1155	1305	1316	1213	1165	1132	801	792	870	887	915	755	841	796	819
937	1016	1287	1316	1204	1192	1157	1306	1317	1214	1166	1133	803	795	872	889	916	758	843	798	822
967	1017	1288	1317	1206	1193	1158	1307	1318	1215	1167	1135	805	796	875	891	918	760	846	800	824
1028	1021	1293	1322	1209	1197	1162	1311	1322	1219	1171	1138	809	800	880	896	924	763	850	805	828
1058	1019	1280	1305	1206	1194	1159	1292	1302	1212	1167	1135	810	801	880	895	922	764	848	804	828
1088	982	1162	1168	1140	1136	1107	1152	1152	1131	1109	1083	794	786	854	868	888	745	813	780	801
1119	908	1003	991	1021	1022	1003	986	977	1001	997	981	755	749	799	811	821	705	750	729	745
1179	753	730	701	786	792	788	720	705	764	777	773	653	649	673	681	683	604	618	614	620
1240	630	557	525	619	627	631	554	538	601	618	620	556	554	566	573	572	511	514	515	518
1301	537	442	412	501	510	517	442	426	487	506	510	477	475	482	487	487	437	436	439	440
1361	465	363	336	417	426	435	363	349	406	424	429	414	412	415	421	421	378	376	378	380
1422	408	306	282	354	362	372	307	294	345	362	367	362	361	363	368	368	331	328	330	331
1483	361	263	242	306	313	324	265	253	298	314	318	321	320	321	325	326	293	291	293	294

TABLE VIII.- MEASURED VALUES OF LOAD, STRAIN, TEMPERATURE, AND DEFLECTION FOR 1,600° F TEST - Continued

(d) Fourth heating cycle: 1 top skin thermocouple, 18 left longitudinal spar cap thermocouples, 73 transverse frame cap thermocouples - Continued

Time, sec	Temperature, °F, at -																		
	TC 230	TC 237	TC 238	TC 239	TC 240	TC 241	TC 242	TC 244	TC 245	TC 246	TC 247	TC 248	TC 249	TC 250	TC 252	TC 253	TC 254	TC 255	TC 256	TC 257
0	79	79	79	78	79	79	79	79	79	78	79	79	79	79	79	79	79	79	80	78
30	79	81	87	94	89	88	84	82	79	79	80	79	79	79	80	81	83	82	80	79
60	81	103	123	140	117	124	117	105	83	82	82	79	81	81	83	102	106	112	82	81
90	88	149	195	222	164	192	186	164	92	91	88	80	88	87	96	151	151	184	91	87
121	105	231	317	354	243	306	308	279	119	118	102	83	106	102	130	242	231	317	114	103
151	141	377	521	565	374	497	505	486	186	181	136	92	144	133	216	410	376	547	174	141
176	185	546	714	746	501	671	677	702	274	258	178	104	187	169	321	602	523	773	254	186
236	312	857	1005	996	745	933	938	1037	501	456	300	145	298	265	592	629	796	1101	473	314
297	436	1000	1105	1082	884	1030	1038	1162	683	619	425	203	408	360	801	1057	922	1218	655	438
357	533	1062	1143	1119	965	1073	1079	1217	802	734	537	275	503	446	925	1108	983	1266	777	547
385	569	1079	1153	1130	993	1084	1090	1232	838	772	581	309	540	480	961	1122	1000	1279	816	588
400	586	1086	1158	1135	1007	1090	1096	1238	853	790	603	327	557	497	976	1129	1008	1284	833	608
415	601	1093	1162	1140	1020	1095	1100	1243	867	805	623	345	574	513	989	1135	1015	1289	848	627
430	615	1099	1165	1145	1032	1100	1104	1249	879	819	641	363	589	527	1000	1140	1022	1294	861	644
485	653	1116	1174	1160	1069	1117	1117	1263	911	868	697	426	634	573	1031	1157	1042	1308	899	697
545	683	1130	1186	1173	1095	1128	1126	1272	935	888	742	489	670	613	1050	1172	1058	1320	928	740
605	703	1138	1192	1182	1113	1136	1134	1279	950	906	775	542	697	639	1053	1183	1070	1329	948	769
635	710	1140	1194	1186	1120	1140	1137	1281	955	913	788	566	708	652	1068	1187	1075	1332	955	780
665	716	1142	1195	1188	1125	1143	1140	1283	960	919	799	588	717	661	1071	1189	1079	1335	961	792
695	720	1143	1196	1190	1128	1145	1142	1284	963	923	808	605	723	667	1074	1192	1082	1337	966	798
726	724	1145	1199	1193	1132	1147	1145	1287	966	928	817	620	728	675	1077	1195	1086	1339	972	806
786	732	1149	1203	1197	1137	1151	1149	1290	972	935	831	645	738	686	1082	1201	1092	1344	980	818
816	735	1150	1206	1200	1140	1154	1150	1292	974	937	836	655	743	693	1084	1203	1096	1346	984	825
846	738	1151	1207	1203	1143	1154	1151	1293	976	940	841	665	747	697	1087	1204	1097	1348	987	828
877	740	1152	1209	1205	1145	1156	1152	1295	978	943	846	673	750	700	1089	1206	1099	1350	990	831
907	742	1153	1210	1208	1148	1159	1154	1296	980	945	849	679	752	705	1091	1208	1102	1353	993	837
937	745	1154	1212	1210	1151	1161	1157	1297	982	947	852	685	755	708	1092	1210	1105	1354	995	840
967	747	1155	1213	1212	1153	1162	1158	1300	983	949	856	691	758	708	1094	1211	1106	1355	998	843
1028	751	1161	1217	1216	1158	1167	1161	1304	988	954	862	701	764	716	1099	1217	1114	1360	1002	848
1058	751	1158	1213	1208	1154	1160	1148	1301	987	953	826	703	762	716	1097	1214	1111	1357	1002	848
1088	735	1093	1146	1132	1102	1097	1082	1234	955	922	844	702	738	697	1059	1150	1057	1279	973	830
1119	697	976	1017	1010	1010	986	983	1118	890	862	800	691	694	661	984	1032	952	1155	914	787
1179	598	742	764	791	835	769	786	884	747	727	691	645	588	568	822	796	746	916	784	677
1240	506	587	598	639	705	618	641	714	632	615	593	585	493	483	694	640	602	751	677	577
1301	433	483	486	531	603	510	534	592	544	527	511	524	417	412	598	536	503	635	593	493
1361	375	410	407	450	522	431	452	502	475	458	446	466	356	355	521	461	431	547	523	423
1422	328	355	349	388	459	371	390	433	420	404	394	417	309	309	460	404	376	478	466	368
1483	291	313	305	339	408	324	339	379	374	360	350	374	272	272	410	359	332	423	419	325

TABLE VIII.- MEASURED VALUES OF LOAD, STRAIN, TEMPERATURE, AND DEFLECTION FOR 1,600° F TEST - Concluded

(d) Fourth heating cycle: 1 top skin thermocouple, 18 left longitudinal spar cap thermocouples, 73 transverse frame cap thermocouples - Concluded

Time, sec	Temperature, °F, at -												
	TC 258	TC 259	TC 260	TC 261	TC 262	TC 263	TC 264	TC 265	TC 266	TC 267	TC 268	TC 269	TC 270
0	79	80	79	(a)	79	79	79	79	78	79	79	79	79
30	79	81	86		79	79	79	82	79	83	80	80	79
60	82	98	108		82	82	82	102	96	105	81	82	82
90	92	140	148		90	89	91	152	129	159	87	91	89
121	120	216	218		113	106	116	250	188	258	102	111	108
151	191	350	335		164	144	176	414	292	431	135	157	149
176	285	500	459		226	191	251	595	415	613	180	215	200
236	538	803	717		401	332	463	904	677	913	312	381	349
297	744	963	873		568	474	656	1042	819	1051	447	544	503
357	875	1037	961	↓	697	596	794	1107	1001	1113	566	677	629
385	915	1057	986	1119	742	641	838	1128	1024	1131	612	725	676
400	933	1066	997	1145	763	664	858	1137	1035	1140	635	748	700
415	948	1073	1008	1147	783	684	876	1146	1044	1148	657	769	722
430	962	1080	1018	1139	800	704	893	1153	1053	1156	678	788	742
485	1000	1104	1048	1120	852	764	940	1179	1082	1181	745	846	808
545	1027	1121	1070	1135	892	811	976	1200	1103	1200	801	891	862
605	1045	1134	1084	1151	920	843	1000	1215	1117	1215	843	921	904
635	1051	1137	1086	1164	930	855	1009	1221	1121	1219	860	933	918
665	1057	1139	1090	1173	939	865	1016	1226	1125	1223	874	943	930
695	1061	1142	1093	1177	946	873	1022	1230	1129	1227	886	950	941
726	1065	1144	1097	1177	952	881	1027	1233	1131	1229	898	956	951
786	1073	1150	1103	1191	963	893	1035	1238	1135	1234	915	965	965
816	1076	1153	1106	1193	967	898	1039	1240	1136	1235	922	968	970
846	1079	1154	1106	1200	971	901	1042	1242	1136	1235	927	971	975
877	1081	1154	1106	1203	974	906	1045	1243	1136	1236	931	973	979
907	1084	1157	1107	1206	977	910	1047	1244	1137	1238	936	976	981
937	1086	1158	1107	1216	980	912	1049	1246	1138	1239	939	979	985
967	1088	1159	1108	1222	982	914	1051	1248	1139	1241	942	980	987
1028	1092	1164	1113	1227	987	919	1056	1252	1143	1247	948	985	993
1058	1092	1162	1112	1219	986	919	1055	1250	1140	1244	950	985	993
1088	1059	1118	1069	1156	965	901	1032	1205	1097	1194	936	966	978
1119	993	1021	975	1058	918	860	977	1114	994	1086	903	919	940
1179	844	814	777	880	805	753	848	923	785	870	813	805	842
1240	723	668	638	739	706	654	738	789	644	726	729	704	733
1301	629	568	539	623	627	571	651	692	546	623	658	623	677
1361	544	493	463	527	562	502	581	617	473	547	597	557	614
1422	493	436	405	447	506	444	521	555	412	488	543	500	559
1483	442	391	358	382	459	397	471	503	359	439	495	452	511

[a]Intermittent short in thermocouple.

TABLE IX.- MEASURED VALUES OF LONGITUDINAL SPAR-CAP LOAD, STRAIN, AND TEMPERATURE FOR 1,000° F TEST

[2 loads; 6 strain gages; 22 thermocouples. SG (strain gage) readings are corrected for temperature, microinches/inch; TC (thermocouple) readings are temperatures, °F]

Time, sec	Total load, lb	Right load, lb	SG 95	SG 99	SG 101	SG 103	SG 105	SG 107	TC 95	TC 99	TC 101	TC 103	TC 105	TC 107	TC 184	TC 185
0	0	0	-21	-21	-18	-15	-18	-15	84	86	85	83	83	83	80	81
66	-69	-38	-15	6	-21	-18	-18	-6	89	88	86	85	85	85	87	90
126	-95	-52	-29	107	-31	-24	-38	11	128	107	93	92	97	93	127	138
196	-47	-24	-47	217	-42	-35	-59	30	192	151	108	104	119	106	192	203
257	-81	-40	-46	264	-41	-31	-65	50	244	196	123	116	139	120	245	254
317	-24	-13	-21	295	-37	-33	-101	55	292	240	137	128	158	135	293	301
453	2659	1314	295	426	-128	-299	-213	-183	378	328	169	155	199	169	380	388
483	3633	1798	399	468	-162	-397	-249	-273	394	345	176	161	207	176	397	405
511	4634	2290	506	510	-195	-498	-286	-367	409	359	182	166	215	183	411	419
542	5654	2794	613	553	-230	-600	-319	-464	423	374	188	171	222	190	425	434
572	6656	3290	717	596	-265	-705	-356	-559	436	388	194	176	230	197	439	447
602	7670	3794	813	639	-299	-810	-389	-656	448	399	200	181	236	203	450	459
630	8709	4306	931	686	-333	-913	-421	-756	458	410	204	184	242	208	461	469
665	9782	4838	1046	729	-368	-1021	-453	-857	469	422	209	188	248	215	473	481
695	9809	4854	1055	736	-365	-1023	-456	-861	479	431	214	193	254	220	482	491
725	9826	4859	1062	742	-360	-1019	-452	-862	488	440	218	196	259	225	490	500
755	9835	4866	1070	746	-356	-1016	-456	-864	496	448	222	200	264	230	498	508
785	9831	4862	1086	750	-351	-1012	-452	-864	503	455	227	204	269	235	505	515
815	8468	4275	961	704	-291	-873	-408	-736	509	462	230	206	273	239	511	521
845	6518	3295	775	640	-208	-665	-351	-554	515	468	233	209	277	243	518	528
875	4551	2309	583	576	-128	-452	-282	-367	521	473	236	212	281	246	523	533
905	1591	819	291	482	-3	-135	-180	-87	526	478	240	215	284	250	528	539
935	90	61	136	436	62	28	-127	55	530	482	242	217	287	254	533	543
965	142	86	145	424	67	30	-125	47	535	486	244	218	291	256	537	547
1084	155	94	216	300	89	47	-73	11	485	457	234	210	271	250	487	488
1204	128	79	170	229	95	43	-32	-20	415	394	207	189	230	225	420	420
1325	236	133	142	202	85	24	-19	-49	357	337	184	171	204	200	362	362

Time, sec	Total load, lb	Right load, lb	TC 186	TC 187	TC 188	TC 97	TC 146	TC 189	TC 190	TC 191	TC 192	TC 168	TC 193	TC 194	TC 195	TC 196
0	0	0	84	84	83	84	84	83	80	80	84	84	83	83	83	84
66	-69	-38	92	90	86	86	86	87	85	83	86	85	84	84	84	85
126	-95	-52	136	131	113	108	106	112	112	108	98	92	90	92	90	95
196	-47	-24	202	196	169	159	152	157	159	162	115	106	102	106	101	109
257	-81	-40	254	248	219	207	198	201	204	212	130	120	114	117	113	123
317	-24	-13	300	295	266	253	243	244	249	260	145	134	126	128	125	137
453	2659	1314	385	380	355	342	332	328	337	352	178	166	155	153	155	170
483	3633	1798	401	397	372	359	349	344	353	370	185	172	161	158	161	178
511	4634	2290	415	410	387	374	363	358	367	385	191	178	166	162	166	184
542	5654	2794	429	424	402	388	378	371	381	400	197	184	172	167	172	191
572	6656	3290	442	438	416	402	392	384	394	415	203	190	177	171	177	198
602	7670	3794	454	449	428	415	405	396	405	427	208	195	182	176	183	203
630	8709	4306	464	459	438	425	415	405	414	438	212	200	186	179	187	209
665	9782	4838	476	471	451	438	427	417	426	451	216	204	191	182	192	215
695	9809	4854	485	480	461	447	437	425	435	461	221	209	195	186	196	220
725	9826	4859	493	488	470	456	446	433	442	469	225	213	199	189	200	225
755	9835	4866	501	496	478	465	454	440	449	478	231	217	203	193	204	230
785	9831	4862	508	503	485	472	462	447	456	486	235	222	207	196	208	235
815	8468	4275	514	509	492	479	468	453	461	492	237	225	209	198	211	238
845	6518	3295	521	515	499	485	474	458	467	499	240	228	213	200	215	242
875	4551	2309	526	521	504	491	480	463	471	505	244	231	216	203	218	246
905	1591	819	531	526	510	496	485	467	476	510	247	234	219	206	221	249
935	90	61	535	530	514	501	490	471	479	515	249	237	221	207	223	253
965	142	86	539	534	519	505	494	475	483	519	250	239	223	209	225	255
1084	155	94	484	482	483	476	467	436	436	484	233	231	218	198	221	245
1204	128	79	413	413	417	411	403	374	368	418	204	205	196	179	199	220
1325	236	133	356	355	359	353	346	320	313	360	182	183	176	162	179	197

TABLE X.- SHEAR-WEB BEAM TESTS

[Fabrication details are shown in fig. 15]

Specimen	Length, in.	d, in.	t, in.	Doubler strip		Hole cutout		Test temp., °F		Beam failure		Flange load, lb	Failure shear stress, ksi
				Depth, in.	Thickness, in.	Diameter, in.	Stiffener	Top	Bottom	Load, lb	Mode		
60° × 1-inch flat corrugation													
1	35.40	18.00	0.0182	----	-----	----	----------	80	80	11,750	Web-cap connection	197	35.3
2	35.40	17.98	.0184	----	-----	----	----------	1232	1220	7,000	Web-cap connection	128	20.8
3	35.45	17.98	.0183	----	-----	----	----------	1202	926	8,000	*Web-cap connection	147	23.9
4	35.44	17.99	.0178	1.62	0.018	----	----------	80	80	15,500	Element buckling	195	47.8
5	35.44	17.98	.0180	1.62	.010	----	----------	80	80	16,075	Element buckling	231	48.9
6	35.39	17.95	.0184	----	-----	8.25	----------	80	80	7,500	Cutout buckling	400	21.5
7	35.41	17.98	.0181	----	-----	8.25	Fig. 15(a)	80	80	8,790	Cutout buckling	288	26.3
8	35.47	17.98	.0180	----	-----	8.25	Fig. 15(a)	1195	916	6,475	*Web-cap connection	256	19.3
Special transverse frame corrugation													
9	34.62	17.20	0.0104	----	-----	----	----------	80	80	2,300	General instability	250	11.4
10	34.65	17.25	.0103	----	-----	----	----------	1194	1194	1,250	Web-cap connection	330	5.2
11	34.70	17.25	.0101	----	-----	----	----------	1186	904	1,350	*Web-cap connection	310	6.0
12	34.58	17.25	.0105	0.75	0.010	----	----------	80	80	2,800	General instability	423	13.1
13	34.74	17.24	.0103	----	-----	8.25	----------	80	80	2,000	General instability	517	8.4
14	34.78	17.26	.0103	----	-----	8.25	Fig. 15(b)	80	80	2,100	General instability	545	8.8
15	34.75	17.26	.0108	----	-----	8.25	Fig. 15(b)	1205	913	1,350	General instability	388	5.2

*Failed on hotter edge.

TABLE XI.- SKIN-PANEL HEAT AND LOAD TESTS

[All specimens are 24.5 inches square unless otherwise noted. Deflection (Defl) readings are inches, strains (SG) are microinches/inch, temperatures (TC) are °F]

(a) Specimen 1; room-temperature loading; instrumentation location, figures 25(a) and 25(b)

Time, sec	Normal load, psf	Defl 1	Defl 2	Defl 3	Defl 4	SG 1	SG 2	SG 3	SG 4	SG 5	SG 6	SG 7	SG 8	SG 9	SG 10	SG 11	SG 12
0	0	0	0	0	0	0	0	0	0	0	0	0	0	0	0	0	0
21	131	.125	.133	.086	.084	798	-344	799	-342	828	-369	546	-211	210	-284	735	-199
53	292	.276	.287	.187	.185	1771	-763	1782	-748	1872	-818	1217	-501	548	-693	1655	-513
105	438	.414	.426	.277	.277	2647	-1137	2658	-1124	2829	-1226	1821	-759	852	-1060	2495	-779
232	553	.521	.532	.346	.346	3298	-1435	3288	-1435	3513	-1566	2257	-968	1100	-1359	3108	-986
252	644	.615	.625	.405	.407	3961	-1697	3974	-1690	4249	-1844	2605	-1130	1294	-1597	3659	-1146
263	685	.674	.684	.441	.444	4490	-1851	4540	-1837	4851	-2004	2764	-1204	1390	-1718	4011	-1220
295	723	.739	.748	.479	.482	(**)	-2007	(**)	-1985	(**)	-2166	2903	-1268	1476	-1835	4392	-1284
305	772	.833	.842	.533	.538		-2231		-2193		-2393	3071	-1345	1587	-1984	4955	-1362
316	806	.921	.929	.582	.584		-2426		-2370		-2588	3183	-1392	1664	-2098	(**)	-1407
358	856	1.069	1.077	(*)	(*)		-2735		-2654		-2914	3341	-1453	1773	-2262		-1454
389	906	1.257	1.264				-3108		-2984		-3275	3470	-1497	1869	-2420		-1480
513	989	1.750	1.750				-3876		-3591		-3962	3635	-1564	1992	-2614		-1511

(b) Specimen 2; 1,600° F uniform heating; instrumentation location, figures 25(a) and 25(c)

Time, sec	Normal load, psf	Defl 1	Defl 2	Defl 3	Defl 4	TC 1	TC 2	TC 3	TC 4	TC 5	TC 6	TC 7	TC 9	TC 10	TC 11	TC 13	TC 14	TC 15	TC 16	TC 17	TC 18	TC 19
0	0	0	0	0	0	80	80	80	80	80	80	80	80	80	80	80	80	80	80	80	80	80
9	0	-.027	-.017	-.012	-.012	80	96	80	98	98	89	86	80	100	91	80	84	85	84	84	84	83
24	0	-.235	-.226	-.155	-.169	102	256	103	279	254	277	275	80	280	281	101	204	260	270	268	245	231
39	0	-.342	-.334	-.229	-.251	178	420	189	441	424	443	443	172	440	447	174	382	418	438	437	398	368
54	0	-.385	-.377	-.259	-.284	295	622	325	596	590	602	606	298	590	609	286	511	566	596	597	546	496
84	0	-.363	-.341	-.238	-.259	534	792	590	812	796	817	819	558	800	803	512	692	769	809	814	754	681
146	0	-.385	-.369	-.266	-.277	892	1162	949	1150	1170	1160	1155	941	1168	1153	869	1036	1121	1162	1164	1085	1018
206	0	-.505	-.483	-.348	-.364	1135	1445	1205	1441	1452	1447	1438	1208	1460	1458	1130	1306	1398	1452	1448	1376	1289
267	0	-.606	-.572	-.412	-.431	1284	1593	1347	1591	1600	1595	1583	1347	1598	1613	1276	1447	1539	1588	1590	1518	1431
297	0	-.606	-.581	-.419	-.438	1300	1606	1363	1600	1603	1604	1590	1359	1598	1621	1291	1453	1540	1590	1595	1524	1435
358	0	-.607	-.605	-.439	-.456	1312	1606	1366	1603	1603	1608	1595	1366	1598	1633	1299	1461	1552	1601	1599	1531	1439
368	18	-.578	-.581	-.424	-.441	1309	1606	1366	1603	1603	1608	1594	1367	1598	1637	1300	1464	1553	1600	1600	1531	1439
378	55	-.552	-.553	-.403	-.424	1292	1606	1341	1602	1603	1599	1584	1345	1598	1639	1293	1465	1551	1587	1587	1526	1436
388	80	-.515	-.528	-.386	-.409	1284	1606	1339	1604	1603	1604	1587	1337	1598	1626	1287	1472	1550	1589	1591	1526	1445
398	101	-.476	-.477	-.353	-.376	1281	1606	1335	1602	1603	1602	1585	1338	1598	1623	1292	1468	1544	1580	1580	1516	1440
408	154	-.367	-.380	-.286	-.313	1281	1606	1333	1597	1603	1597	1580	1335	1598	1631	1285	1478	1551	1584	1583	1521	1440
418	217	-.178	-.198	-.167	-.193	1274	1606	1322	1591	1603	1591	1577	1334	1598	1620	1279	1480	1553	1585	1584	1524	1436
428	256	-.077	-.094	-.102	-.125	1269	1609	1325	1603	1603	1603	1590	1336	1598	1626	1290	1491	1562	1594	1596	1544	1457
438	305	.074	.055	-.012	-.026	1270	1608	1330	1601	1603	1601	1592	1339	1598	1620	1292	1506	1576	1602	1602	1555	1469
443	313	.121	.107	.020	.008	1263	1608	1322	1593	1603	1598	1588	1337	1598	1624	1291	1508	1577	1604	1603	1556	1471
448	332	.198	.190	.070	.065	1263	1608	1329	1598	1603	1596	1582	1334	1598	1628	1293	1504	1568	1597	1596	1546	1464
453	313	1.025	.446	.221	.226	1259	1608	1337	1595	1603	1585	1582	1337	1598	1625	1289	1505	1569	1594	1594	1540	1461

*Deflection exceeded capability of deflectometer.
**Signal went off scale on recorder.

TABLE XI.- SKIN-PANEL HEAT AND LOAD TESTS - Continued

(c) Specimen 3; 1,600° to 1,300° F gradient heating; instrumentation location, figures 25(a) and 25(c)

Time, sec	Normal load, psf	Defl 1	Defl 2	Defl 3	Defl 4	TC 1	TC 2	TC 3	TC 4	TC 5	TC 6	TC 8	TC 9	TC 10	TC 11	TC 12	TC 13	TC 14	TC 15	TC 16	TC 17	TC 18	TC 19
0	0	0	0	0	0	80	80	80	80	80	80	80	80	80	80	80	80	80	80	80	80	80	80
124	0	-.065	-.056	-.046	-.043	128	188	129	169	188	191	225	158	230	178	174	124	219	224	228	229	216	205
244	0	-.119	-.106	-.085	-.077	242	357	275	352	380	395	442	344	450	382	376	272	403	432	454	451	432	378
364	0	-.176	-.155	-.126	-.115	379	521	429	534	570	593	662	531	660	579	569	422	612	649	675	674	636	584
515	0	-.221	-.206	-.166	-.149	549	730	613	747	792	820	903	754	910	785	748	577	855	888	917	915	869	827
756	0	-.391	-.327	-.282	-.253	828	1052	894	1082	1132	1184	1305	1107	1310	1132	1053	831	1268	1286	1328	1325	1258	1240
996	0	-.570	-.472	(***)	(***)	1110	1339	1170	1393	1450	1496	1612	1390	1601	1430	1337	1084	1578	1593	1633	1627	1556	1542
1122	0	-.568	-.462	(***)	(***)	1119	1339	1174	1395	1450	1497	1613	1393	1601	1424	1307	1079	1581	1590	1636	1629	1559	1544
1127	27	-.521	-.419	(***)	(***)	1119	1337	1173	1392	1450	1494	1610	1392	1600	1422	1307	1077	1581	1590	1635	1629	1557	1542
1147	124	-.360	-.288	-.271	-.244	1088	1333	1142	1382	1448	1485	1597	1364	1598	1417	1297	1051	1577	1577	1620	1616	1551	1540
1163	230	-.174	-.116	-.152	-.138	1076	1331	1133	1383	1447	1488	1594	1350	1592	1415	1293	1034	1588	1581	1610	1609	1549	1545
1171	286	-.041	-.022	-.064	-.063	1061	1332	1118	1380	1447	1483	1592	1346	1589	1422	1295	1025	1591	1579	1604	1607	1547	1554
1179	335	.122	.109	.036	.028	1062	1337	1121	1386	1446	1490	1588	1332	1585	1430	1301	1021	1603	1586	1607	1605	1556	1563
1187	388	.239	.196	.104	.090	1062	1337	1123	1392	1448	1496	1587	1337	1584	1430	1304	1014	1610	1596	1623	1609	1560	1579
1195	444	.407	.339	.199	.184	1062	1337	1129	1392	1448	1495	1581	1335	1580	1432	1306	1024	1607	1590	1611	1608	1553	1582
1203	511	.653	.549	.328	.321	1057	1338	1132	1391	1448	1494	1579	1330	1575	1433	1308	1024	1607	1583	1600	1598	1560	1596
1210	554	.906	.756	.489	(*)	1056	1338	1127	1394	1448	1495	1575	1321	1570	1435	1306	1018	1615	1586	1599	1587	1562	1612
1212	141	1.162	.996	.611	(*)	1062	1338	1126	1385	1448	1488	1580	1325	1562	1402	1325	1010	1620	1583	1589	1584	1550	1590

(d) Specimen 4; 600° to 300° F gradient heating; instrumentation location, figures 25(a) and 25(c)

Time, sec	Normal load, psf	Defl 1	Defl 2	Defl 3	Defl 4	TC 1	TC 3	TC 4	TC 6	TC 9	TC 10	TC 11	TC 12	TC 13	TC 14	TC 15	TC 16	TC 17	TC 18	TC 19
0	0	0	0	0	0	77	84	83	82	89	85	77	77	77	76	77	85	85	77	76
12	0	-.080	-.108	-.076	-.081	77	85	130	137	91	162	135	119	77	155	162	159	156	154	149
21	0	-.139	-.185	-.131	-.138	81	90	179	197	101	237	195	163	81	226	241	232	229	229	214
30	0	-.187	-.251	-.177	-.189	91	103	231	260	125	318	259	208	91	302	325	313	311	313	284
39	0	-.225	-.295	-.213	-.232	106	122	286	326	164	401	324	255	108	376	410	394	393	395	353
51	0	-.266	-.332	-.249	-.269	132	159	360	416	235	514	412	320	137	477	524	507	505	505	446
60	0	-.230	-.271	-.193	-.209	157	192	388	446	294	535	442	340	164	490	537	532	530	523	458
91	0	-.127	-.162	-.116	-.120	215	270	394	462	398	547	450	333	228	495	542	551	543	527	463
304	0	-.090	-.119	-.088	-.087	266	326	406	471	448	549	448	346	284	524	544	551	549	537	497
406	139	.027	-.013	-.022	-.013	217	298	405	469	416	542	446	345	249	541	528	535	542	521	485
450	278	.138	.098	.051	.063	185	276	409	465	383	548	449	342	218	561	522	527	552	526	472
509	431	.284	.261	.159	.176	195	269	409	473	353	537	448	343	215	560	517	517	545	543	484
539	497	.351	.335	.208	.225	204	269	406	471	336	534	430	339	216	566	527	525	538	546	506
568	571	.438	.436	.270	.290	207	270	407	469	329	532	423	338	212	568	528	529	536	543	511
627	674	.604	.627	.378	.406	208	256	404	465	324	540	432	327	203	590	548	546	545	562	535
728	746	.840	.867	.508	.552	219	264	408	463	335	539	448	328	218	610	556	543	542	556	560
743	790	1.016	1.046	.599	(*)	207	259	409	465	332	545	458	338	217	630	576	557	550	569	577
755	817	1.153	1.180	(*)	(*)	202	263	413	469	333	548	463	346	215	639	595	563	556	579	584
764	845	1.300	1.322	(*)	(*)	204	266	419	474	337	549	467	353	215	646	597	567	557	581	588
785	893	(*)	(*)	(*)	(*)	213	276	416	485	352	547	459	351	210	655	599	568	562	577	590

*Deflection exceeded capability of deflectometer.
***Deflection exceeded negative capability of deflectometer.

TABLE XI.- SKIN-PANEL HEAT AND LOAD TESTS - Concluded

(e) Specimen 5; 10° F/sec rise rate; temperature distribution in corrugation element cross section; instrumentation location, figure 26(c)

Time, sec	TC 20	TC 21	TC 22	TC 23	TC 24	TC 25	TC 26
0	76	76	76	76	76	76	76
8	223	221	153	157	84	76	77
28	495	482	360	371	206	124	116
48	706	694	567	583	380	249	236
69	891	882	764	782	572	425	410
89	1091	1085	967	987	770	625	611
109	1283	1281	1157	1179	962	829	817
129	1483	1482	1352	1379	1146	1029	1018
144	1614	1613	1483	1514	1276	1164	1152
148	1642	1642	1516	1546	1313	1203	1192
150	1646	1647	1524	1553	1329	1222	1210
160	1646	1647	1531	1555	1362	1278	1268
168	1649	1650	1531	1554	1368	1292	1282
188	1660	1662	1538	1560	1377	1300	1291
217	1665	1666	1538	1559	1379	1301	1292
247	1671	1673	1541	1563	1380	1299	1291

(f) Elevated-temperature buckling of skin-panel surfaces heated cyclically to a maximum of 1,200° F in the seam-welded flat element in the sequence indicated

Specimen	Normal load, psf	Temperature rise rate, °F/sec	Number of residual buckles
6	0	0	10
		10	10
		20	10
		30	10
		40	26
		50	35
		60	80
		70	86
7	288	0	5
		10	8
		15	13
		20	28
		25	52
		30	89
		35	123
		40	166
		45	191

(g) Specimen 7; room-temperature loading after surface was buckled as described in table XI(f) above; instrumentation location, figure 25(a)

Time, sec	Normal load, psf	Defl 1	Defl 2	Defl 3	Defl 4
0	0	0.026	0.005	0.005	0.005
30	111	.146	.108	.074	.073
48	198	.241	.190	.129	.126
69	294	.344	.280	.189	.186
84	370	.425	.351	.236	.233
103	436	.497	.415	.278	.275
130	506	.581	.487	.326	.322
153	630	.738	.625	.416	.412
162	689	.858	.726	.475	.473
168	720	.931	.788	.512	.512
178	772	1.077	.917	.584	.589
184	810	1.195	1.027	.644	(*)
196	868	1.408	1.238	.757	(*)
202	900	1.524	1.356	(*)	(*)
211	929	1.661	1.493	(*)	(*)

*Deflection exceeded capability of deflectometer.

(h) Room-temperature compression buckling; single element of corrugated skin panel, 6.1 in. long × 1.8 in. wide with 0.0193-in.-thick corrugation welded to 0.0107-in.-thick beaded sheet

Specimen	Buckling stress, psi
8	63,500
9	64,200

TABLE XII.- SKIN-PANEL ACOUSTIC TESTS

Specimen	Corrugation orientation relative to airflow	Sound pressure level, db	Temperature, °F	Accumulated exposure time, min	Remarks
10	Perpendicular	160	Room temperature	5	No damage noted
				16	↓
				51	3 skin cracks along one end
				61	↓
				81	↓
				91	↓
				121	Crack growth across one end
11	Parallel	160	Room temperature	10	No damage noted
				20	Weld failures, Z-stiffener to panel corrugation crests
				30	↓
				40	Skin crack, 1 inch long
				50	↓
				60	↓
				70	Crack growth
12	Perpendicular	160	Room temperature	20	Weld failures, transverse spar cap to shear web
Z-stiffener welds replaced by rivets				30	↓
				40	↓
				50	↓
				70	Skin crack
				90	↓
				120	Crack growth, additional weld failures
13	Perpendicular	151	1,600	5	Rivet failures, panel to spar caps new rivets installed
Z-stiffener welds replaced by rivets			1,200	15	No damage noted
				30	Weld failure, transverse spar cap to shear web
				50	↓
				70	↓
				100	↓
				120	Small crack in expansion joint
				150	↓
				180	No change in crack, additional weld failures

TABLE XIII.- SKIN-PANEL FLUTTER TESTS

[Tested at Mach 1.87 in the Langley Unitary Plan wind tunnel]

Specimen	Corrugation orientation relative to airflow	Temperature, °F	Dynamic pressure, psf	Remarks
14	Perpendicular	125	2,050	Flutter
15	Parallel	125	2,400	No flutter
15	Parallel	600	2,400	No flutter

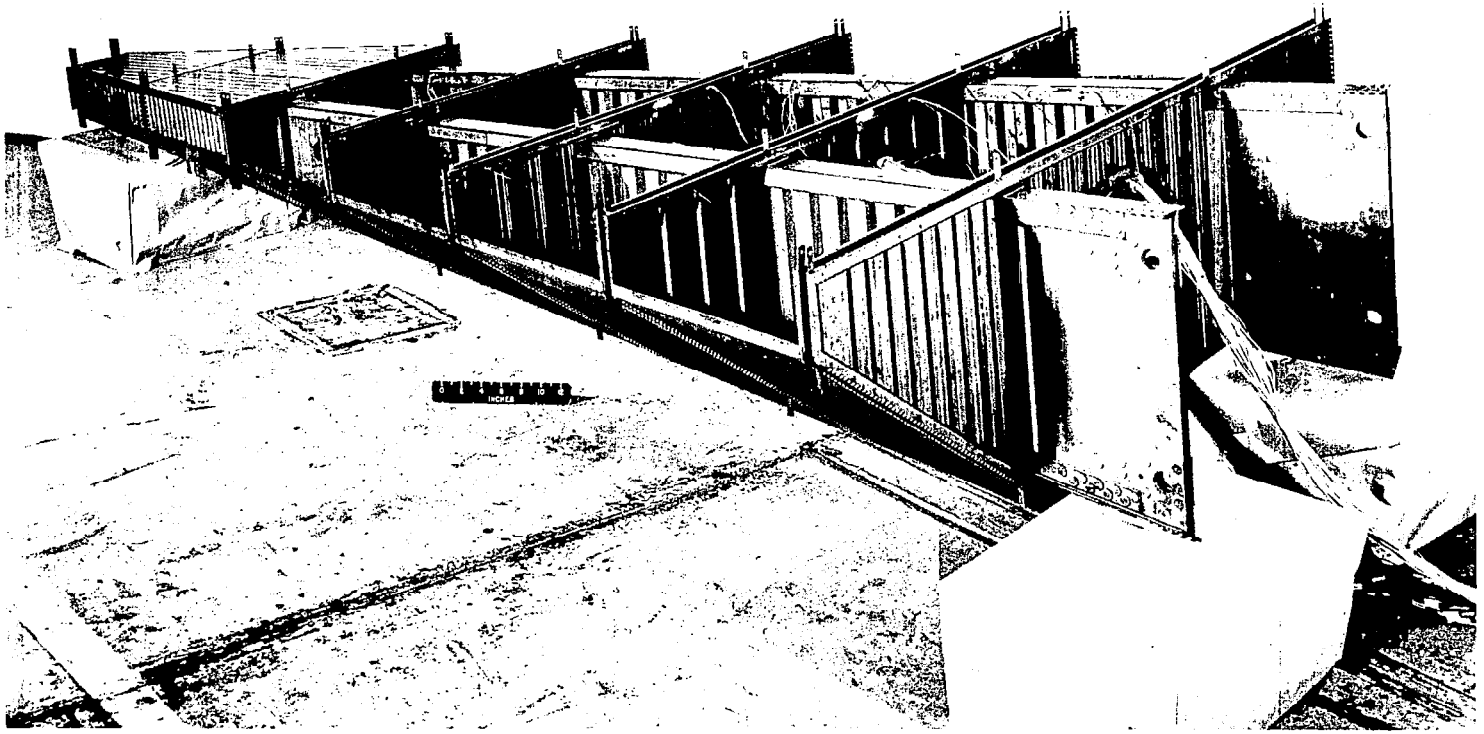

Figure 1.- Structural concept model of lifting reentry glider. L-59-4916

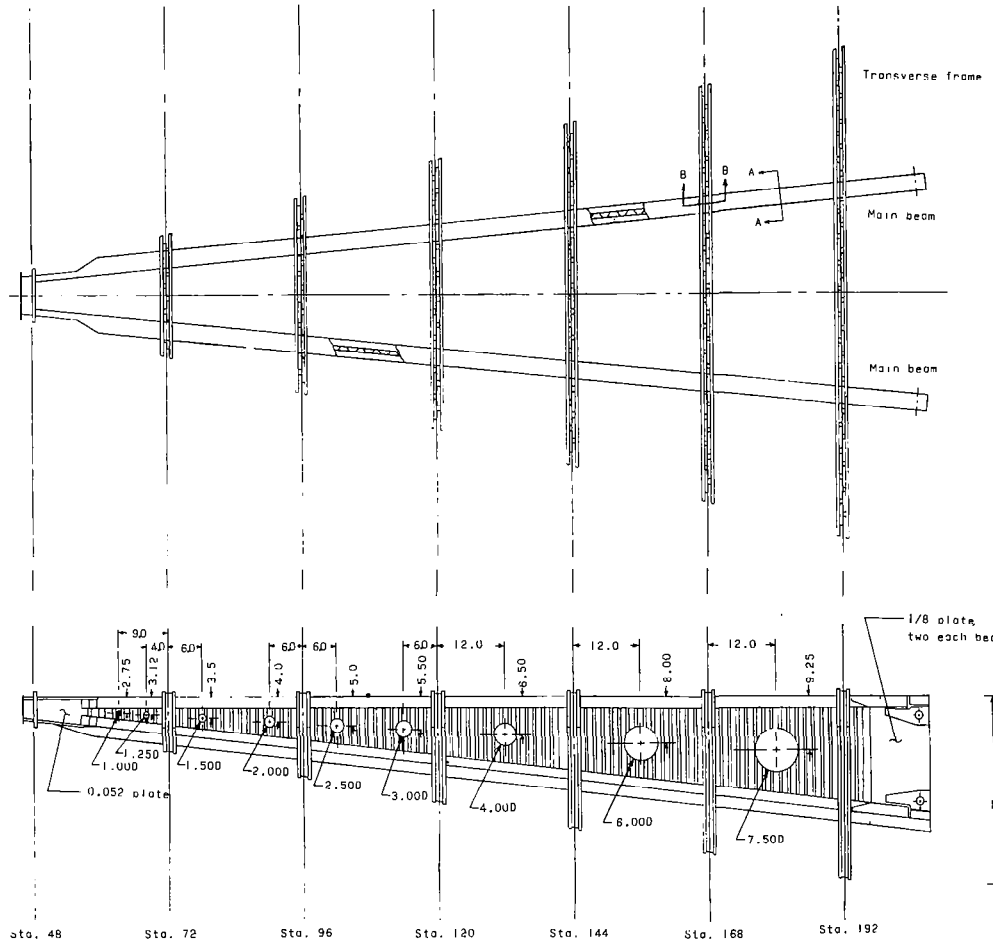

TRANSVERSE FRAME DETAILS

Station	F	K	N	D	U
48	14.57	8.57	6.0		
72	21.43	14.25	10.5	3.75	5.18
96	34.28	18.60	15.0	7.50	7.34
120	47.13	22.95	19.5	11.25	9.50
144	59.98	27.30	24.0	15.00	11.66
168	72.84	31.65	28.5	18.75	13.82
192	85.69	36.00	33.0	22.50	16.00

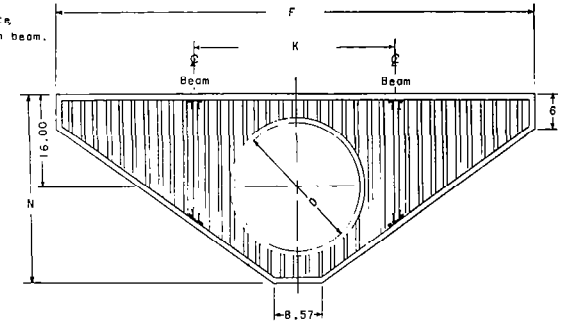

(a) Overall views.

Figure 2.- Interior structure of structural concept model for lifting reentry glider. Dimensions are in inches.

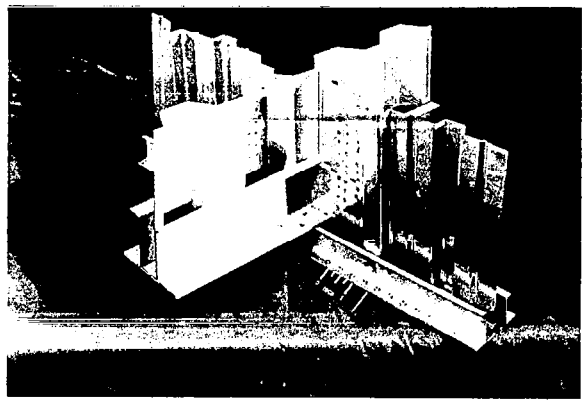

L-60-571

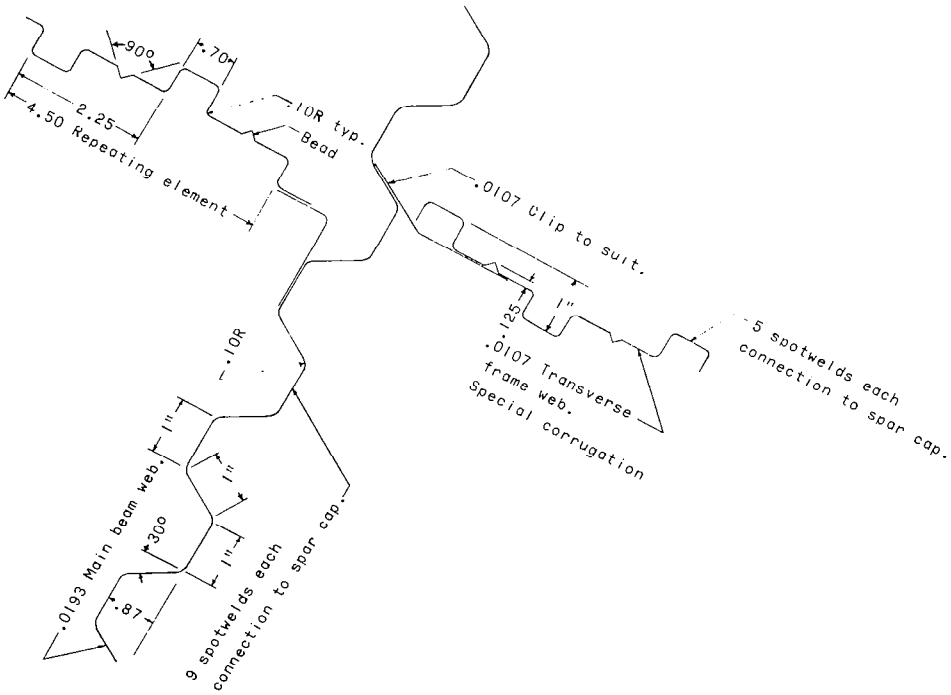

(b) Spar-web details.

Figure 2.- Continued.

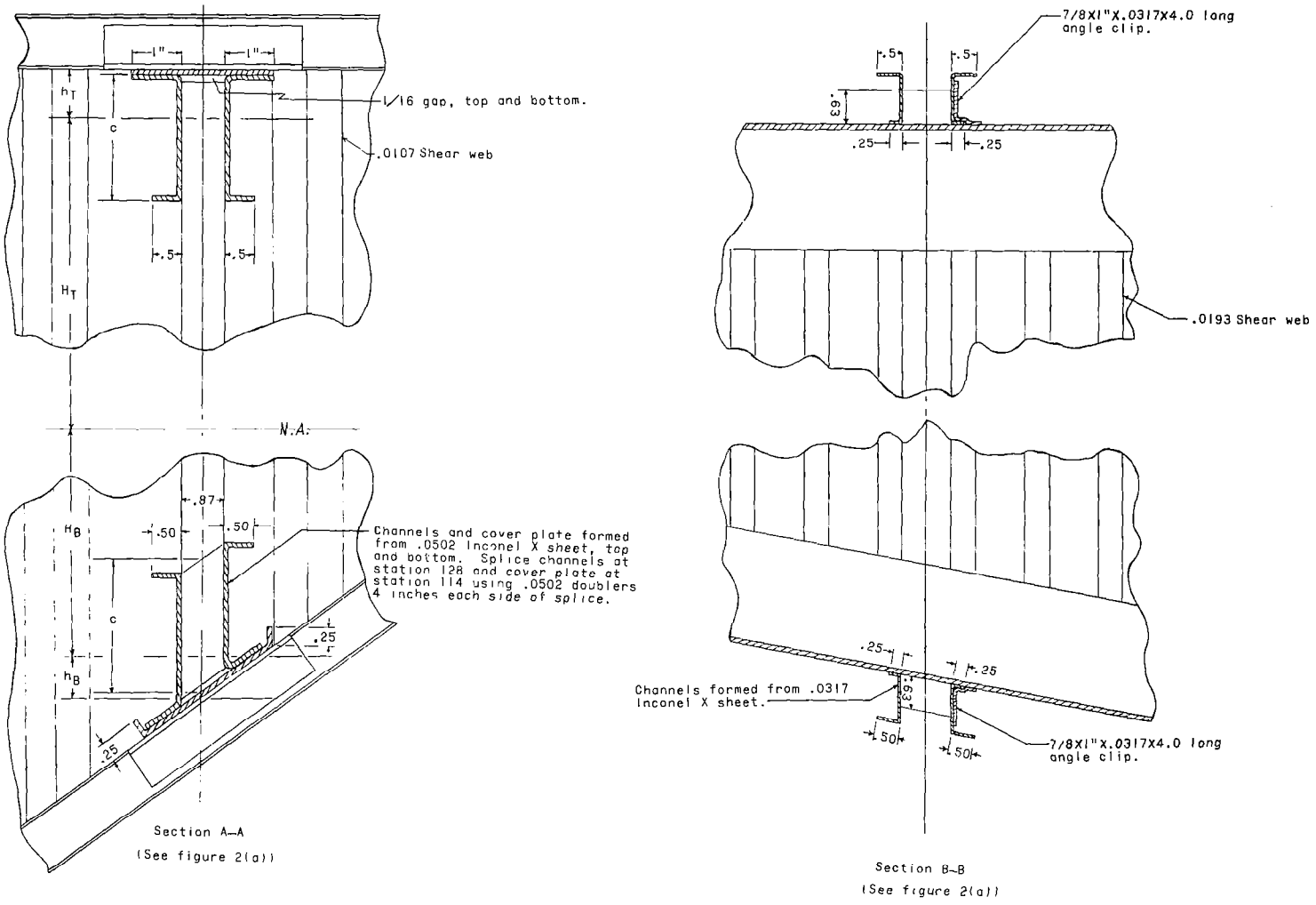

(c) Spar-cap details.

Figure 2.- Concluded.

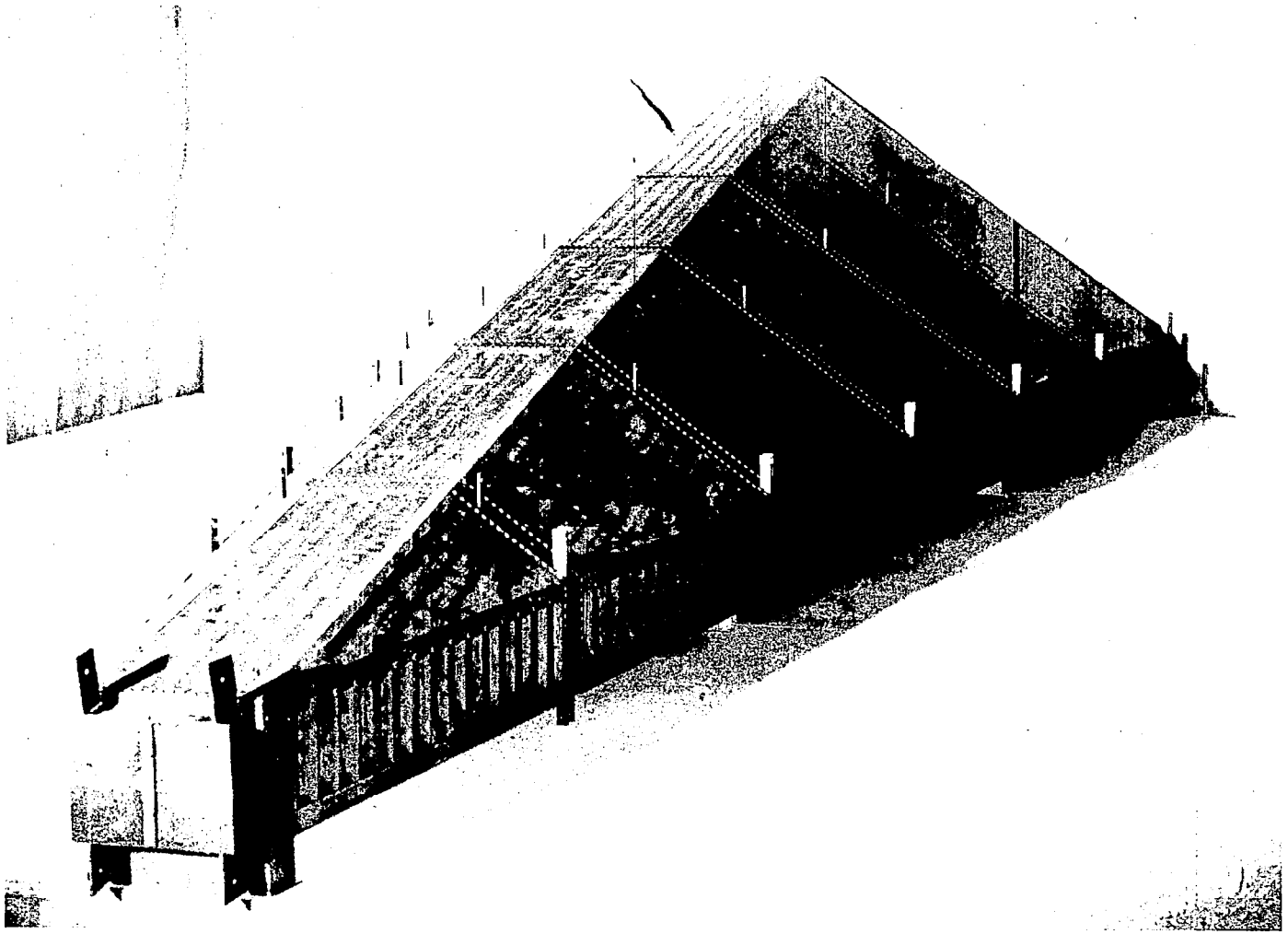

(a) Perspective, looking aft from nose. L-62-6797

Figure 3.- Exterior of structural concept model.

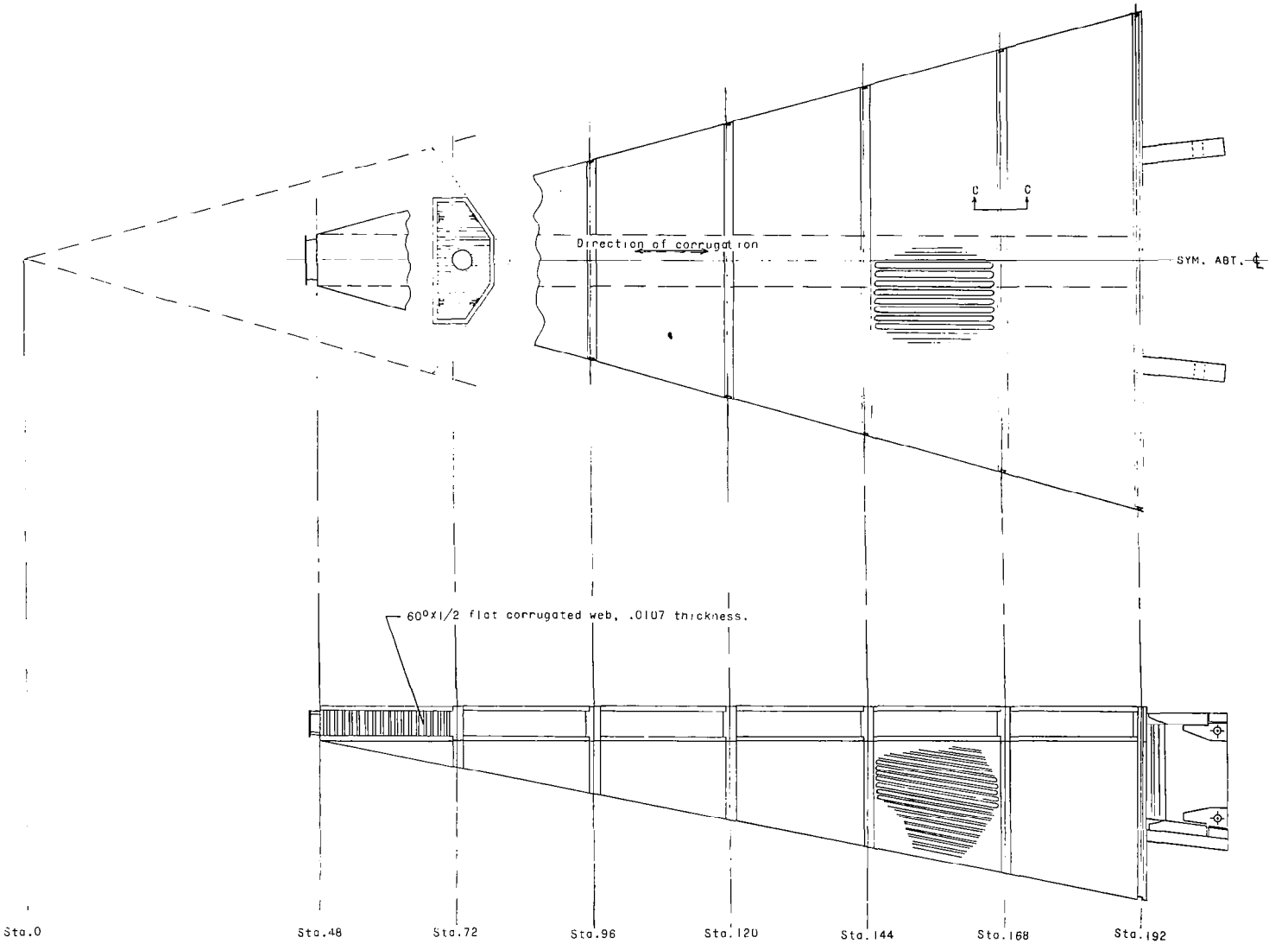

(b) Overall drawing.

Figure 3.- Continued.

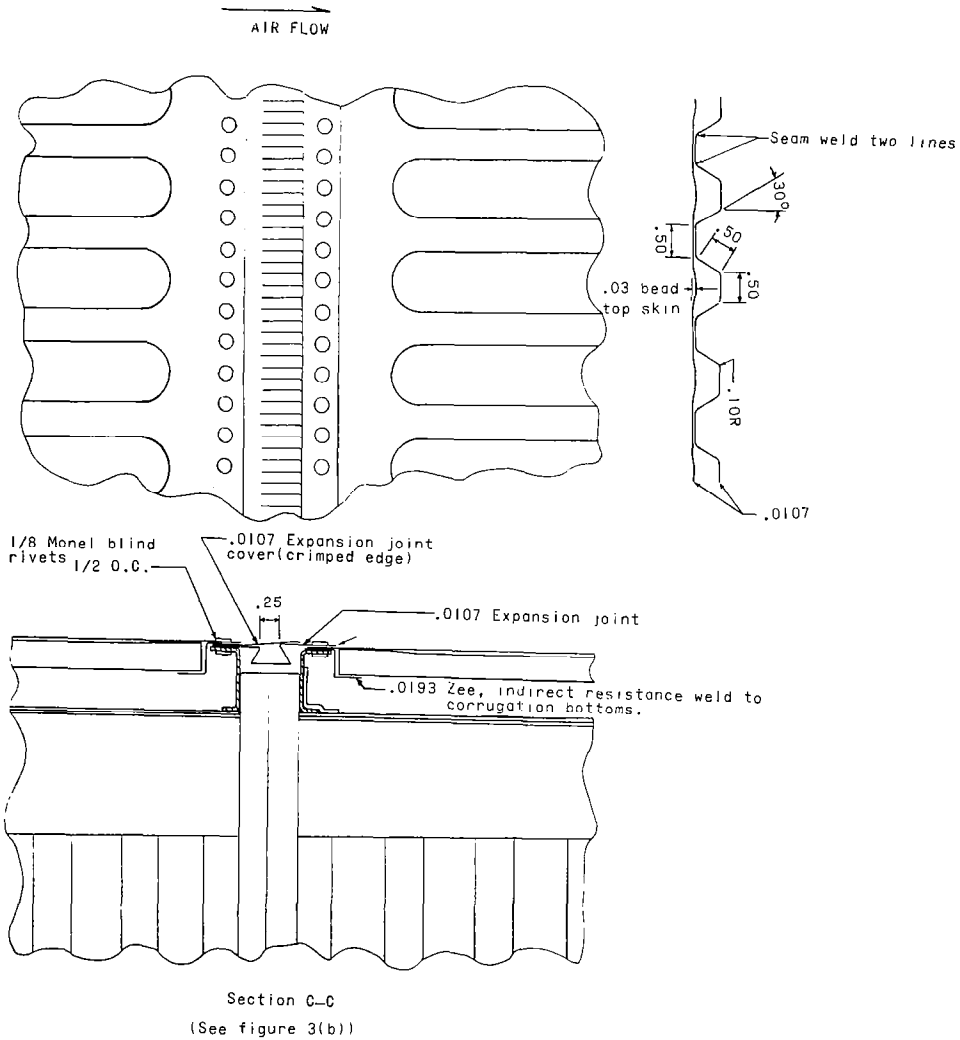

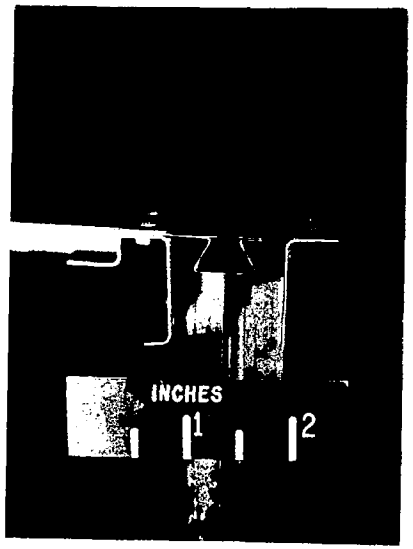

L-62-5981

(c) Skin-panel details.

Figure 3.- Continued.

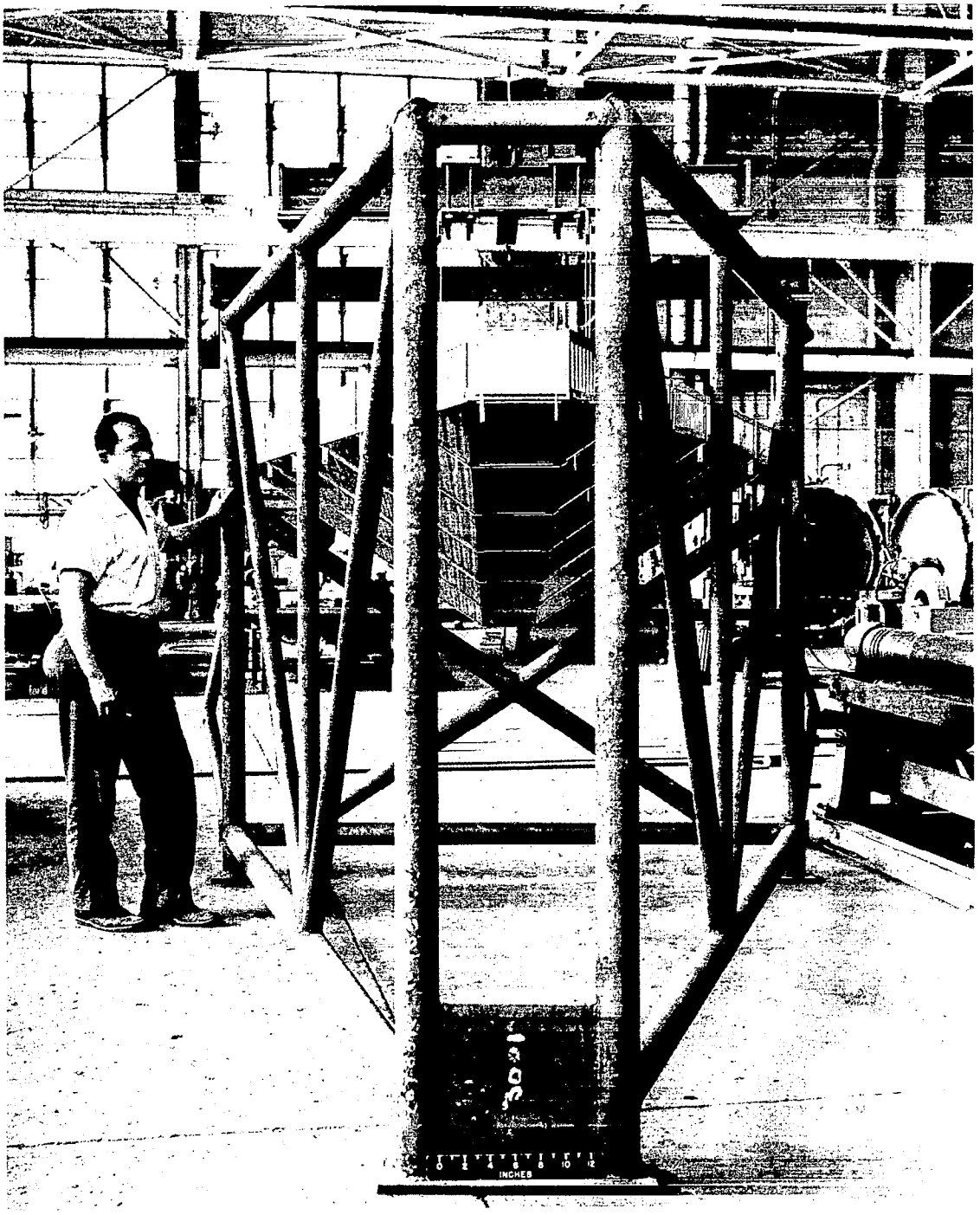

(d) Assembled model in supporting frame prior to heat treatment. L-59-3871

Figure 3.- Concluded.

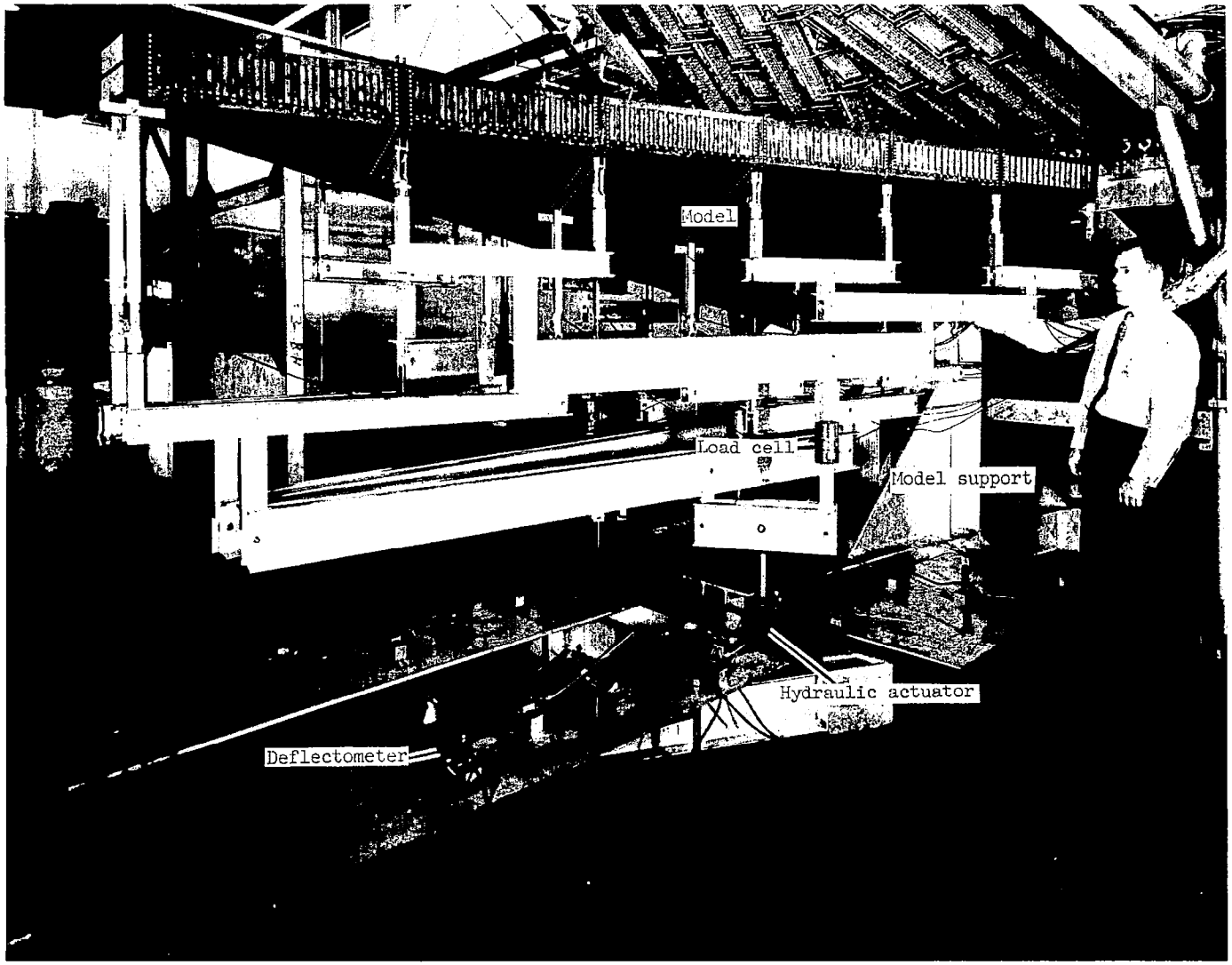

(a) Loading.

Figure 4.- Model test setup. L-59-7693.1

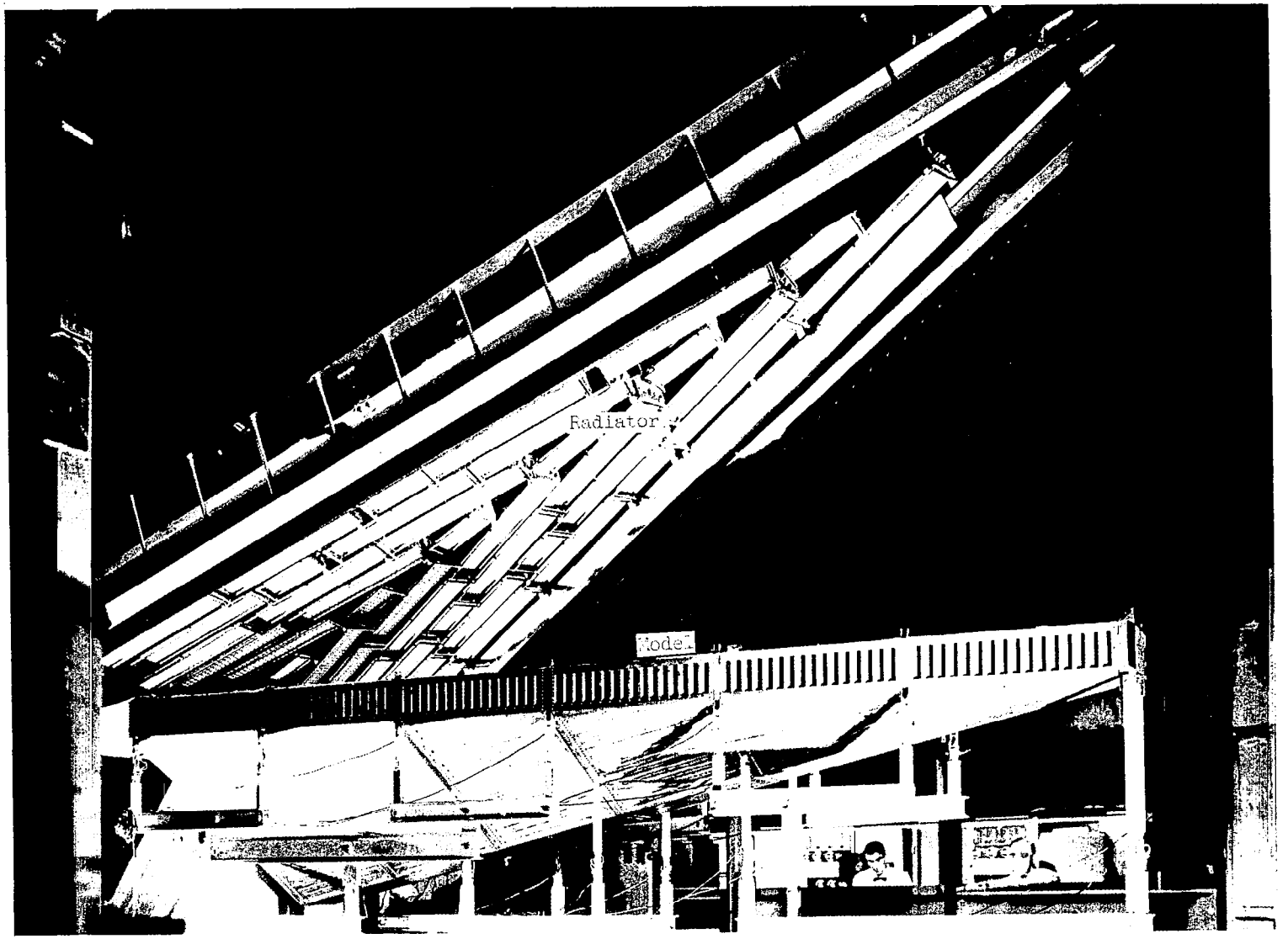

(b) Heating and loading. L-59-6745.1

Figure 4.- Concluded.

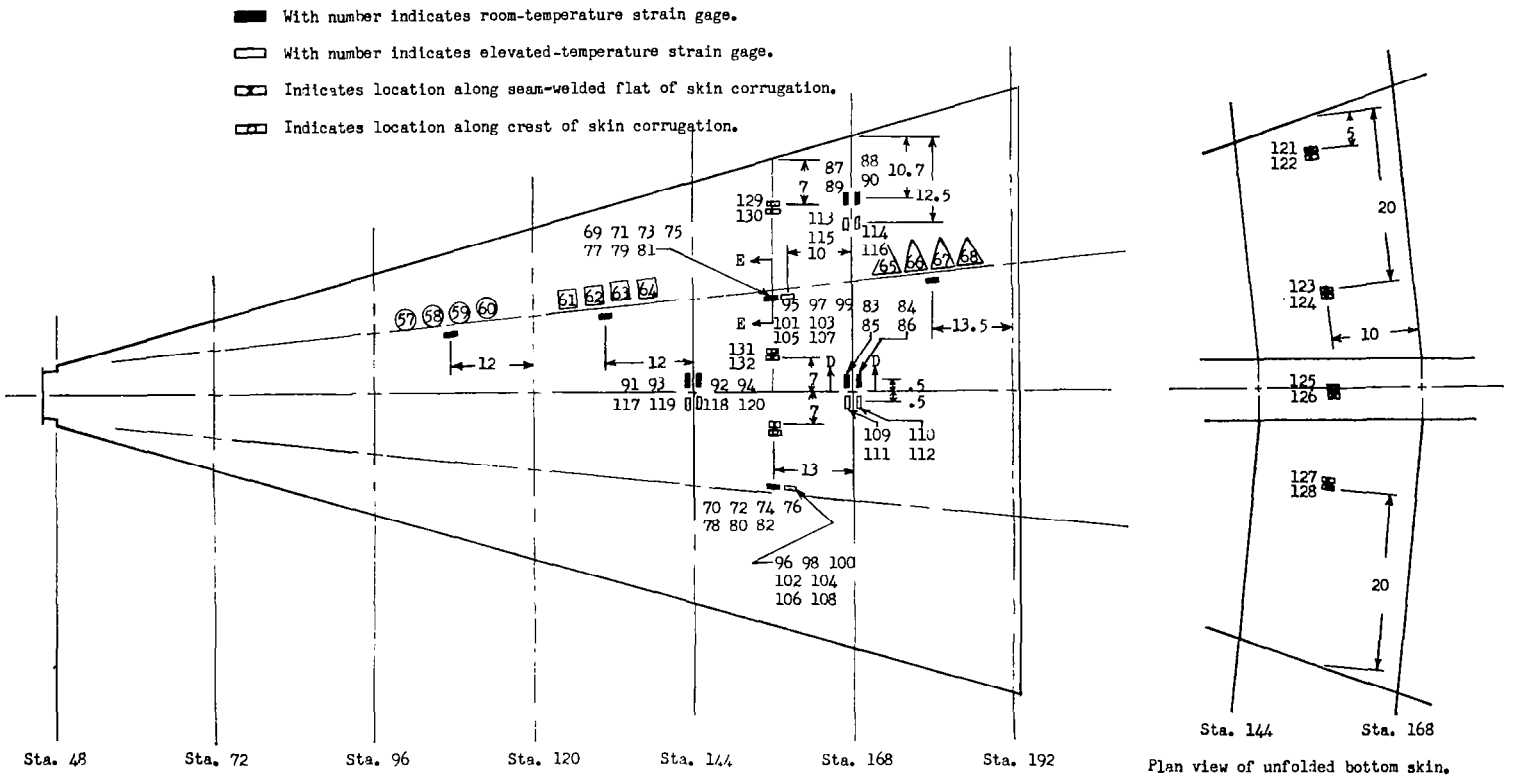

(a) Strain gages, plan view.

Figure 5.- Instrumentation location.

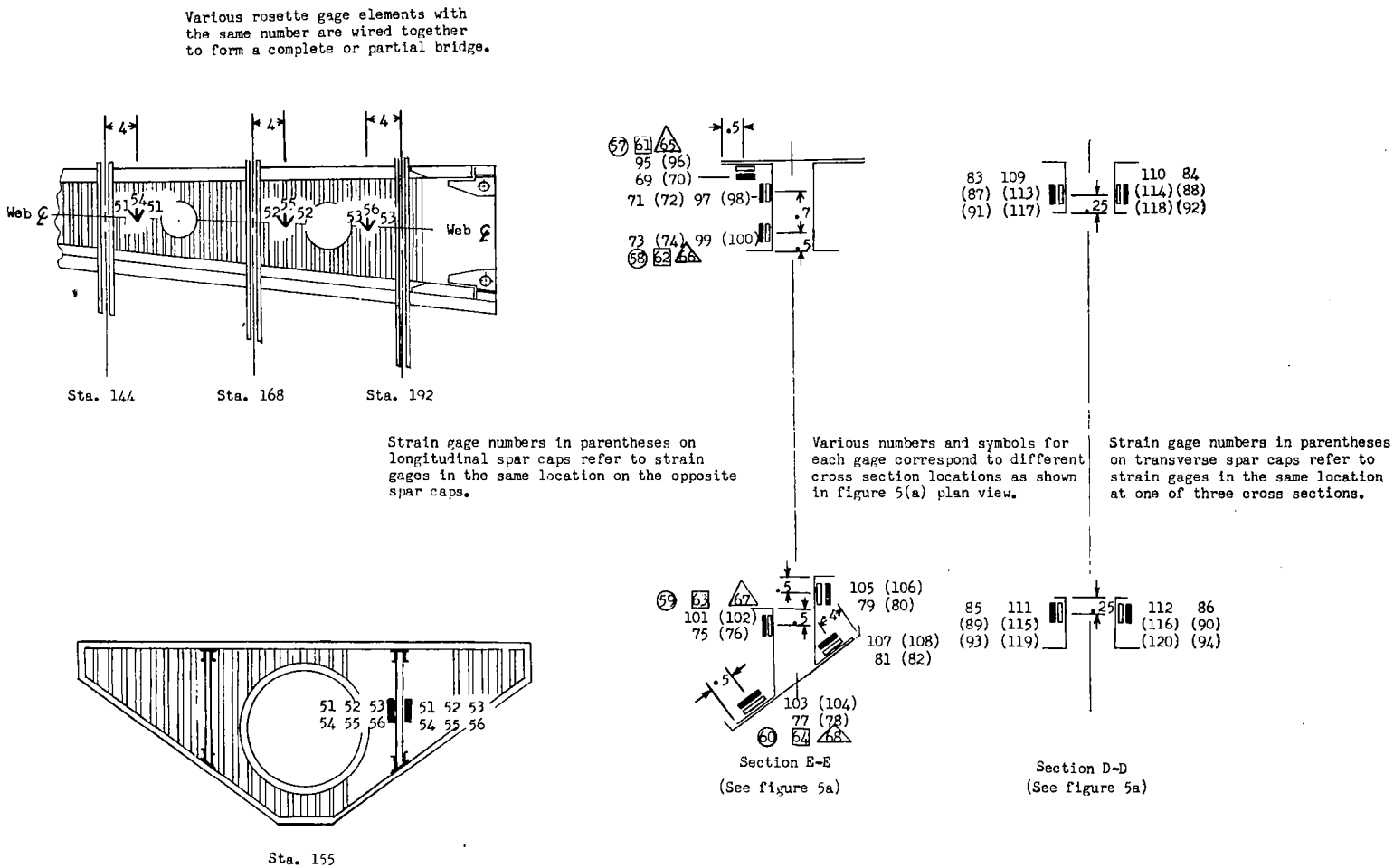

(b) Strain gages, elevation views.

Figure 5.- Continued.

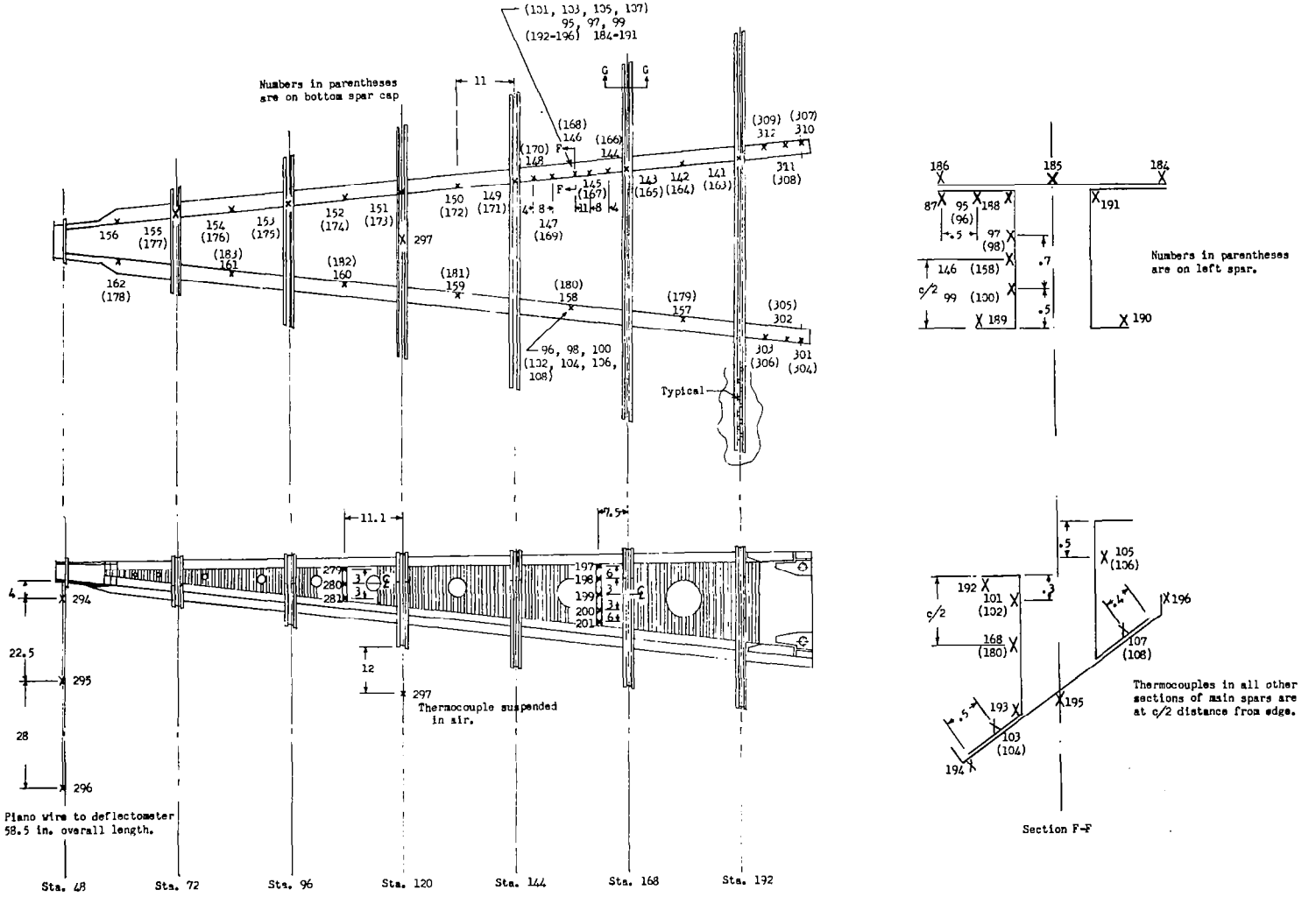

(c) Thermocouples, longitudinal spars.

Figure 5.- Continued.

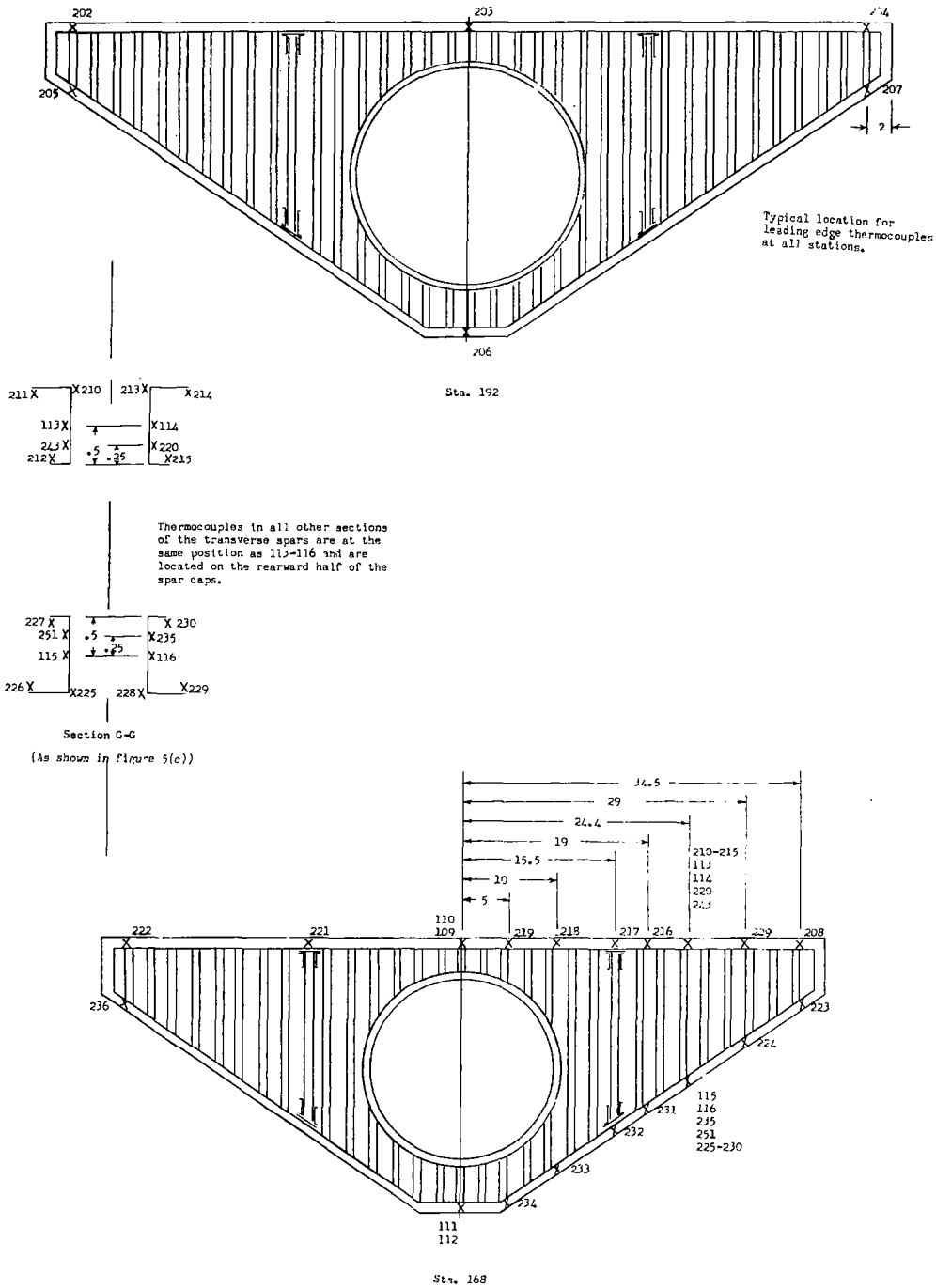

(d) Thermocouples, transverse spars.

Figure 5.- Continued.

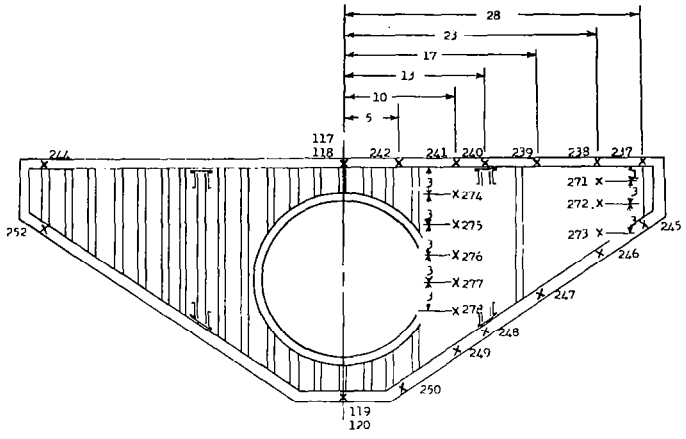

Sta. 144

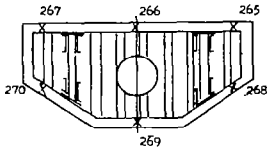

Sta. 72

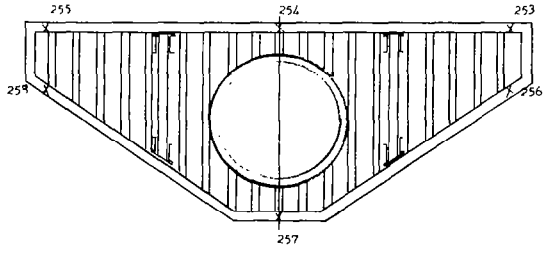

Sta. 120

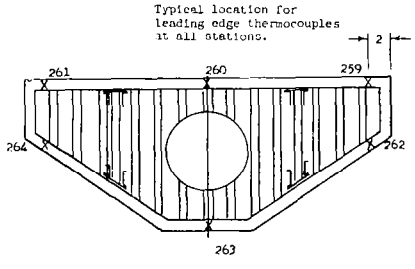

Sta. 96

(d) Concluded.

Figure 5.- Continued.

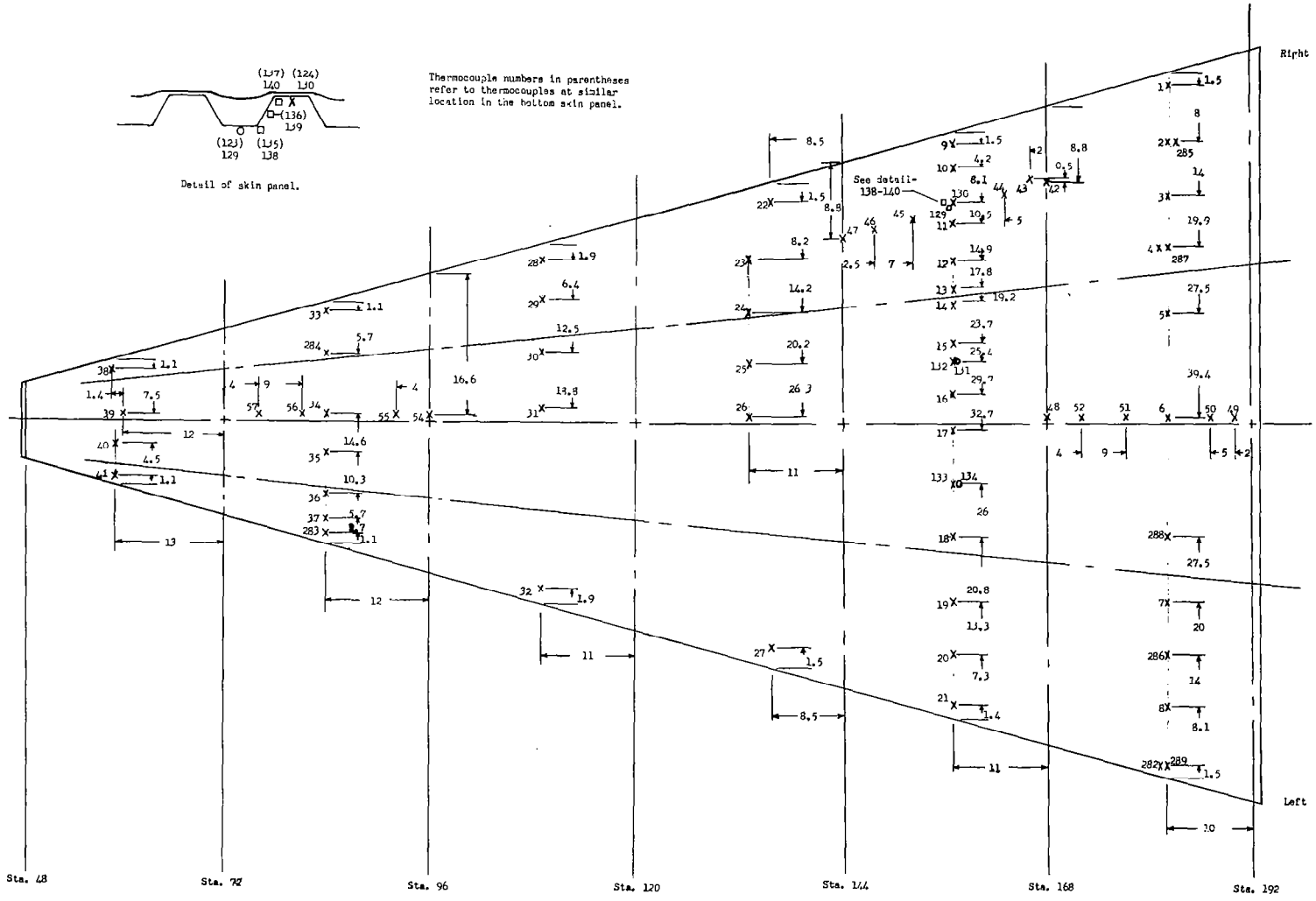

(e) Thermocouples, top skin.

Figure 5.- Continued.

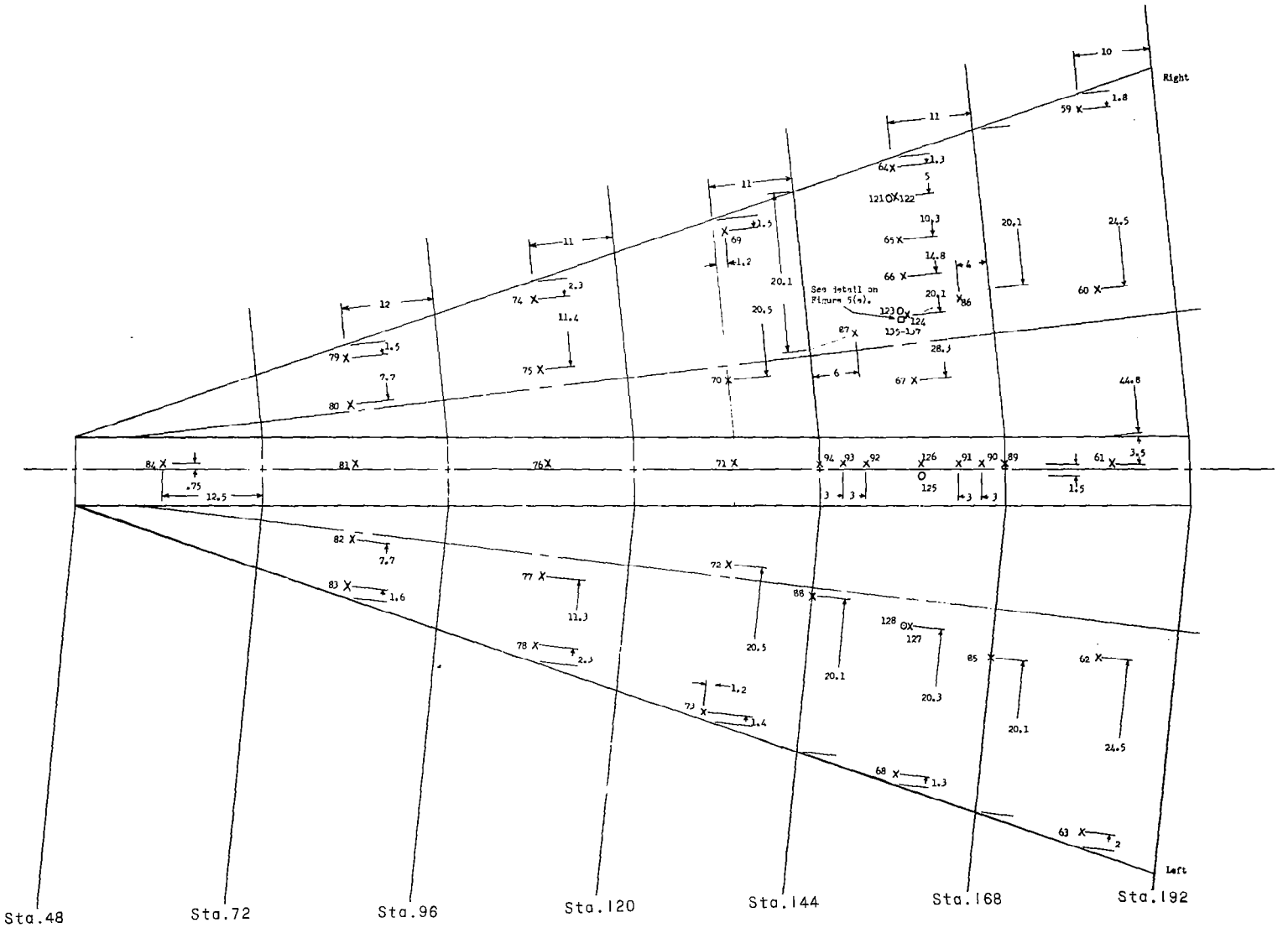

(f) Thermocouples, bottom skin (unfolded).

Figure 5.- Continued.

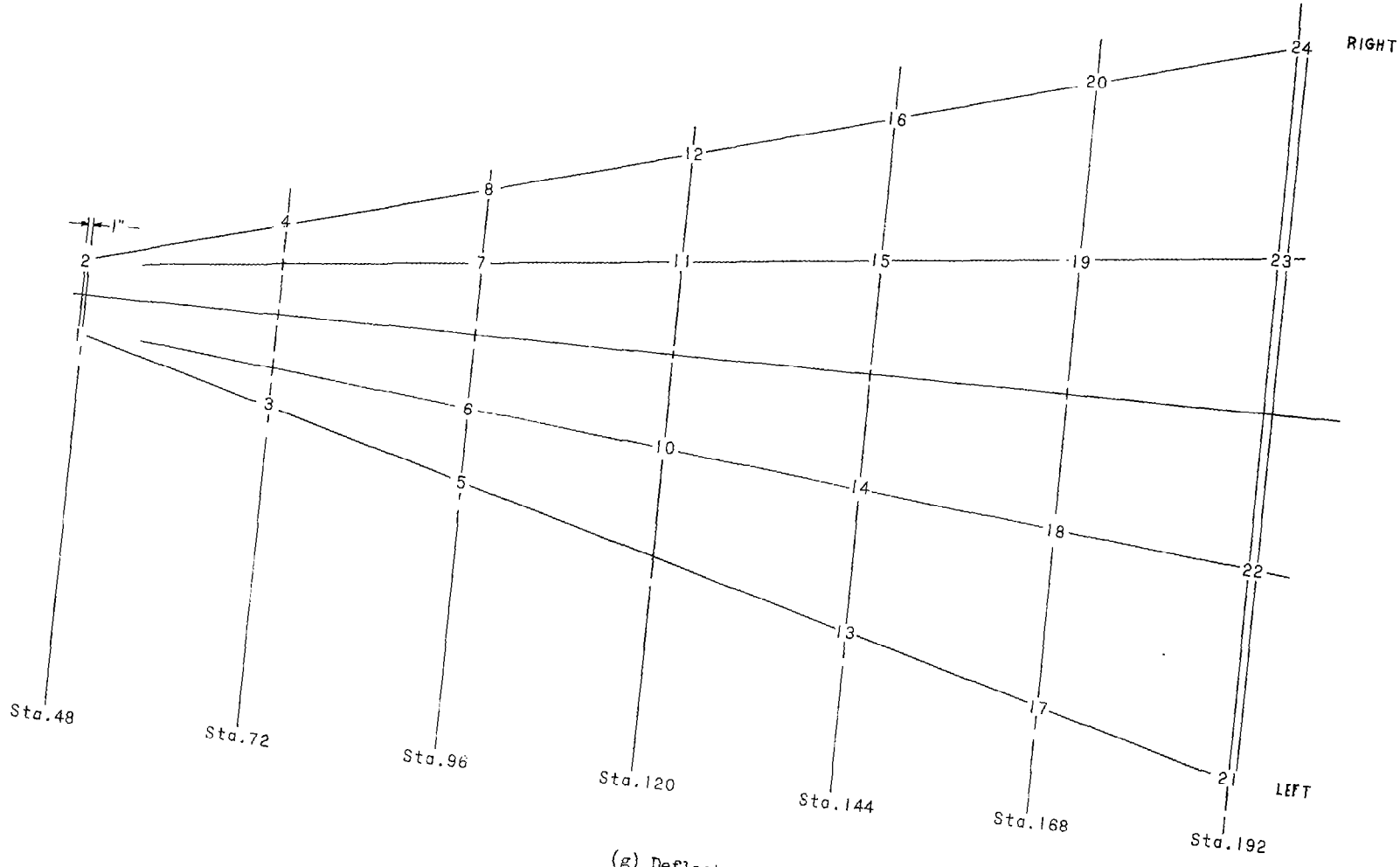

(g) Deflectometers.

Figure 5.- Concluded.

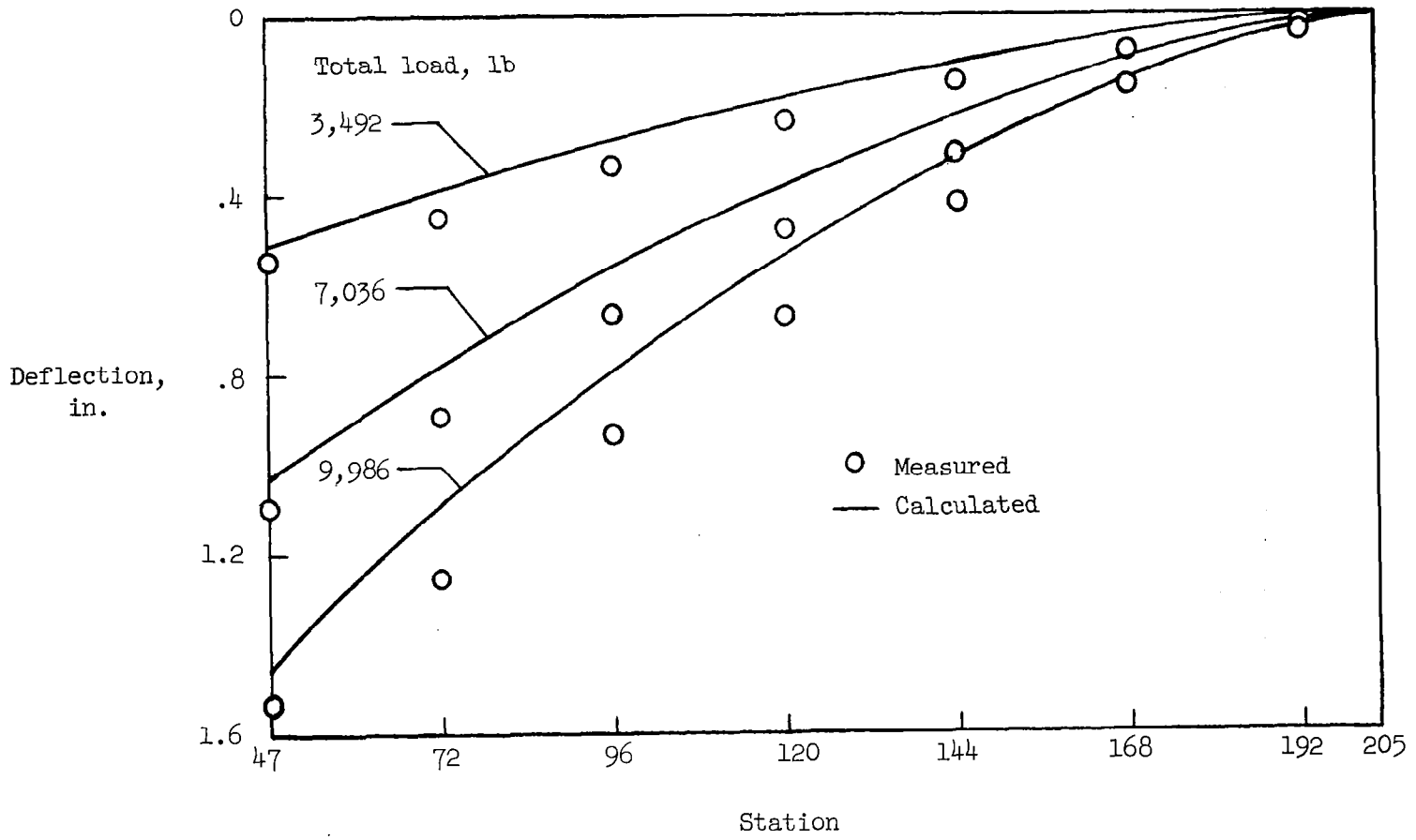

(a) Comparison between measured and calculated deflections.

Figure 6.- Model deflections for room-temperature distributed load.

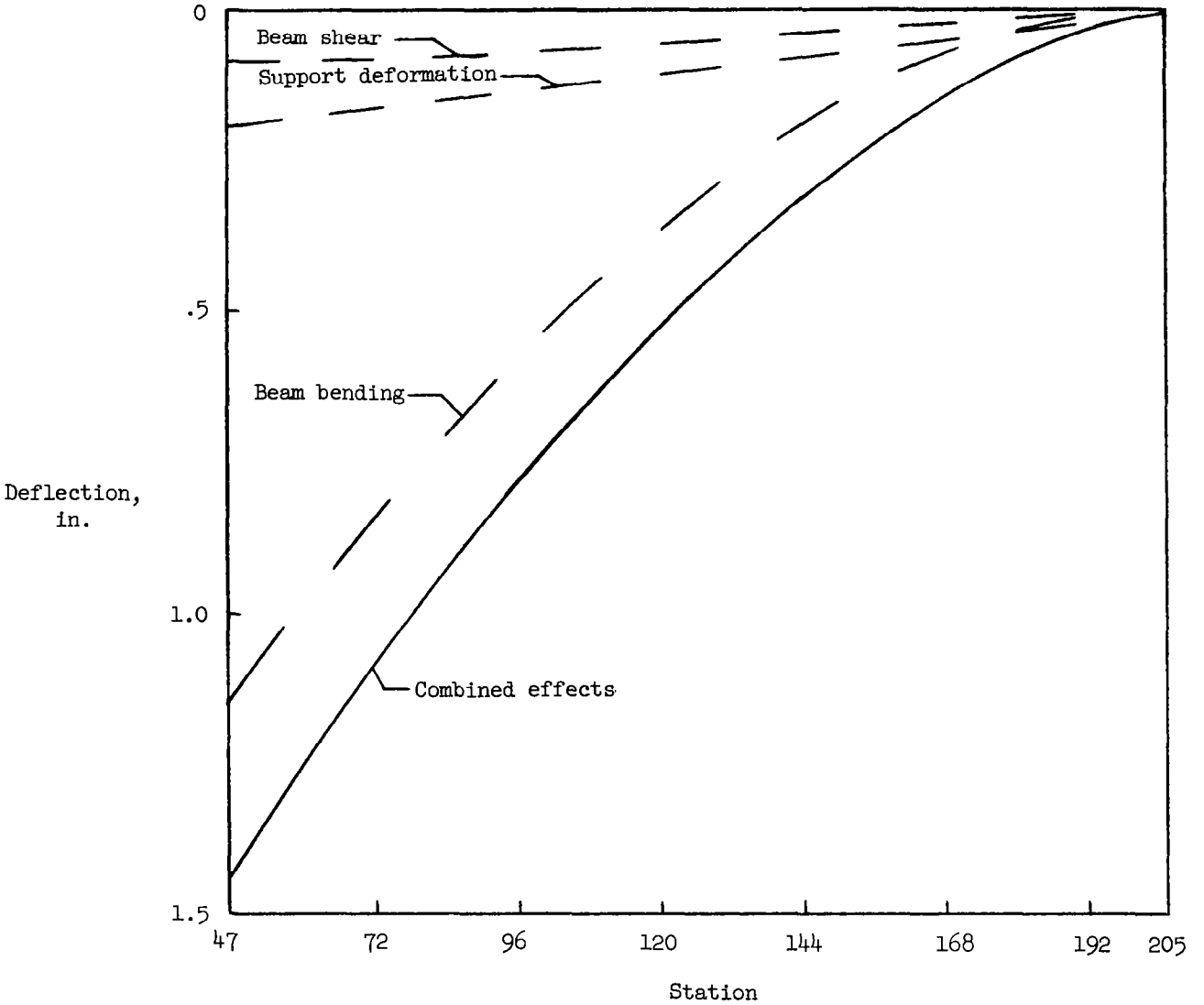

(b) Contributions of various factors to calculate model deflection for 9,986-pound distributed load.

Figure 6.- Concluded.

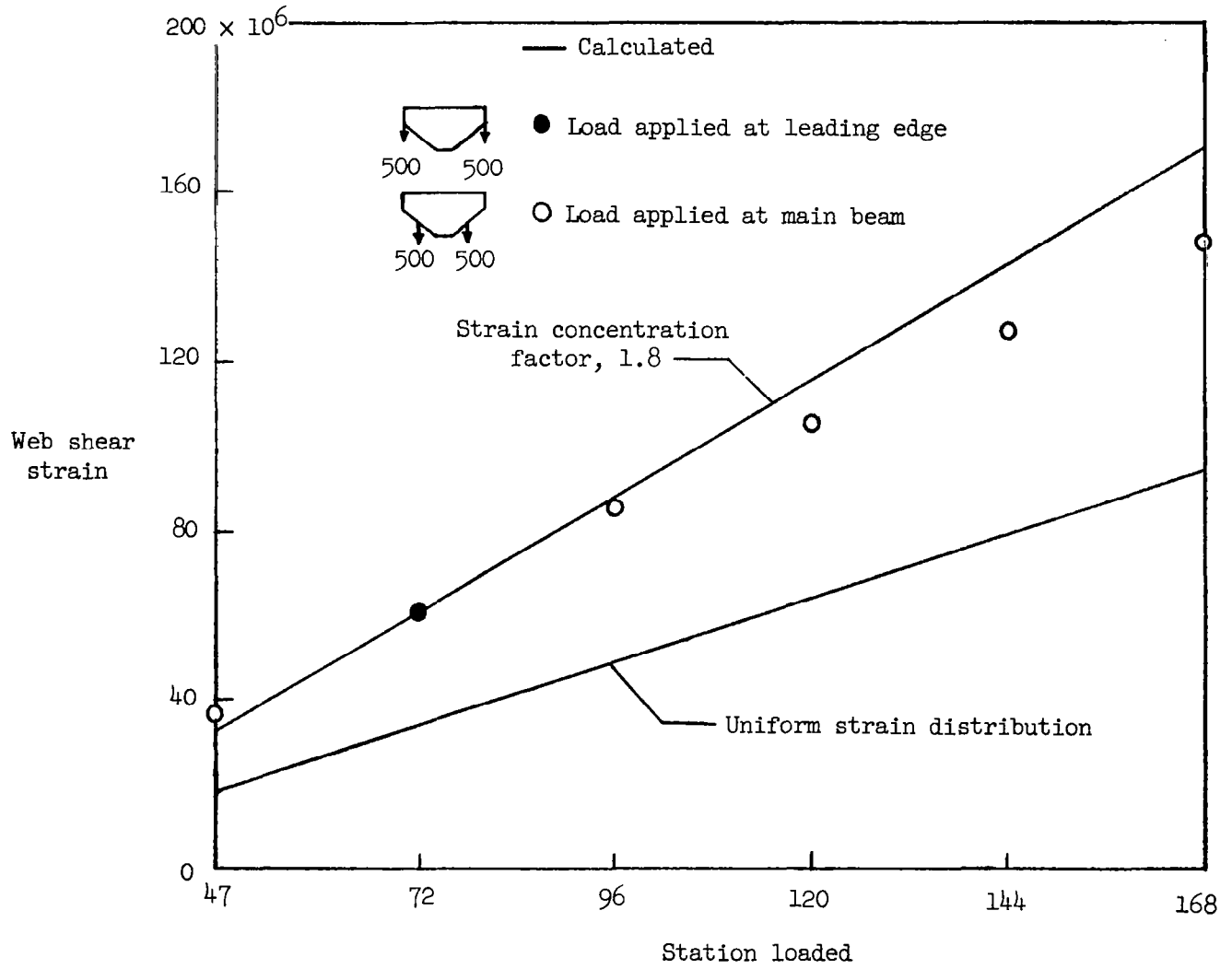

(a) Shear strain in corrugated web of main beam at station 188 for 1,000-pound concentrated load applied at various stations.

Figure 7.- Strain in model due to loading at room temperature.

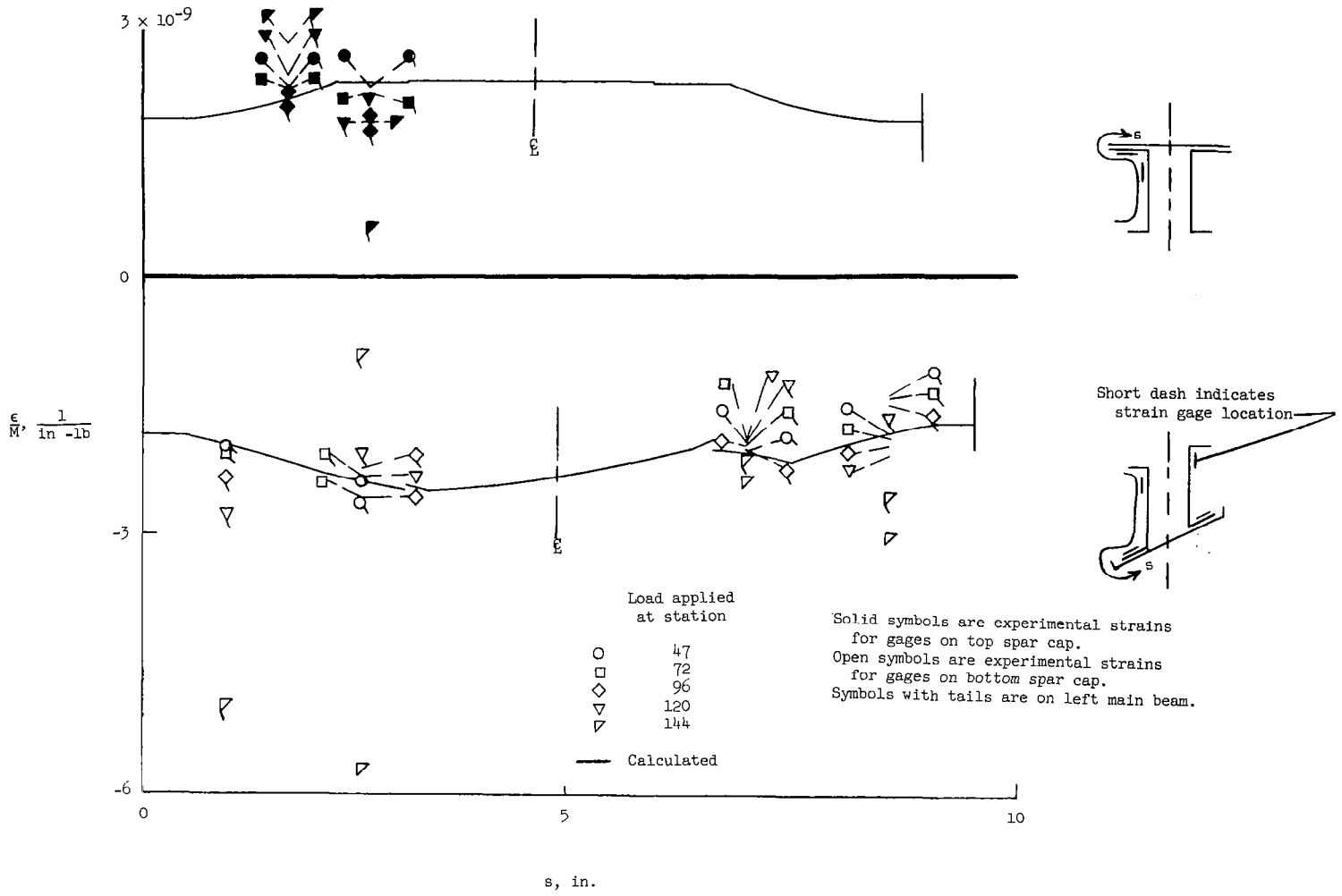

(b) Main beam spar-cap strain in cross section at station 155.

Figure 7.- Continued.

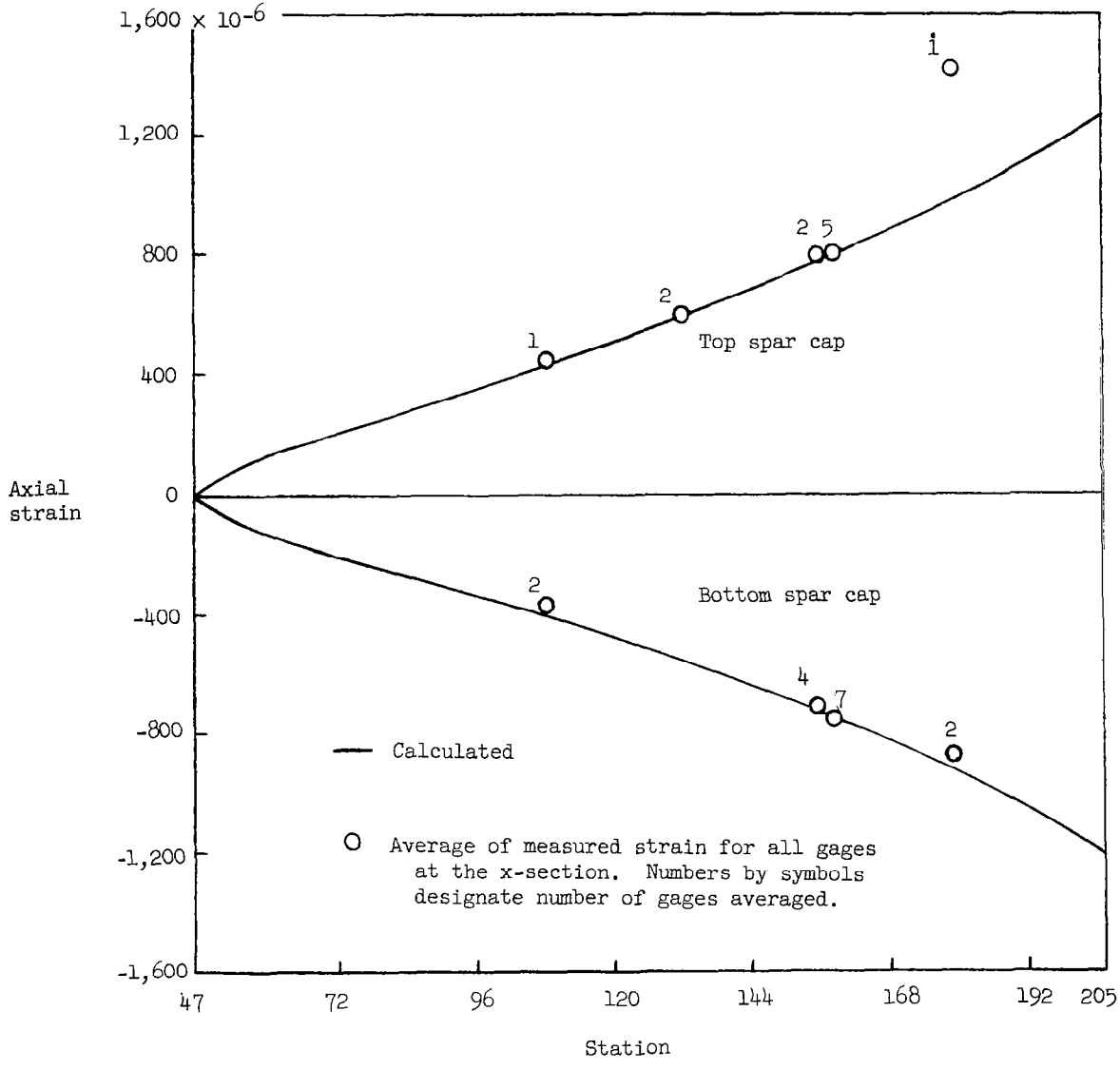

(c) Strains in longitudinal spar cap for distributed load.

Figure 7.- Concluded.

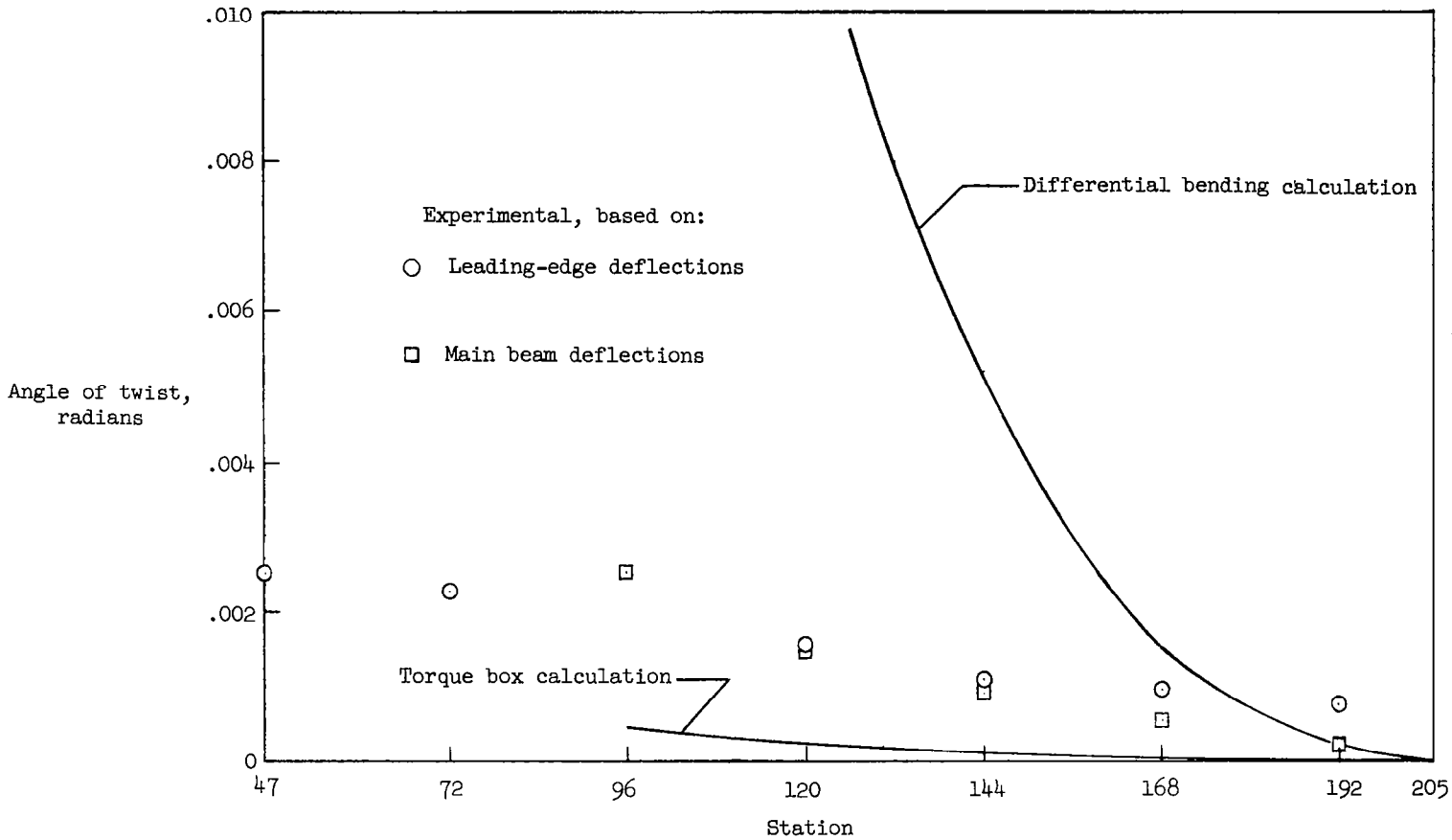

Figure 8.- Comparison of experimental and calculated angles of twist for 16,650 in-lb torque applied at station 96, at room temperature.

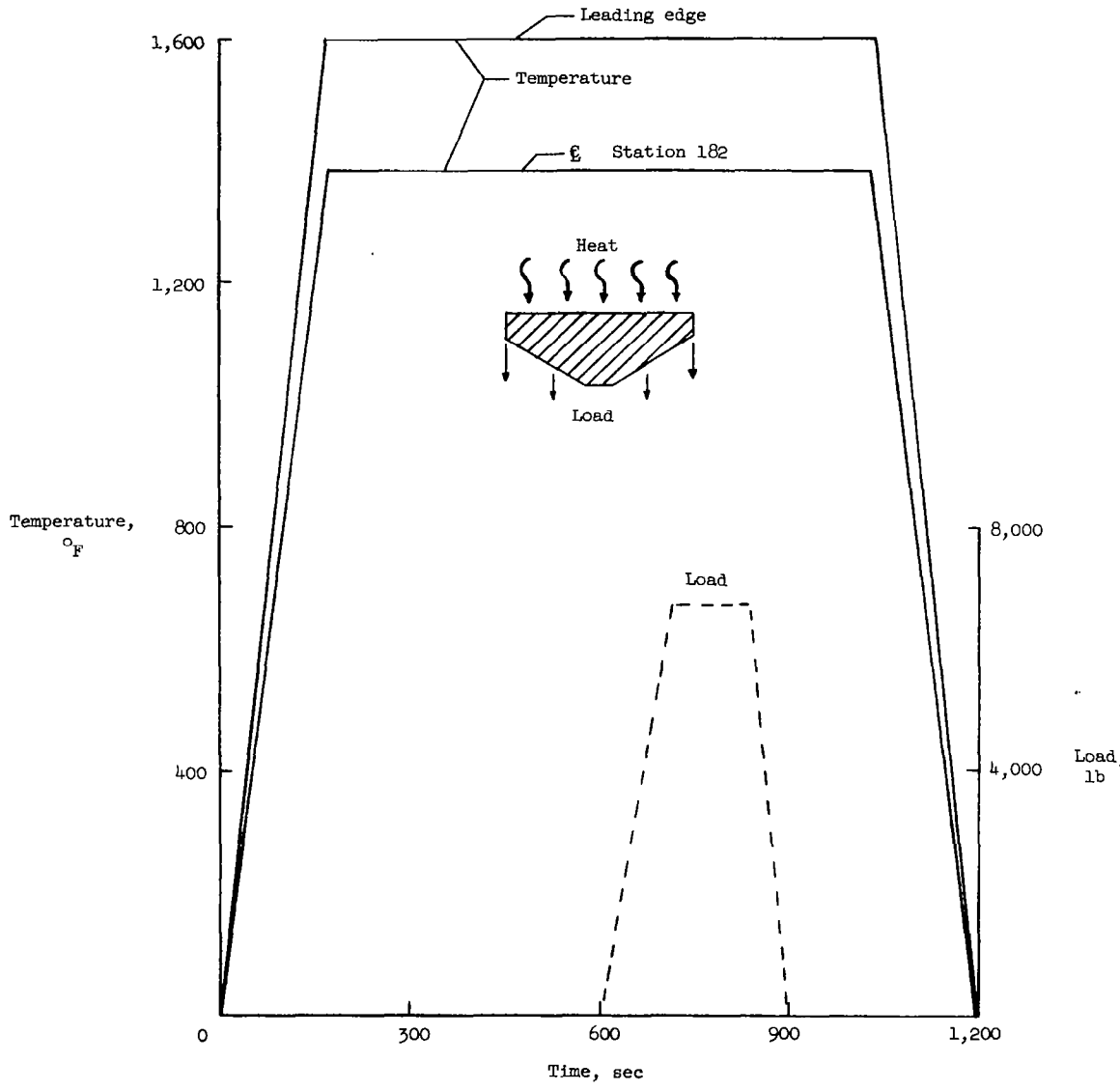

Figure 9.- Programed test environment.

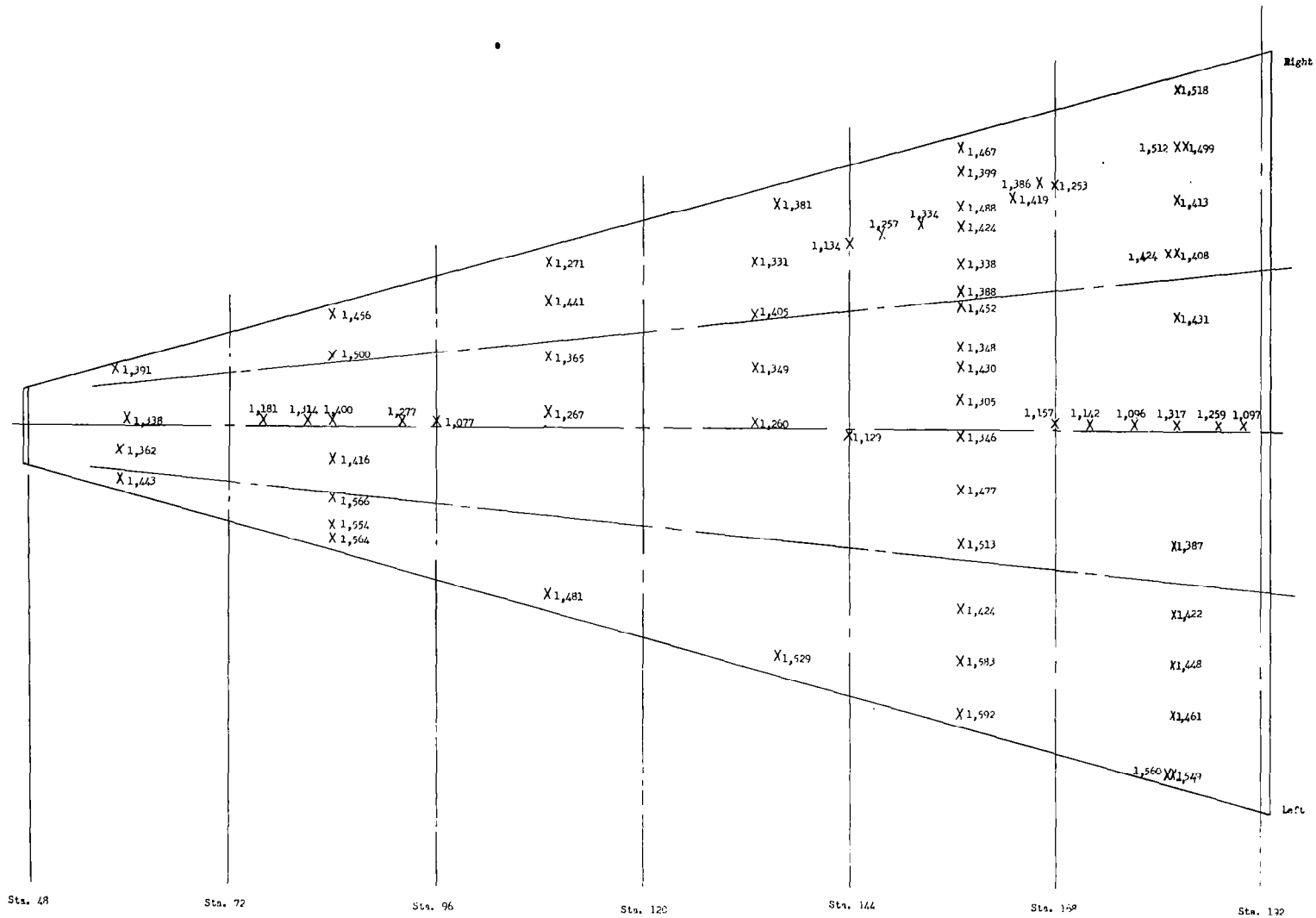

(a) Top skin temperature, °F, are listed at each thermocouple location.

Figure 10.- Temperature distribution of structure at 7 minutes.

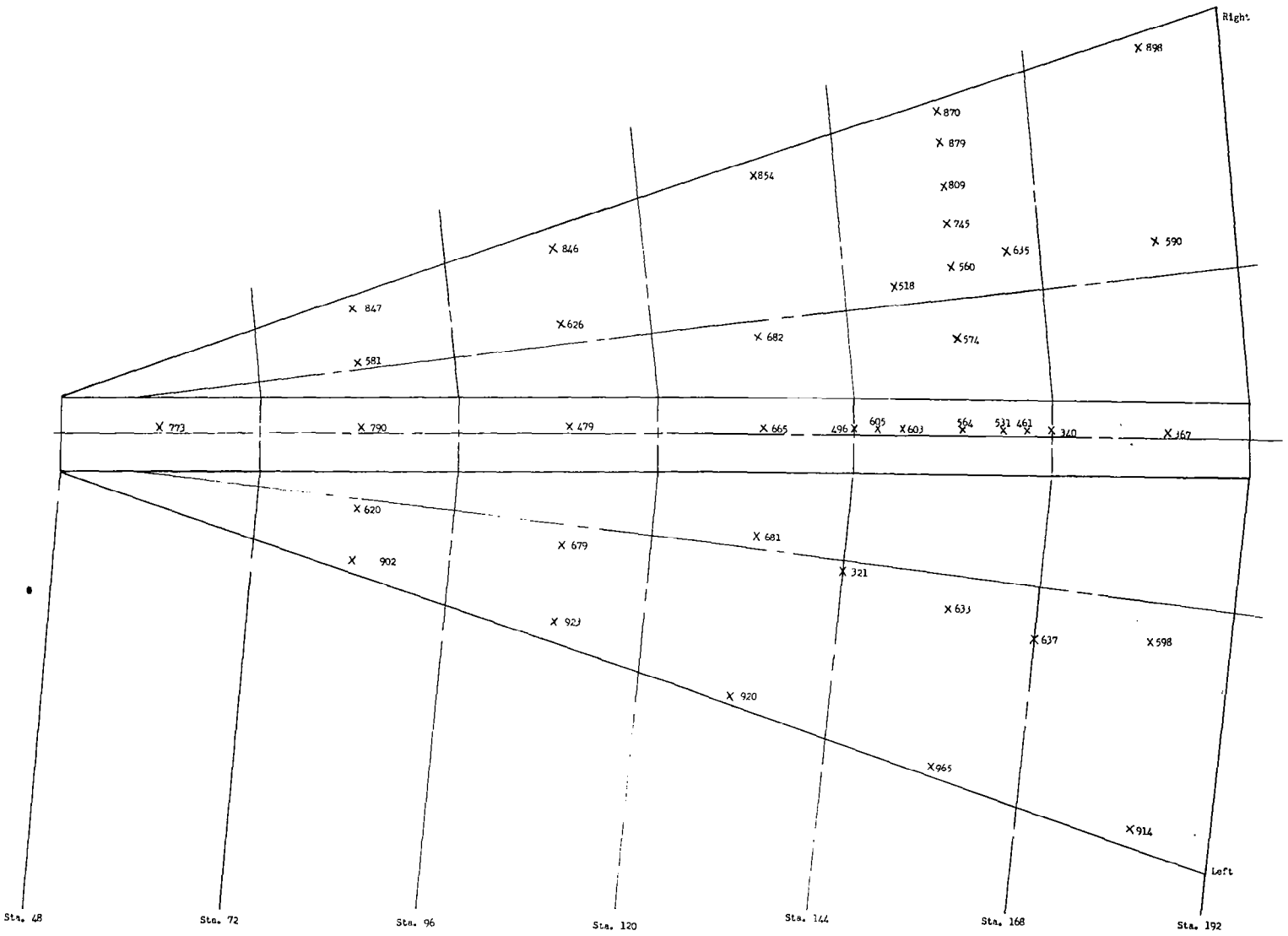

(b) Bottom skin temperature, ^{o}F, are listed at each thermocouple location.

Figure 10.- Continued.

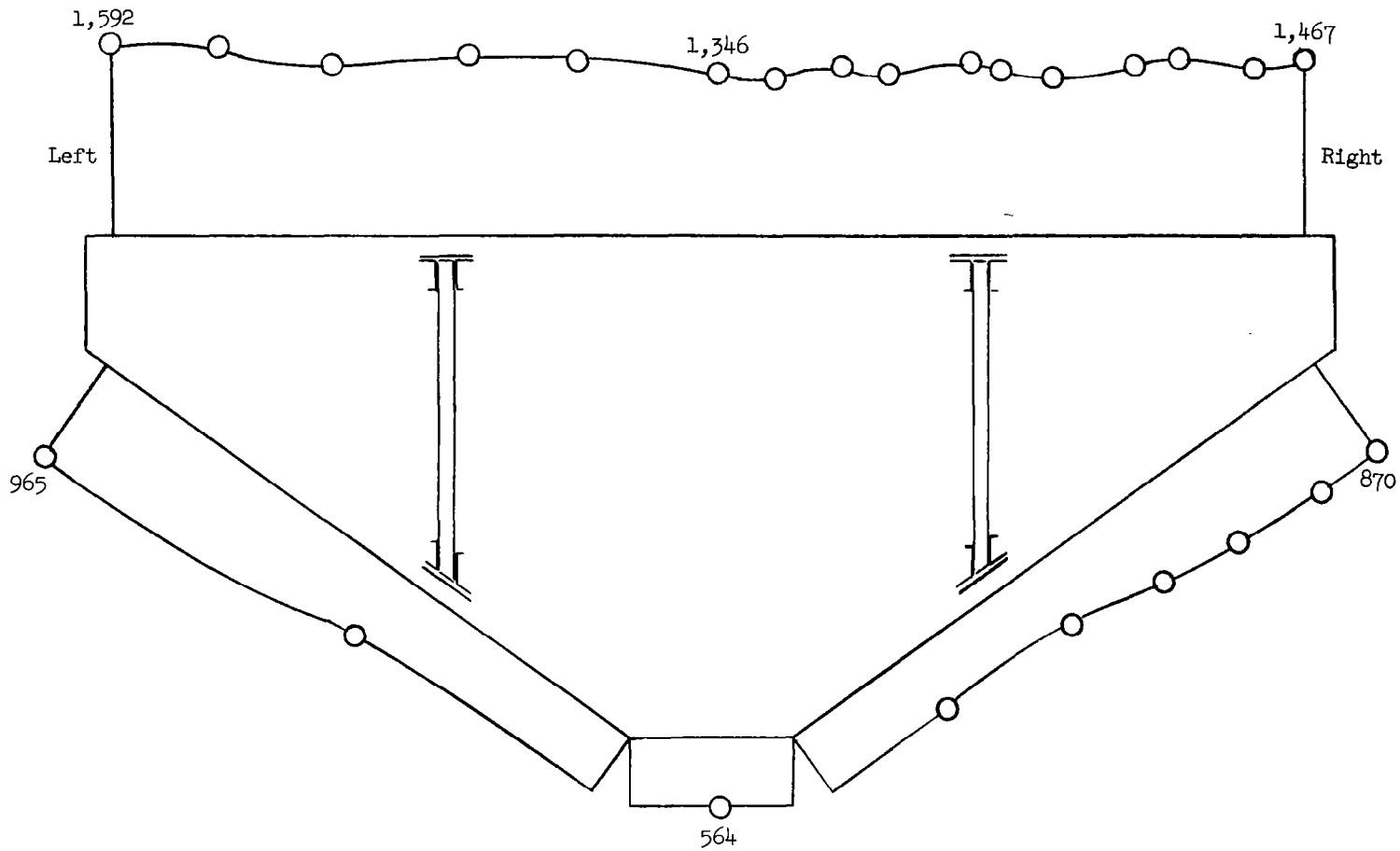

(c) Skin temperatures, ^{o}F, in transverse section at station 157.

Figure 10.- Continued.

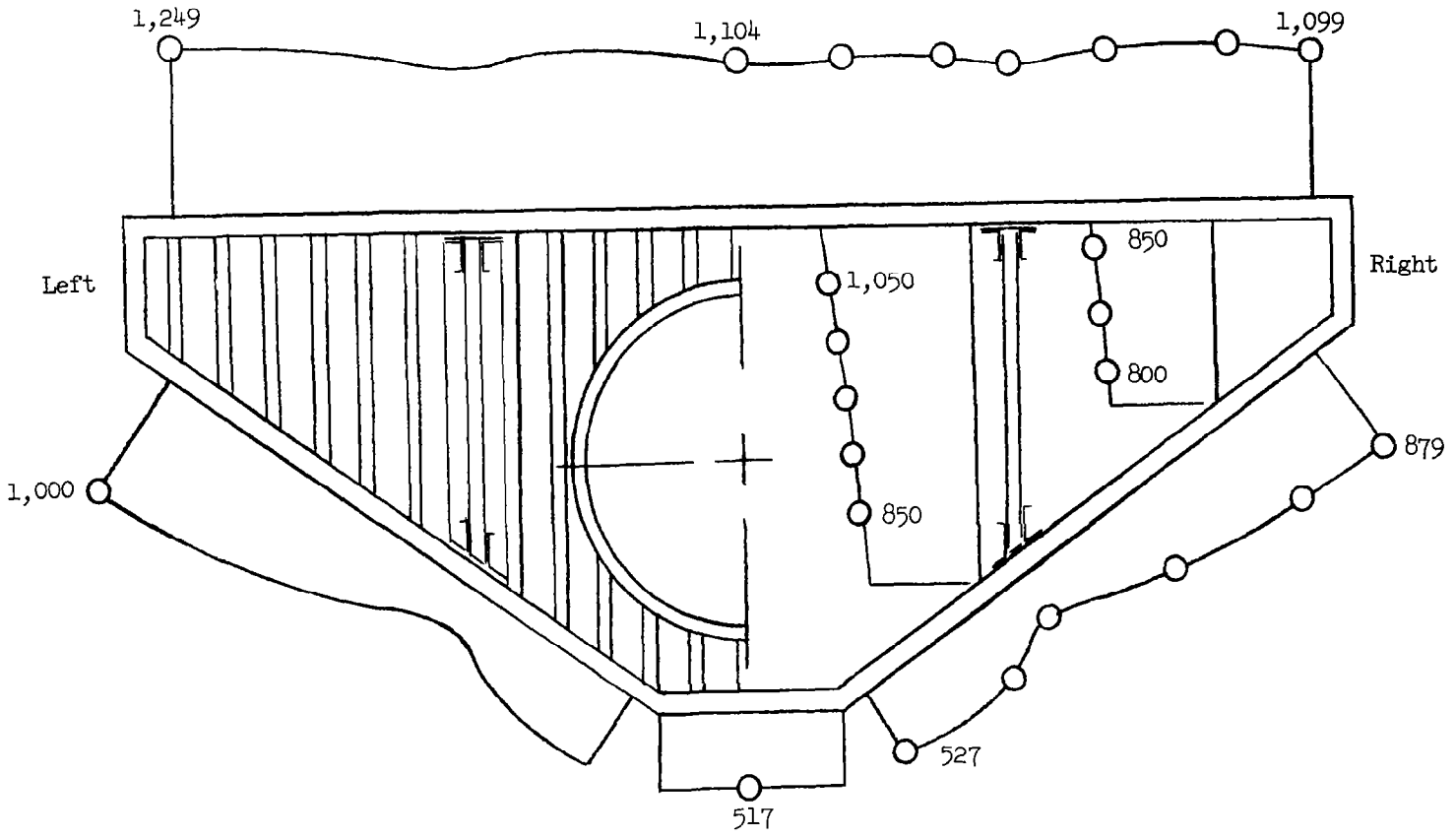

(d) Temperatures, ^{o}F, in transverse frame at station 144.

Figure 10.- Continued.

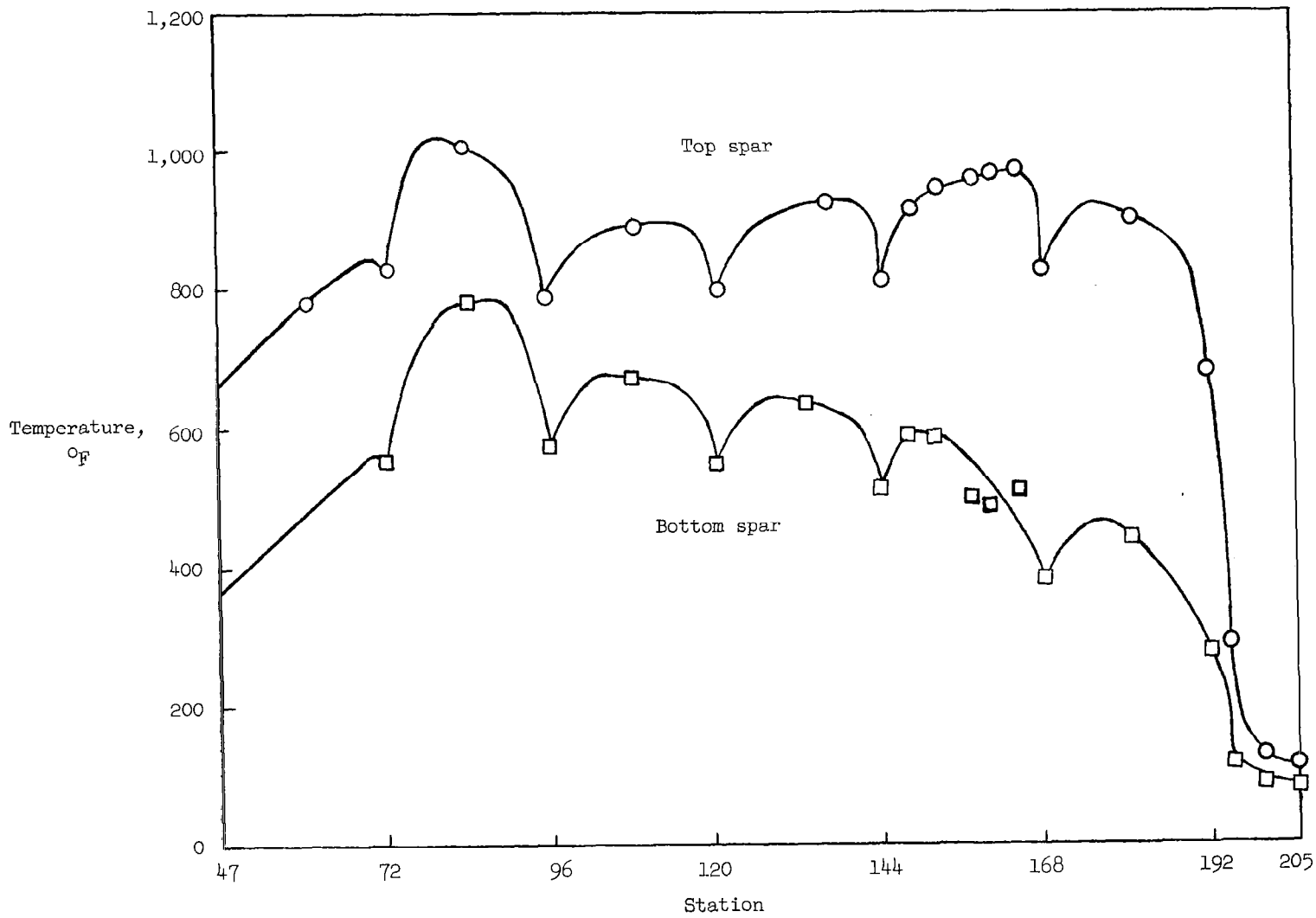

(e) Temperature in right longitudinal spar caps.

Figure 10.- Concluded.

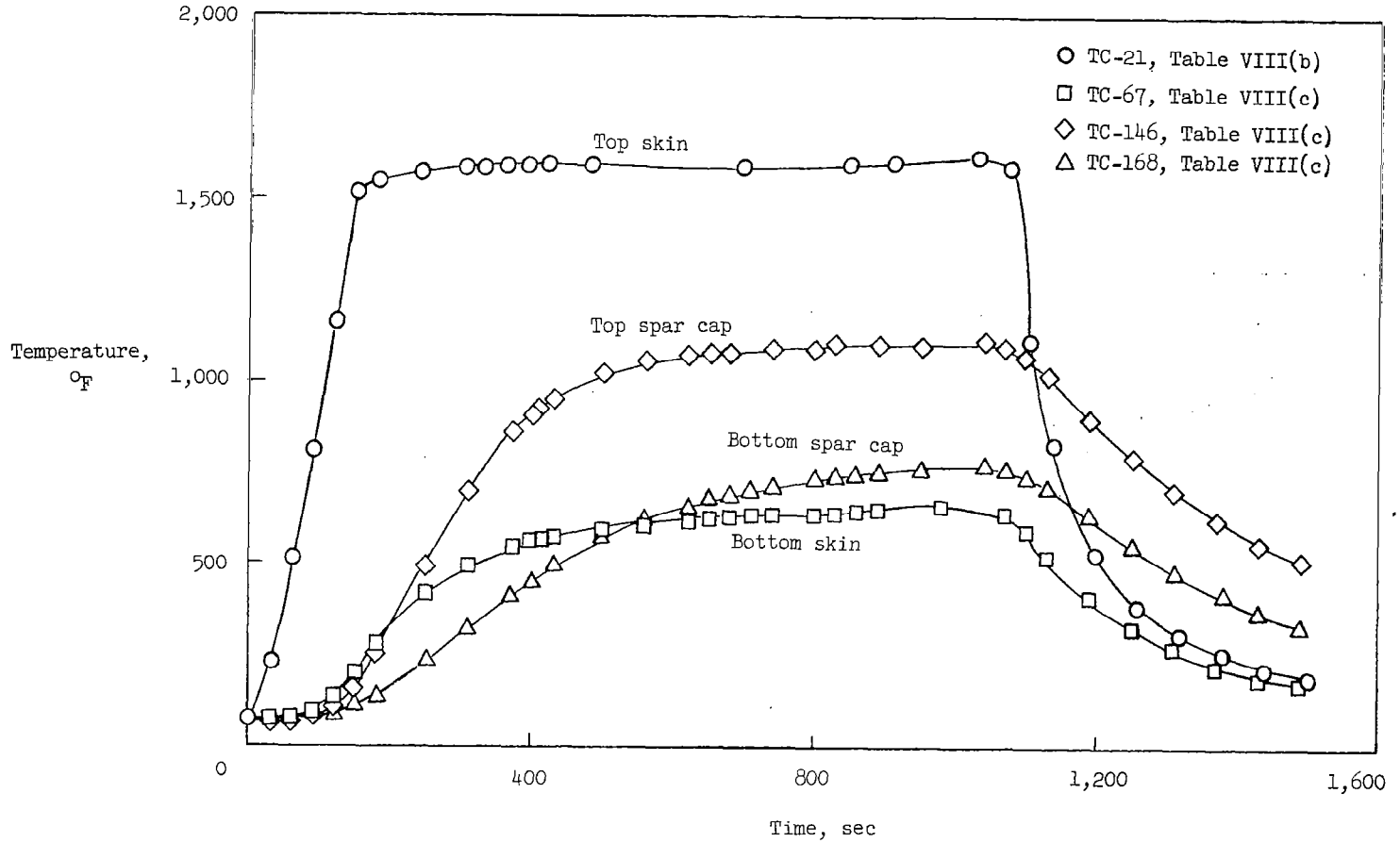

Figure 11.- Variation of temperature with time in model cross section at station 157.

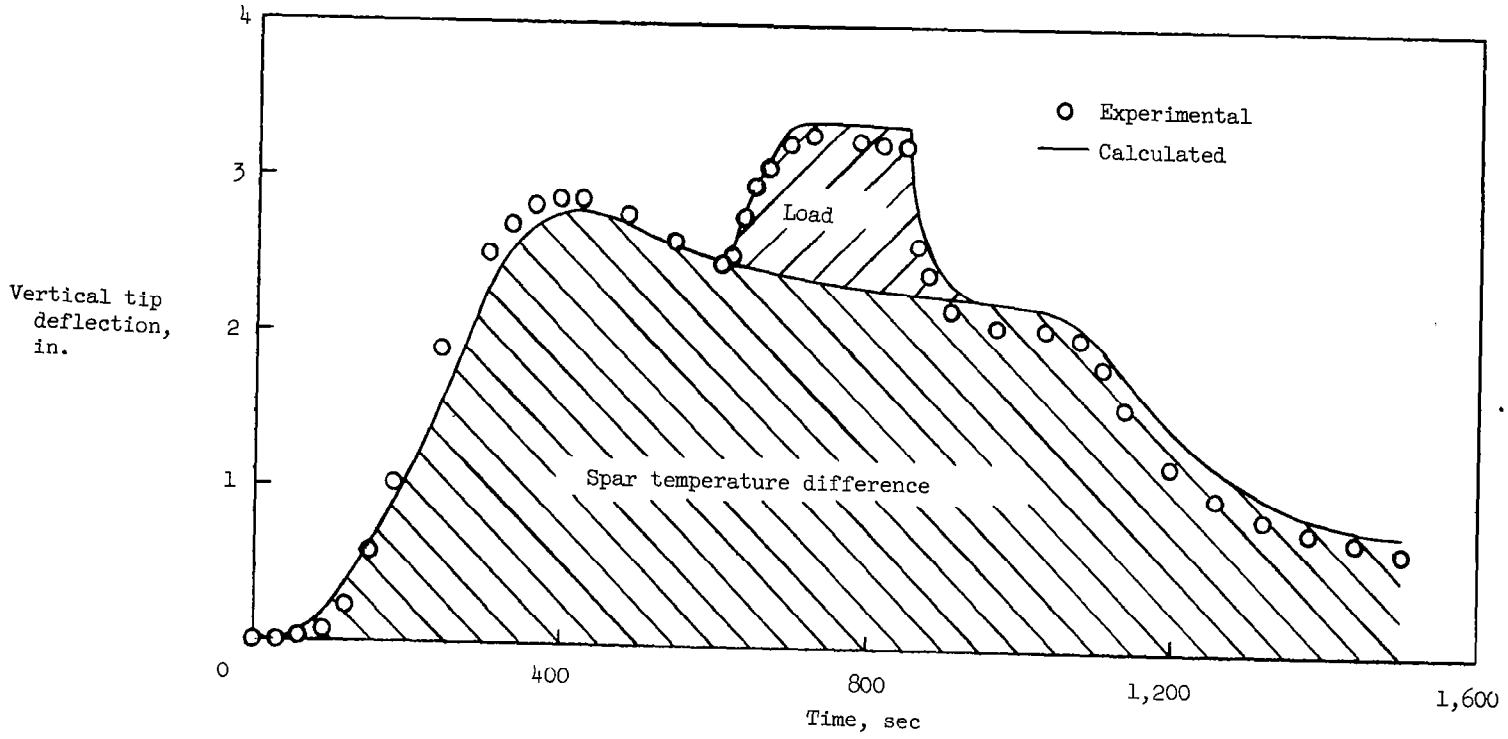

(a) Vertical.

Figure 12.- Tip deflection of model for 1,600° F test.

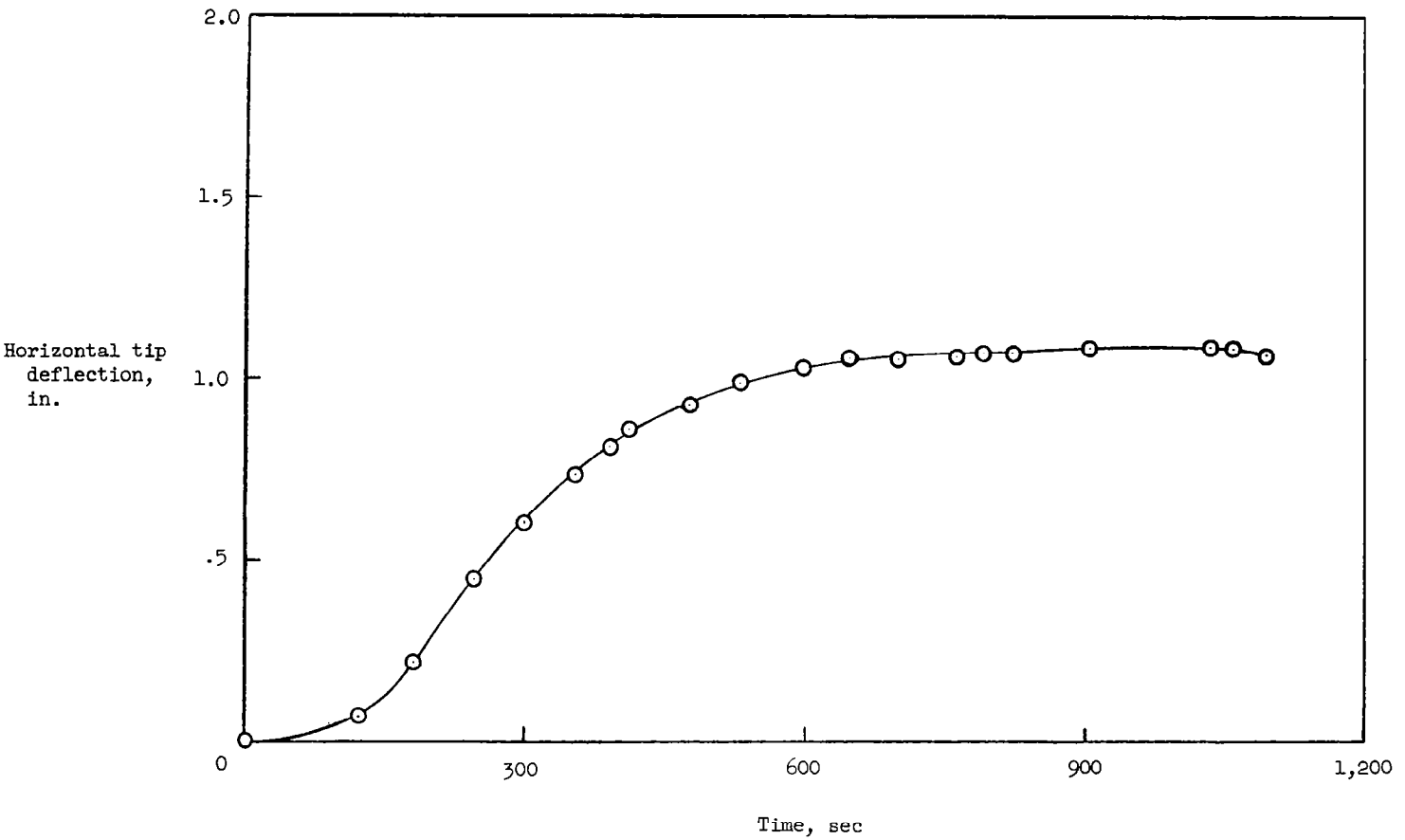

(b) Horizontal.

Figure 12.- Concluded.

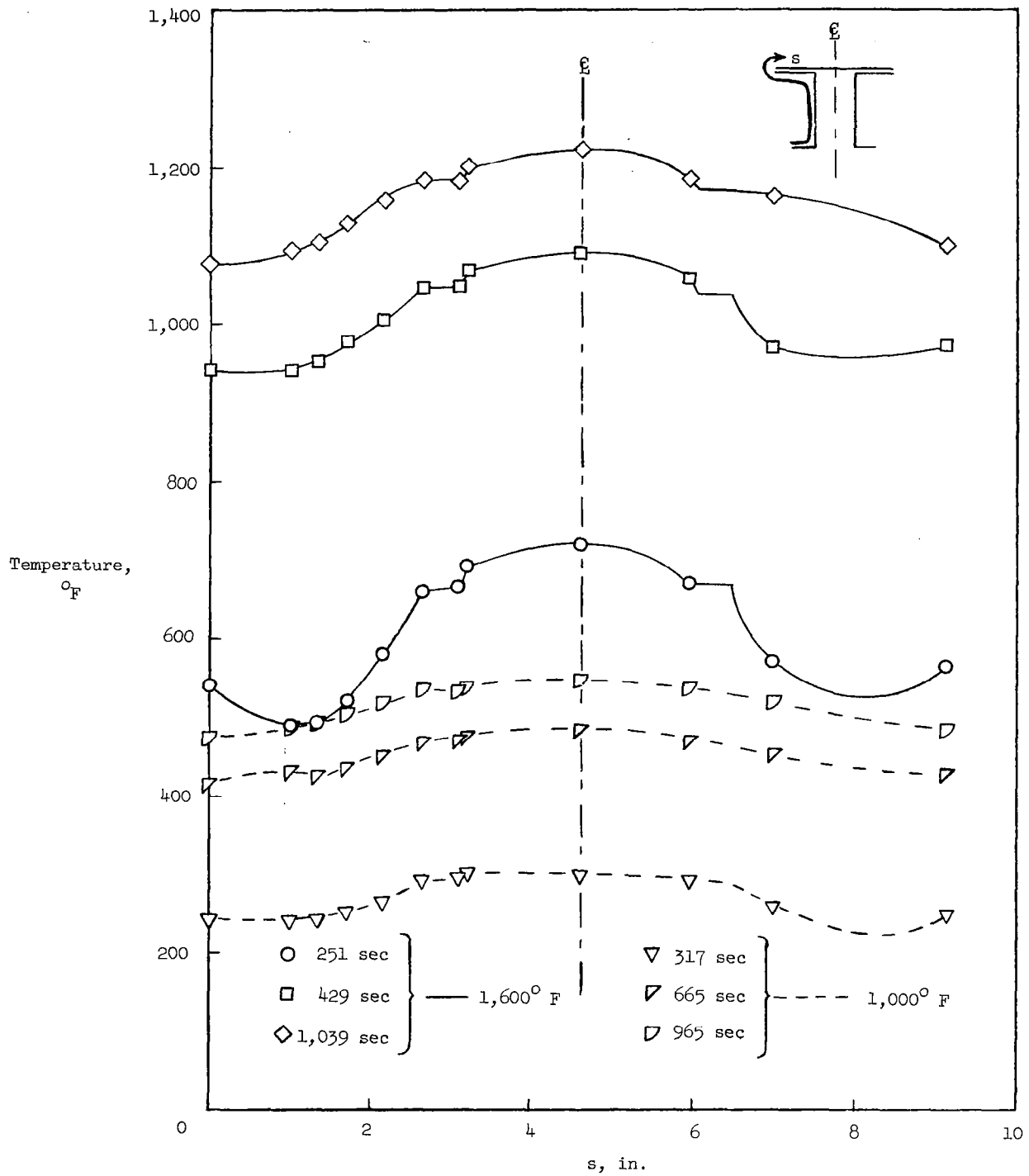

Figure 13.- Temperature distribution in longitudinal spar cap at station 157.

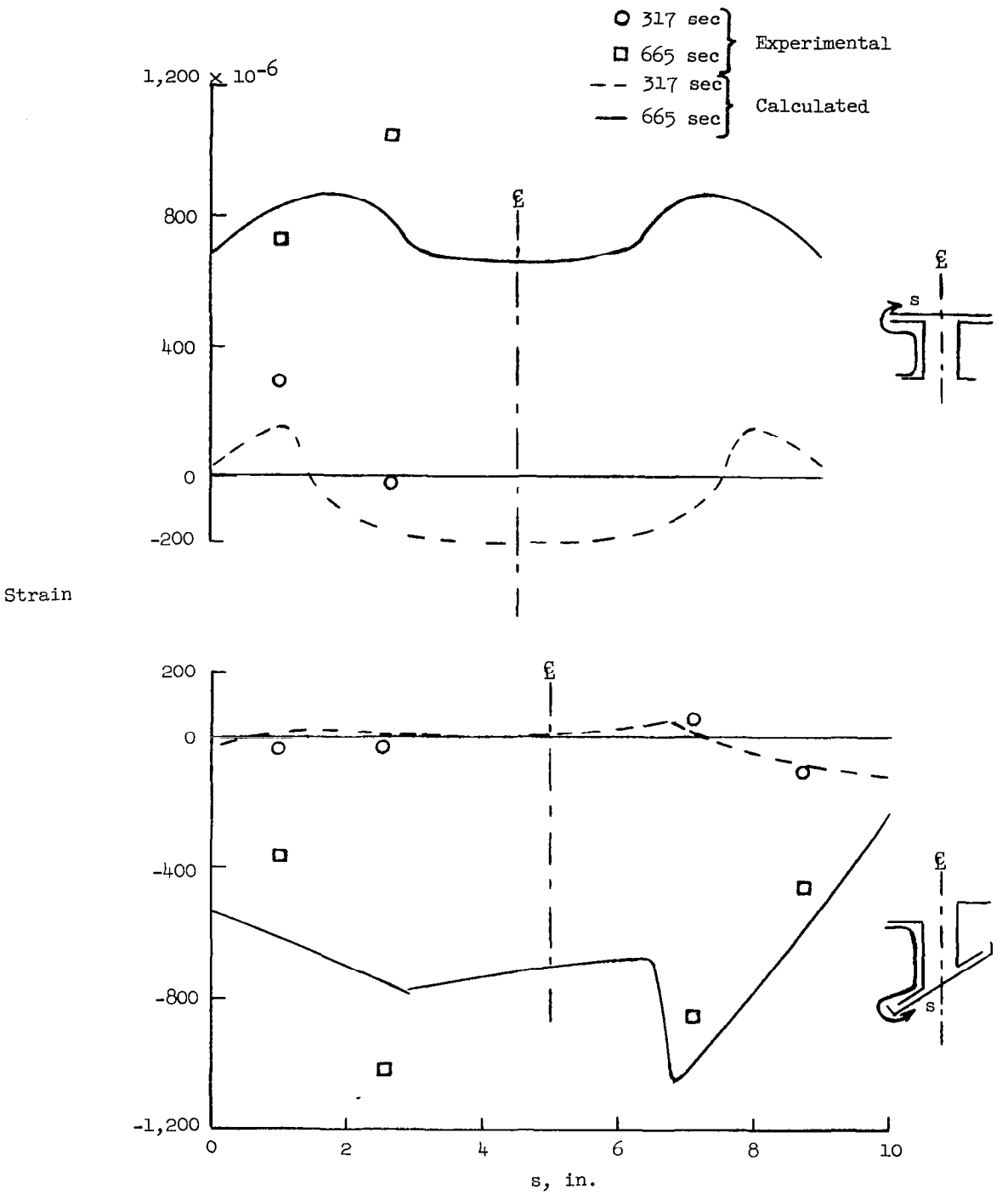

Figure 14.- Strains in longitudinal spar-cap cross section due to thermal and load stress for 1,000° F test (table IX).

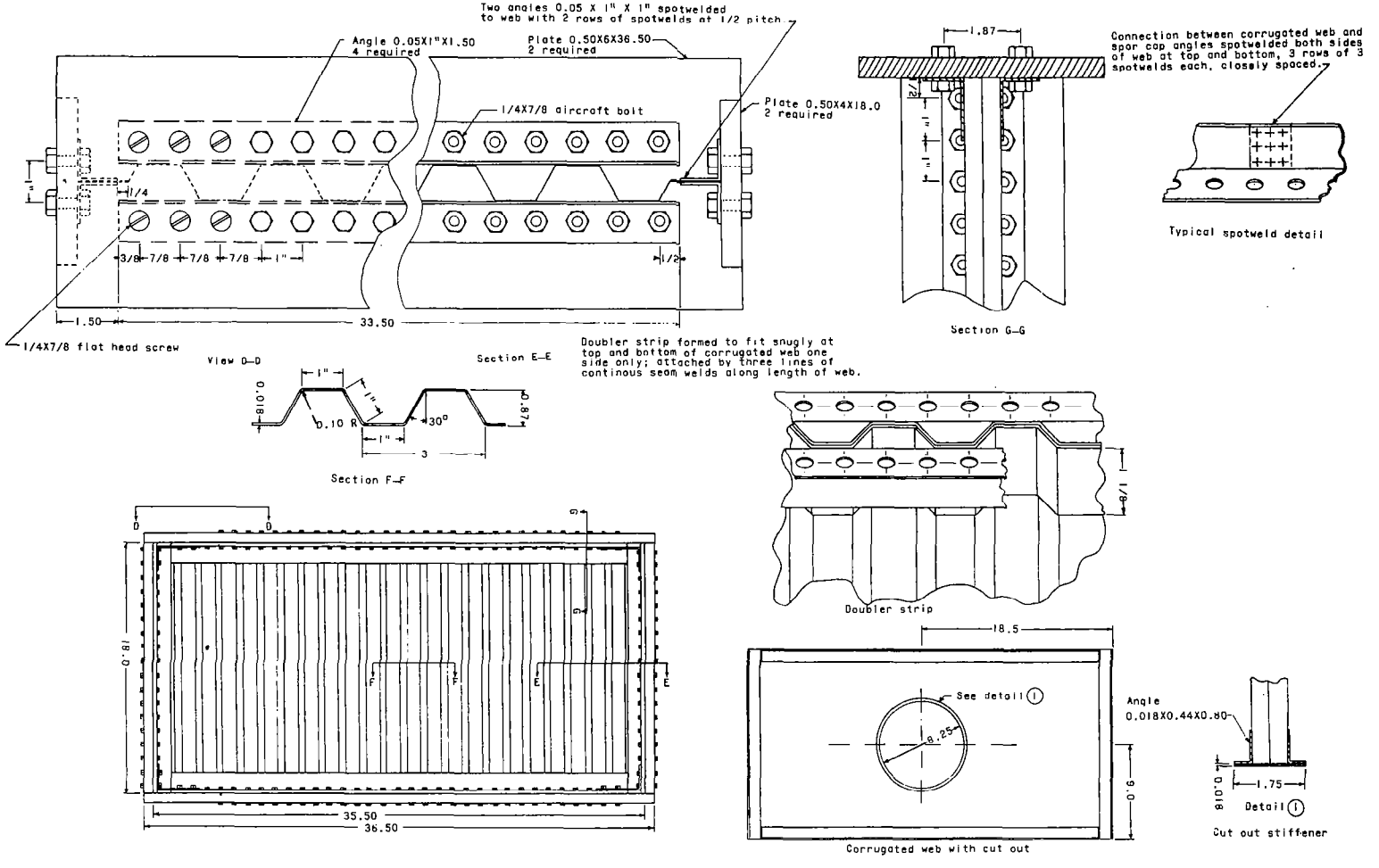

(a) 60° by 1-inch flat corrugation.

Figure 15.- Shear-web test specimen.

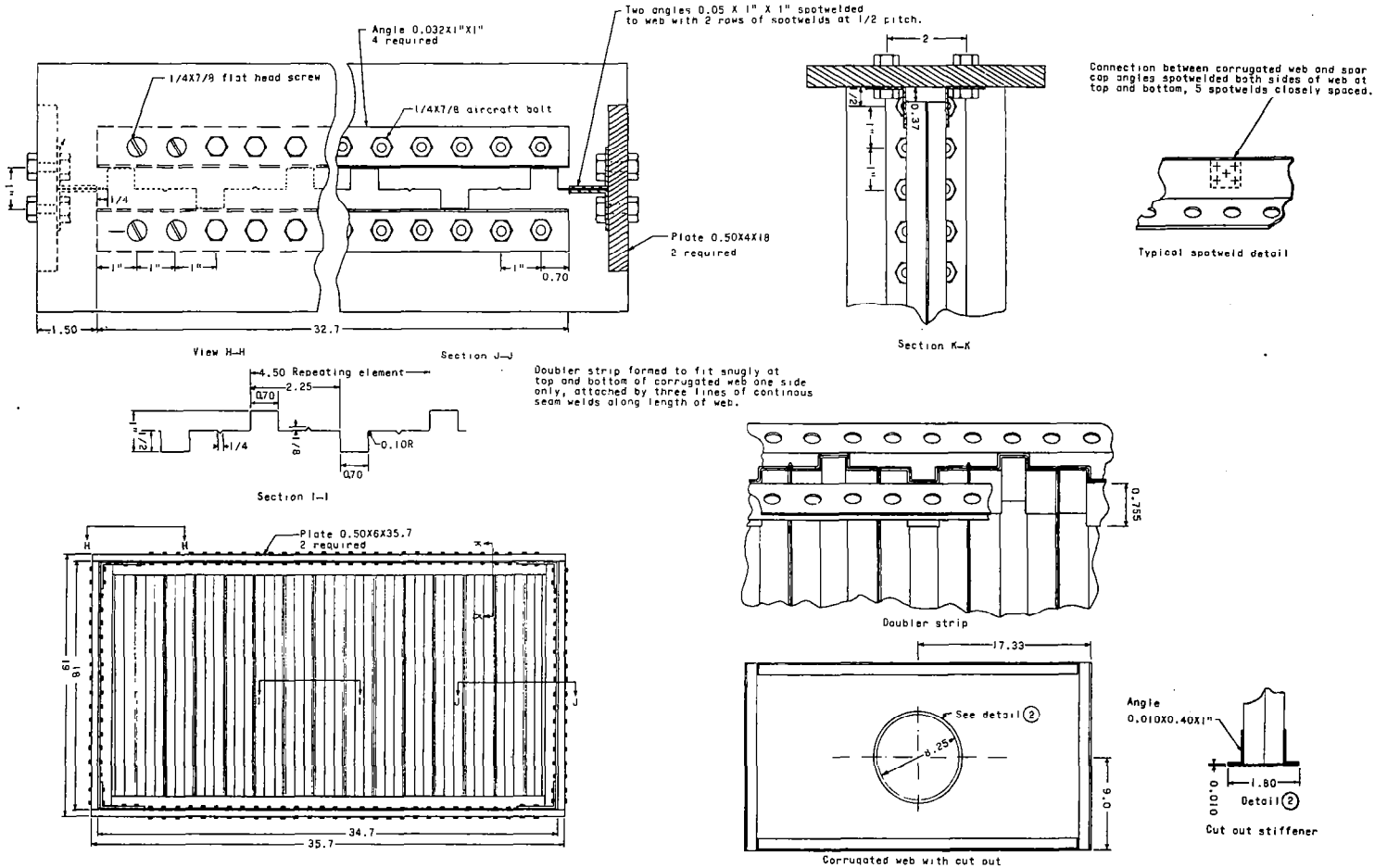

(b) Special transverse-frame corrugation.

Figure 15.- Concluded.

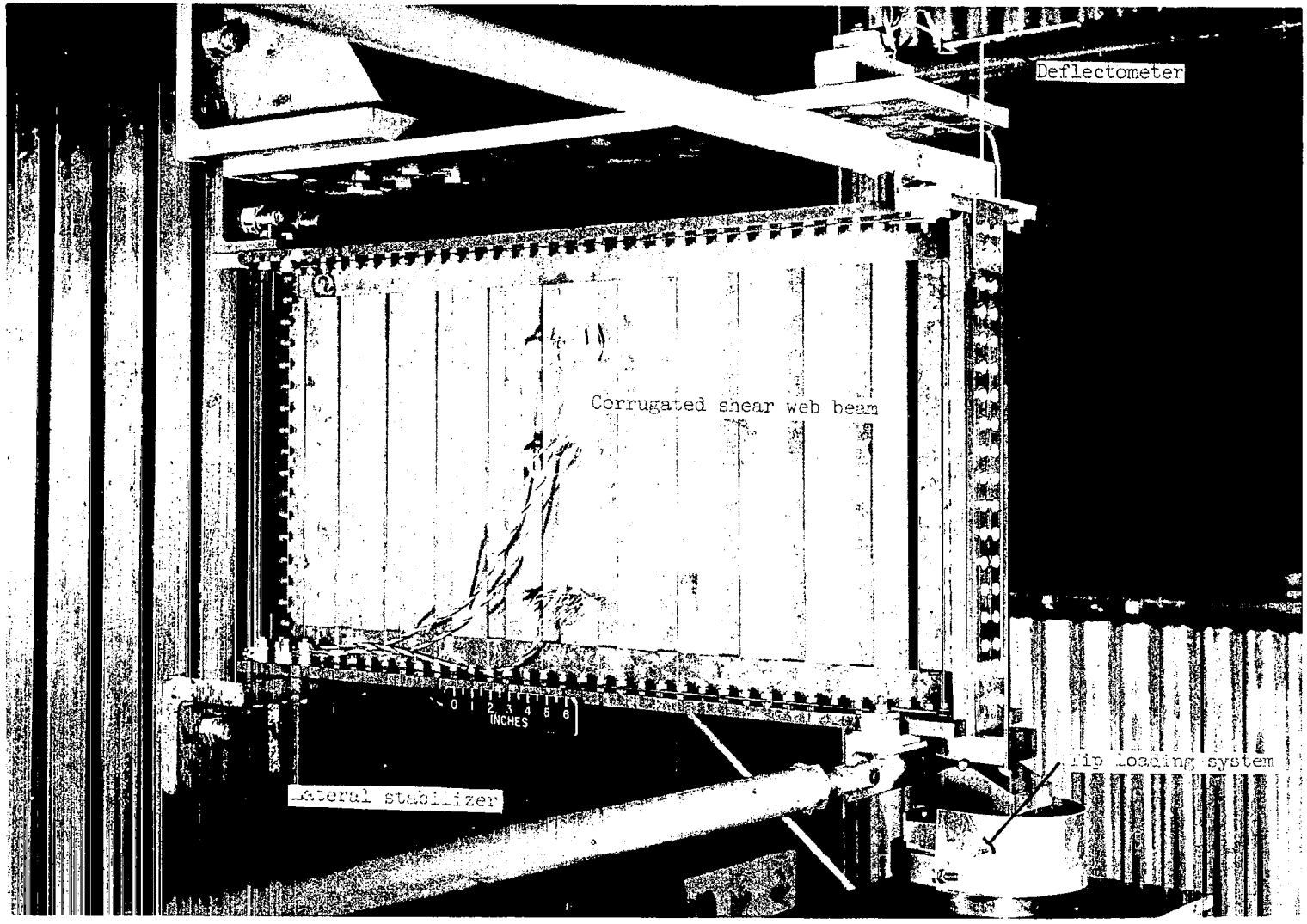

(a) Room temperature. L-60-1743.1

Figure 16.- Shear-web test setup.

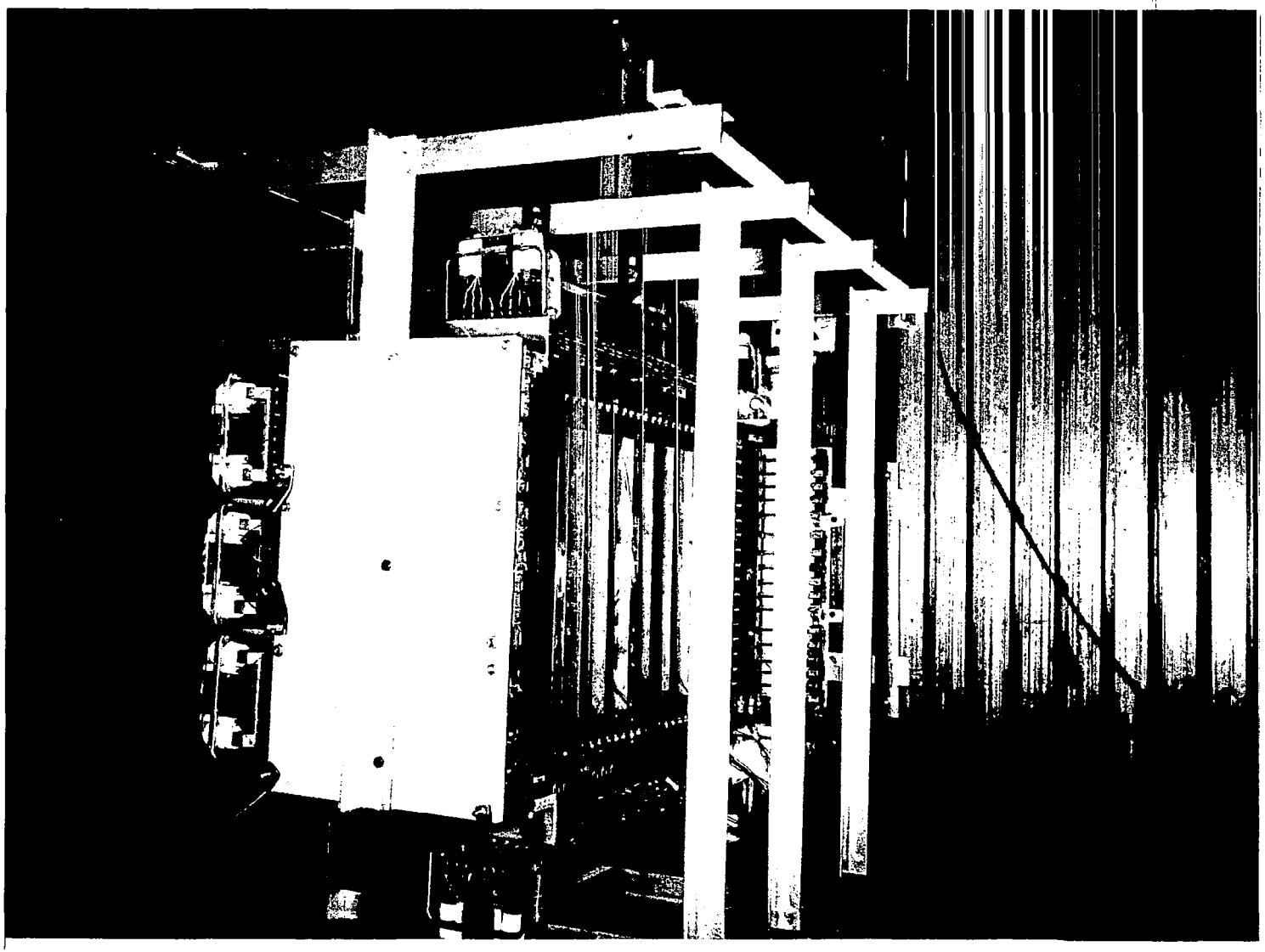

(b) Elevated-temperature setup with one side-radiator and hydraulic loading system removed. L-60-2749

Figure 16.- Concluded.

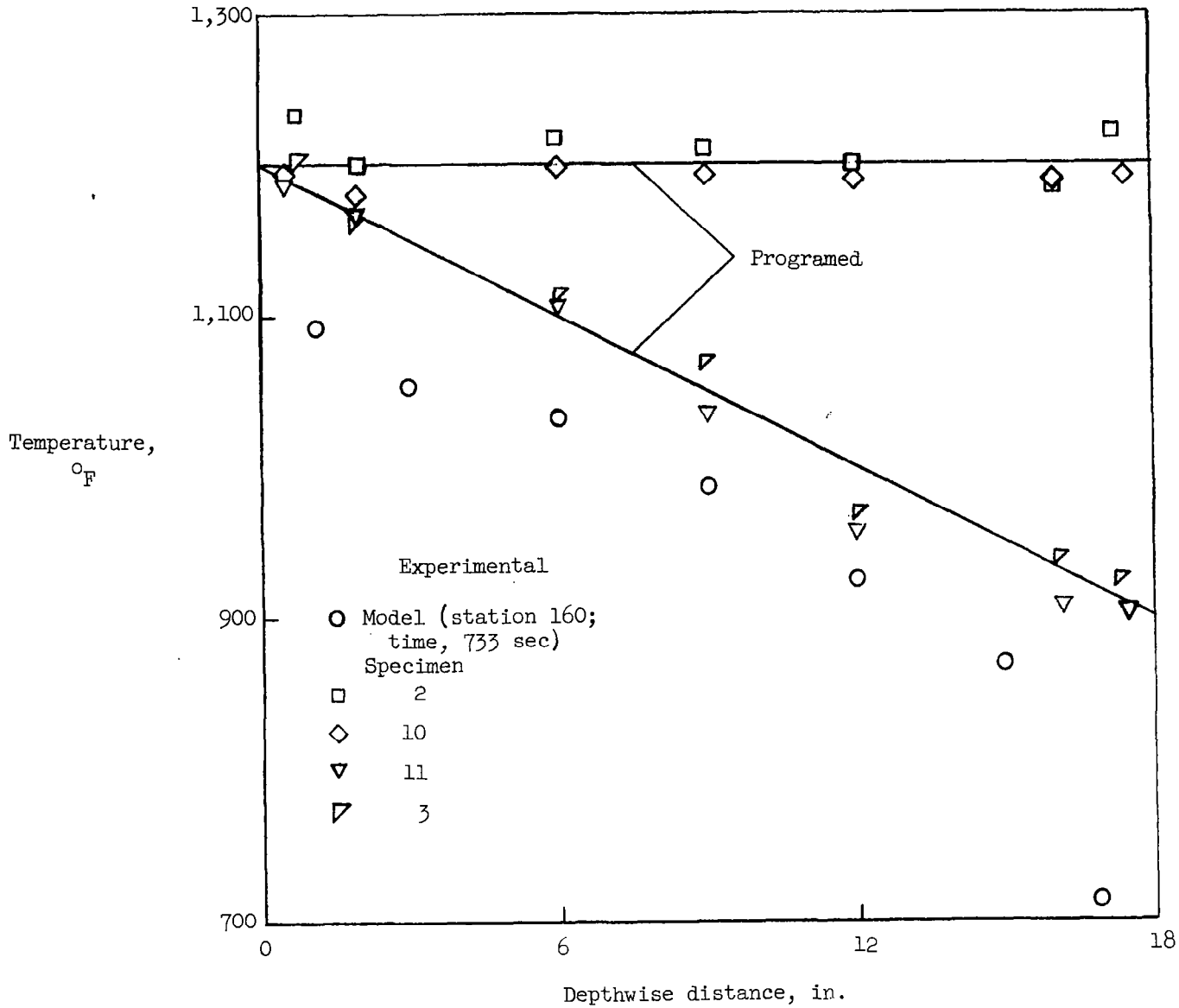

Figure 17.- Shear-web temperature distributions for combined heat and load tests.

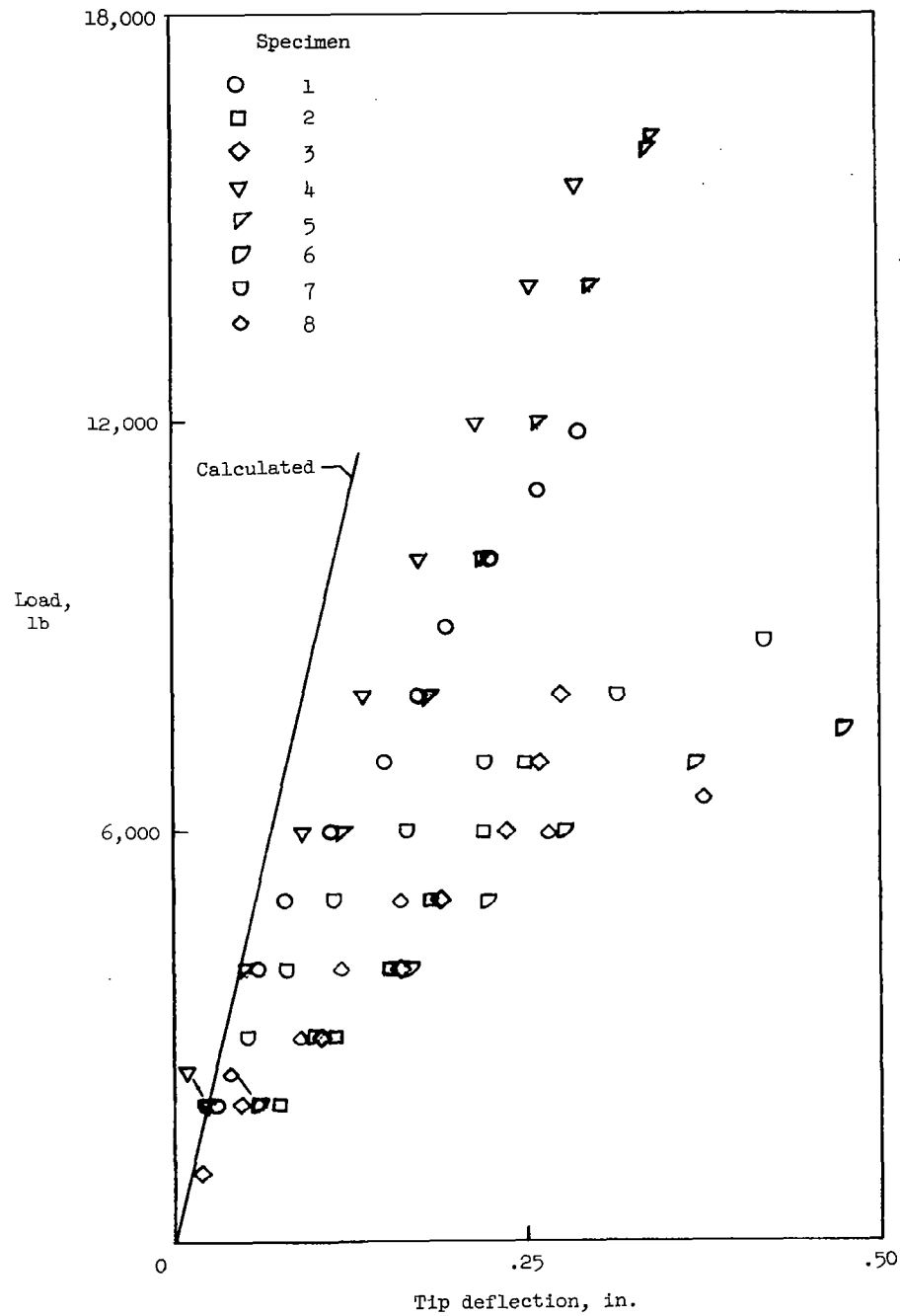

(a) 60^{o} by 1-inch flat corrugation.

Figure 18.- Tip deflection for corrugated shear-web beams. See table X for description of specimens and test conditions.

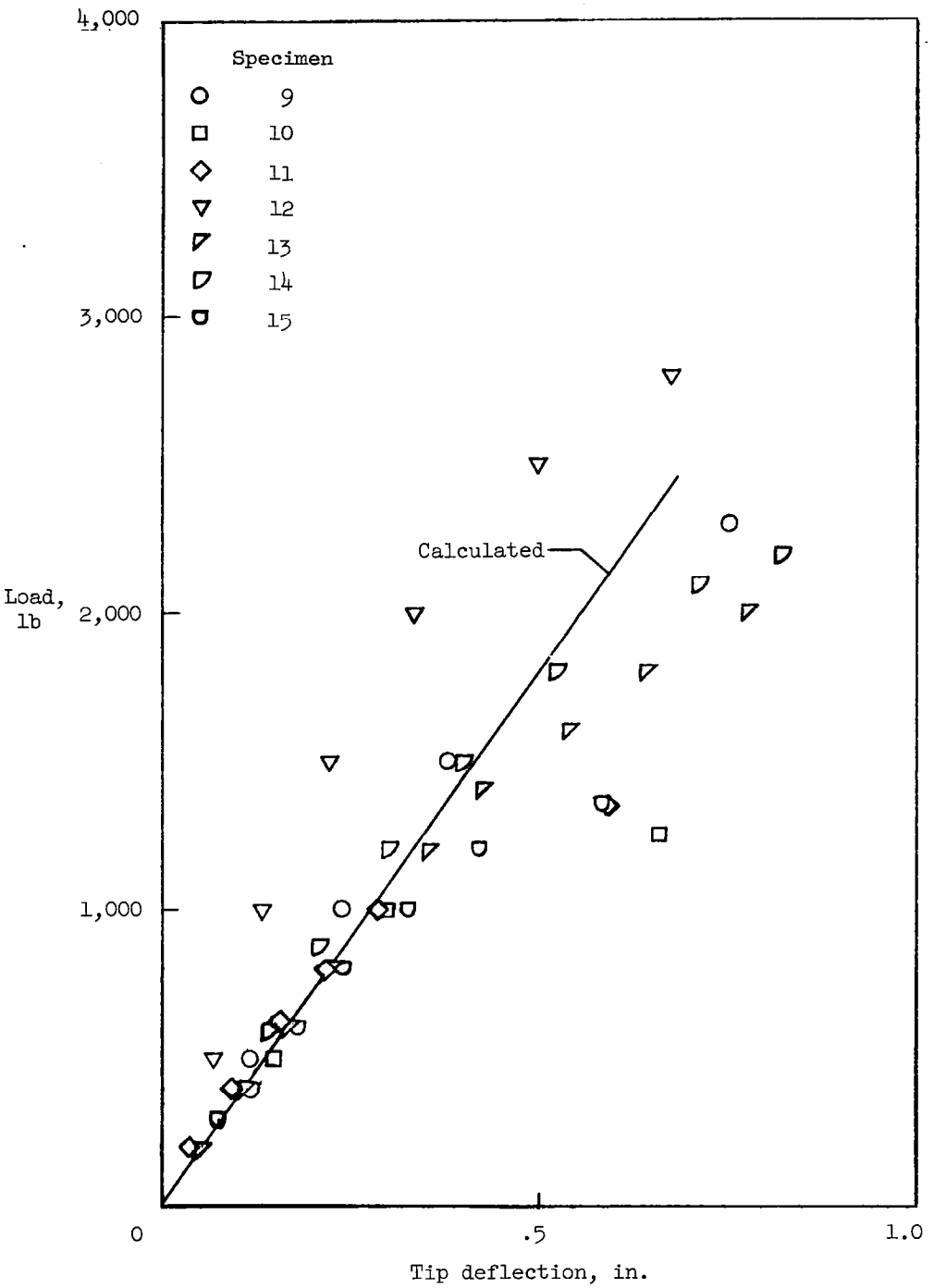

(b) Special transverse-frame corrugation design from structural concept model.

Figure 18.- Concluded.

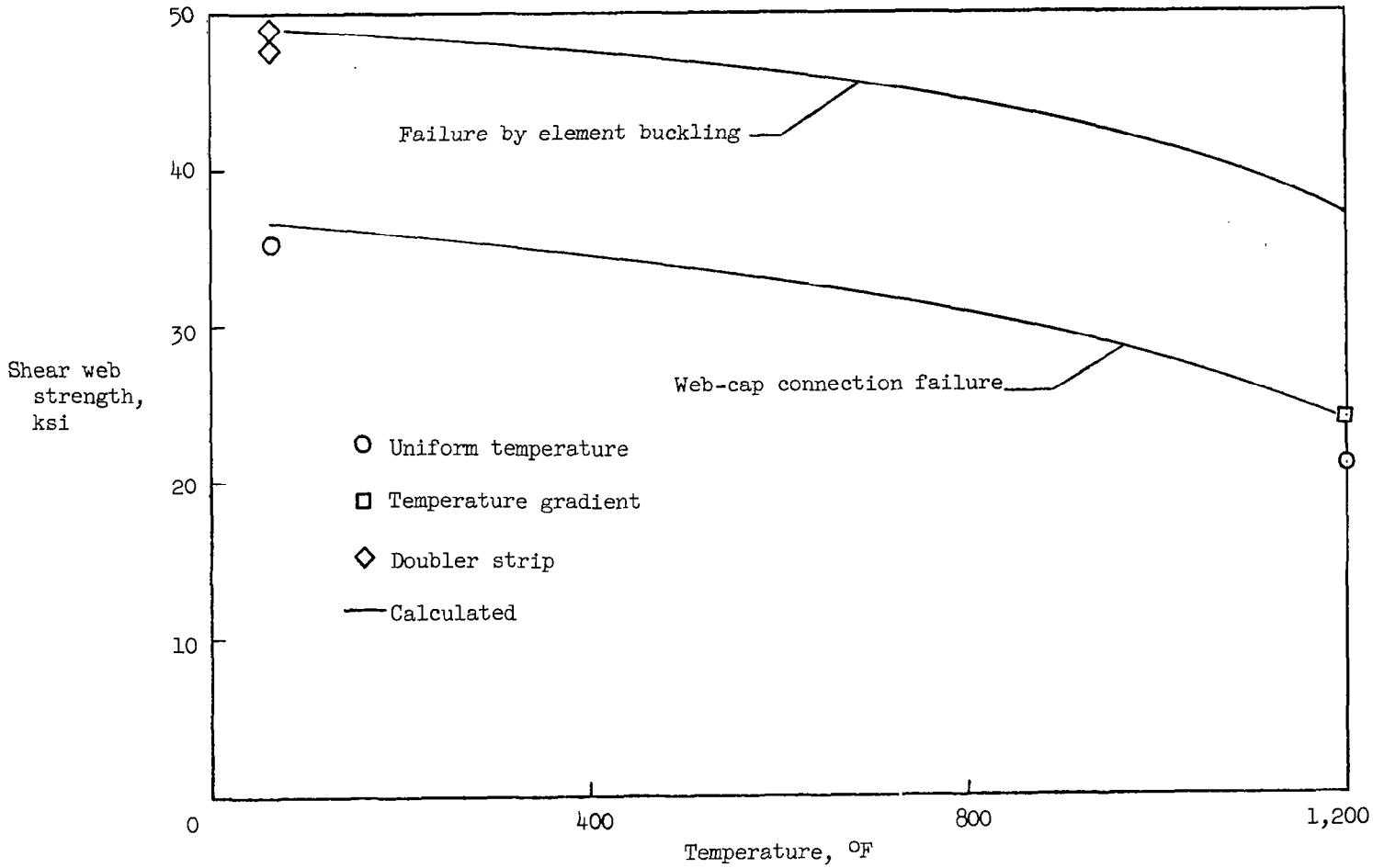

(a) 60° corrugation.

Figure 19.- Influence of elevated temperature and connection doubler strips on failure strength of corrugated shear webs.

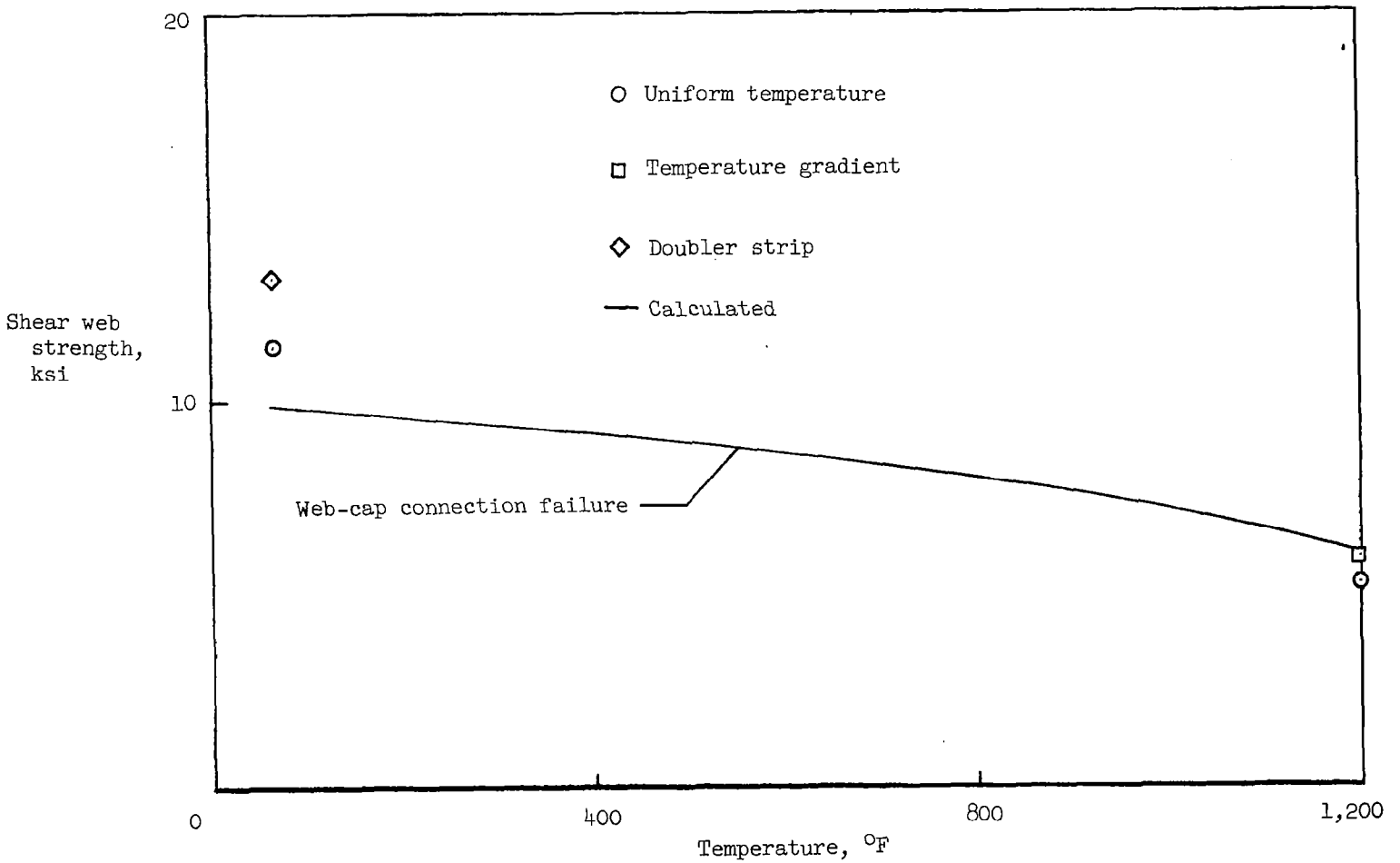

(b) Transverse-frame corrugation.

Figure 19.- Concluded.

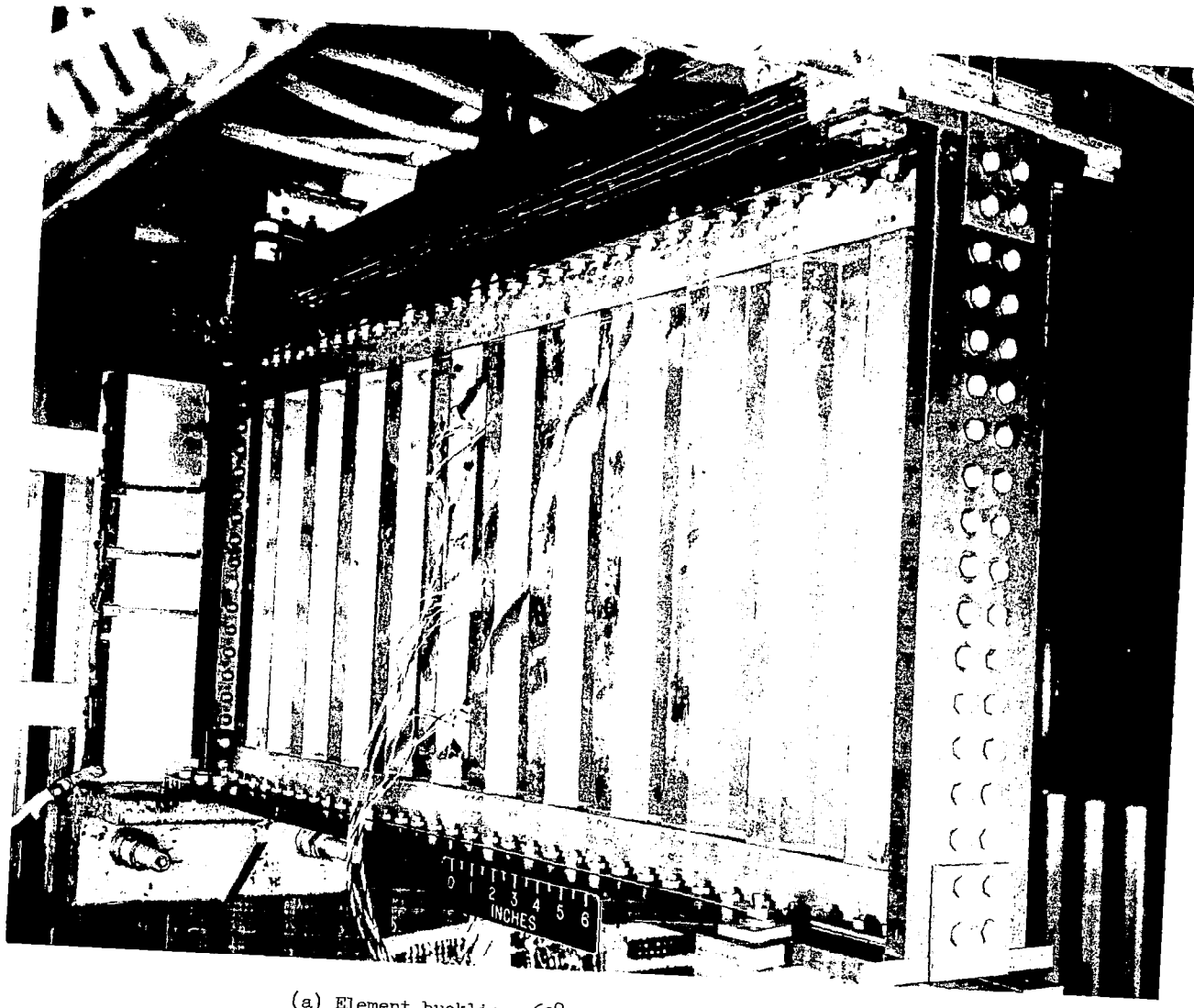

(a) Element buckling, 60° corrugation specimen 5. L-61-1819

Figure 20.- Modes of shear-web failure.

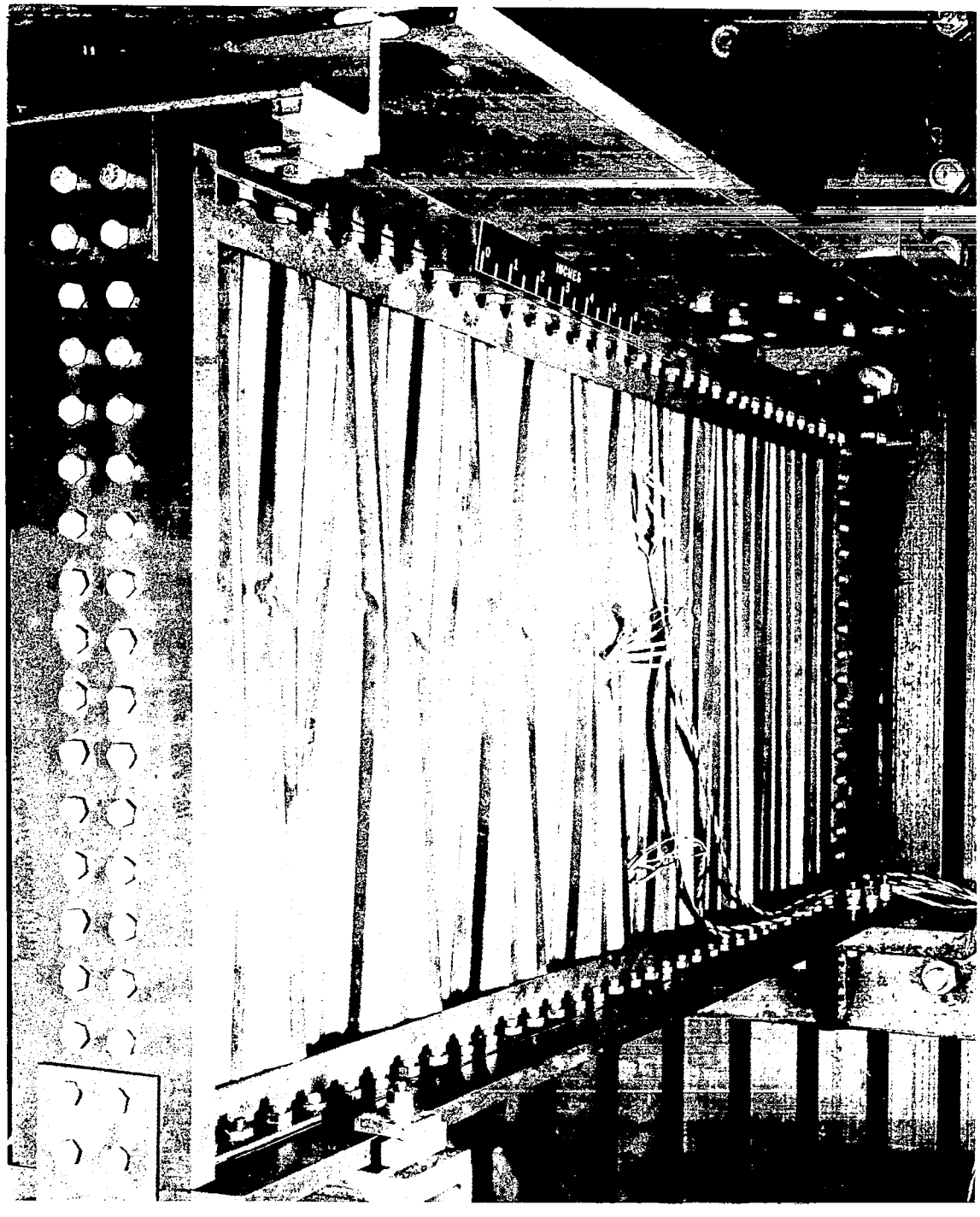

(b) General instability, transverse-frame corrugation specimen 9. L-60-2106

Figure 20.- Concluded.

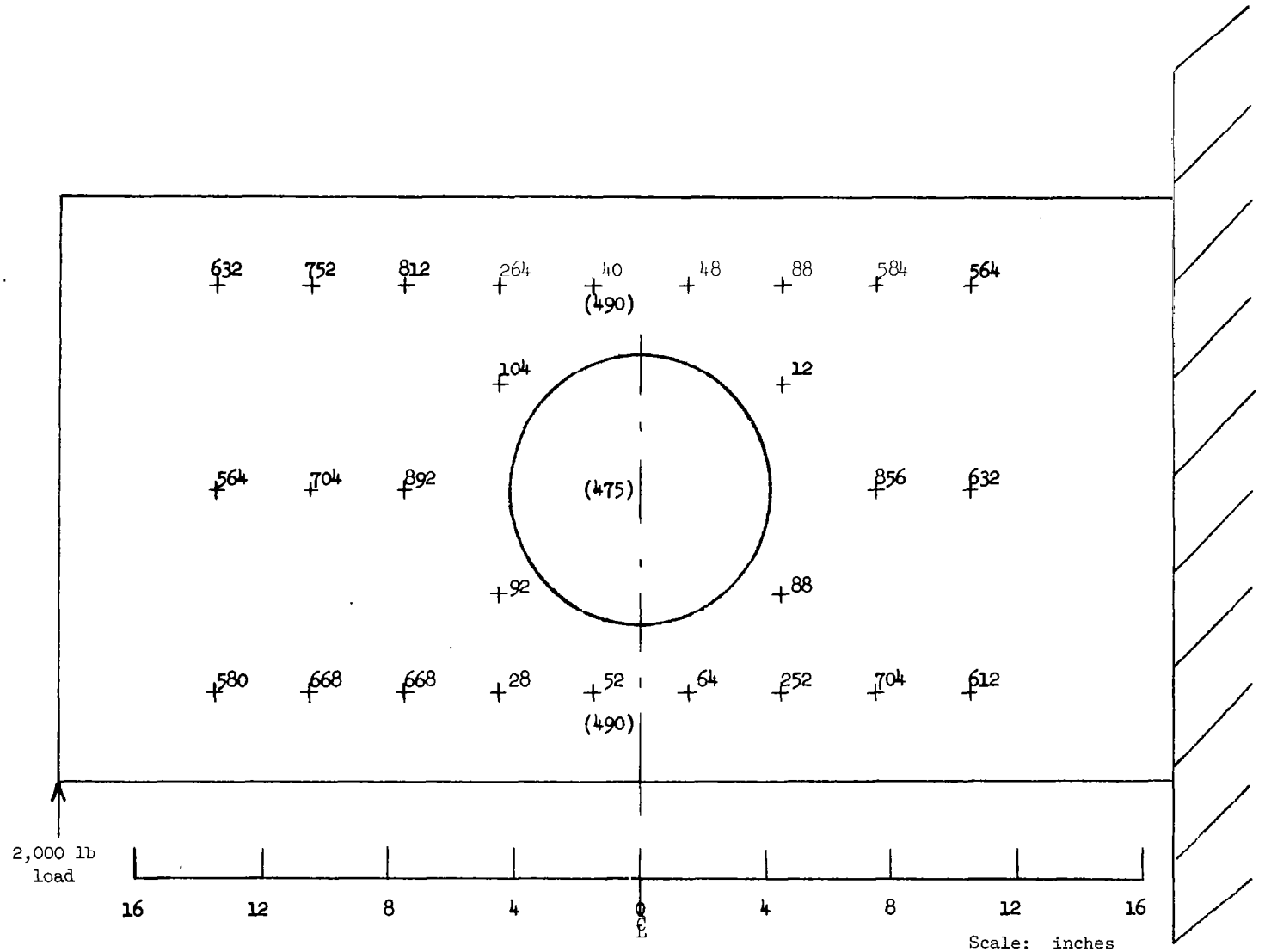

Figure 21.- Shear-strain distribution in web with cutout, specimen 6. Numbers are strains in microinches per inch. Numbers in parentheses are from specimen 1 (no cutout). Calculated average $\gamma = 504$.

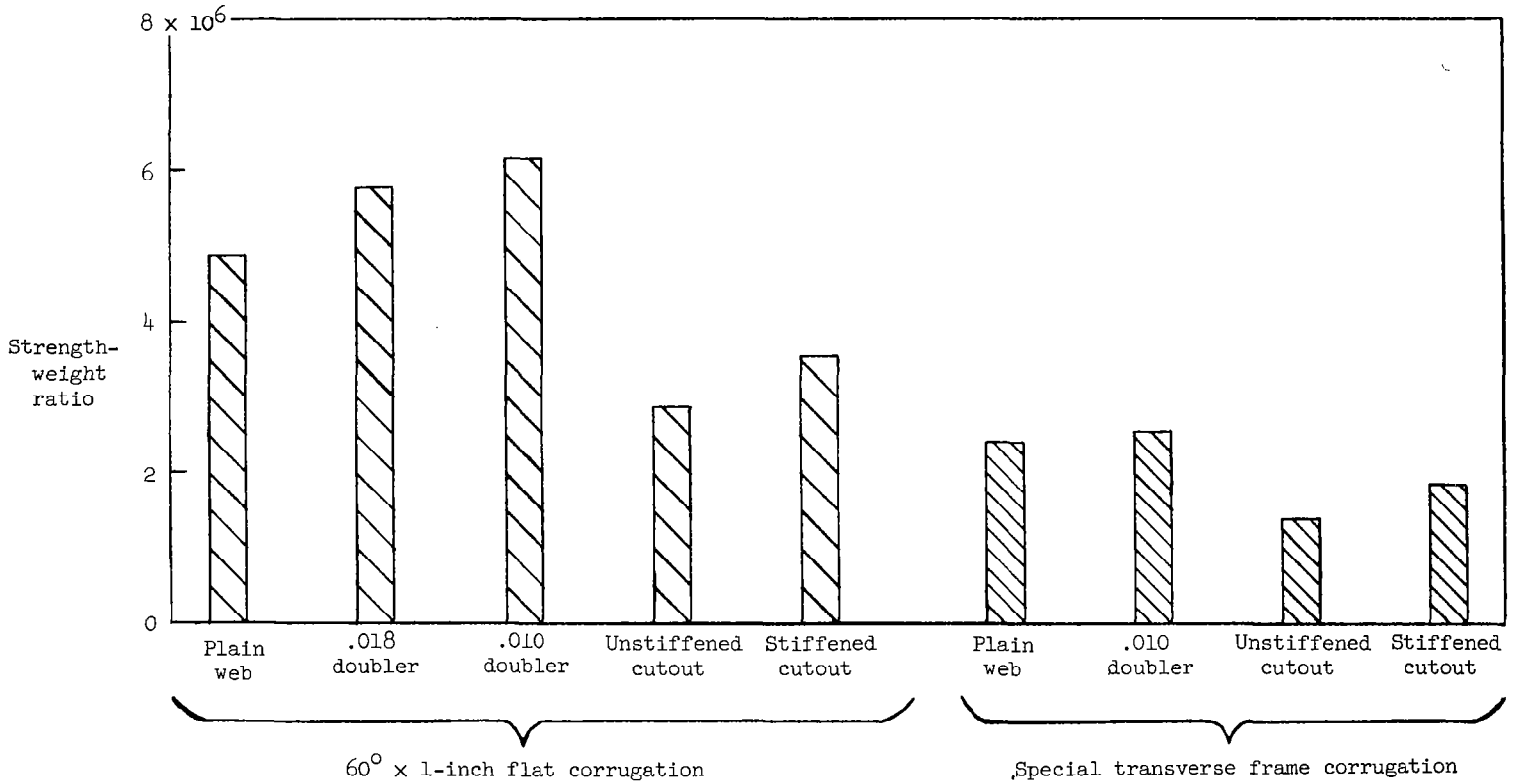

Figure 22.- Factors affecting room-temperature strength-unit weight ratio for corrugated web beams.

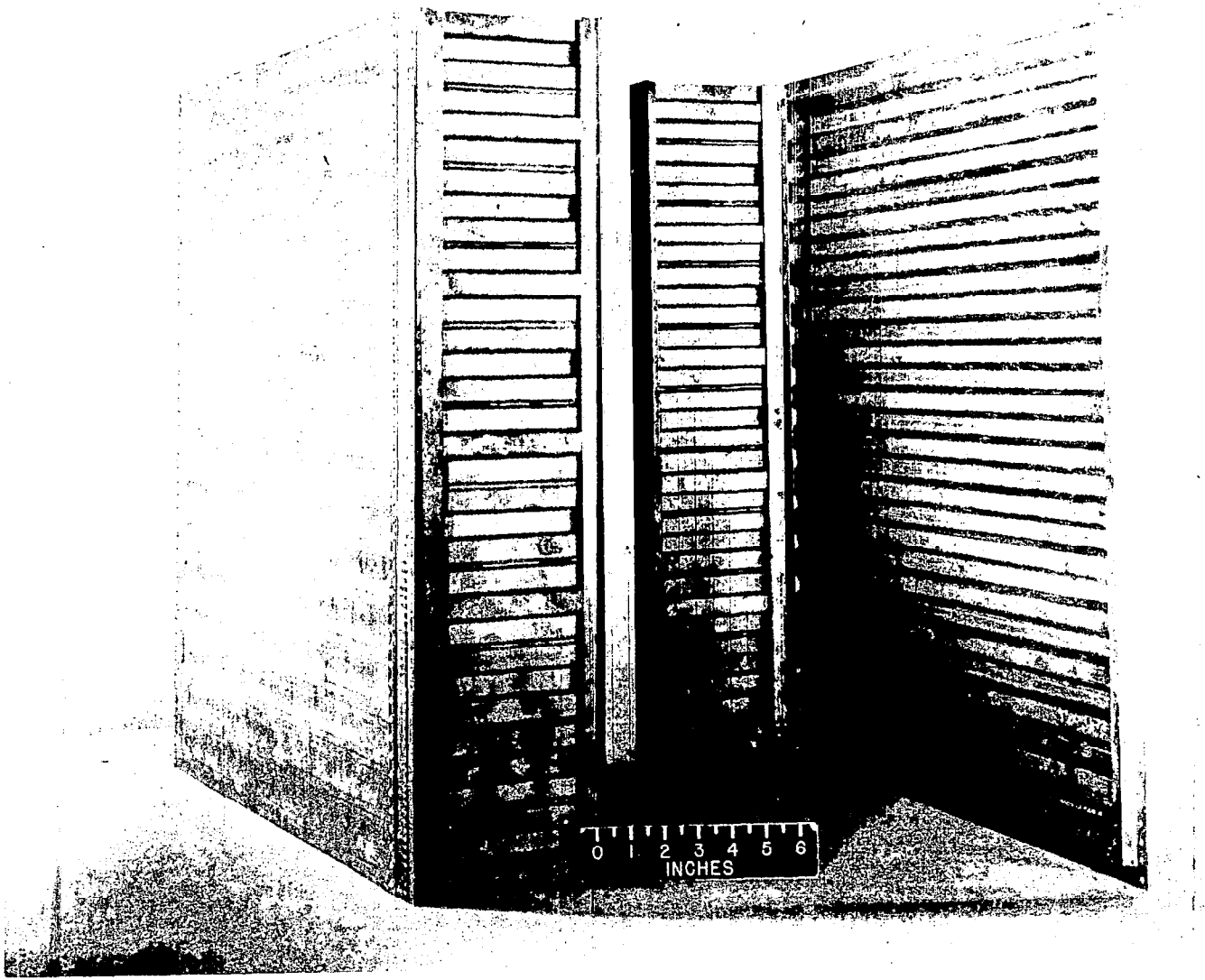

Figure 23.- Skin-panel test specimens.

L-60-1512

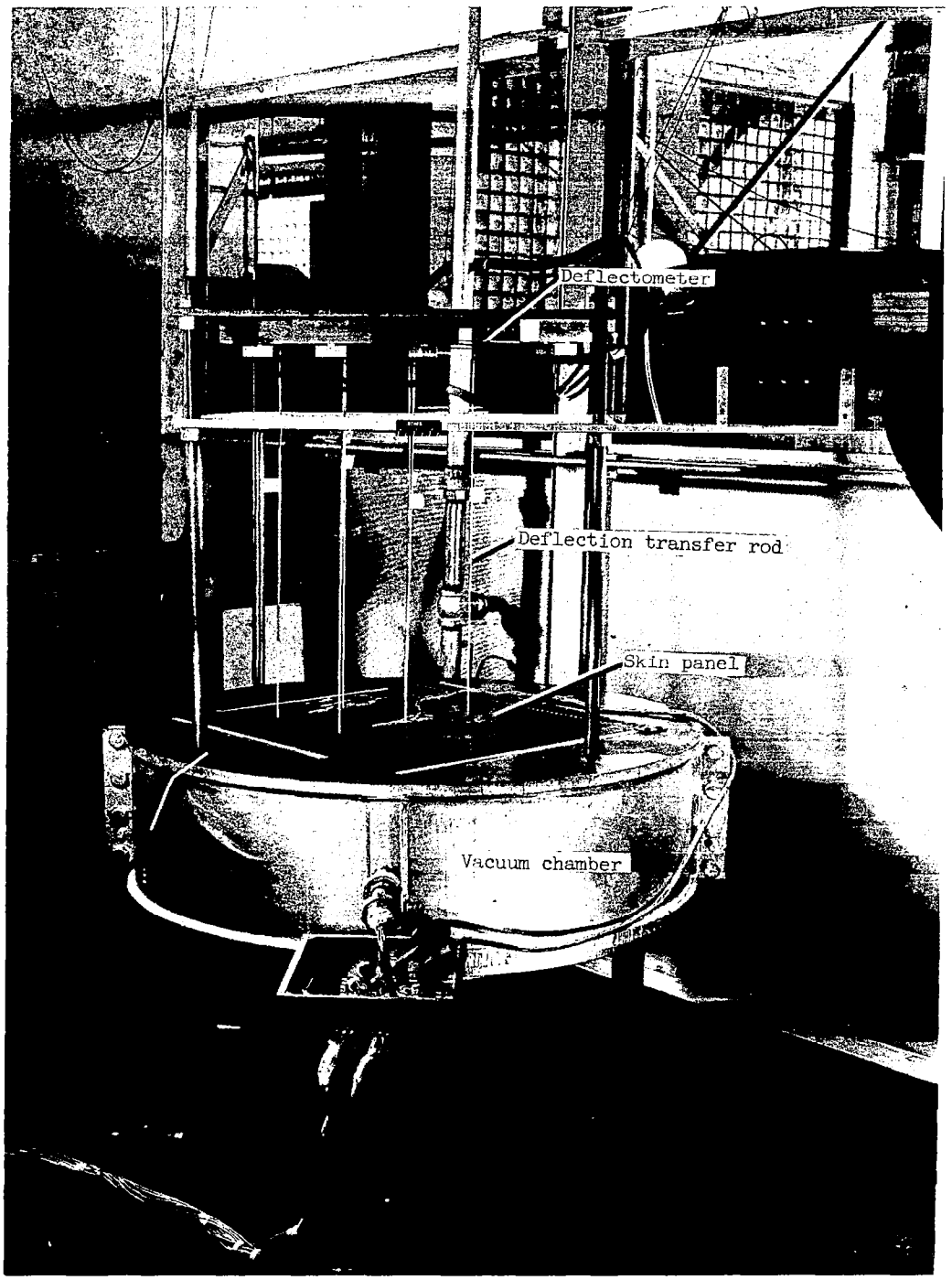

(a) Room temperature. L-60-5765.1

Figure 24.- Skin-panel heat and load test setup.

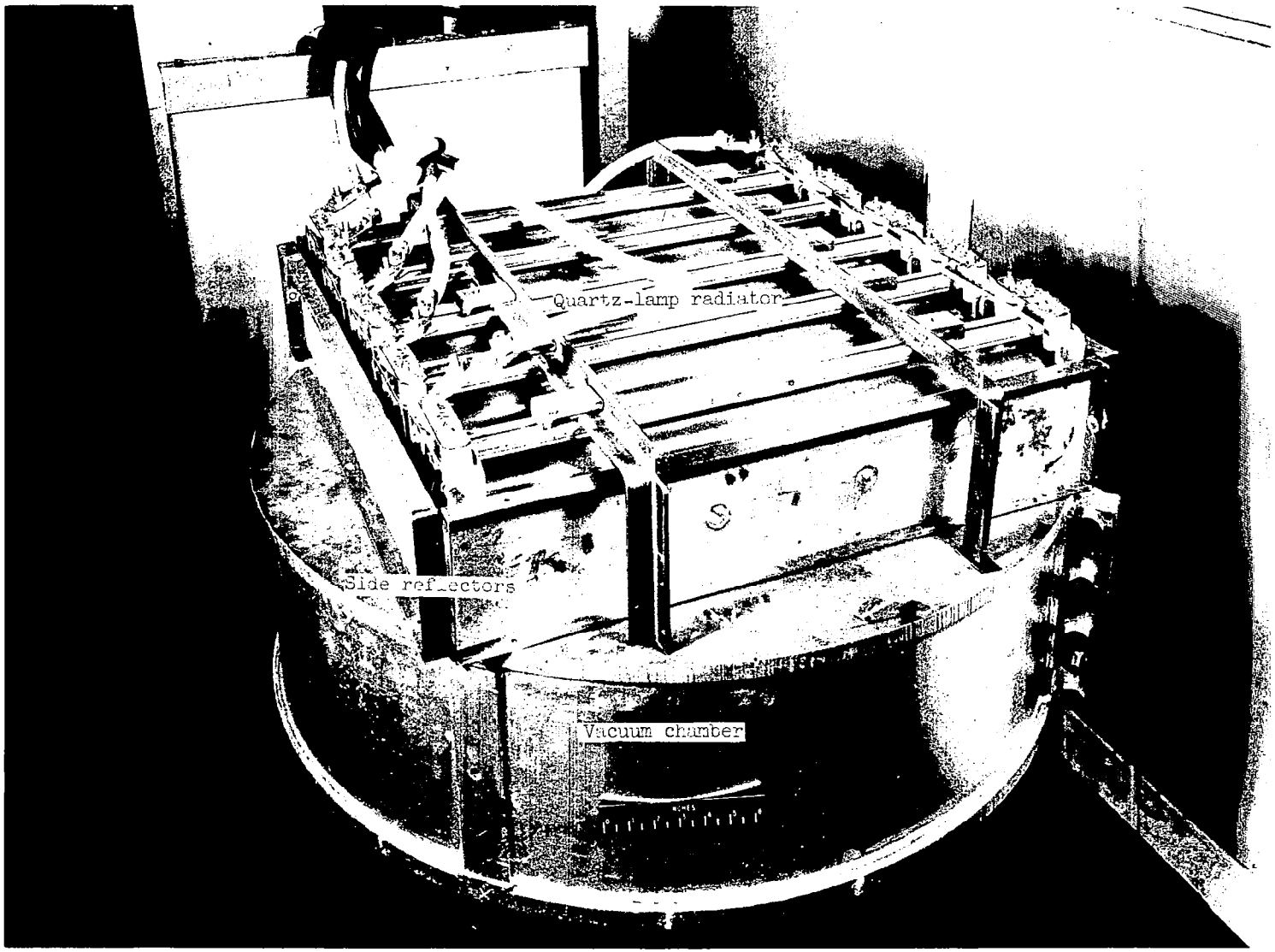

(b) Elevated-temperature test setup with deflectometer assembly removed. L-60-2654.1

Figure 24.- Concluded.

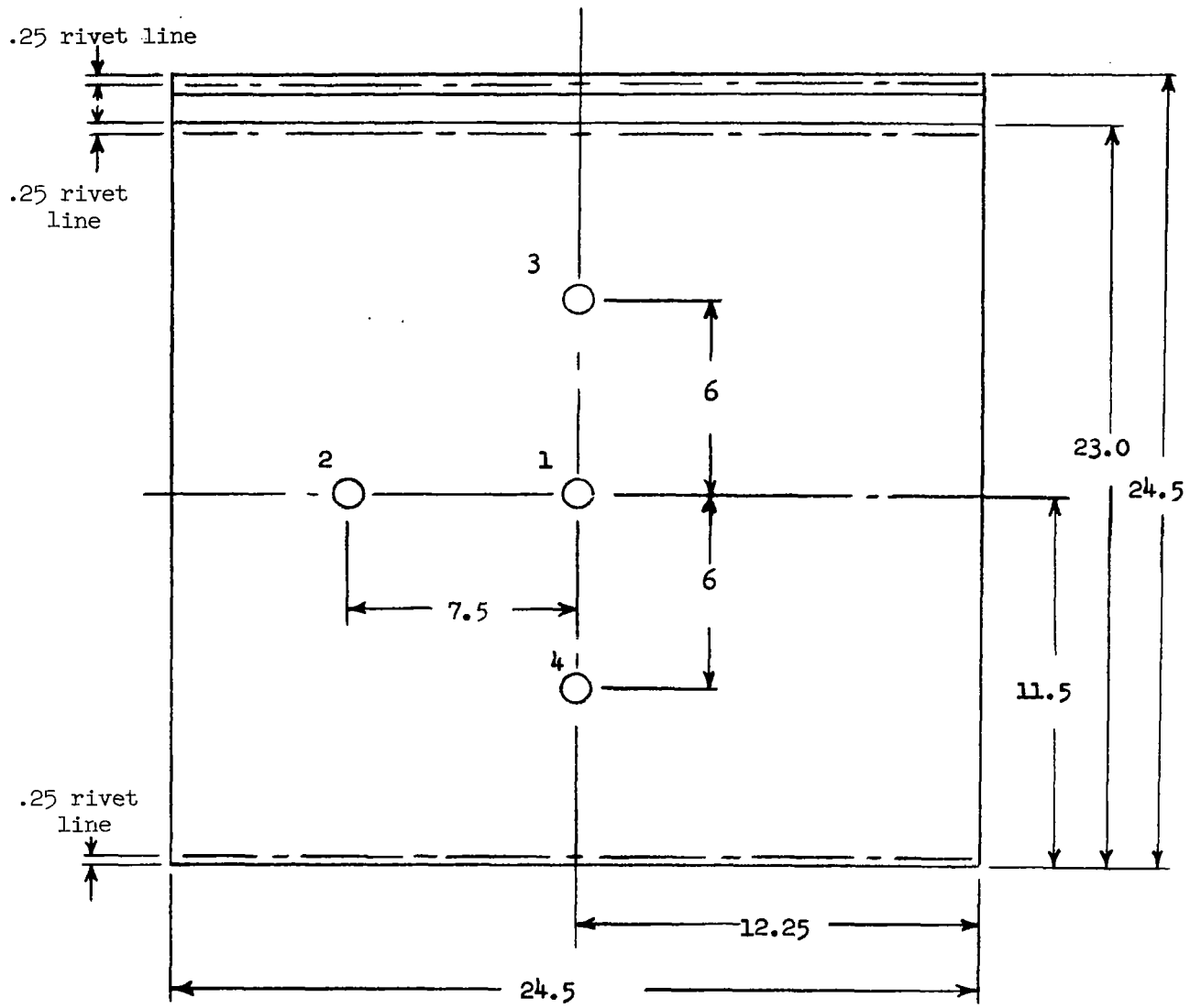

(a) Deflectometers.

Figure 25.- Skin-panel instrumentation location.

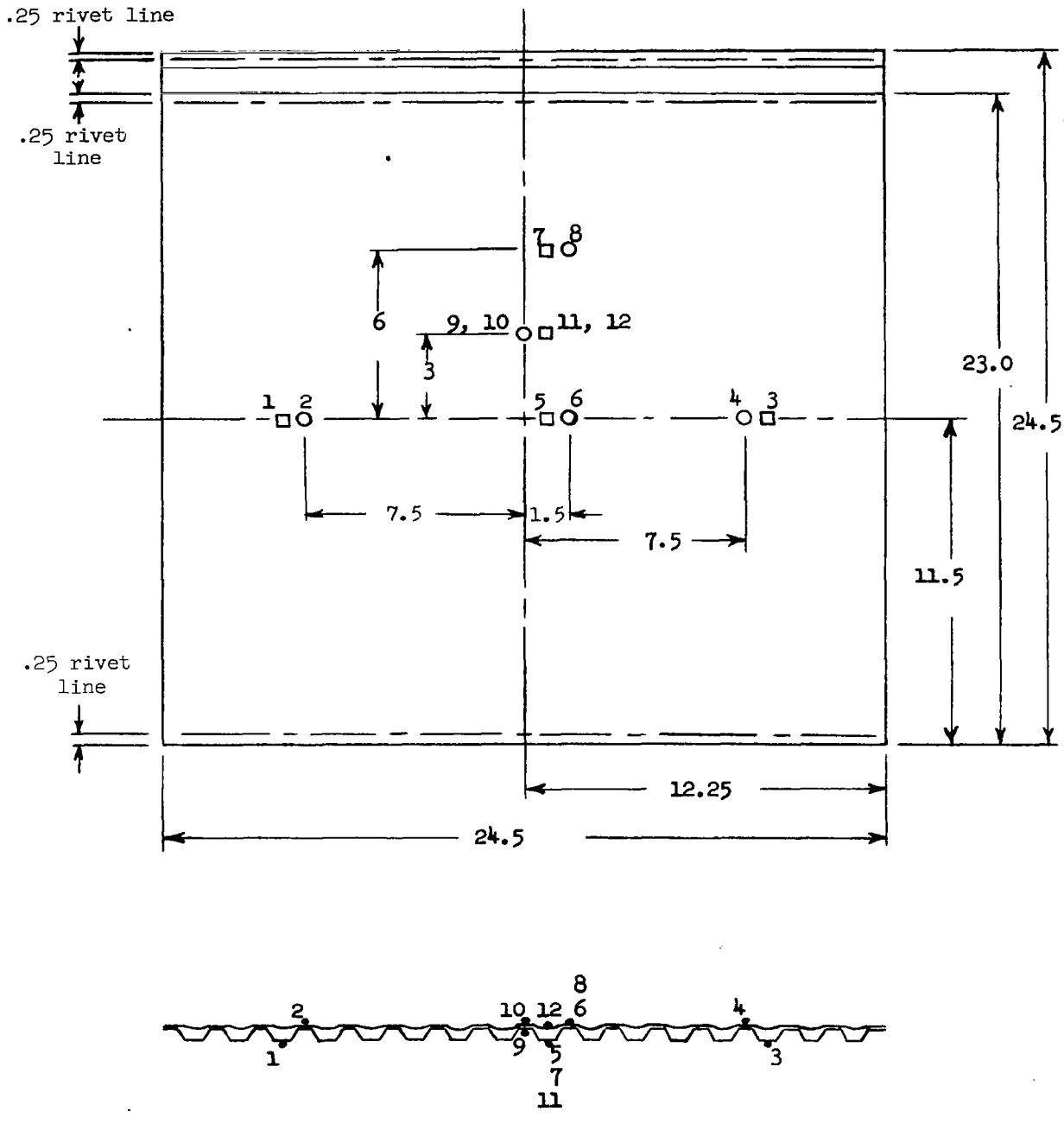

(b) Strain gages.

Figure 25.- Continued.

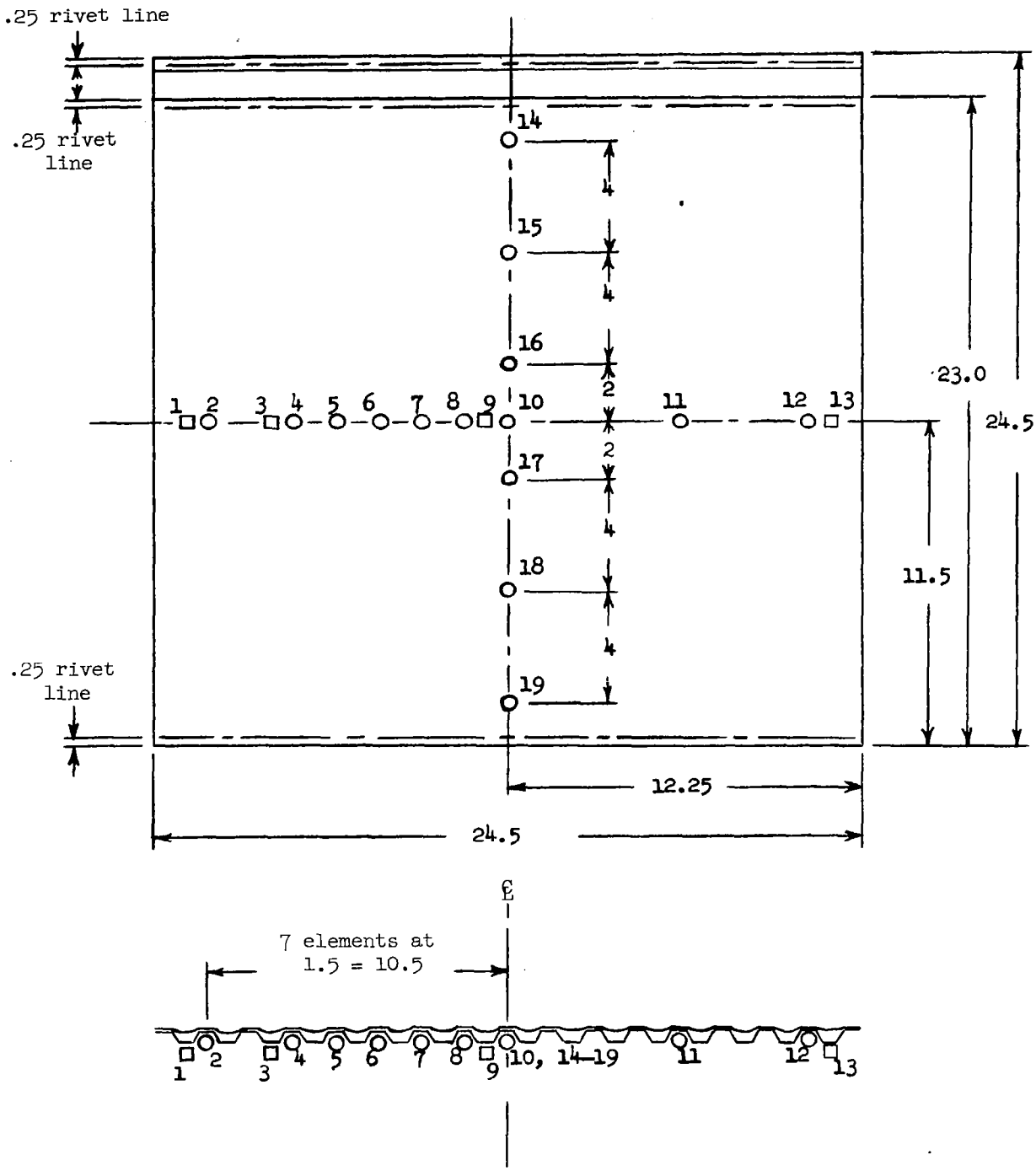

(c) Thermocouples.

Figure 25.- Concluded.

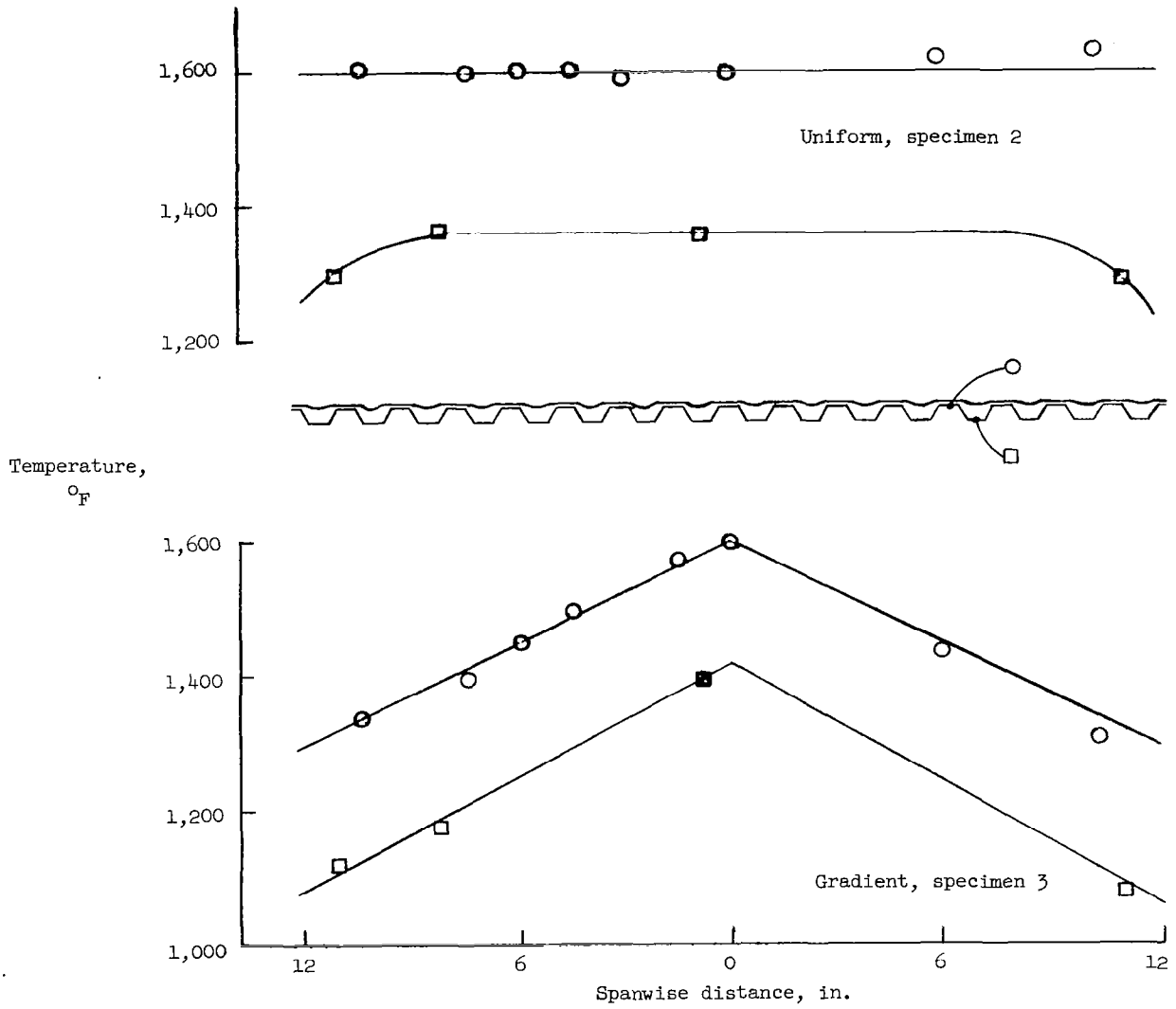

(a) Spanwise, steady state.

Figure 26.- Temperature distribution for corrugation-stiffened skin panels.

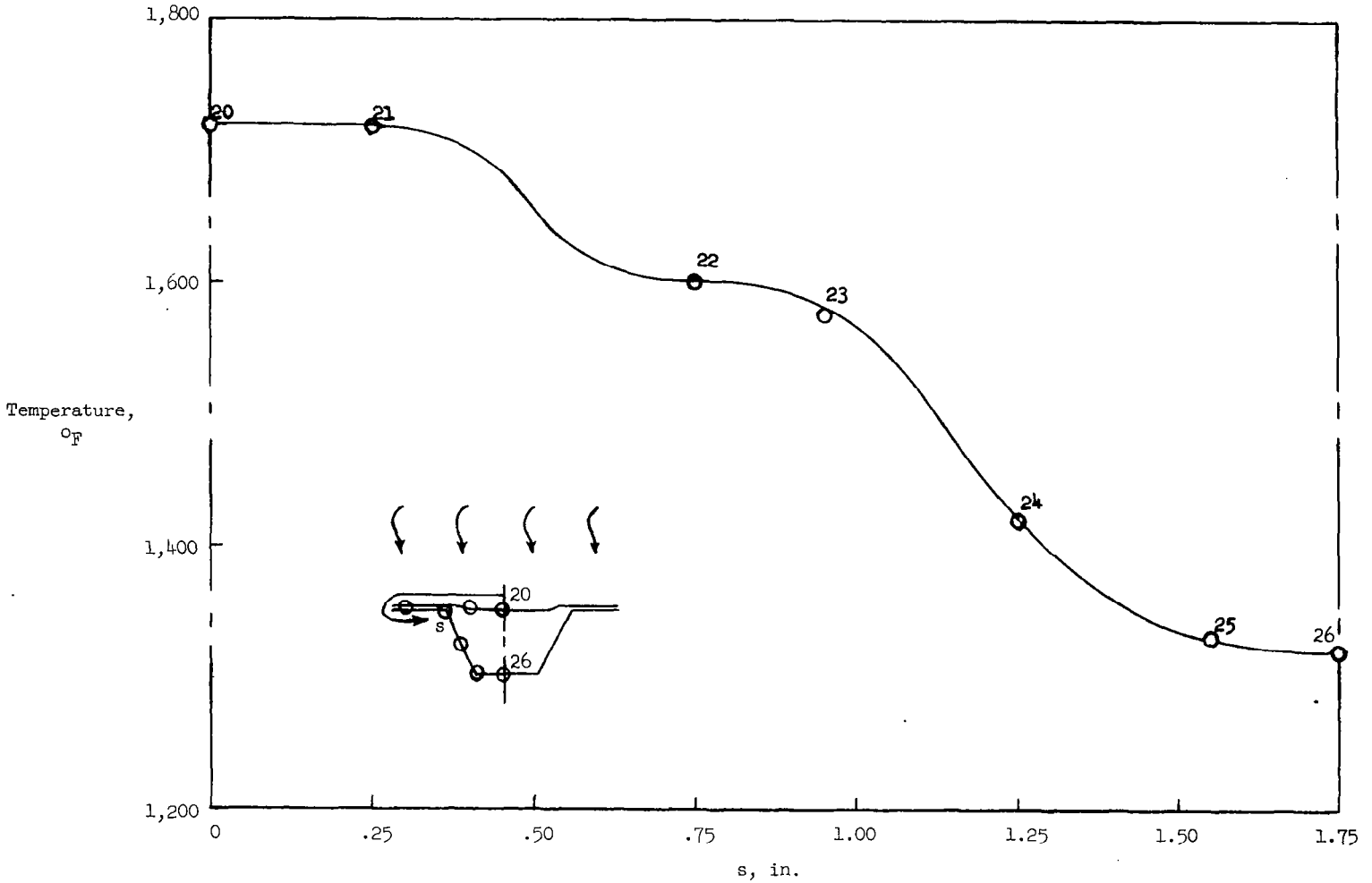

(b) Panel element, steady state.

Figure 26.- Continued.

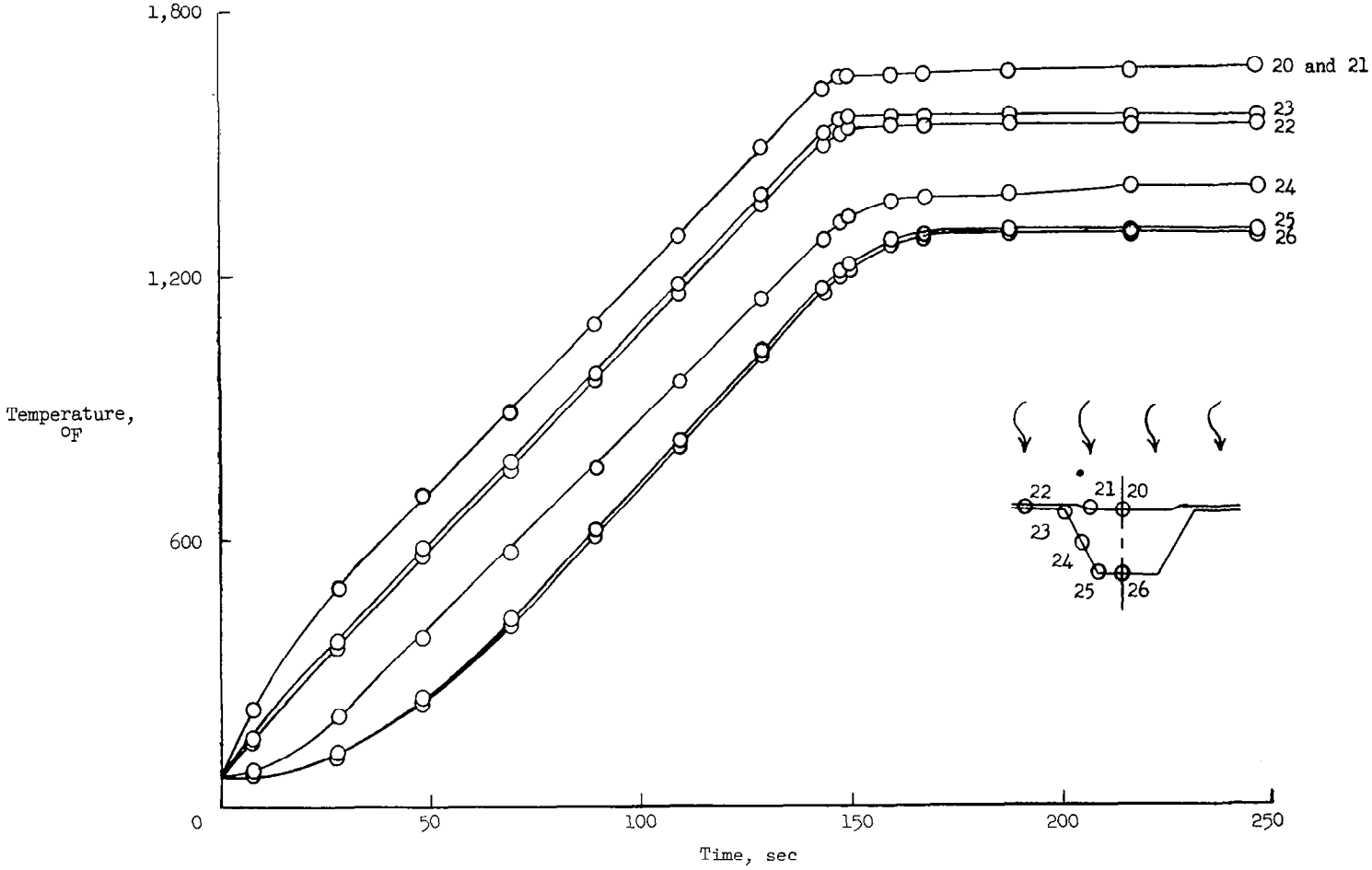

(c) Panel element, transient.

Figure 26.- Continued.

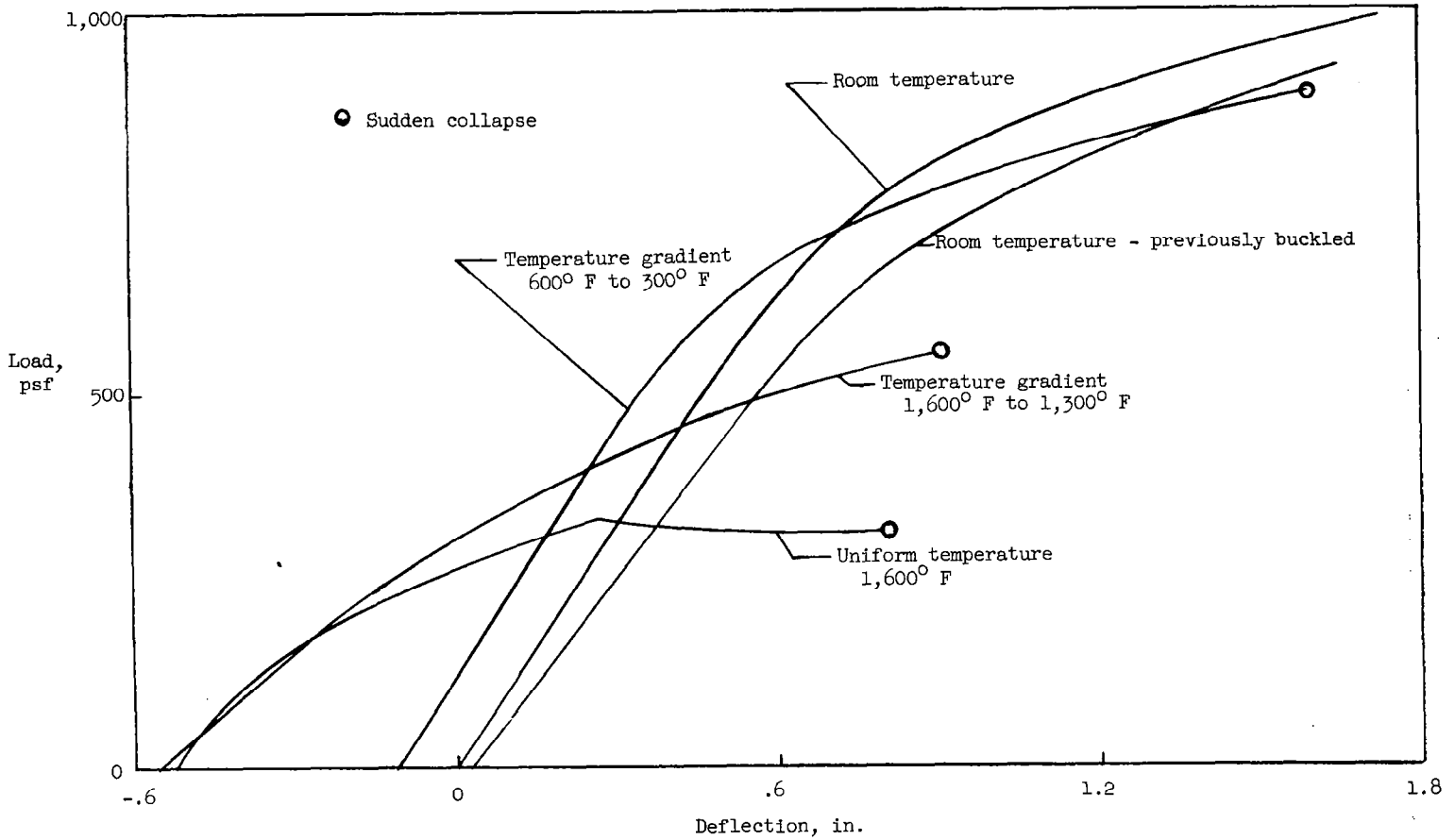

(a) Experimental.

Figure 28.- Normal load, center deflection for corrugation-stiffened skin panels.

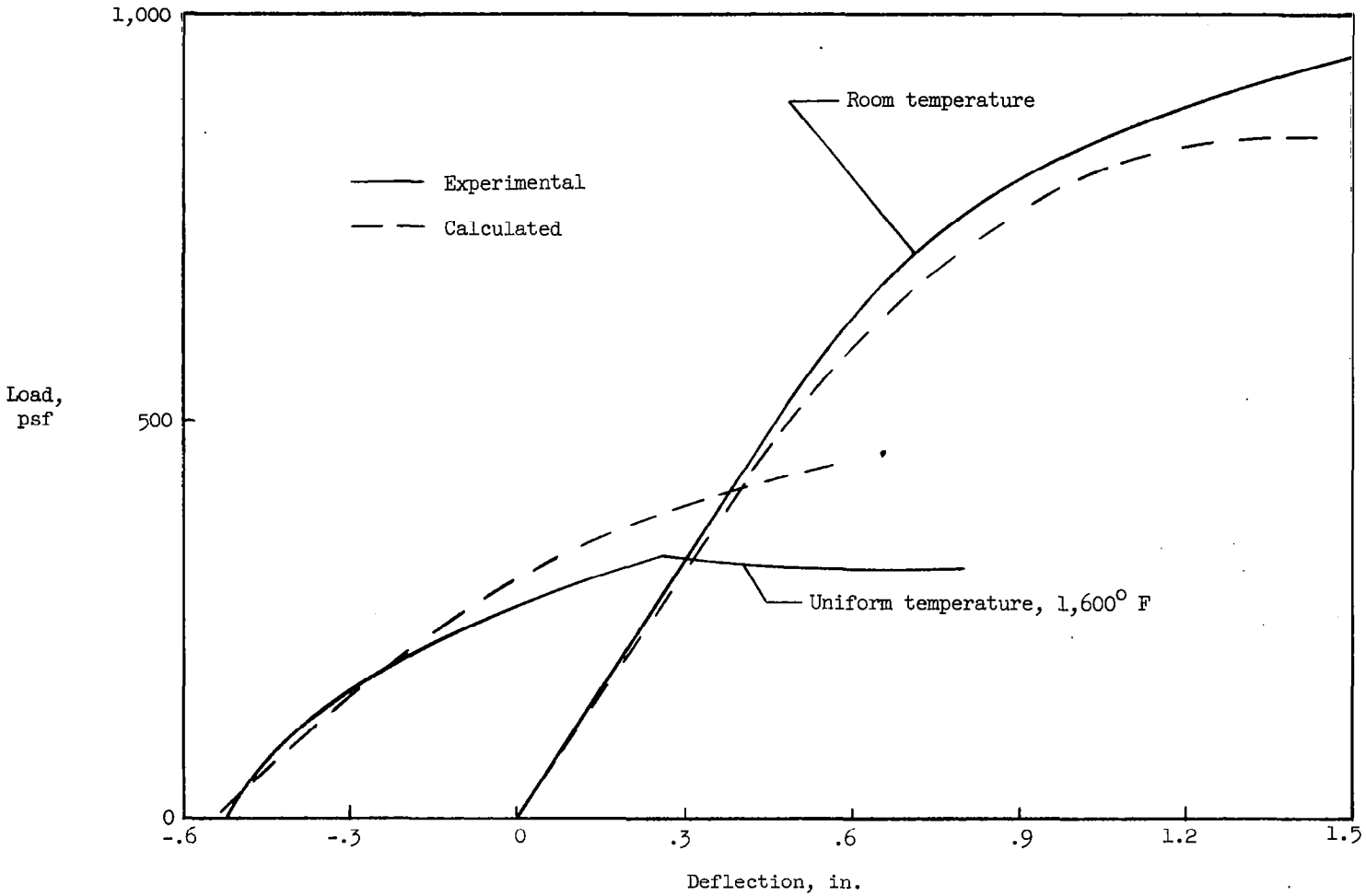

(b) Comparison of experimental with calculated skin-panel deflections.

Figure 28.- Concluded.

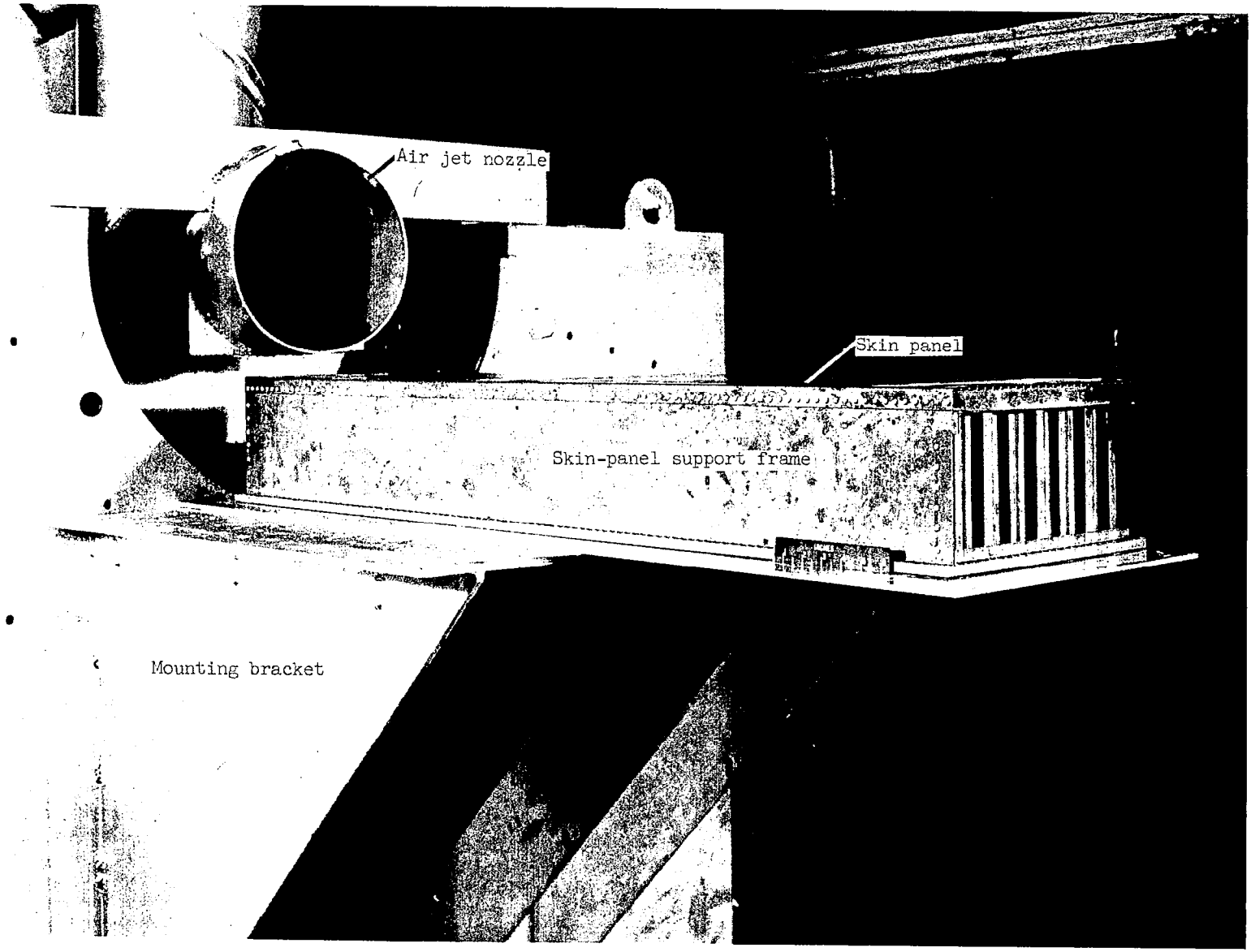

Figure 29.- Acoustic test setup.

L-61-4805.1

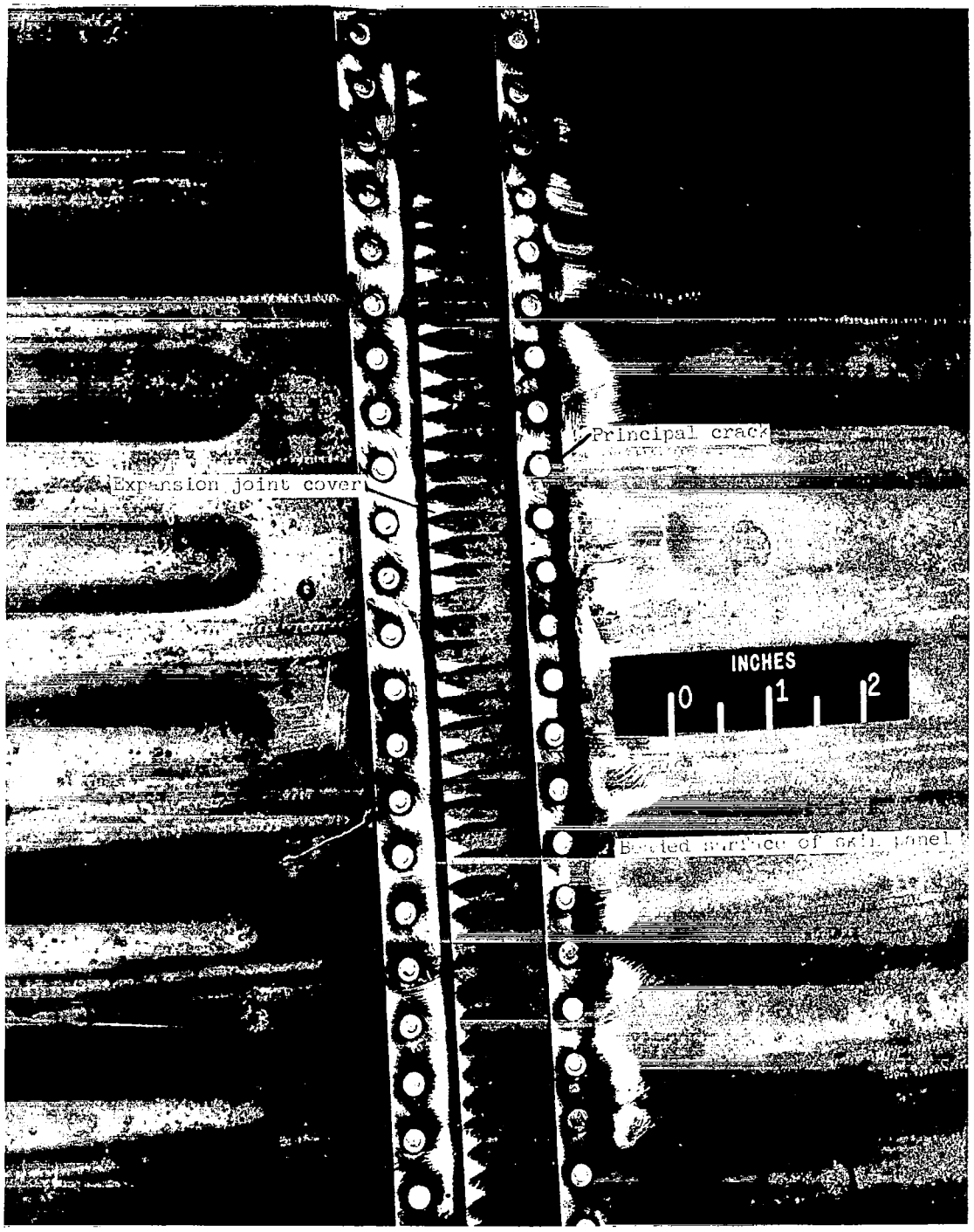

L-60-579.1

Figure 30.- Growth of skin cracks at end of 121 minutes of exposure to 160-db sound-pressure level at room temperature, specimen 10.

Figure 31.- Failure of indirect resistance welds on back side of skin-panel specimen 10 at end of test. L-60-577.1

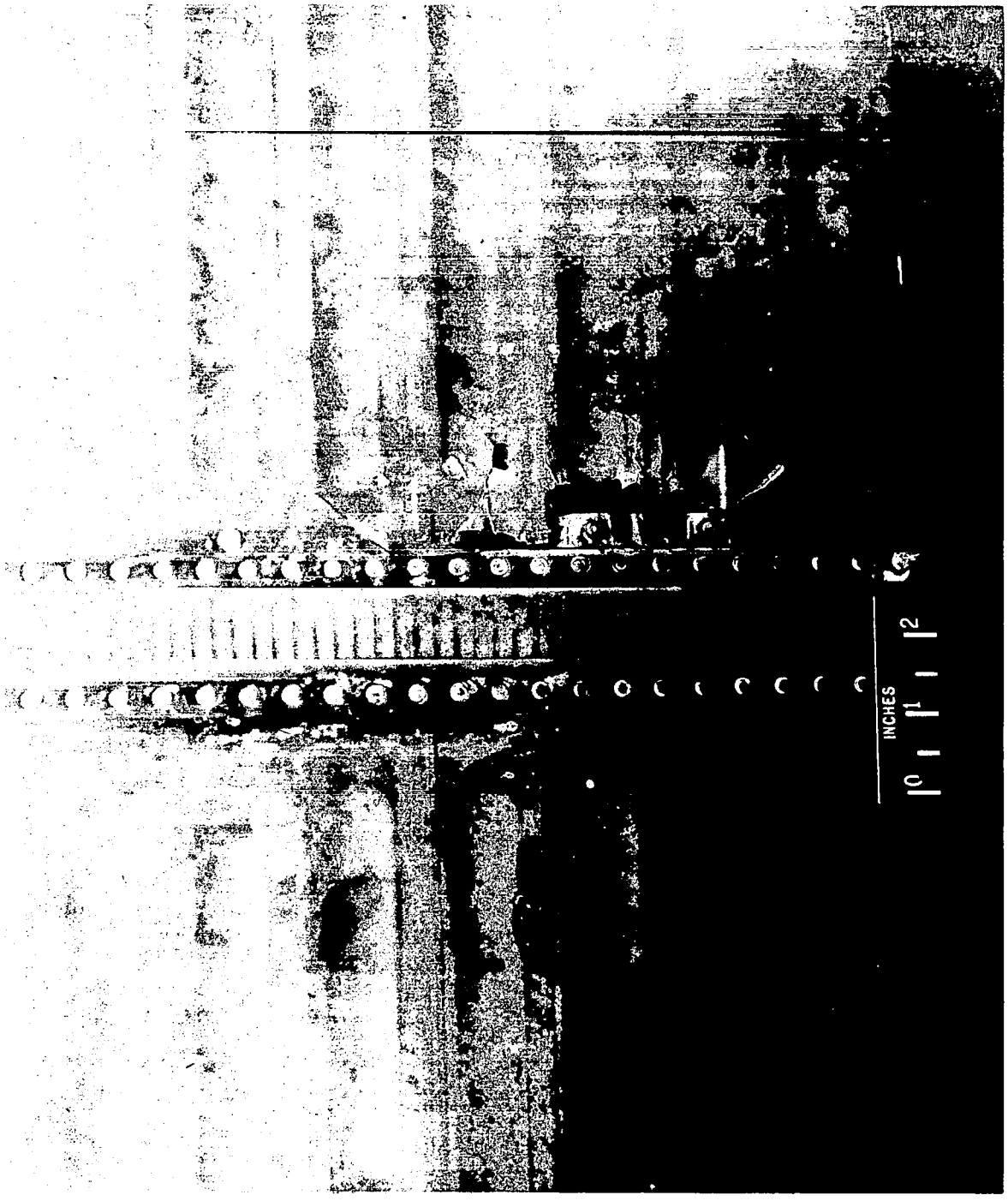

L-61-5385

Figure 32.- Growth of skin cracks at end of 120 minutes of exposure at 160-db sound-pressure level at room temperature, modified specimen 12.

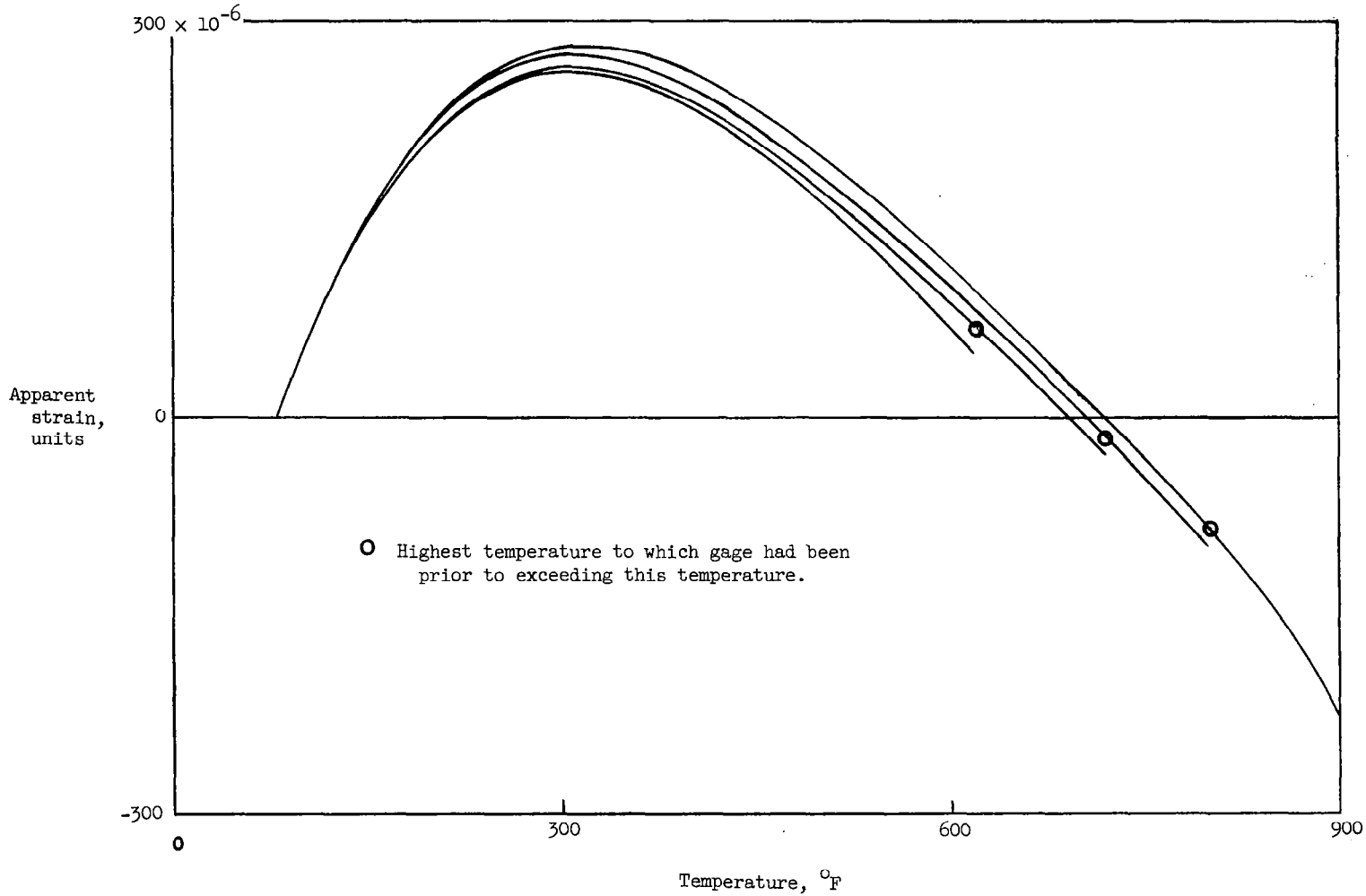

(a) Apparent strain for gage type rated at <600° F on Inconel X. Gage was cyclicly heated and cooled four times to temperatures of 620°, 720°, and 800° F.

Figure 33.- Strain-gage temperature effects. Gage installation was cured at 600° F for 1 hour prior to testing.

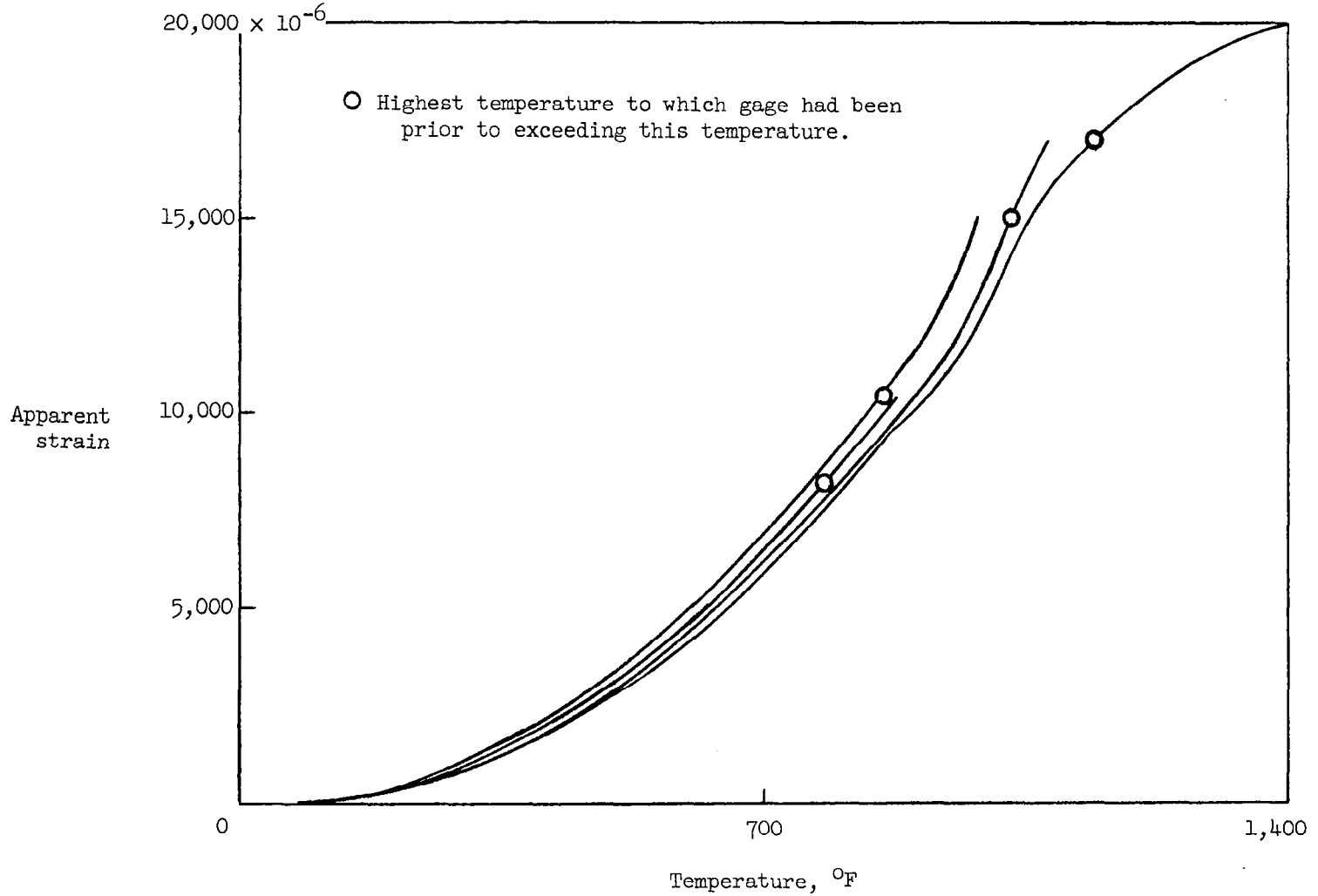

(b) Apparent strain for gage type rated at >600° F on Inconel X. Gage was cyclicly heated and cooled four times to temperatures of 780°, 860°, 1,030°, and 1,140° F.

Figure 33.- Continued.

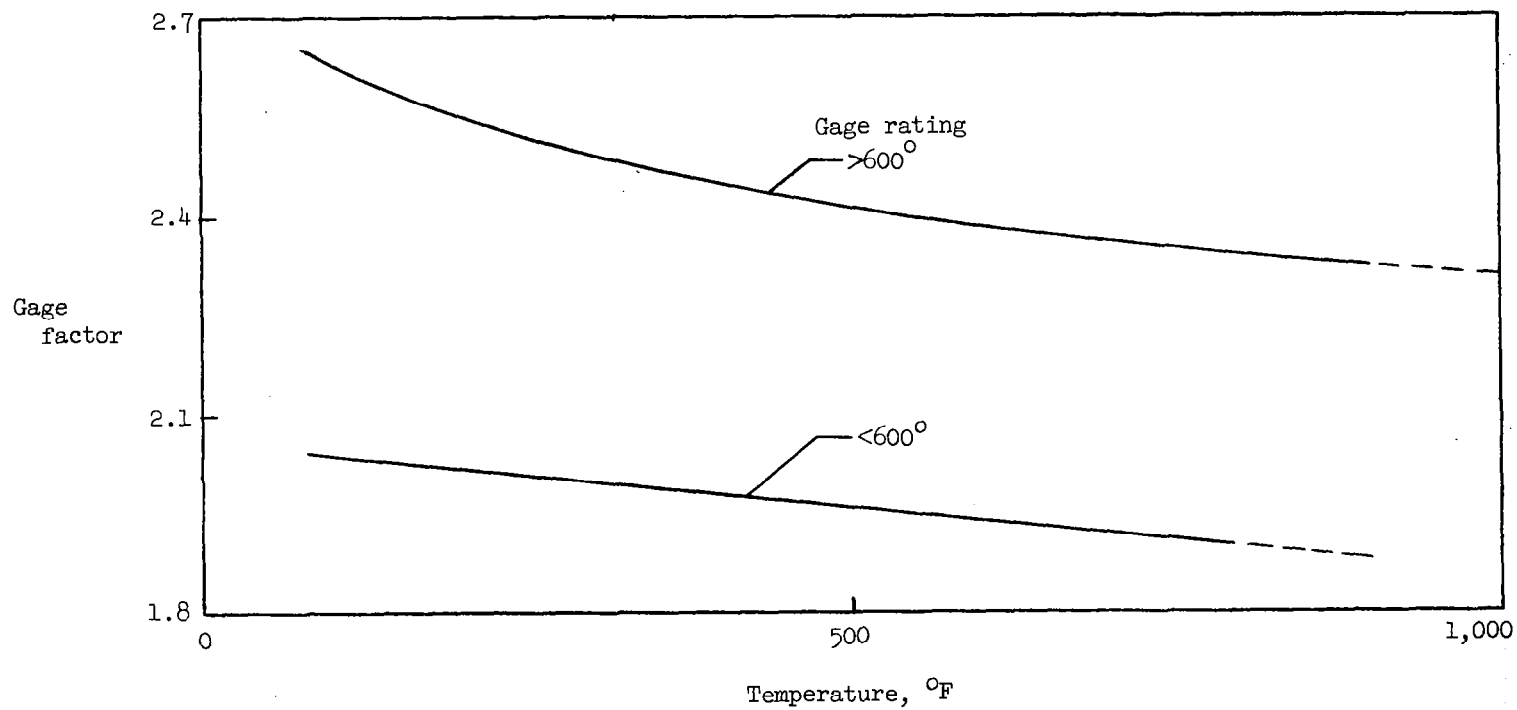

(c) Gage factor for foil gages.

Figure 33.- Concluded.

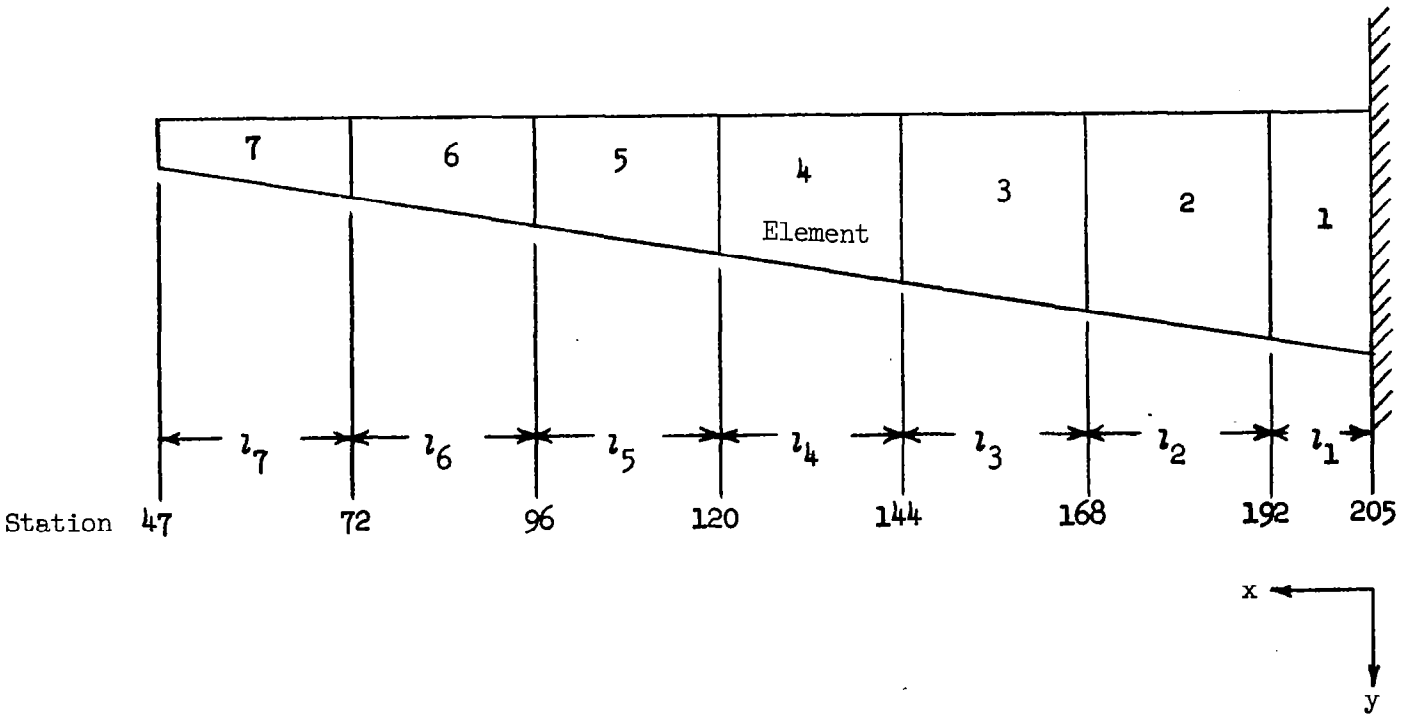

Figure 34.- Division of main beams into seven elements of length for deflection calculations.

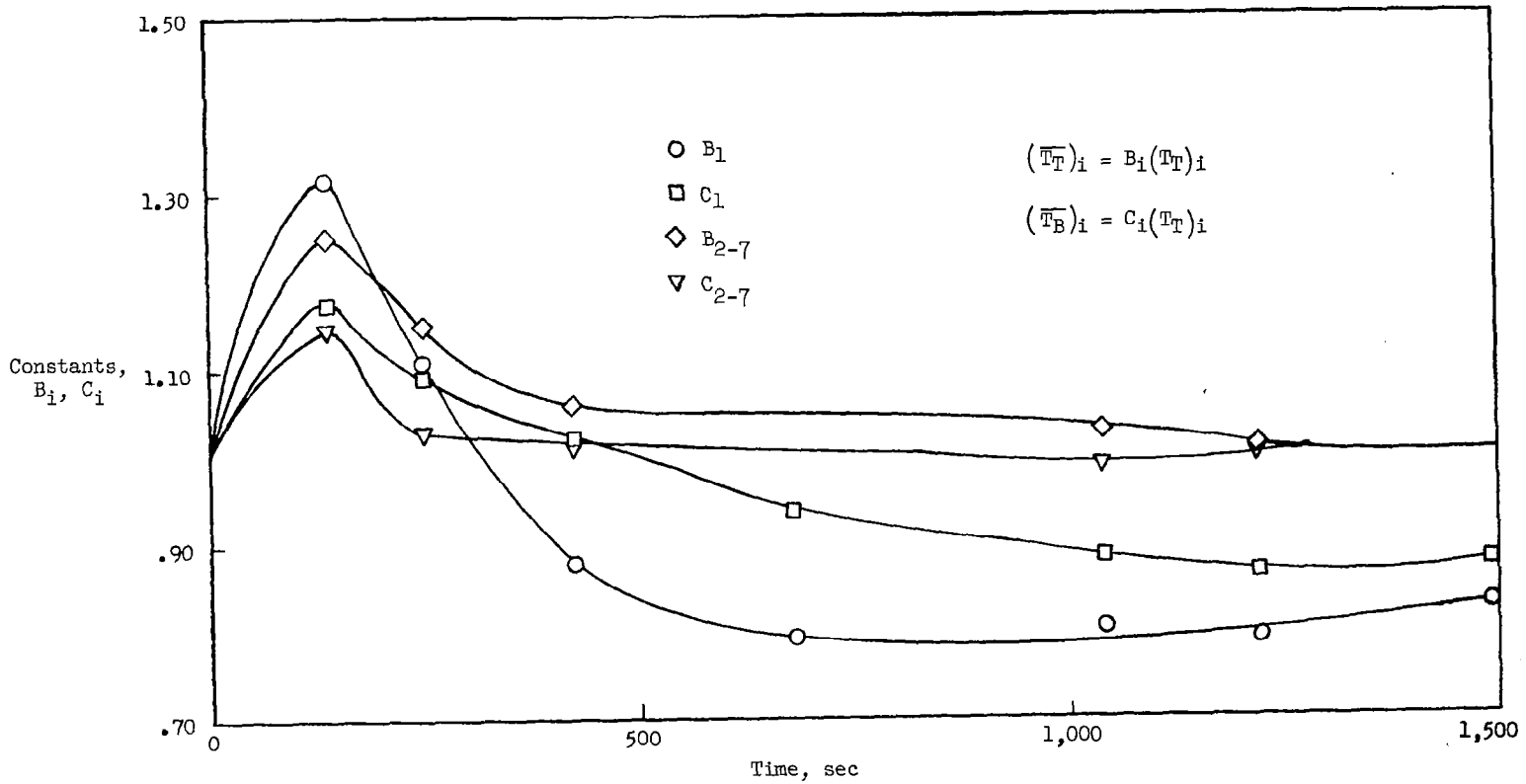

Figure 35.- Correction terms to be applied to measured temperature to get average temperatures in each element of length for main-beam spar caps.

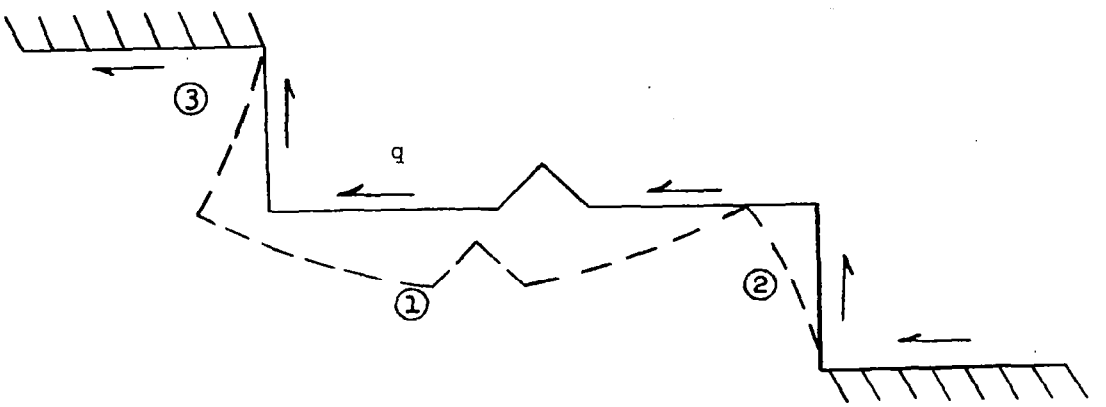

(a) Bending deformation in one repeating element.

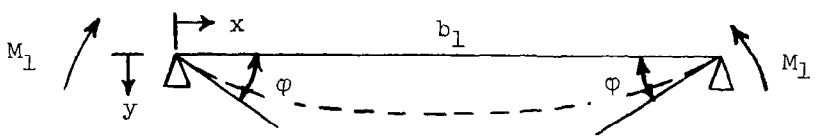

(b) Bending of element (1).

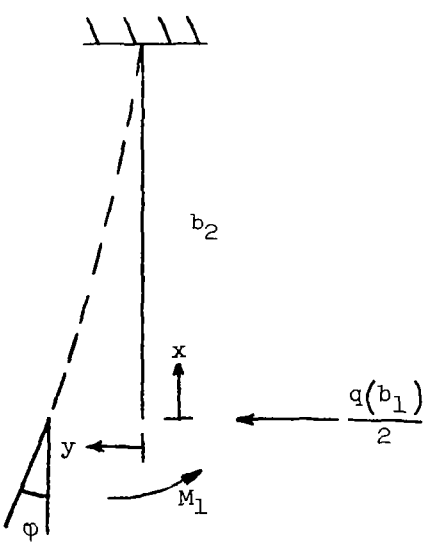

(c) Bending of element (2) or (3).

Figure 36.- Deformation of special transverse-frame corrugation considered in shear-web deflection calculation.

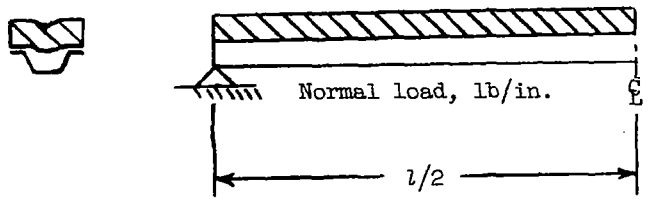

(a) Beam-loading diagram.

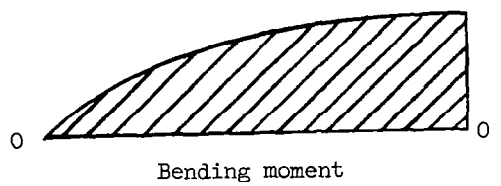

(b) Beam-bending-moment diagram.

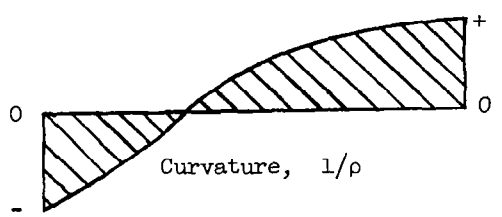

(c) Beam-curvature diagram.

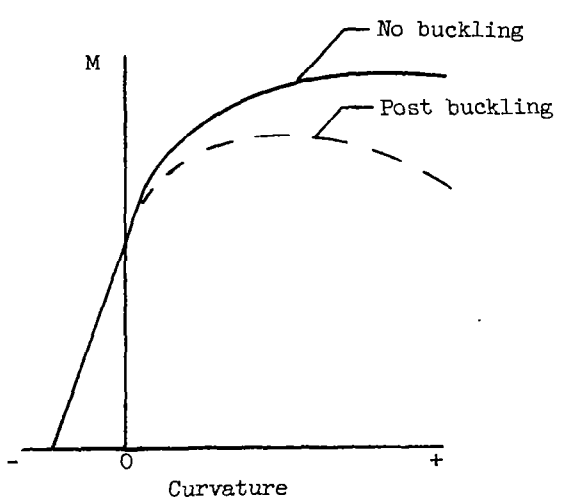

(d) Moment-curvature relationship for cross section of beam.

Figure 37.- Graphical construction used in the calculation of plastic beam bending.

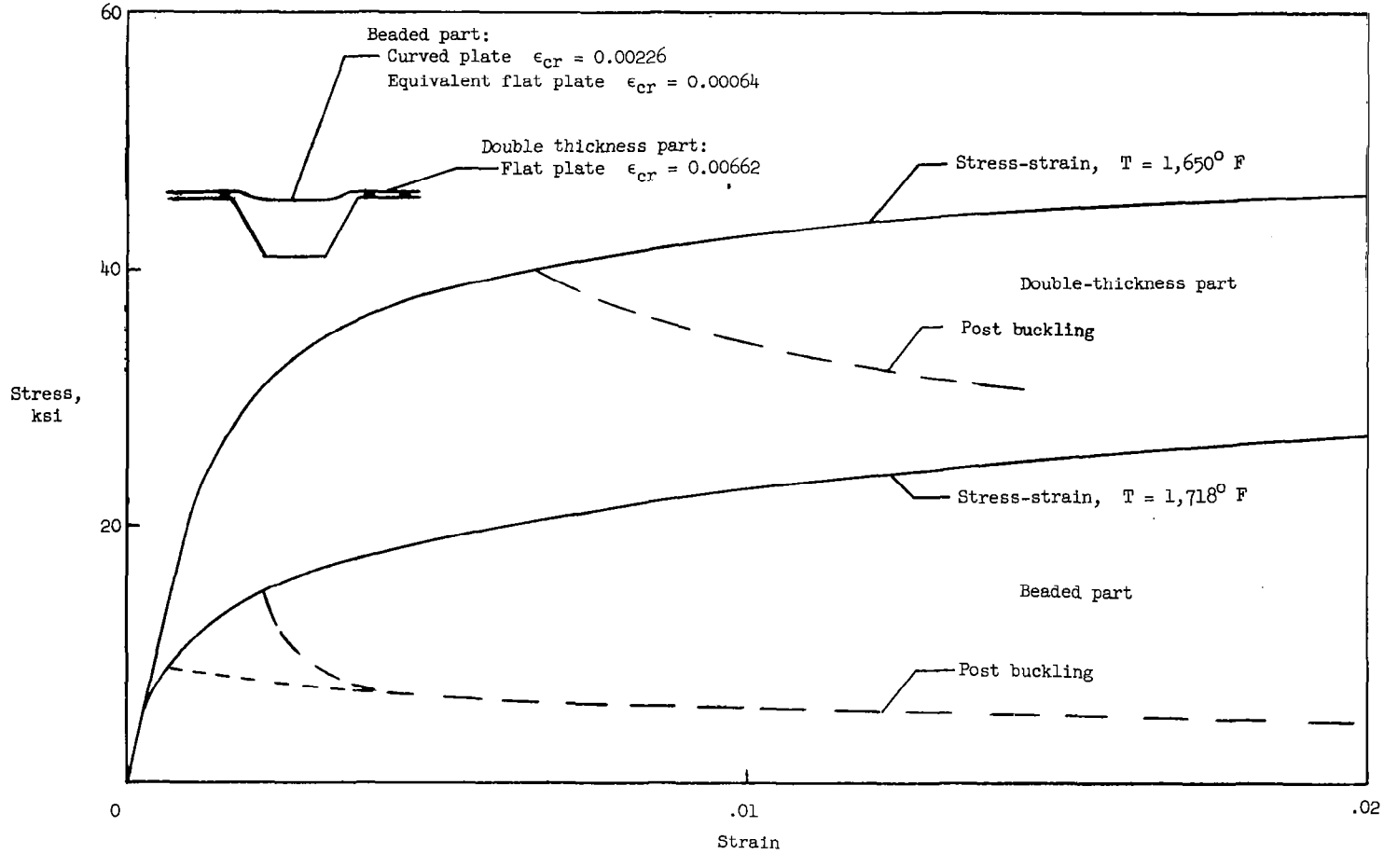

Figure 38.- Effective stress-strain curves for postbuckled parts of the corrugation-stiffened skin panel.